Title
Regulation of Bacterial Type IIA Topoisomerases

Author
Vos, Seychelle Monique

Publication Date
2013

Peer reviewed|Thesis/dissertation

Regulation of Bacterial Type IIA Topoisomerases

By

Seychelle Monique Vos

A dissertation submitted in partial satisfaction of the

requirements for the degree of

Doctor of Philosophy

in

Molecular and Cell Biology

in the

Graduate Division

of the

University of California, Berkeley

Committee in charge:

Professor James M. Berger, Chair
Professor Jamie H. D. Cate
Professor Douglas Koshland
Professor Daniel Fletcher

Fall 2013

Abstract

Regulation of Bacterial Type IIA Topoisomerases

by

Seychelle Monique Vos

Doctor of Philosophy in Molecular and Cell Biology

University of California, Berkeley

Professor James M. Berger, Chair

DNA topoisomerases are ubiquitous and essential enzymes that maintain the supercoiling homeostasis of chromosomes. Decades of research have elucidated how topoisomerases manipulate DNA to introduce or remove supercoils. Recently it has become apparent that these enzymes are highly regulated by cells, often through direct physical interactions with other proteins involved in diverse cellular processes such as replication, chromosome condensation, transcription, and repair. It is largely unknown how these interactions affect enzyme function and localization in cells.

To gain a better understanding of topoisomerase regulation, I have explored some of the intrinsic and extrinsic mechanisms bacteria use to control their type IIA topoisomerases, topoisomerase (topo) IV and gyrase. This work has revealed intrinsic features that contribute to substrate discrimination by topo IV, determined how a condensin homolog binds and activates topo IV, and uncovered a novel proteinaceous mechanism to inhibit gyrase function. These initial studies provide a framework for understanding how gyrase and topo IV function are integrated into the broader context of the cell through enzyme specific modifications and associations and may provide novel targets for small molecule inhibitors.

TABLE OF CONTENTS

ACKNOWLEDGEMENTS

I thank my advisor, James Berger, for his undying patience, excitement, and encouragement. The Berger Lab for being a constant source of inspiration with special thanks to Allyn Schoeffler, Nathan Thomsen, Elsa Tretter, Kevin Jude, Imsang Lee, Glenn Hauk, Tim Blower, Tim Wendorff, Artem Lyubimov, David Hershey, Richard Rymer, Karl Duderstadt, Ernesto Arias, Franziska Bleichert and Iris Hood for their encouragement, suggestions, and collaborations.

I thank my generous and helpful collaborators Nichole Stewart and Martha Oakley at Indiana University for their advice and collaboration on the MukB project. I thank Valakunja "Raj" Nagaraja for sharing unpublished data and inspiring our group to investigate YacG. I thank Jane Tanamachi, James Holton, and George Meigs at ALS Beamline 8.3.1 for their assistance scheduling and collecting crystallography data.

I thank my backpacking friends for encouraging me to escape for a few weekends each year to experience the beauty of California: Damian Trujillo, Dan Richter, Alec Sexton, Dorothy Tegler, Aaron Cantor, Tera Levin, Phil Cleves, Pricilla Erickson, Eric Estrin, Debbie Thurtle, and Lauren Booth. I thank Aaron Cantor for his patience, enthusiasm, and many delightful scientific discussions. I thank Neutron, Bubbles and Peter for brightening gloomy days. I thank my family for supporting and encouraging my educational endeavors.

I thank Jasper Rine and his crash of "Rhinos" for providing me with an awesome working environment for my last few months in Berkeley. I thank my committee members Jamie Cate, Doug Koshland, and Dan Fletcher for their helpful advice and support over the years.

This research was supported by a National Science Foundation Pre-Doctoral Fellowship and the NCI (R01-CA077373).

Chapter 1-Introduction to Topoisomerases and their Regulation in Cells

(Portions reproduced from: Vos, S.M., Tretter, E.M., Schmidt, B.H., and Berger, J.M. *Nature Reviews Molecular Cell Biology* (2011) **12**, 827-841)

The extended, double-helical structure of DNA poses a unique challenge to living organisms. Chromosomes must be folded and compacted in an orderly manner to fit within the confines of the cell. Natural nucleic-acid transactions such as transcription, replication, and repair – all of which require access to nucleotide sequence information – necessitate duplex melting events that overwind and underwind (or supercoil) (**Fig. 1.1A**) nucleic acid segments, interfering with appropriate gene expression. DNA repair and replication further generate entanglements between chromosomal regions that, if left unresolved, can lead to potentially mutagenic or cytotoxic DNA strand breaks.

Enzymes known as topoisomerases manage these transactions. Endowed with an ability to cut, shuffle, and religate DNA strands, topoisomerases can add or remove DNA supercoils, and disentangle snarled DNA segments. How topoisomerases carry out such complex functions has long been a significant question of both biochemical and biophysical interest. However, in recent years it has become evident that topoisomerases do not work at random; they can instead preferentially distinguish between different types of DNA juxtapositions and collaborate with disparate factors direct their action. It also has become clear that a rich and growing variety of natural and synthetic agents block topoisomerase function for the purposes of evolutionary competition or therapeutic gain.

Topoisomerase families

At first glance, a bewildering number of different topoisomerases exist. However, nature's topoisomerase collection is not as complicated as it first appears. For example, all topoisomerases contain a nucleophilic tyrosine, which they use to promote strand scission. This feature links DNA cleavage to the formation of a transient, covalent enzyme–DNA adduct, which in turn prevents the inadvertent release of nicked or broken DNA duplexes that might otherwise damage the chromosome. All topoisomerases also can be assigned into one of two primal classes, type I and type II, depending on whether they cleave one or two strands of DNA, respectively. Enzymes with an odd Roman numeral (for example, "I" or "V") after their name fall into the type I class, whereas those with an even-numbered Roman numeral after their name are type II. Topoisomerase subtypes – "A," "B," or "C" – are then used to distinguish between enzyme families that have significantly different amino acid sequence relationships and/or structures. Some topoisomerase subtypes further encompass multiple paralogs that have

diverged from one another in terms of their specific activities. A brief overview of these groupings follows to provide a context for subsequent discussion. For more extensive coverage of topoisomerase evolution, structure, and mechanism see (Forterre et al, 2007; Schoeffler & Berger, 2008).

Type IA: single-stranded 'strand-passage' enzymes.
Type IA topoisomerases have a toroidal protein structure that bears a superficial resemblance to a padlock (Lima et al, 1994). These enzymes effect topological changes in DNA through a "strand-passage" mechanism (Brown & Cozzarelli, 1981; Tse et al, 1980), in which a single DNA strand is cleaved and physically opened, and a second DNA is navigated through the gap; following passage of the second DNA, the broken DNA is resealed. Type IA topoisomerases comprise three distinct subfamilies that are found throughout all three cellular domains of life cellular (Woese *et al*, 1990; Forterre *et al*, 2007). These subfamilies are bacterial topo I (hereafter called topo IA), bacterial and eukaryotic topo III, and reverse gyrase (Forterre et al, 2007). The primary activity of topo IA is to relax negatively-supercoiled DNA (Hiasa et al, 1994; Wang, 1971). By contrast, topo III preferentially acts to resolve single-stranded DNA entanglements that can arise during DNA replication and repair (DiGate & Marians, 1988; Harmon et al, 1999; Hiasa et al, 1994; Lopez et al, 2005; Wallis et al, 1989). Reverse gyrase, found exclusively in thermophilic bacteria and archaea, positively supercoils DNA and renatures melted DNA strands through the action of an ATP-dependent superfamily-2 (SF-2) helicase domain fused to its type IA topoisomerase element(Kikuchi & Asai, 1984) (Hsieh & Plank, 2006).

Type IB: DNA "swivelases".
Type IB topoisomerases differ fundamentally in structure and mechanism from type IA enzymes (Redinbo et al, 1998) Rather than relying on strand passage, type IB topoisomerases effect supercoil relaxation by nicking a single strand of duplex DNA, and allowing one DNA end to rotate with respect to the other around the intact phosphodiester bond on the opposing strand (Koster et al, 2005). Rotation is controlled by friction between the DNA and the enzyme, which aids in aligning the broken ends for resealing (Champoux & Dulbecco, 1972; Koster et al, 2005). Type IB proteins preferentially bind positively- or negatively- supercoiled substrates rather than relaxed substrates (Frohlich et al, 2007; Madden et al, 1995) using an interaction surface outside of its primary active site to bridge distal DNA segments (Patel et al, 2010). Some variants show a proclivity for positively-supercoiled DNA, which they can relax at a faster rate (Frohlich et al, 2007).

The active site architecture of type IB topoisomerases is evolutionarily related to that of tyrosine recombinases and integrases (Cheng et al, 1998; Stewart et al, 1998). Type IB enzymes are ubiquitous among eukaryotes, with some scattered homologs extant in certain viruses and bacteria (Krogh & Shuman, 2002). Type IB topoisomerases appear to be represented by a single family member (topo IB), although architectural differences that influence the rate

and mechanism of supercoil relaxation are evident between various homologs in this group (Koster et al, 2005).

Type IC: a second class of swivelase.
Type IC topoisomerases thus far have been found only in the archaeal genus *Methanopyrus* (Forterre, 2006). Like topo IB, type IC topoisomerases relax positively- and negatively-supercoiled DNA through a nicking and rotation mechanism (Slesarev et al, 1993; Taneja et al, 2007). However, the type IC active site shows little structural similarity to that of type IB enzymes, and appears to have a different evolutionary lineage (Forterre, 2006; Taneja et al, 2006). Type IC enzymes also retain functional elements that exhibit apurinic site lysase activity, which they can use for repairing abasic lesions in DNA (Belova et al, 2001; Taneja et al, 2006). Only one topoisomerase variant, topo V, is presently known to comprise the type IC family (Slesarev et al, 1993).

Type IIA: duplex DNA 'strand-passage' enzymes.
As with their type IA counterparts, type IIA topoisomerases employ an active strand-passage mechanism for effecting topological changes in DNA. Type IA and IIA topoisomerases also share certain catalytic domains used for DNA cleavage (Aravind et al, 1998; Berger et al, 1998). However, type IIA enzymes differ in that they cleave both strands of a DNA duplex and pass a second intact duplex through the transient break (Brown & Cozzarelli, 1979; Liu et al, 1980; Mizuuchi et al, 1980) (**Fig 1.2**), and they use ATP to power strand passage (Brown & Cozzarelli, 1979; Gellert et al, 1976; Goto & Wang, 1982). These activities allow type IIA topoisomerases to resolve both positive and negative DNA supercoils, as well as disentangle long intertwined chromosomes and DNA catenanes (Hsieh & Brutlag, 1980; Mizuuchi et al, 1980). Type IIA topoisomerases are found throughout all cellular organisms, as well as in some viruses and organelles, and can be partitioned into three paralogous subfamilies – eukaryotic topo II, bacterial topo IV, and prokaryotic gyrase – that exhibit distinct functional properties (Forterre et al, 2007; Schoeffler & Berger, 2008). For instance, gyrase actively adds negative supercoils to DNA and is only weakly able to unlink catenanes (Gellert et al, 1976; Peng & Marians, 1993a; Zechiedrich & Cozzarelli, 1995), while topo IV (and certain topo II isoforms) is a robust decatenase that preferentially relaxes positively-supercoiled substrates over negatively-supercoiled ones (Crisona *et al*, 2000; McClendon *et al*, 2005; Woese *et al*, 1990; Charvin *et al*, 2003). Interestingly, type IIA topoisomerases show some ability to discriminate between, and preferentially act on, regions of high DNA curvature or DNA crossovers due to their ability to sharply bend DNA segments (Baxter et al, 2011; Dong & Berger, 2007; Laponogov et al, 2010; Vologodskii et al, 2001; Zechiedrich & Cozzarelli, 1995). By contrast, yeast and *Drosophila melanogaster* topo II do not show any preference for one type of supercoiled DNA over another (Charvin et al, 2003; Roca & Wang, 1996).

Type IIB: a second class of duplex DNA strand-passage enzyme.
Type IIB topoisomerases are found in archaea, plants, and a few bacterial, protist, and algal lineages (Bergerat et al, 1997; Malik et al, 2007). As with their type IIA cousins, type IIB topoisomerases unlink tangled DNA duplexes by strand passage and relax both negative and positive supercoils (Bergerat et al, 1994). Type IIB topoisomerases also possess ATPase and DNA-cleavage domains similar to those found in type IIA enzymes, although the relative arrangement of these elements in primary sequence space and their overall structural organization differs significantly (Bergerat et al, 1997; Bergerat et al, 1994; Corbett et al, 2007; Corbett & Berger, 2003; Nichols et al, 1999). The principal DNA binding subunit of type IIB topoisomerases is noteworthy in that it is evolutionarily related to Spo11, the factor responsible for creating double-stranded DNA breaks that initiate meiotic recombination (Bergerat et al, 1997; Keeney et al, 1997). Thus far, only one family member, topo VI, is known to comprise the type IIB topoisomerase clade (Bergerat et al, 1997).

Topoisomerase families – why so many?
Given this diversity of topoisomerases, and the seeming overlap in their basic function, how do cells decide which one to use for a particular purpose? This question has been difficult to address, in part because different organisms often possess markedly different topoisomerase repertoires (Forterre et al, 2007; Schoeffler & Berger, 2008). Moreover, the regulatory strategies for a given topoisomerase can vary widely among species. At present, there appears to be no single answer. Rather, the molecular logic behind topoisomerase choice appears to derive from a confluence of factors, including: the type of topological problem that needs to be addressed, which topoisomerase genes happen to be present in the resident genome, whether specific architectural elements have been acquired to modulate topoisomerase function, and if different accessory factors and/or modifications that alter topoisomerase localization and activity are in use (**Table 1.1**). Topoisomerases utilize a combination of these regulatory strategies in the majority of nucleic-acid transactions in which they participate. A discussion of the role of specific topoisomerases in different cellular processes follows.

DNA packaging
The length of chromosomal DNA far exceeds that of the cell in which it resides. Organisms thus employ a variety of mechanisms to assist with DNA compaction, including supercoiling and the use of chromosome organizing factors such as histones or nucleoid associated proteins (Luijsterburg et al, 2008). Plectonemic supercoiling alone has been estimated to condense DNA by two to three orders of magnitude (**Figure 1.1A**)(Boles et al, 1990).

In bacteria, a need for compaction has been invoked as one of the principal reasons why chromosomal DNA is negatively supercoiled, and why gyrase, which adds those supercoils to DNA, is so ubiquitous throughout the bacterial kingdom (Luijsterburg et al, 2008; Zechiedrich et al, 2000). More recent

studies, however, suggest that there are additional layers of complexity to this view. For example, two very closely related bacterial species, *E. coli* and *S. typhimurium*, share about 90% sequence identity across homologous genes (McClelland et al, 2001), but have highly-dissimilar superhelical densities, with *E. coli* DNA being significantly more underwound (Champion & Higgins, 2007). Gyrase itself is not always necessary for DNA packaging, as the lone type IIA topoisomerase present in the hyperthermophilic bacterium *Aquifex aeolicus* is not a gyrase, as might be predicted on the basis of its sequence similarity with other gyrase N-terminal domains, but rather a topo IV (Tretter et al, 2010). However, many thermophiles also possess reverse gyrase (Brochier-Armanet & Forterre, 2007), which introduces positive supercoils that may aid compaction, as well as counteract thermal denaturation (Forterre et al, 1985; Perugino et al, 2009). Although the steady-state superhelical density of DNA in most prokaryotes has not been measured directly, multiple findings suggest that many species, particularly those that are adapted to growth at high temperatures, may have relatively relaxed chromosomes (Charbonnier & Forterre, 1994). How such organisms are able to sufficiently compact their chromosomes in the absence of supercoiling remains an open question, but the mechanism almost certainly relies on proteinaceous factors. Overall, the role of supercoiling in DNA compaction, and how topoisomerases collaborate to define the superhelical "setpoint" of the chromosome, is not fully understood.

Topoisomerases play another role in chromosome compaction by working with large condensation machineries (**Table 1.1**), principally a group of ATP binding cassette (ABC)-family ATPases known as Structural Maintenance of Chromosomes (SMC) proteins (Bhat et al, 1996; Hayama & Marians, 2010; Li et al, 2010b; Maeshima & Laemmli, 2003; Tadesse et al, 2005). SMCs, and their counterparts Rad50 (eukaryotes) and SbcC and RecF (*E. coli)*, are conserved factors involved in multiple aspects of chromosome cohesion, condensation, and DNA repair (Hirano, 2006). SMCs and type IIA topoisomerases indirectly co-localize as part of the protein network that helps stabilize long-range contacts between chromosomal segments (Bhalla et al, 2002; Maeshima & Laemmli, 2003). SMCs, or their affiliated accessory factors, also have been reported to directly associate with both topo II and topo IV. For example, the *Drosophila melanogaster* Barren subunit (an ortholog of the condensin H protein) co-immunoprecipiates with topo II *in vitro* (Bhat et al, 1996), while a dimerization region of the *E. coli* SMC homolog MukB interacts with the C-terminal domain of the ParC subunit of topo IV (Hayama & Marians, 2010; Li et al, 2010b). Interestingly, both interactions appear to potentiate the relaxation of negatively-supercoiled DNA by the associated topoisomerase, although how stimulation is achieved is unresolved. At present, little is known about the effect and role of these interactions on global DNA superstructure or about their utility to the cell, although the MukB–ParC interaction is important for cell viability (Li et al, 2010b). Whether these associations are preserved in other species is not clear, and constitutes a clear avenue for additional investigation.

Replication and chromosome segregation

Topoisomerases are required both for the successful management of DNA replication, and for specific developmental strategies that depend on replication. In the latter instance, the type IIB topoisomerase found in plants (topo VI) is required for a particular form of replication known as endoreduplication, a process by which chromosomes are copied multiple times in the absence of cell division (Breuer et al, 2007; Hartung et al, 2002; Sugimoto-Shirasu et al, 2002; Yin et al, 2002). Endoreduplication gives rise to polyploid nuclei, which in turn can be used to regulate cell size (Lee et al, 2009). Why topo VI is needed specifically for endoreduplication, and why topo II cannot rescue a topo VI deficiency, is not clear (Sugimoto-Shirasu et al, 2005). Similarly, replication of vertebrate mitochondrial DNA requires a special mitochondrial type IB topoisomerase, top1mt, a paralog of the nuclear type IB topoisomerase, top1 (Rosa et al, 2009; Zhang & Pommier, 2008). Mitochondrial DNA replication requires top1mt to form its regulatory displacement (D)-loop (Zhang & Pommier, 2008), which in turn is thought to regulate DNA replication initiation and transcription (Zhang & Pommier, 2008). Surprisingly, when nuclear top1 is localized to the mitochondria, it cannot complement top1mt function and arrests the cell cycle (Rosa et al, 2009). At present, it remains to be seen whether similar topoisomerase-dependent roles exist in other organisms. The role of topoisomerases in conventional DNA replication is better understood, with recent studies uncovering specific roles for topoisomerases in each of the three major replicative phases: initiation, fork progression, and termination.

Topoisomerases in replication initiation

In *E. coli*, replication initiation is dependent on local supercoiling at a lone origin *oriC*, that is regulated by the opposing activities of topo I and gyrase (Hiasa & Marians, 1994; Kaguni & Kornberg, 1984). During DNA replication initiation in eukaryotes, topoisomerases have been seen to associate directly with certain origins to aid in activation. For example, human topo IB and topo IIα co-localize with both the lamin B2 origin (an early firing, widely studied replication start site found on human chromosome 19) and the Orc2 subunit of the origin recognition complex, while inhibition of topo IB interferes directly with origin firing (Abdurashidova et al, 2007) (**Table 1.1**). Formation of replication initiation complexes at the human Ors8 origin, (a late firing origin), as well as the lamin B2 origin, also have been reported to require DNA cleavage by topo IIβ – a topoisomerase associated with repair and development (Ju et al, 2006; Lyu et al, 2006; Yang et al, 2000) – and the association of DNA repair proteins such as Ku70/80 and poly (adenosine diphosphate-ribose) polymerase-1 (PARP1) (Rampakakis & Zannis-Hadjopoulos, 2009). Why topoisomerases are needed during these early stages of eukaryotic replication is not well understood, but they may be involved in the control of torsional stress or DNA deformations that could be used either to help clear DNA regions for replisome assembly, or to promote DNA unwinding in the early stages of replisome assembly.

Topoisomerases in replication fork progression

During strand synthesis, topoisomerases are required to relieve positive supercoiling that arises from DNA unwinding by replicative helicases (**Fig 1.1B**). In bacteria, this role is typically fulfilled by DNA gyrase and/or topo IV (Hiasa & Marians, 1996b; Khodursky et al, 2000; Wang et al, 2011; Zechiedrich & Cozzarelli, 1995). By contrast, eukaryotes rely primarily on topo IB for positive supercoil relaxation, although topo II can assist or even substitute for topo IB in this capacity (Brill et al, 1987; Kegel et al, 2011; Kim & Wang, 1989; Yang et al, 1987). Some type II topoisomerases (for example, topo IV and human topo IIα) are markedly more adept at removing positive supercoils than negative ones (Baxter et al, 2011; Crisona et al, 2000; McClendon et al, 2005), suggesting that cells may be under evolutionary pressure to acquire particularly robust relaxases that can accommodate rapidly moving replication forks.

A second consequence of a progressing fork is the formation of daughter duplex intertwinings (termed precatenanes in circular chromosomes) behind it (**Fig. 1.1B**). Such structures are produced as a natural byproduct of replicating the double helix of the mother chromosome and, if left unchecked, give rise to tangled or catenated DNAs that can lead to abnormal DNA segregation upon entry into cell division (Baxter & Diffley, 2008a; Champoux & Been, 1980; Holm et al, 1985; Peter et al, 1998; Uemura & Yanagida, 1984). The duplex strand-passage activity of type II topoisomerases plays a key role in resolving these topological linkages.

As two forks converge, the unreplicated region between them represents a topological linkage, known as a hemicatenane, which must be resolved before chromosome segregation can occur. If the two strands of the hemicatenane can be fully replicated prior to resolution, the resulting duplex DNA segments become a natural substrate for type II topoisomerases. Consistent with a need for these enzymes in resolving inter-chromosome crossovers, the removal or inactivation of topo II or topo IV can lead to hyper-catenated DNAs and the production of broken chromosomes during cell division (Adams et al, 1992; Baxter & Diffley, 2008a; DiNardo et al, 1984; Holm et al, 1989; Uemura et al, 1987; Uemura & Tanagida, 1986).

However, there also is mounting evidence that type IA topoisomerases, particularly topo III, can participate directly in hemicatenane resolution before forks converge. For example, in bacteria, topo IV temperature-sensitive alleles can be rescued by overexpression of topo III (Nurse et al, 2003). Topo III, which decatenates single-stranded DNA *in vitro*, has been shown to collaborate with RecQ-family helicases in disentangling hemicatenated structures (**Table 1.1**); in this partnership, the helicase may help generate single-stranded DNA to aid topo III function. The connection between these two enzyme classes is sufficiently entwined that they frequently form stable or co-localized complexes, along with auxiliary single-stranded DNA binding proteins such as SSB (in bacteria), or replication protein A (RPA)-like factors (Rmi1 in eukaryotes and Rmi2 in metazoans) (Chang et al, 2005; Harmon et al, 1999; Suski & Marians, 2008; Xu

et al, 2008). Consistent with the collaboration between these proteins as part of a functional "resolvosome", ablation of the RecQ-partner of topo III in eukaryotes, the BLM helicase, leads to the enhanced formation of ultrafine DNA tangles, termed "microbridges," between condensed chromosomes (Chan et al, 2007). The natural fusion of a RecQ-like (SF-2**)** helicase domain with a type IA topoisomerase module in reverse gyrase – which likewise can resolve hemicatenanes (Confalonieri et al, 1993; Déclais et al, 2000; Hsieh & Plank, 2006) – further highlights the frequent need for paired, RecQ-family helicase–topoisomerase activities in the cell.

Topoisomerases in replication termination

With respect to replication termination, topoisomerases have been found to play a role in at least two instances. In bacteria, the completion of DNA synthesis can be assisted by chromosomally-encoded termination regions (*Ter*s), which bind dedicated factors that help arrest replicative helicases. In *E. coli*, the absence of topo IA diminishes the ability of the bacterium's cognate termination factor (Tus) to block progression of the replicative DnaB helicase (Valjavec-Gratian et al, 2005). This effect may arise as a consequence of the increased levels of negative supercoiling left by topo IA's absence, which can stimulate DNA unwinding by the replicative helicase, DnaB, and may also serve to reduce the duration of the Tus–DnaB interaction. In yeast, topo II appears to facilitate fork progression at termination elements by localizing to such sites and working with the Rrm3 helicase to resolve the torsional stress arising from converging forks (Fachinetti et al, 2010). This controlled pausing at termination elements ensures complete replication and counteracts abnormal genome rearrangements and breaks arising from fork convergence at replication termination (**Table 1.1**). Whether there exist other, more specific connections between topoisomerases and replication termination remains to be determined.

Topoisomerases in chromosome segregation

Once replication is complete, daughter chromosomes must be pulled apart and separated from each other. Topoisomerases promote these events by facilitating DNA compaction and disentangling (as described above) and by working directly with chromosome partitioning machineries and/or cytoskeletal elements. For instance, many bacteria use a dedicated motor protein, FtsK or SpoIIIE, to move newly replicated chromosomes into different cellular locales to aid segregation (Crozat & Grainge, 2010). In *E. coli*, topo IV physically associates with, and is stimulated by, FtsK, possibly as a means to both counteract the supercoils created by the translocating motor and to help unlink tangled DNA regions (Bigot & Marians, 2010; Espeli et al, 2003a) (**Table 1.1**). Although no eukaryotic topoisomerase has been reported to bind to cytoskeletal elements, topo II does associate with factors responsible for centromere formation and chromosome segregation, including the aurora B kinase and the polo-like kinase (Plk)-1 (Coelho et al, 2008; Li et al, 2008) (**Table 1.1**). The biological rationale for these interactions is not fully understood; however, the colocalization of topo II with

aurora B and Plk-1 may be important for centromere resolution between sister chromatids. Additional links between topoisomerases and chromosome segregation appear likely to exist, but have yet to be discovered.

What attracts a given topoisomerase to a particular point in the replicative process? As the aforementioned examples highlight, this control can be achieved not only by the types of DNA intermediates that derive from a particular process (for example, hemicatenanes, pre-catenanes and supercoils), but also by topoisomerase-associated partner proteins. Other intriguing interactions have been implicated in topoisomerase function during replication. For example, topo IV can associate with both the polymerase processivity clamp-loader assembly, which may localize the enzyme to *oriC* to decatenate newly synthesized chromosomes (Espeli et al, 2003b), and the SeqA factor, a protein that prevents replication reinitiation by sequestering hemimethylated DNA within *oriC,* and that stimulates topo IV decatenation and supercoil relaxation activity (Kang et al, 2003) (**Table 1.1**). These connections further highlight cellular needs for particular topoisomerase activities during elongation and initiation, respectively.

Transcription and gene regulation

As with replication, transcription induces changes in DNA topology. A moving RNA polymerase produces localized positive supercoiling ahead of the transcription bubble and negative supercoiling in its wake (Liu & Wang, 1987; Wu et al, 1988) (**Fig. 1.1C**). Left unchecked, these supercoiling alterations can lead to significant changes in gene expression (Blot et al, 2006). Underwound DNA also has a higher propensity to form stable RNA–DNA hybrids (R-loops) than relaxed duplexes (Drolet et al, 1994). Such structures can block cell growth and may contribute to genomic instability by stalling replication forks and promoting DNA breaks at highly transcribed genes (Drolet et al, 1995; Tuduri et al, 2009).

Both type IA and type IB topoisomerases have been implicated in the removal of negative supercoils and the resulting suppression of R-loop formation (Massé & Drolet, 1999; Tuduri et al, 2009). Indeed, the *E. coli* topo IA C-terminus interacts directly with RNA polymerase, and this interaction may help recruit the topoisomerase to negative supercoils (Cheng et al, 2003; Zechiedrich et al, 2000). Type IB and type II topoisomerases further help relax positive supercoils in front of transcribing polymerases, with topo IB playing a more significant role in eukaryotic transcription and topo IV and gyrase handling these substrates in bacteria (Durand-Dubief et al, 2010; Merino et al, 1993; Mondal et al, 2003; Zechiedrich & Cozzarelli, 1995; Zechiedrich et al, 2000).

Topoisomerases have been linked to specific transcriptionally-related events, such as the activation or repression of particular promoters or nucleosome remodeling. For example, inactivation of topo IB in *S. cerevisiae* leads to histone-specific acetylation and methylation events that increase the transcription of telomere-proximal genes (Lotito et al, 2008). In *S. pombe*, there is evidence that the presence or absence of topo IB activity can influence nucleosome disassembly and assembly, respectively, at certain promoter regions (Durand-Dubief et al, 2010). Eukaryotic topo IB has been implicated in the control

of gene expression through an associated kinase activity, which is reported to phosphorylate splicing factors such as SR (serine/arginine-rich) proteins(Rossi et al, 1996), regulating splicing factor localization and enhancing their activity(Juge et al, 2010; Malanga et al, 2008); topo IB-mediated phosphorylation of SR proteins in turn can be negatively regulated by the presence of poly(ADP-ribose) (Malanga et al, 2008) (**Table 1.1**).

Remarkably, the transient, site-specific cleavage of DNA by human topo IIβ has been reported to be required to activate the transcription of genes regulated by certain nuclear receptors, a process that requires the activity of PARP and Ku80/Ku70, as well as DNA repair proteins such as DNA-PK (DNA-dependent protein kinase) (Ju et al, 2006; Lyu et al, 2006). DNA cleavage and the subsequent recruitment of PARP and associated repair proteins appears necessary to exchange histone-1 for the high mobility group (HMG)B-1/2 factor, and to stimulate transcription (Ju et al, 2006). Similarly, Topo IIβ associates with the promoter region of genes in human acute promyelocytic leukemia cell lines that are regulated by retinoic acid receptor elements, initially stimulating transcription; sustained transcriptional activation then leads to decreased transcript levels and the inhibition of granulocytic differentiation in a topo IIβ-dependent manner (Mcnamara et al, 2008).

Some of these findings, such as those suggesting that topo IB might directly phosphorylate target proteins, or that cells might rely on a potentially mutagenic topo IIβ-meditated DNA-cleavage event to control gene expression, raise as many questions as they answer. Nonetheless, even though it can be difficult to definitively determine whether the effects of topoisomerases on promoter function and structure are direct or indirect, it seems that these enzymes can influence transcriptional events in a manner that may not depend solely on their ability to control supercoiling. This complex area of investigation is likely to yield many more surprises.

Recombination and repair

Yet another area where topoisomerases play a critical role is in forming and managing double-stranded DNA (dsDNA) breaks. As noted earlier, DNA cleavage by at least one topoisomerase, topo IIβ, has been implicated in the control of promoter activity (Ju et al, 2006; Lyu et al, 2006; Mcnamara et al, 2008). However, double-stranded DNA-break formation through a variety of topoisomerases and topoisomerase-like proteins also impacts processes such as meiotic recombination, cell cycle checkpoint activation, and DNA repair. For instance, during meiotic recombination, the type IIB topoisomerase A-subunit homolog, Spo11, creates double-strand breaks that allow chromosomes to exchange segments through homologous recombination (Bergerat et al, 1997; Keeney et al, 1997; Peciña et al, 2002). Although there is no evidence presently linking Spo11 to a *bona fide* topoisomerase activity (in the sense that it would be capable of DNA strand passage) (Keeney, 2008), its DNA-cleavage activity during meiosis is clearly controlled, as only a fraction of the total Spo11 pool bound to chromosomal loci is used to form DNA breaks and recombinogenic

sites (Neale et al, 2005). Eukaryotes (with the exception of plants) do not appear to possess any clear homologs of the ATP-binding B-subunit of topo VI, and how Spo11 is activated is unknown at present (Keeney, 2008).

The creation of nicks and double-strand DNA breaks are potentially deleterious events for the cell. Hence, DNA cleavage by topoisomerases or topoisomerase-like factors has the capacity to elicit DNA damage responses. For example, following DNA-breakage by Spo11, the protein remains covalently attached to the DNA and must be removed (Neale et al, 2005). The removal of Spo11 and downstream DNA-end processing events appear to be carried out by double-strand break repair proteins such as the Rad50–Mre11–Nbs1 (MRN) complex (Keeney, 2008; Neale et al, 2005), Rad51 and Dmc1-like factors (Baudat et al, 2000; Li & Ma, 2006), and the nuclease Sae2/CtIP (Hartsuiker et al, 2009). Meiotic recombination elicits a p53 damage response, which appears to be independent of the ATM and ATR (ataxia telangiectasia mutated and ATM Rad3-related) kinases and their associated repair pathways (Lu et al, 2010). Similar responses are seen when topoisomerases become inactivated (Baxter & Diffley, 2008a), or are aberrantly linked to DNA through the action of DNA lesions or small-molecule inhibitors that promote the formation of topoisomerase-DNA cleavage complexes. However, additional systems also can be activated in these instances (for example, the ATM and ATR pathways, and BRCA1 or BRCA2 proteins (Cliby, 2002; Treszezamsky et al, 2007)) that induce cell cycle arrest and DNA repair. When topoisomerases become inadvertently trapped in a covalent complex with DNA, they further can be targeted for destruction by SUMOylation- and ubiquitinylation-mediated mechanisms, and the covalent tyrosine-DNA adducts can be repaired by enzymes such as Tdp1 and Tdp2 (Cortes Ledesma et al, 2009; Desai et al, 1997; Lin et al, 2009; Mao et al, 2000a; Mao et al, 2001; Mao et al, 2000b; Nitiss et al, 2006; Pouliot et al, 1999; Treszezamsky et al, 2007; Zeng et al) (**Table 1.1**). Some of these latter events may be promoted by collision encounters with proteins such as RNA polymerase(Desai et al, 2003; Sordet et al, 2008; Xiao et al, 2003).

Other evidence also exists linking topoisomerase activity to mutagenesis. For instance, highly transcribed genes in eukaryotes are sometimes associated with enhanced levels of genetic instability and spontaneous mutation (Datta & Jinks-Robertson, 1995). Several recent studies have found that 2-3 nucleotide deletions commonly observed in these regions are the result of topo IB activity (Lippert et al, 2011; Takahashi et al, 2011). The mechanism behind these alterations has not been fully elucidated; topo IB may generate lesions by binding and cleaving within and adjacent to tandem dinucleotide repeats, forming a stable covalent DNA link that is then processed in part by endonucleases such as Mus81 and Rad1 (Lippert et al, 2011; Takahashi et al, 2011). Alternatively, topo IB may cleave at the scissile phosphate of a misincorporated ribonucleotide within or adjacent to the tandem dinucleotide repeats. The misincorporated ribonucleotide would then undergo an internal 2'-3' cyclization event to release the enzyme and leave a small nick or gap in the DNA (Kim et al, 2011), giving

rise to microdeletions from DNA misalignments during repair. In this regard, it is interesting to note that type II and type IB topoisomerases form stable adducts at sites of ribonucleotide incorporation in DNA (Wang et al, 1999), as well as at DNA lesions such as nicks (Deweese & Osheroff, 2009) and abasic sites (Sayer et al, 2004) (Kingma & Osheroff, 1997a; Kingma & Osheroff, 1997b). Thus, both classes of enzymes may contribute to a steady-state background of damage events with mutagenic potential.

Topoisomerases further play an important role during and after the repair of damaged DNA strands. This is particularly true during homologous recombination (HR), which generates interlinked intermediates that bear some similarities to those occurring during replication fork convergence. Recent work has found ample evidence for the participation of topo III in HR where, as with hemicatenane resolution during replication, it breaks up double-Holliday junctions in concert with both a RecQ-type helicase (Sgs1 in yeast (Ira et al, 2003), BLM in metazoans (Plank et al, 2006; Wu & Hickson, 2003)) and single-stranded DNA binding proteins such as SSB(Harmon et al, 2003) , Rmi1 (Chang et al, 2005) and Rmi2 (Singh et al, 2008; Xu et al, 2008) (**Table 1.1**). Notably, the cooperative activity of this resolvosome allows HR to proceed without the generation of crossover products that exchange large chromosomal segments, which occurs when branch-endonucleases resolve double-Holliday junctions, and may therefore constitute the dominant means for resolving Holliday junctions in mitotic cells (Chang et al, 2005; Plank et al, 2006; Wu & Hickson, 2003). Topo III also may help recruit other HR proteins to broken DNA ends. For example, Sgs1, Dna2, and RPA derived from budding yeast can resect DSBs in a topo III-independent manner *in vitro*; however, topo III stimulates Sgs1 helicase activity and is probably required at physiological concentrations to recruit Sgs1 to broken DNA ends (Cejka et al, 2010; Niu et al, 2010). How disparate topoisomerase, helicase, and SSB protein activities collaborate to disentangle hemicatenated substrates is not known; studies of reverse gyrase may provide some mechanistic insights into this problem, since reverse gyrase is composed of an Sgs1-like (SF-2) helicase domain fused to a type IA topoisomerase element (Confalonieri et al, 1993; Déclais et al, 2000).

PTM of eukaryotic topoisomerases

Eukaryotic topoisomerases are subject to a number of post-translational modifications (PTMs) that can alter their localization and activities at various stages in the cell cycle. These modifications may also influence the types of DNA structures on which topoisomerases preferentially act. Thus far, four types of topoisomerase PTM have been observed: phosphorylation (Wells et al, 1994), acetylation (Choudhary et al, 2009), SUMOylation (Mao et al, 2000a; Mao et al, 2000b), and ubiquitinylation(Mao et al, 2001).

The modification of poisoned topoisomerases trapped on DNA by SUMOylation and ubiquitinylation, in response to DNA damage, appears to target these enzymes for processing and/or degradation (Desai et al, 1997; Desai et al, 2003; Mao et al, 2000a; Mao et al, 2001; Mao et al, 2000b; Sordet et al, 2008;

Xiao et al, 2003). However, apart from this function, the physiological role of topoisomerase PTMs has been somewhat controversial. Indeed, it is not uncommon to find studies that link the same type of modification to the regulation of different protein–protein partnering events, the activation or repression of specific topoisomerase activities, and/or proper and improper topoisomerase localization, sometimes in a mutually-exclusive manner. An example of this complexity is the role of SUMOylation in the temporal activation and localization of topo IIα through two E3 ligases RanBP2 and protein-inhibitor-of-activated-STAT-1 γ (PIASγ). In *Xenopus laevis,* PIASγ has been linked to the SUMOylation of topo IIα, a modification that appears to reduce topo IIα's ability to decatenate DNA *in vitro* (Ryu et al, 2010). By contrast, PIASγ is reported to have no effect on topo IIα in mouse embryonic fibroblasts; instead, these cells appear to SUMOylate topo IIα through RanBP2, which enhances topo IIα localization and activation at centromeres during sister chromosome resolution in anaphase (Bachant et al, 2002; Dawlaty et al, 2008). The role of phosphorylation has been similarly difficult to tease apart, with studies variously reporting that this modification can potentiate, depress, or exert no effect on topoisomerase function (Kimura et al, 1996; Li et al, 2008; Plo et al, 2002; Shapiro et al, 1999a). Nonetheless, some of these differences are almost certainly due to the particular site on the topoisomerase that is being modified. The regulation of eukaryotic topoisomerases through PTMs is a highly-interesting, but still relatively murky, area of research that undoubtedly holds significant surprises.

Topoisomerase inhibition

Although indispensible for cell viability, it is clear that topoisomerases also present a fundamental peril: they can be inadvertently inactivated, or their DNA cleavage activity can be corrupted, resulting in cytotoxic or mutagenic DNA breaks, which leads to cell death. The evolution of general repair systems, as well as more specific ones such as the tyrosyl-DNA phosphodiesterases (Tdps) (Cortes Ledesma et al, 2009; Nitiss et al, 2006; Pouliot et al, 1999; Zeng et al), help cells to deal with these problems. However, nature and humans also have been able to exploit topoisomerase inactivity and stalling through diverse means to deliberately kill cells, at times for tangible therapeutic benefit.

A number of proteins and protein-like factors have been found that specifically inhibit topoisomerase activity, particularly in bacteria (**Table 1.1**). These proteins range from toxins that control plasmid stability (CcdB) (Bernard & Couturier, 1992; Smith & Maxwell, 2006) to agents that are involved in microbial competition (microcin B17) (Vizán et al, 1991) and antibiotic resistance (Qnr and MfpA) (Hegde et al, 2005). Such factors have varied modes of action that include attenuating the DNA binding activity of topoisomerases, or promoting their ability to cleave DNA. In considering protein-based anti-topoisomerase factors, it is interesting to note that their identification has come not through directed screens, but from basic research and serendipity. The continual discovery of new proteinaceous inhibitors points to the utility – and potentially relative ease – by

which topoisomerase activity can be subverted, and strongly suggests that more anti-topoisomerase systems remain to be discovered.

On the biomedical side, topoisomerase inhibition has proven to be a highly versatile and useful approach for therapeutic intervention. Small-molecule agents targeting topoisomerases fall into two broad classes based on their mode of action: “inhibitors,” which attenuate enzyme activity, and “poisons”, which stabilize DNA-cleavage complexes (see **Fig. 1.3** for a partial list of type II topoisomerase antagonists and their modes of action). Although many of the most significant therapeutics (for example, epipodophyllotoxins, quinolones, and camptothecins) have been used for decades, only relatively recently have their mechanisms of action been understood in molecular detail. For instance, camptothecin, and its derivatives such as Topotecan, poison topo IB by intercalating between cleaved DNA ends in the enzyme active site (Staker et al, 2002), impeding DNA religation and the relaxation of supercoils. Fluoroquinolones, which are used primarily as antibiotics that target gyrase and topo IV, as well as topo II poisons such as etoposide, act in a similar manner, binding between the 5’ and 3’ end of a broken DNA strand to prevent resealing and release (Laponogov et al, 2010). Other compounds that act in a very different manner, blocking either ATPase activity (for example, novo- and cholorobiocins (Lewis et al, 1996; Tsai et al, 1997), bisdioxopiperazines (Classen et al, 2003), and radicicol (Corbett & Berger, 2006)), DNA binding (simocyclinone D8) (Edwards et al, 2009), or DNA cleavage (NTBI GSK299423)(Bax et al, 2010). These compounds have been imaged in the presence of their respective targets, yielding insights into their function. Together, these findings have not only highlighted the molecular determinants that enable drug binding and explained their inhibitory effects, but further demonstrated that there are a rich abundance of molecular scaffolds capable of inhibiting topoisomerases. At present, no small-molecule agent is known to target type IA topoisomerases, although biochemical studies have suggested that such compounds likely would be cytotoxic (Cheng et al, 2009). A hopeful, but presently unrealized, goal for these combined efforts is to point the way toward design of new inhibitors that show improved patient tolerance and that can circumvent emerging problems with drug-resistance.

Concluding remarks

Topoisomerases are complex molecular machines that modulate DNA topology to maintain chromosome superstructure and integrity. Although capable of stand-alone activity *in vitro*, topoisomerases frequently are linked to larger pathways and systems that resolve specific DNA superstructures and intermediates arising from cellular processes such as DNA repair, transcription, replication, and chromosome compaction. Topoisomerase activity is indispensible to cells, but requires the transient breakage of DNA strands. This property has been exploited, often for significant clinical benefit, by various exogenous agents that interfere with cell proliferation. Despite decades of study, surprising findings involving topoisomerases continue to emerge with respect to their cellular function, regulation, and utility as therapeutic targets.

Table 1.1: A partial list of the topoisomerase interactome

TOPOISOMERASE	PROTEIN PARTNER	SUGGESTED CELLULAR ROLE FOR INTERACTION	SYSTEM(S) OBSERVED	REFERENCE (S)
COMPACTION				
Topo IV, Topo II	SMCs and MukB	Potential role in chromosome compaction and segregation	*E. coli, Drosophila*	(Bhat et al, 1996; Hayama et al, 2013; Hayama & Marians, 2010; Li et al, 2010b)
DNA REPLICATION AND CHROMOSOME SEGREGATION				
Topo IV, Topo IIα	Clamp loader assembly, PCNA	Localizes ParC subunit to replication factory, localizes Topo IIα to origin of replication	*E. coli,* Avian DT40 cell line	(Espeli et al, 2003b; Niimi et al, 2001)
Topo II	Rrm3	Assists in permitting replication fork passage and replication termination at genomic pausing elements in eukaryotes	Yeast	(Fachinetti et al, 2010)
Topo IV	SeqA	Stimulates Topo IV relaxation and decatenation activity through direct interaction	*E. coli*	(Joshi et al, 2013; Kang et al, 2003)
Topo IV	Ftsk	Promotes chromosome segregation in bacteria	*E. coli*, *Caulobacter crescentus*	(Espeli et al, 2003a; Wang et al, 2006b)
Topo IIα	RanBP2	Induces sumoylation of topo IIα to influence its localization and activity	Mice	(Dawlaty et al, 2008)
Topo IIα	PIASγ	Catalyzes sumoylation of topo IIα to negatively regulate its activity	*Xenopus*	(Ryu et al, 2010)
Topo IIα	Polo-like kinase (PLK)	Activates Topo IIα for chromosome decatenation	Human cell lines	(Li et al, 2008)
Topo II	Aurora B Kinase	May promote centromere resolution	*Drosophila*, Human HeLa cell line	(Coelho et al, 2008)
Topo IIα/ Topo II	HMGB1/ HMO1	Chaperone topoisomerase to specific DNA structures	*S. cerevisiae*, human proteins *in vitro*	(Stros et al, 2007)
Gyrase	MarR	Sequester the MarR repressor of the *marRAB* operon	*E. coli*	(Domain & Levy, 2010)

TopoII α/β	HDAC 1/HDAC2	May localize to specific chromosomal regions or influence activity of the enzyme; it was recently reported that Topo IIβ is acetylated(Choudhary et al, 2009)	Human	(Tsai et al, 2000)
Topo IB	SR proteins	Topo IB dependent phosphorylation of SR protein RS domain	Human	(Kowalska-Loth et al, 2005; Labourier et al, 1998; Rossi et al, 1996)
Topo IB	Hrp	Chromatin remodeling	*S. pombe*	(Durand-Dubief et al, 2010)
Topo II	CHRAC	Chromatin remodeling	*Drosophila*	(Varga-Weisz et al, 1997)
Topo IIα/ Topo II	Sgs1/BLM/ RECQL5	Stimulates decatentation activity and may be important for proper cell cycle progression.	*S. cerevisiae*, Human cell lines	(Kennedy et al, 2013; Ramamoorthy et al, 2011; Russell et al, 2011; Watt et al, 1995)
Topo IIα	BAF complex	Chromatin remodeling complex that may stimulate Topo IIα to resolve catenanes	Human and mouse cell lines	(Dykhuizen et al, 2013)

TRANSCRIPTION

Topo IIβ	PARP	Promotes steroid receptor mediated transcription initiation	APL human cells, MCF cells	(Ju et al, 2006; Mcnamara et al, 2008)
Topo IIβ	RARα	Promotes the negative transcriptional regulation of retinoic acid regulated genes	PML human cell lines	(Mcnamara et al, 2008)
Topo IA	RNA polymerase	Physical interaction with the C-terminus of topo IA may stimulate Topo IA or localize it to supercoils produced by the RNA polymerase	*E. coli*	(Cheng et al, 2003)
Topo IIIβ	FMRP	Promote expression of mRNAs required for neurodevlopment	Human cell line	(Xu et al, 2013)
Topo IB	SR proteins	Leads to Topo IB dependent phosphorylation of SR proteins RS domain	*Drosophila*	(Juge et al, 2010)
Topo IIα	RRN3	Interacts with RNA polymerase I transcription factor RRN3 to potentially assist in pre-initiation complex formation	Human cell lines	(Ray et al, 2013)

POSTRANANSLATIONAL MODIFICATIONS

Topo II	Pkc1	Possible role in thermal regulation pathway	*S. cerevisiae*	(Mouchel & Jenkins, 2006)
Topo II	Siz1/Siz2	Mediate Smt3 sumoylation of topo II to localize topo II to pericentric chromosome regions	*S. cerevisiae*	(Takahashi, 2005)

RECOMBINATION AND REPAIR

Topo III	RecQ helicases such as BLM, Sgs1, and RecQ	Assists in homologous recombination to resolve Holliday junctions and hemicatenanes resulting during DNA replication	Yeast, PML human cell line, *E. coli*	(Gangloff et al, 1994; Harmon et al, 1999; Hu et al, 2001; Kennedy et al, 2013)
Topo III	SSB,RPA,Rmi1 and Rmi2	Stabilize RecQ helicase/topo III complex	HeLa human cell line, avian DT40 cell line, *E. coli*, yeast	(Chang et al, 2005; Suski & Marians, 2008; Xu et al, 2008)
Topo IB, Topo II α/β	Ubc9, SUMO-1	SUMO conjugation in response to topoisomerase mediated DNA-damage	Human	(Mao et al, 2000a; Mao et al, 2000b)
Topo IB, Topo II	Tdp1 and Tdp2	Phosphodiesterases that remove topos covalently attached to DNA ends	*S. cerevisiae*, human cell extracts, avian DT40 cell line	(Cortes Ledesma et al, 2009; Nitiss et al, 2006; Pouliot et al, 1999; Zeng et al)

PROTEINACEOUS INHIBITORS

Gyrase	CcdB	F plasmid derived poison of gyrase that promotes F plasmid maintenance by killing cells that do not possess the CcdB inhibitor CcdA	*E. coli*	(Bernard & Couturier, 1992)
Gyrase and Topo IV	Qnr, Mfpa, and Albicidin	Qnr and Mfpa are structurally reminiscent of DNA and inhibit quinolone binding by gyrase/topo IV	*E. coli*, *M. tuberculosis, Xanthomonas albilineans*	(Hashimi et al, 2007; Hegde et al, 2005; Tran et al, 2005)
Gyrase	Microcin B17	Peptide poison of gyrase	*E. coli*	(Vizán et al, 1991)
Gyrase	MurI (Glutamate racemase)	Negatively regulates gyrase function	*E. coli*, *M. smegmatis*, *M. tuberculosis*	(Ashiuchi et al, 2003; Sengupta & Nagaraja, 2008a; Sengupta et al, 2006)
Gyrase	LdACT	Leishmania actin inhibits *E. coli* gyrase decatenation function through physical interaction	*In vitro* assays	(Kapoor et al, 2010)
Gyrase	YacG	Endogenous inhibitor of GyrB in *E. coli*	*E. coli*	(Sengupta & Nagaraja, 2008b)

OTHER INTERACTIONS

Topo IIα	14-3-3-e	Modulates topo IIα interaction with drugs and DNA	HeLa cell line	(Kurz et al, 2000)
Topo IV Gyrase	YejK	Nucleoid associated protein. Inhibits gyrase DNA supercoiling and relaxation activity. Stimulates topo IV relaxation activity.	*E. coli*	(Lee & Marians, 2013)
Gyrase	TrxA/ TrxC	Negatively and positively affect gyrase supercoiling activity; potential way to link cell redox state to gene expression profile.	*R. capsulatus, R. sphaeroides, E. coli in vivo* and *in vitro* assays	(Li et al, 2004)

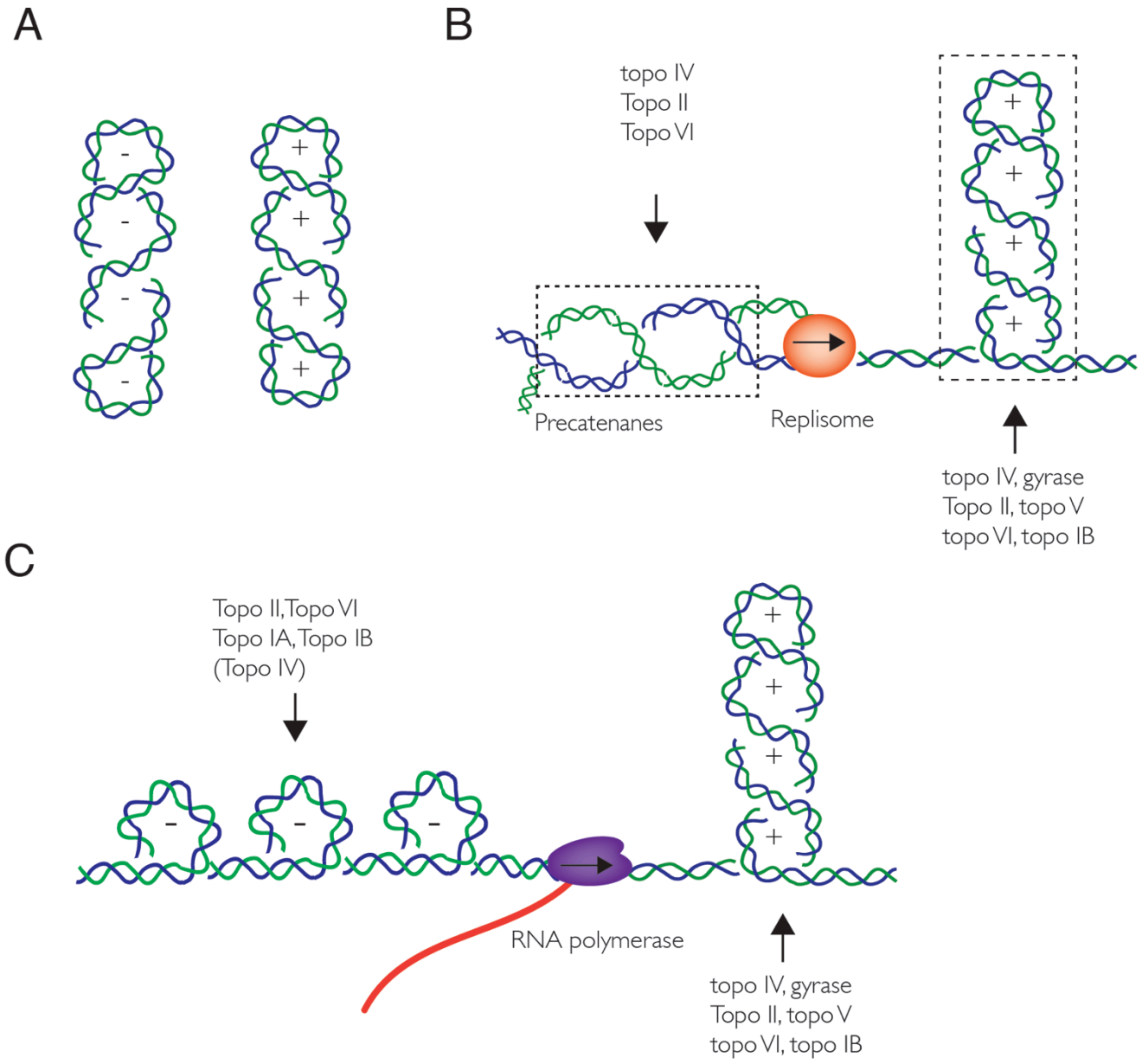

Figure 1.1.
A Negative and positive plectonemic supercoiling. Supercoils are distinguished by their right and left handed superhelical wrapping respectively.
B Topological challenges arising during DNA replication. As a replisome (orange) translocates through a DNA substrate, the DNA becomes overwound (positively-supercoiled) ahead of the moving fork and intertwined behind the fork, into structures known as precatenanes. Failure to remove the positive supercoils ahead of the fork can impede replication fork progression, eventually stalling the fork. If not resolved, precatenanes result in catenanes, which link the chromosomes together and cause cells

to receive asymmetric amounts of DNA at the time of cell division. Topoisomerases that remove these challenges are listed.
C Topological challenges arising during transcription. As RNA polymerase (purple) translocates, positive supercoils are generated ahead of the polymerase assembly whereas negative supercoils develop behind the polymerase assembly. Failure to remove positive supercoils can cause the polymerase assembly to stall resulting incomplete transcription. If the negative supercoils behind the fork are not removed, they can form toxic RNA:DNA hybrids known as R-loops with the nascent RNA (red). Topoisomerases responsible for removing these challenges are listed. Topo IV is less apt at removing negative supercoils and is shown in brackets to indicate that it is not the primary enzyme responsible for removing negative supercoils.

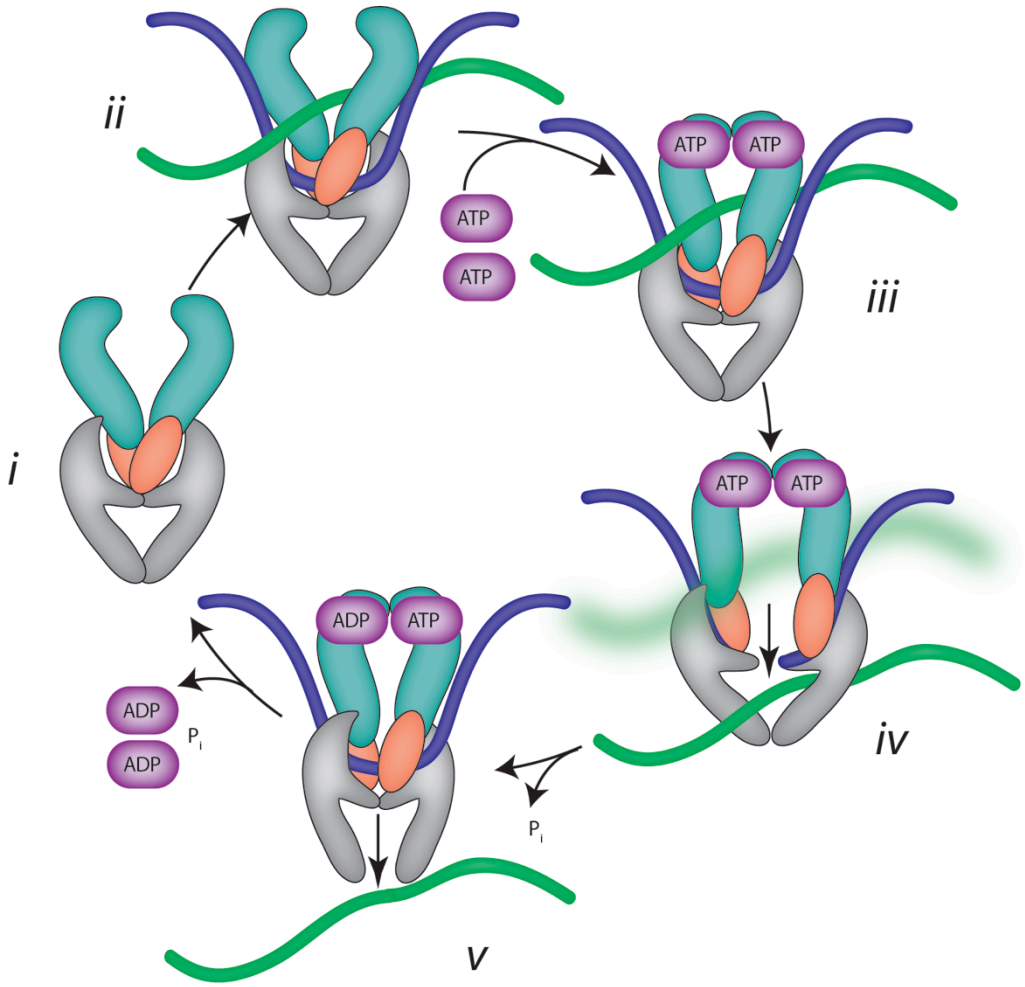

Figure 1.2 Simplified model of the type IIA Topoisomerase Catalytic Cycle. GHKL ATPase domain colored cyan, Topoisomerase/Primase (TOPRIM) domain red, DNA binding cleavage core, grey. ***i.*** Enzyme in the absence of substrate. ***ii.*** The enzyme first binds to duplex DNA known as a gate or g-segment through its central DNA binding channel (blue). It then associates with a second duplex DNA strand known as a transfer or t-segment (green). ***iii.*** Binding of ATP causes the ATPase domain to dimerize. ***iv.*** A transient opening is made in the G-segment DNA. The enzyme breaks the DNA through the formation of a phosphotyrosyl bond. The T-segment can then be passed from the upper cavity of the enzyme through the transient break to the lower enzyme cavity. One ATP is hydrolyzed during this process ***v.*** Hydrolysis of another ATP results in T-segment release and relegation of the G-segment. The enzyme can disassociate from the DNA or remain on the same DNA to act further.

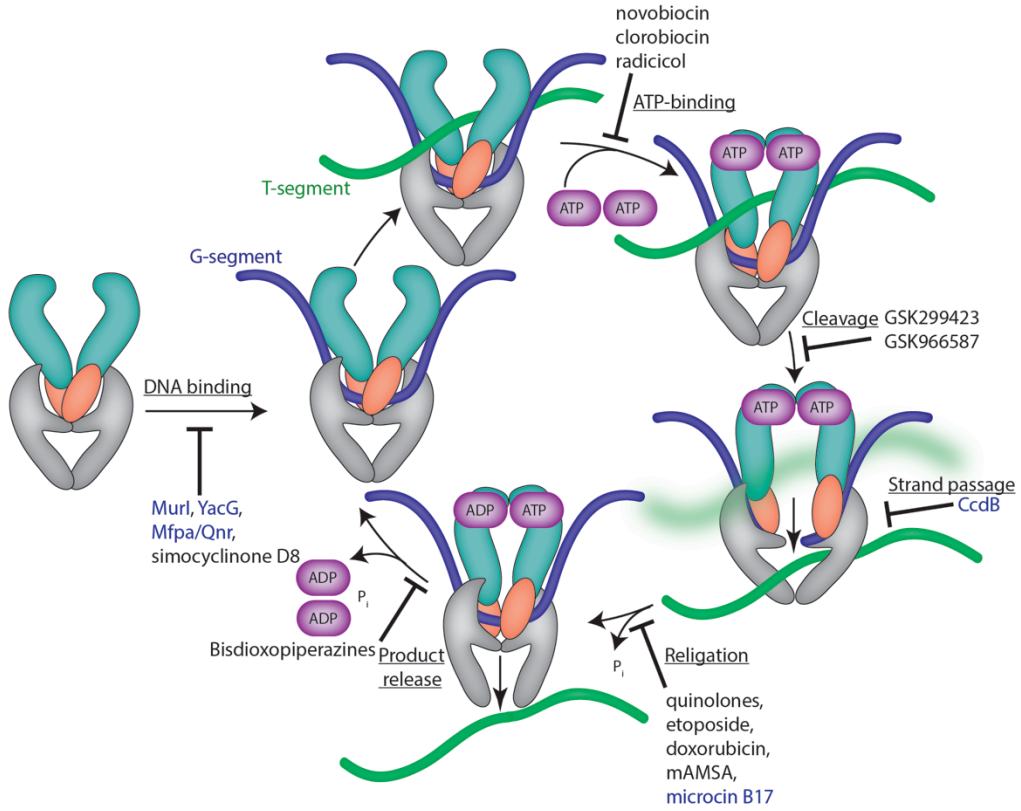

Figure 1.3. Proteinaceous and pharmaceutical inhibition of the type IIA topoisomerase catalytic cycle.
The type IIA topoisomerase catalytic cycle is illustrated. Steps that can be disrupted by proteinaceous (blue) and pharmaceutical agents (black) are indicated.

Chapter 2- Distinct Regions of the *Escherichia coli* ParC C-Terminal Domain Are Required for Substrate Discrimination by Topoisomerase IV

(Portions reproduced from: Vos, S.M., Lee, I., and Berger, J.M. (2013). Journal of Molecular Biology **425** (17) 3029-3045)

Introduction

DNA topoisomerases are ubiquitous and essential enzymes that maintain the topological homeostasis of chromosomes. Type IIA topoisomerases use ATP to modulate chromosome supercoiling and interlinking (catenation) by binding and cleaving one duplex DNA (termed the gate or G-segment), passing another duplex DNA (the transfer or T-segment) through the transient opening, and religating the break (Brown & Cozzarelli, 1979; Liu & Liu, 1980; Roca & Wang, 1992; Roca & Wang, 1994). Since the type IIA topoisomerase catalytic cycle has the potential to create toxic, double-stranded DNA breaks, topoisomerases are highly regulated to ensure proper activity and localization. Regulation can be mediated both intrinsically, through specific physical elements and post-translational modifications, and extrinsically, through direct physical interactions with other proteins. The regulatory programs that define type IIA topoisomerase function on specific substrates or during particular periods of the cell cycle are still emerging.

Most bacteria encode two type IIA topoisomerase paralogs, gyrase and topoisomerase IV (topo IV) (Gadelle et al, 2003; Gellert et al, 1976; Kato et al, 1990). Gyrase and topo IV share a common heterotetrameric architecture ($GyrA_2$•$GyrB_2$ or $ParE_2$•$ParC_2$), as well as substantial sequence homology. Despite these similarities, however, gyrase and topo IV perform distinct functions. Gyrase actively introduces negative-supercoils into DNA to counteract the introduction of positive-supercoils by processes such as replication and transcription (Gellert et al, 1976; Zechiedrich et al, 2000). By contrast, topo IV preferentially removes positive supercoils and resolves catenanes from DNA formed during DNA replication, but is less active on negatively-supercoiled substrates (Charvin et al, 2003; Crisona et al, 2000; Neuman et al, 2009; Stone et al, 2003; Ullsperger & Cozzarelli, 1996; Zechiedrich & Cozzarelli, 1995).

The functional differences between gyrase and topo IV have been ascribed (at least in part) to variations in the C-terminal domains (CTD) of their respective GyrA and ParC subunits. The GyrA and ParC CTD share a common β-pinwheel fold that is formed by a series of repeating Greek key motifs or “blades” (**Figures 1.1A, 1.1B**) (Corbett et al, 2005; Corbett et al, 2004; Hsieh et al, 2004). The GyrA CTD is a DNA binding and wrapping domain composed of 6 blades (Corbett et al, 2005; Reece & Maxwell, 1991; Tretter & Berger, 2012), along with a conserved motif known as the “GyrA-box”, which latches the first blade of the domain to the last blade (Hsieh et al, 2010; Ward & Newton, 1997). Loss of either the GyrA CTD or the GyrA box abolishes the ability of gyrase to supercoil DNA, but does not abrogate strand passage (Kampranis & Maxwell, 1996; Kramlinger & Hiasa, 2006; Lanz & Klostermeier, 2012).

ParC CTDs can bind, but not wrap DNA substrates and have a variable number of blades (from 3-8, proteobacterial versions possess five) (Corbett et al, 2005; Corbett et al, 2004; Tretter et al, 2010). Although the ParC CTD does not contain a canonical GyrA box, degenerate remnants of the motif are found in each of its blades (**Figs 2.1A and S2.1**)(Tretter et al, 2010). Loss of the *E. coli* ParC CTD does not completely abolish relaxation and decatenation function by topo IV, but does generally disrupt the ability of the enzyme to discriminate between topologically distinct substrates (Corbett et al, 2005).

How topo IV discriminates between positively- and negatively- supercoiled substrates has been a subject of debate. In one study, multiple DNA molecules were braided at the single molecule level to simulate crossovers found in positively- and negatively-supercoiled substrates. These experiments found that topo IV relaxed crossovers found in positively-supercoiled substrates more readily than crossovers found in negatively-supercoiled DNAs, suggesting specificity was determined by an ability of the enzyme to sense the chirality of G- and T- segment crossing angles within the topo IV active site (Stone et al, 2003). A subsequent single-molecule study set out to test this model by assaying the ability of topo IV to act on a variety of crossover angles between only two DNA duplexes, rather than braids; however, these experiments found that topo IV showed no preference for positive versus negative crossovers (Neuman et al, 2009), and that discrimination instead arose from differences in enzyme processivity on positively- and negatively- supercoiled substrates (Neuman et al, 2009). In yet a third effort, structural and biochemical studies of ParC have suggested that the CTD may associate with T-segment DNAs and hence provide a means to influence activity (Corbett et al, 2005).

To better understand how the ParC CTD might aid in topology discrimination by *E. coli* topo IV, we mutated potential DNA interacting residues on the positively-charged outer surface of the domain and tested the effect of these substitutions on enzyme function. Unexpectedly, we found that distinct regions of the ParC CTD contribute differentially to DNA binding affinity and the action of topo IV on specific types of DNA substrates. Some sites appear to actively repress activity on negatively-supercoiled and catenated substrates, whereas others are more important for functions such as G-segment bending. Together, these studies indicate that topo IV can indeed sense the juxtaposition of G- and T-segment crossovers, but that this discrimination – which acts in part through controlling enzyme processivity – occurs outside the active site where strand passage takes place.

RESULTS

Construction and solution behavior of ParC CTD mutants

Although the C-terminal domain (CTD) of *E. coli* ParC has been shown to be important in topology discrimination by topo IV (Corbett et al, 2005), the mechanism of this effect has remained unknown. The CTDs of ParC and GyrA have been suggested to bind DNA using the positively-charged rim that encircles the domain (Corbett et al, 2005; Corbett et al, 2004; Hsieh et al, 2004; Ruthenburg et al, 2005)(**Fig 2.1C**). To more finely dissect of the role of this region, we set out to identify prospective DNA binding residues using multiple-sequence alignments of ParC CTD homologs that contain only five blades. We focused first on residues that are both highly-conserved and positively-charged (**Fig S2.1**), and mapped these residues onto the *E. coli* ParC CTD crystal structure to find surface-exposed amino acids that did not appear to be required for structural stability. This analysis revealed that many of the most highly-conserved positions reside in degenerate GyrA-box motifs that reside on the extended loops that latch adjoining blades together (**Fig 2.1D, Fig S2.1**). We also identified a positively-charged patch on the fifth blade that contains two arginines previously suggested to interact with the *E. coli* condensin homolog, MukB (Arg705 and Arg729) (Hayama et al, 2013; Hayama & Marians, 2010).

Given the criteria described above, we next mutated representative basic residues from each of the five blades to aspartate, using charge substitutions to more actively disfavor potential electrostatic interactions that might occur with DNA. Full-length ParC mutants were purified to homogeneity and then subjected to size-exclusion chromatography to confirm that the introduced mutations did not cause the proteins to aggregate (**Fig S2.2**). Of all the mutations surveyed, only one (Arg721Asp) did not behave as a monodisperse species and so was discarded; interestingly, this locus lies in close proximity to a previously identified ParC temperature-sensitive allele, Gly725Asp (Kato et al, 1990). An alternative residue within this region, Arg723Asp, which is nearly as well conserved (**Fig S2.1**), was chosen in lieu of Arg721, and found to behave as per the wild-type protein in solution. To ensure that the CTD mutants were properly folded at the temperatures used in our enzymatic assays, we measured circular dichroism (CD) spectra for each mutant at 25˚C and 37˚C (**Fig S2.2**). In each case, the CD spectra for all mutants were similar to that of WT ParC, indicating that the substitutions did not lead to gross perturbations in protein structure (**Fig S2.2**).

Conserved, basic amino acids in the ParC CTD are important for positive-supercoil relaxation

After purifying the mutants, we proceeded to conduct enzyme assays for standard topo IV activities on different types of DNA substrates using native agarose gel-electrophoresis. In the absence of a DNA intercalating agent, supercoiled DNA migrates faster than intermediate, relaxed, and nicked topoisomers through the gel matrix. We initially tested the ability of our ParC mutants to relax topo IV's favored substrate, positively-supercoiled DNA. Different concentrations of enzyme were titrated against a fixed concentration of DNA to look for general defects in activity (**Fig 2.2**). We discovered that mutations within the CTD of ParC exhibited a broad range of activity profiles, ranging from essentially WT behavior to severe defects in the efficiency and/or

processivity of supercoil relaxation (a detailed explanation of topoisomerase processivity is provided in **Fig S2.3**; relative defects in processivity are roughly quantified by comparing the amount of mutant topo IV required to produce a final topoisomer distribution similar to that seen for the WT enzyme (boxed in blue **Fig 2.2**)).). For example, mutation of positions within blade 5 (Arg705Asp/Arg729Asp) resulted in no change in activity or processivity, whereas mutation of blade 1 (Arg564Asp) significantly impaired both (~10-fold decrease). Other mutations primarily affected enzyme processivity; substitutions to blades 2-4 (Arg616Asp, Lys665Asp. Arg723Asp) led to particularly distributive behavior.

To further characterize the effects of ParC CTD mutations on positively-supercoiled DNA, we looked at relaxation using a fixed molar excess of DNA compared to topo IV (~50 fold) as a function of time. This regime permitted us to observe differences in rate of relaxation in addition to changes in processivity. Interestingly, all mutations tested actually modestly enhanced the overall rate of positive-supercoil relaxation by topo IV compared to the WT protein, with the exception of Arg564Asp in blade I, which was severely compromised (**Fig 2.3**). As with the enzyme titration assays, however, defects in processivity were again observed for mutations in blades 2, 3, and to a lesser extent blade 4. Together, these data demonstrate that positively-charged amino acids on the CTD of ParC not only influence the activity of topo IV on positively-supercoiled DNA, yet also unexpectedly show that different blades make different contributions to activity.

Basic residues on the ParC CTD differentially affect decatenation and negative-supercoil relaxation

We next tested the ability of our ParC CTD mutants to act on kinetoplast DNA (kDNA), a singly network of ~5000 2.5kb minicircles that is also a favored substrate of topo IV (Anderson et al, 1998; Nurse et al, 2000; Peng & Marians, 1993c; Sugisaki & Ray, 1987). When visualized by agarose gel-electrophoresis, the kDNA network is too large to pass into the gel-matrix and remains trapped in the wells; however, in the presence of topo IV or other topoisomerases, kDNA minicircles are released into the gel matrix (Marini et al, 1980). Although the processivity of topo IV on kDNA cannot be evaluated in this assay, the activity of the enzyme can be monitored as an increase in the amount of minicircle produced as a function of either protein concentration or time. We first examined the ability of different quantities of topo IV to decatenate the substrate at a fixed concentration of kDNA (**Fig 2.4**). As with the relaxation of positively-supercoiled DNA, mutations in the ParC CTD exhibited a broad range of functional effects. Mutation of blades 2 and 4 had only a modest affect on decatenation. By contrast, mutation of blade 3 markedly reduced enzymatic activity (~10 fold), while the blade 1 substitution almost entirely abrogated minicircle release. Unexpectedly, the blade 5 mutation appeared to increase the activity of topo IV on kDNA nearly 10-fold (as indicated by a need for a lower amount of enzyme to fully unlink the catenated network).

Based on the outcome of this study, we proceeded to perform time-course reactions of topo IV on kDNA (**Fig 2.5**). As with the enzyme titrations, topo IV containing a mutation in blade 2 displayed essentially WT activity. An enhanced ability of the blade 5 mutations in catalyzing minicircle release was also seen; a similar behavior was

observed for the mutation in blade 4. The substitution to blade 3 again impaired minicircle release (~5-fold decrease), while the blade 1 alteration failed to produce virtually any detectable minicircle product. Overall, these data indicate that blade 1, and to a lesser extent blade 3, play a critical role in supporting the activity of topo IV on catenated substrates. Moreover, as with our positive-supercoil relaxation study, different positions on the ParC CTD appear to play an unequal part in the enzyme's decatenation function.

To round out our analysis, we next tested the ability of our ParC CTD mutants to relax topo IV's least favored substrate, negatively-supercoiled DNA. As with the experiments using positively-supercoiled substrates, enzyme titrations were first performed to look at overall catalytic prowess (**Fig 2.6**). Mutations in nearly every blade led to reproducible changes in the relative amount of enzyme required to produce comparable amounts of relaxed product, with exception of the mutation to blade 4, which displayed essentially WT activity. Interestingly, activity was actually subtly enhanced by the substitutions in blade 5 (~2-3 fold), but reduced by the alterations made to blades 2 and 3 (~10-fold). The blade 1 mutation nearly completely abolished activity overall (~20-fold decrease).

To examine these functional effects further, we performed time course assays using a fixed molar ratio of topo IV to DNA (**Fig 2.7**). Since there proved to be a significant difference in general activity between the blade 4 and 5 mutants of ParC compared to the other constructs, we examined activity with two slightly different enzyme concentrations to observe relaxation within a common timeframe (a 1.5-fold molar excess of DNA to topo IV for blades 4 and 5, and a 1.3-fold molar excess of topo IV to DNA for blades 1-3). Under these conditions, we again observed an enhanced rate of relaxation by the blade 5 mutant (~2-fold), whereas the blade 4 mutant exhibited WT behavior. By contrast, the blade 2 and 3 mutants removed negative supercoils very slowly (~10-fold less quickly), while the blade 1 mutant was incapable of removing negative supercoils in the time period assayed. These results, as with the other substrates, indicate that the outer surface of the ParC CTD is important for the control of negative-supercoil relaxation, but that different blades again do not contribute equivalently to this activity.

Different blades on the CTD have a non-equivalent affect on DNA binding

Because the CTD is thought to be a T-segment binding element, the functional disparities between different mutants in our assays suggested that individual substitutions might be affecting the affinity of the domain for DNA. To test this idea, we assessed the ability of different CTD mutants to bind DNA using fluorescence anisotropy. Because full-length ParC and the topo IV holoenzyme both bind DNA, we looked at the isolated CTD to establish the effects of our substitutions on this region alone. In our initial experiments, we found that the isolated CTD (498-752) tended to aggregate over time. Since this domain is well-behaved when connected to the N-terminal DNA binding region of ParC, we overcame this poor solution behavior by fusing the CTD to an inert carrier protein, MBP. The MBP-CTD construct proved well-behaved, showing no observable tendency to aggregate by gel-filtration. We then proceeded to examine the properties of each of our various CTD mutants by incubating different

concentrations of the MBP fusion with 20nM of a fluorescein labeled 20mer duplex oligonucleotide. The mutants exhibited a broad range of DNA binding activity, with the mutations closest to the N-terminal half of the CTD displaying near WT levels of affinity. By contrast, DNA binding became progressively impaired as substitutions were made to more C-terminal regions of the domain (**Fig 2.8A**). Thus, as with activity assays, different regions of the ParC CTD contributed differently to DNA binding by the domain. Interestingly, however, the mutations that most significantly affected DNA binding did not necessary correlate with substitutions that showed the greatest effect on enzyme activity.

Blade 1 of ParC CTD is required for G-segment bending

Through the course of conducting our DNA relaxation and decatenation assays, it became apparent that one mutant in particular, Arg564Asp in blade 1, showed greatly impaired activity on all substrates (>90-95% decreases, comparable to deletion of the CTD entirely (Corbett et al, 2005)). However, when we assessed this substitution either in the context of the CTD alone or in topo IV holoenzyme, it had one of the least severe effects on DNA binding (**Fig 2.8A, 2.8B**). Given this dichotomy, we were curious as to whether the mutation might disrupt not T-segment interactions *per se*, but rather some other aspect of topo IV function. Type IIA topoisomerases have been shown to bend the G-segment DNA (Dong & Berger, 2007; Hardin et al, 2011; Laponogov et al, 2010; Lee et al, 2012; Schmidt et al, 2010; Vologodskii et al, 2001; Wendorff et al, 2012; Wohlkonig et al, 2010) (Lee et al, 2013); inspection of the structure of full-length ParC shows that Arg564 lies close to the G- segment binding site of the protein, near the point where the bent DNA arms emanate from the active site (**Fig S2.4**). This juxtaposition would appear to be sterically incompatible with the binding of Arg564 to a T-segment, as the transport-DNA would clash with a bound G-segment.

Based on this structural consideration, we hypothesized that blade 1 might play a role in linking the CTD to a G-segment associated with topo IV. Because the G-segment binding site of type IIA topoisomerases is large and extensive (>2500Å^2 surface area (Bax et al, 2010; Dong & Berger, 2007; Laponogov et al, 2010; Schmidt et al, 2010; Schmidt et al, 2012; Wendorff et al, 2012; Wohlkonig et al, 2010; Wu et al, 2011)), we did not anticipate observing a strong defect in G-segment affinity *per se*, an expectation borne out by our affinity measurements (**Fig 2.8B**). Instead, the proximity of blade 1 to the bent arms of a prospective G-segment suggested to us that the amino acid might interrogate the geometry of the associated DNA.

To test this idea, we looked to see whether G-segment bending might be affected by the integrity of the CTD using FRET. In these experiments, we utilized a 45mer duplex oligonucleotide labeled on opposite strands with Cy3 and Cy5 and the topo IV holoenzyme. Bending was observed after exciting Cy3 with 530nm and observing changes in the emission from 545-720nm. Consistent with earlier studies, WT topo IV gave rise to a strong FRET signal consistent with the introduction of a sharp DNA bend (Hardin et al, 2011; Lee et al, 2013) (**Fig 2.8C**). By contrast, the Arg564Asp mutant gave rise to no appreciable change in FRET, indicating that DNA bending was severely compromised in this mutant. To confirm this result, we next tested a ParC construct lacking its C-terminal domain entirely. As with the Arg564Asp mutation, this construct

likewise failed to induce any observable change in FRET, again indicative of a bending deficiency. Together, these data reveal that the CTD plays an unexpected role in the establishment of a stable G-segment bend by topo IV, and further suggest that the significant enzymatic defects we observe in the Arg564Asp mutant are due at least in part to this defect.

Discussion

Although all type IIA topoisomerases rely on a generally-conserved, ATP-dependent strand passage mechanism for effecting topological changes in DNA, the substrate specificities of different enzyme subfamilies vary significantly. Topo IV discriminates between topologically distinct DNA substrates in a manner that requires the CTD of its ParC subunit (Corbett et al, 2005); however, the molecular basis for this discrimination has remained ill-defined. It has been postulated that the GyrA and ParC CTDs contribute to substrate discrimination by associating with DNA substrates using their positively-charged, outer rim (Corbett et al, 2004). To better understand how the ParC CTD might mediate these effects, we identified highly-conserved, basic amino acids on CTD surface and mutated these regions to aspartate. We then tested whether these substitutions altered topo IV function on positively-supercoiled, catenated, and negatively-supercoiled DNA substrates, and whether they altered DNA binding by the isolated domain itself.

Our ParC CTD substitutions reveal an unexpectedly rich pattern of functional contributions emanating from each blade of the domain (**Fig 2.9**). For example, blade 1 is critical for overall topo IV activity on all substrates. By contrast, blade 4 is not essential for general activity on any substrate. Catenane resolution strongly depends on blade 3, while efficient removal of negative-supercoils (and to a lesser extent positive supercoils) depends not only on an intact blade 3 but also blade 2. In addition to modulating general topo IV activity, different substitutions also affected overall processivity, as well as DNA binding by the isolated CTD. Processivity defects were most apparent with blade 2 and 3 substitutions, yet milder defects were also observed upon altering blade 4. We discovered that DNA binding by the isolated domain was strongly perturbed by substitutions to blades 4 and 5, whereas mutations in other blades had a more subtle impact on DNA binding (**Fig 2.8**). Interestingly, the blade 5 mutation actually enhanced the activity of topo IV in relaxing negatively-supercoiled DNA and in decatenating kDNA substrates. This result indicates that the strong DNA binding site associated with blade 5 is actually an auto-inhibitory element that specifically represses negative-supercoil relaxation and catenane resolution. Together, our data show that single mutations made to the positively-charged surface of the CTD give rise to specific, but differential effects on enzyme activity and processivity depending upon which blade they reside (**Fig 2.10A**).

Overall, these findings unexpectedly demonstrate that the ParC CTD is not a uniform, non-specific DNA binding domain, but rather a complex sensor element that can both interrogate the topological status of DNA and use this information to control topoisomerase response. An additional surprise is the finding that one region of the CTD (blade 1) is not only required for activity on all substrates, but also for the bending of G-segment DNA. At present, it is unknown how topo IV associates with DNAs outside of the active site; however, this study clearly indicates specificity for and activity differences on distinct DNA substrates can be attributed to non-equivalent surfaces of the ParC CTD. It is similarly unclear whether ParC orthologs whose CTD blade number varies compared to that of *E. coli* ParC are able to discriminate between different DNA topologies.

An additional outcome of these data is their ability to help reconcile a debate insofar as how topo IV discriminates between positively-supercoiled and negatively-supercoiled DNA segments. Early single molecule experiments using braided DNA substrates led to the hypothesis that topo IV could discriminate between different DNA topologies by recognizing the chiral juxtaposition between G- and T-segments in the topo IV active site (Stone et al, 2003). However, a subsequent single molecule study using single duplex crossovers indicated that topo IV has no preference for DNA duplex crossing angle, and that lowered enzyme processivity on negatively-supercoiled DNA was instead responsible for the difference in supercoil relaxation rates between underwound and overwound substrates (Neuman et al, 2009). Our data suggest that topo IV can indeed read out crossover geometry, but that sensing of this geometry occurs *outside* the active site, where it influences not only strand passage efficiency but also enzyme processivity. In this model, positively-supercoiled substrates would interact with blades 2, 3, and 4. Negatively-supercoiled DNA would also interact with blades 2 and 3, but could further associate with a strong DNA binding site on blade 5 that impedes strand transport and lowers processivity. Catenated DNAs would preferentially engage blades 3 and 4, but likewise be subject to an interaction with blade 5 that slows enzyme function. Blade 1 would play a role in binding the G-segment as a means to both facilitate the bending of this DNA through the active site and to help orient the CTD for appropriate readout of substrate DNA topology.

How might the CTD physically mediate such differential effects? One possible mechanistic model for the action of the ParC CTD can be derived by docking a G-segment from a DNA-bound type IIA topoisomerase into the structure of the full-length ParC dimer and modeling T-segment DNA over the active site (**Fig 2.10B**). Such an exercise indicates that the ParC CTD likely adopts alternate conformations with respect to the N-terminal domains to engage the flanking arms of positive or negative-handed T-segment DNAs *after* they exit the active site (**Fig 2.10C**). The degenerate GyrA box that resides on the surface of blade 1 would help stabilize G-segment bending, a property we recently have found to be critical for enzyme function (Lee et al, 2013). The equivalent motifs in other blades, particularly 2 and 3 would be brought to bear on a T-segment by using distinct CTD orientations to distinguish between different types of DNA topologies; when engaged, these elements would promote processive strand passage events, as has been seen on positively-supercoiled DNA (Crisona et al, 2000; Neuman et al, 2009; Stone et al, 2003). However, in some instances, particular CTD configurations would allow the strong DNA-binding site on blade 5 to counteract the other blades and actively impede strand transport, possibly by slowing T-segment release and contributing to the lowered processivity seen on negatively-supercoiled DNA (Neuman et al, 2009). Although it is not known at present if the CTDs of topo IV are mobile, precedence for such movement can be found in gyrase, whose related domains appear to transit with a T-segment during strand passage (Baker et al, 2011; Costenaro et al, 2005; Kirchhausen et al, 1985). The suggestion that the ParC CTD interacts with both the G- and T-segments also has parallels with gyrase, whose CTDs also are known to engage DNA sufficiently tightly as it exits the nucleolytic active site that they wrap the duplex back through the enzyme to provide the transport strand *in cis*

(Kampranis & Maxwell, 1996). A more precise physical model that can account for how an extended DNA segment can writhe spatially to selectively engage specific regions of the CTD, as well as snake through the arms of a second bent DNA, will require future investigation.

MATERIALS AND METHODS

Cloning and protein expression

Cloning of the full-length coding regions of *E. coli* ParC (1-752), ParE (1-630), and the ParC N-terminal domain (NTD) (1-482) has been previously described (Corbett et al, 2005). The ParC C-terminal domain (CTD) (498-752) was amplified from *E. coli* MG1655 K-12 genomic DNA and cloned into vector pSV272, which possesses an N-terminal hexahistidine (His_6) tag followed by maltose binding protein (MBP) tag and tobacco etch virus (TEV) protease cleavable site. Point mutations were introduced into the full-length ParC or the His6-MBP ParC CTD using QuikChange (Stratagene).

Proteins (except for the ParC NTD) were over-expressed in E. coli BL21codon-plus (DE3) RIL cells (Stratagene) at 37°C. Protein expression was induced at 37°C by adding 0.25-0.5mM isopropyl β-D-1-thiogalactopyranoside (IPTG) to 2xYT liquid media cultures after cells had grown to OD600 0.3-0.5. After induction, cells were grown at 37°C for an additional 3-4 hours, centrifuged, resuspended in buffer A800 (10% (v/v) glycerol, 20mM Tris-HCl pH 7.9, 800mM NaCl, 30mM imidazole pH 8.0, 2mM β-mercaptoethanol (BME), 1µg/mL pepstatin A, 1µg/mL leupeptin, and 1mM phenyl methylsulfonyl fluoride(PMSF)), frozen drop-wise into liquid nitrogen, and stored at -80°C prior to purification.

Purification of E. coli ParE, ParC and His_6-MBP ParC CTD

Protein expression and purification are described in detail in **Appendix 5**.

Expression and Purification of the ParC NTD

The ParC NTD was over-expressed in E. coli BL21codon-plus (DE3) RIL cells (Stratagene) from a fresh transformation. Protein expression was induced at 30°C by adding 0.3mM IPTG to 1L 2xYT liquid media cultures after cells had grown to OD600 0.3-0.5. Cells were grown for six more hours, resuspended in A800, drop frozen, and stored at -80˚C.

For purification of the ParC NTD, cells were thawed, lysed by sonication, and centrifuged. The clarified lysate was applied to a 5mL HiTrap Ni2+ column (GE), and the column was washed extensively with a buffer containing 800mM NaCl, 10mM imidazole pH 8.0, 50mM Tris-HCl pH 7.9, 20% (v/v) glycerol, 2mM BME, 1µg/mL pepstatin A, 1µg/mL leupeptin, and 1mM PMSF. The column was then washed in a buffer A200 (200mM NaCl, 10mM imidazole pH 8.0, 50mM Tris-HCl pH 7.9, 20% (v/v) glycerol, 2mM BME, 1µg/mL pepstatin A, 1µg/mL leupeptin, and 1mM PMSF). The protein was eluted in a buffer containing 200mM NaCl, 400mM imidazole pH 8.0, 50mM Tris-HCl pH 7.9, 20% (v/v) glycerol, 2mM BME, 1µg/mL pepstatin A, 1µg/mL leupeptin, and 1mM PMSF and concentrated by centrifugation (Millipore Amicon Ultra 30). To remove the His6 tag, the protein was dialyzed overnight in Slide-A-Lyzer cassettes (Thermo Scientific, 10K MWCO), at 4°C against A200 in the presence of 1mg His6 TEV protease. Following TEV cleavage, the protein was run over a HiTrap Ni2+column equilibrated in A200 to isolate tagless proteins and remove the tagged TEV protease. The protein was concentrated by centrifugation (Millipore Amicon Ultra 30) and then applied to a S-300 gel filtration column (GE) equilibrated and run in a buffer containing 800mM KCl, 50mM

Tris-HCl pH 7.9, 20% (v/v) glycerol, 2mM BME, 1µg/mL pepstatin A, 1µg/mL leupeptin, and 1mM PMSF. Peak fractions were collected and concentrated by centrifugation (Millipore Amicon Ultra 30). The ParC NTD was flash frozen in a final buffer containing 30% (v/v) glycerol, 20mM Tris-HCl pH 7.9, 400mM KCl, and 2mM BME, and stored at -80°C. Protein purity was assessed by SDS-PAGE/Coomassie staining, and protein concentration was measured by absorbance at 280nm.

Circular Dichroism

Aliquots of full-length WT and mutant ParCs were thawed and dialyzed overnight at 4˚C against a buffer containing 200mM KCl and 10mM Tris-HCl pH 7.9. After dialysis, the proteins were diluted to a final concentration of 0.25mg/mL. Circular dichroism spectra were taken at 25˚C and 37˚C with an Aviv model 410 Circular Dichroism Spectrophotometer in a 1cm pathlength cuvette. Data were obtained from 250-200nm, at 1nm intervals. Each point is averaged over 5 seconds and each read was performed three times.

Preparation of Supercoiled Plasmid Substrates and kDNA

Negatively-supercoiled pSG483 (2927bp), a pBluescript SK derivative, was prepared from E. coli using a maxiprep kit (Machery-Nagel). To produce positively-supercoiled pSG483, negatively-supercoiled pSG483 was treated with *A. fulgidus* reverse gyrase following the method of Rodriguez (Rodriguez, 2002). A detailed protocol for preparing positively-supercoiled DNA and reverse gyrase is provided in **Appendices 6** and **7**. Kinetoplast DNA (kDNA) from *Crithidia fasciculata* was purified as described by Shaprio et al (Shapiro et al, 1999b).

DNA Supercoil Relaxation Assays and Decatenation Assays

A detailed protocol is provided in **Appendix 8**. The topo IV holoenzyme was formed on ice by incubating equimolar amounts of ParE and ParC (final concentration tetramer ~ 20-40µM) for 10 minutes. Topo IV was then serially diluted in protein dilution buffer (2-3 fold steps in 150mM potassium glutamate, 50mM Tris-HCl pH 7.9, 10% (v/v) glycerol, and 6mM MgCl2) and mixed with supercoiled DNA (7.9 nM final concentration) or kDNA (9.2 nM). The final reaction (20µL) contained 30mM potassium glutamate, 1% (v/v) glycerol, 10mM dithiothreitol (DTT), 1mM spermidine, 10µg/mL bovine serum albumen (BSA), 50mM Tris-HCl pH 7.9, 6mM MgCl2, and 2mM ATP pH 7.5. For enzyme titration experiments, samples were incubated at 37˚C for 10 minutes after addition of ATP. The reactions were quenched by the addition of 2% (w/v) SDS and 20mM EDTA pH 8.0 (final concentrations). Sucrose loading dye was added to the samples, which were then run on 1% (w/v) TAE agarose gels (40mM sodium acetate, 50mM Tris-HCl pH 7.9, 1mM EDTA pH 8.0) for 6-15 hours at 2-2.5 volts/cm. For visualization, gels were stained with 0.5µg/mL ethidium bromide in 1% TAE buffer for 20 minutes, then destained in 1% TAE buffer for 30 minutes and exposed to UV transillumination. For time course experiments, the reaction volume was increased to 180µL. After the addition of ATP, samples were incubated at 37˚C. For each time point, 18µl of the sample was removed and quenched by the addition of 2% (w/v) SDS and 20mM EDTA pH 8.0 (final concentrations). All other experimental parameters are identical to those utilized in the enzyme titration

experiments. All gel-based experiments were performed at least three times with at least two different protein preparations for each ParC construct.

DNA Binding Experiments with the Isolated His_6-MBP ParC CTD

A randomly generated, 20bp annealed duplex oligonucleotide was purchased from Integrated DNA Technologies (IDT) and resuspended in water (50% G/C content, Tm = 50°C, 5'-l56-FAMl-TTAGGCGTAAACCTCCATGC-3' and 5'-GCATCCGCATTTACGCCTAA-3', where l56-FAMl indicates the position of a carboxyfluorescein dye used for analysis. A short DNA was chosen to prevent binding of the multiple CTDs to a single duplex. All proteins were diluted on ice in protein dilution buffer A (150mM potassium glutamate, 20mM Tris-HCl pH 7.5, 10% (v/v) glycerol, and 50 µg/mL BSA). The assay (80µL) contained 16µL of the diluted His6-MBP ParC CTD protein and 20nM of the fluorescently labeled 20mer oligonucleotide. DNA and proteins were initially incubated on ice in the dark for 10 minutes, after which they were diluted to the final assay volume and kept at room temperature in the dark for 10-15 minutes (final assay conditions: 2.4mM DTT, 20mM Tris-HCl pH 7.5, 10% (v/v) glycerol, 1mM $MgCl_2$, 50 µg /mL BSA, 30mM potassium glutamate). Measurements were made with a Perkin Elmer Victor 3V 1420 multilabel plate reader at 535 nm. Data points are the average of three independent reads and all points are normalized to wells where protein is absent. Data were plotted in GraphPad Prism Version 5 using the following single site binding model equation:

$$Y = Bmax\left(\frac{([L]+[P]+K_{d,app}))-\sqrt{([L]+[P]+K_{d,app})^2-4[L][P]}}{2[L]}\right)$$

where Bmax is the maximum specific binding, L is the DNA concentration, P is the concentration of the His_6-MBP ParC CTD, and Kd, app is the apparent dissociation constant for His_6-MBP ParC CTD and DNA (Datta & LiCata, 2003; Heyduk & Lee, 1990).

DNA binding experiments with the topo IV holoenzyme

The topo IV holoenzyme was reconstituted as described for the DNA relaxation and decatenation assays. A 45bp annealed duplex DNA with a strong topoisomerase II binding site was obtained from IDT and resuspended in water (Mueller-Planitz & Herschlag, 2007). The sequences for the two strands were: 5'-GCCTATCCGAGGATGACGATGCGCGCATCGTCATACAGCGAATGG-3' and 5'-l56-FAMl- CCATTCGCTGTATGACGATGCGCGCATCGTCATCCTCGGATAGGC - 3'. A longer DNA was chosen for this study because the central DNA binding and cleavage core of type IIA topoisomerases footprints an ~34bp span of the duplex (Peng & Marians, 1995); the DNA was extended slightly further to match the oligo used for obtaining a robust FRET signal in the recent DNA bending studies (Lee et al, 2013). To conduct the assay, topo IV was titrated on ice and mixed with DNA (20nM final) for ten minutes prior to further dilution. The final reaction (80µL) contained 25mM Tris-HCl pH 7.5, 20mM NaCl, 10mM $MgCl_2$, 10% (v/v) glycerol, and 100ug/mL BSA. Reactions were incubated at RT for 15 minutes prior to taking measurements. Measurements were made with a Perkin Elmer Victor 3V 1420 multilabel plate reader at 535nm. Data were

plotted in Prism Graphpad Version 5 and fit to the single-site binding model described earlier.

FRET-based DNA bending experiments.
A 45mer duplex DNA of identical sequence to that employed for the binding assays was used to conduct the bending experiments. One strand contained a 5'-Cy5 dye:
5'-GCCTATCCGAGGATGACGATGCGCGCATCGTCATACAGCGAATGG-3',
while the other bore a 5'-Cy3 label:
5'-CCATTCGCTGTATGACGATGCGCGCATCGTCATCCTCGGATAGGC-3'.
For the assay, 0-1000 nM topo IV was titrated against 100 nM labeled DNA in 14 μL reactions containing 25 mM Tris-HCl (pH 7.5), 20 mM NaCl, 10 mM MgCl2, 10% (v/v) glycerol, and 100 µg/mL BSA. Emission spectra of Cy5 (545-720 nm) were measured after excitation of Cy3 by 530 nm using a Fluoromax fluorometer 4 (HORIBA Jobin Yvon, Edison, NJ, USA). The loss of emission signal with topo IV constructs containing either the blade 1 ParC mutant or the ParC NTD alone reflects a loss of the ability of the enzyme to bend DNA (Lee et al, 2013) (Hardin et al, 2011).

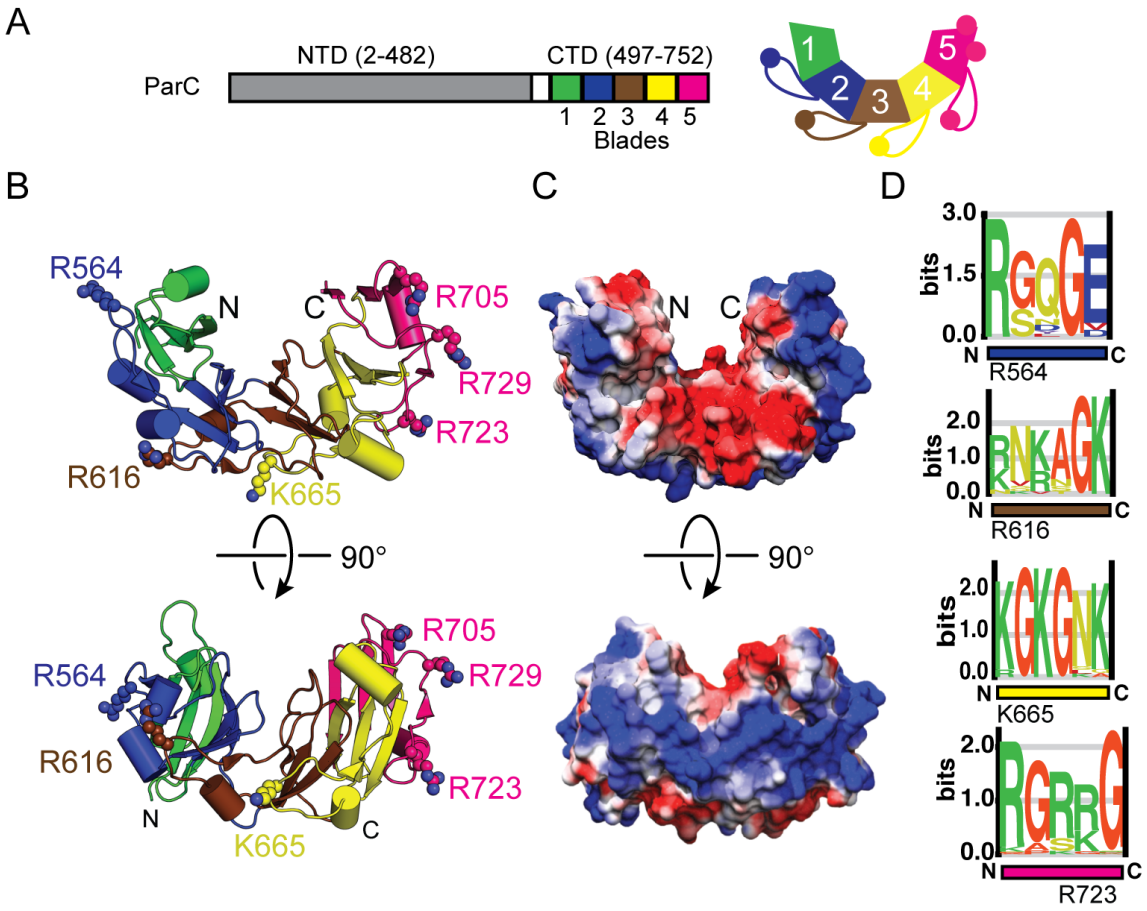

Figure 2.1. ParC CTD structure and organization.
A Primary structure of ParC. The ParC NTD is colored in grey and the blades of the ParC CTD are colored according to number. A cartoon schematic of the ParC CTD is on the right (colored spots correspond to positions assayed in this work).
B Cartoon representation of the *E. coli* ParC CTD crystal structure (PDB id: 1ZVT), top and side views. Residues assayed in this work are shown by stick representation. All figures depicting crystal structures were generated in PyMol[56].
C Electrostatic representation of the *E. coli* ParC CTD crystal structure (PDB id: 1ZVT) outer surface, top and side views. The outer, curved surface of the domain is rich in positive-charges.
D Sequence conservation of γ-proteobacterial ParC CTD residues residing in remnant GyrA boxes. Sequence logos generated in enoLOGOs[57]. Residues assessed in this work are indicated under each logo. For a more complete sequence alignment see **Fig S2.1**.

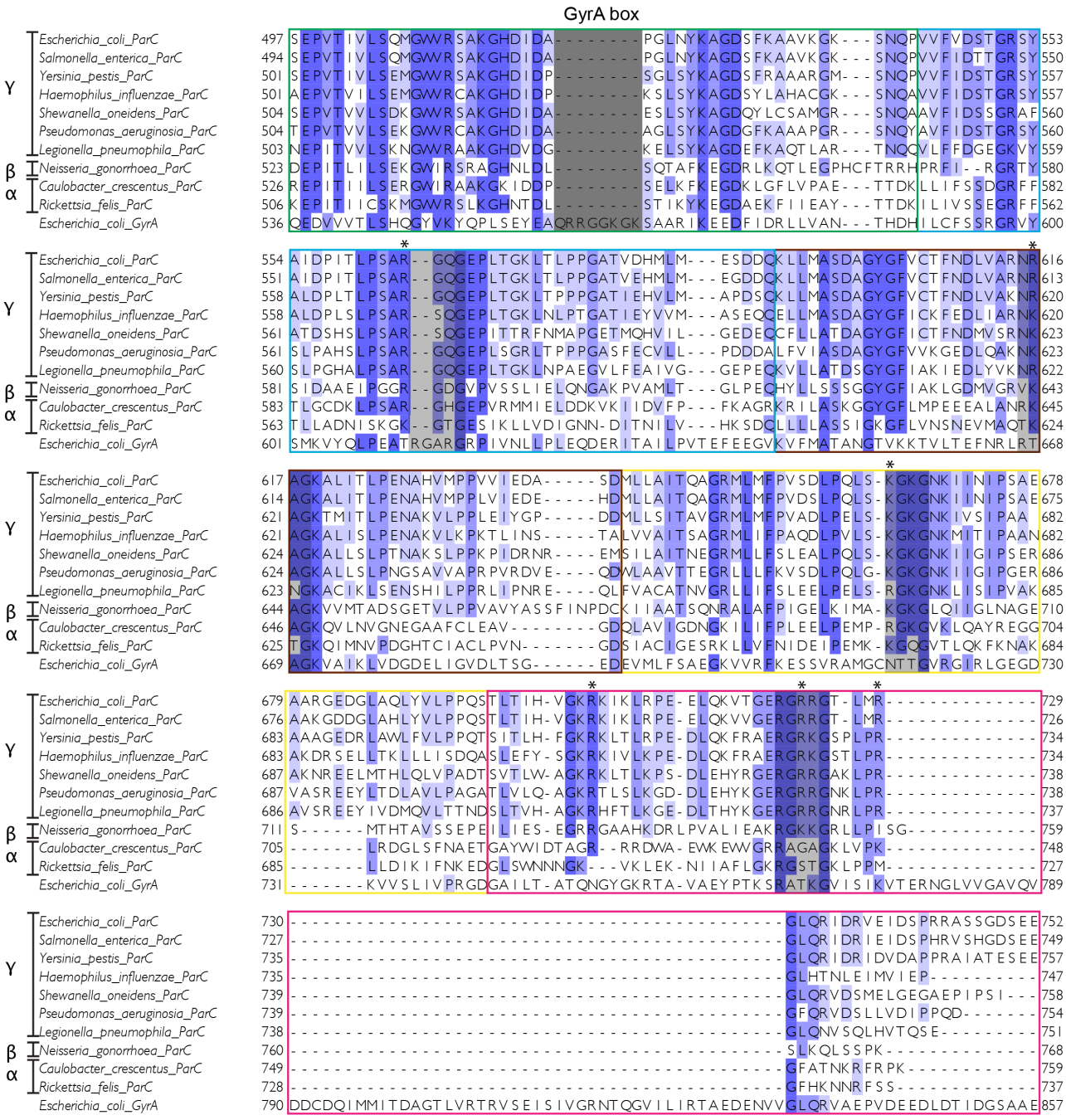

Figure S2.1. Sequence alignment of proteobacterial ParC CTDs.
Sequences of various α,β, and γ proteobacterial ParC CTDs and the *E. coli* GyrA CTD were aligned in MAFFT [1]. The figure is representative of a larger sequence alignment containing ~60 sequences. Blades of the ParC CTD are boxed and colored according to figure 1. Residues residing in each blade are mapped to the *E. coli* ParC CTD crystal structure (PDB id: 1ZVT). The GyrA box found in GyrA, but not in ParC CTDs, is shaded dark grey. The GyrA box remnants found in the ParC CTD are shaded in grey. Residues mutated in this study are asterisked above the alignment. Figure was made in JALVIEW (Waterhouse et al, 2009).

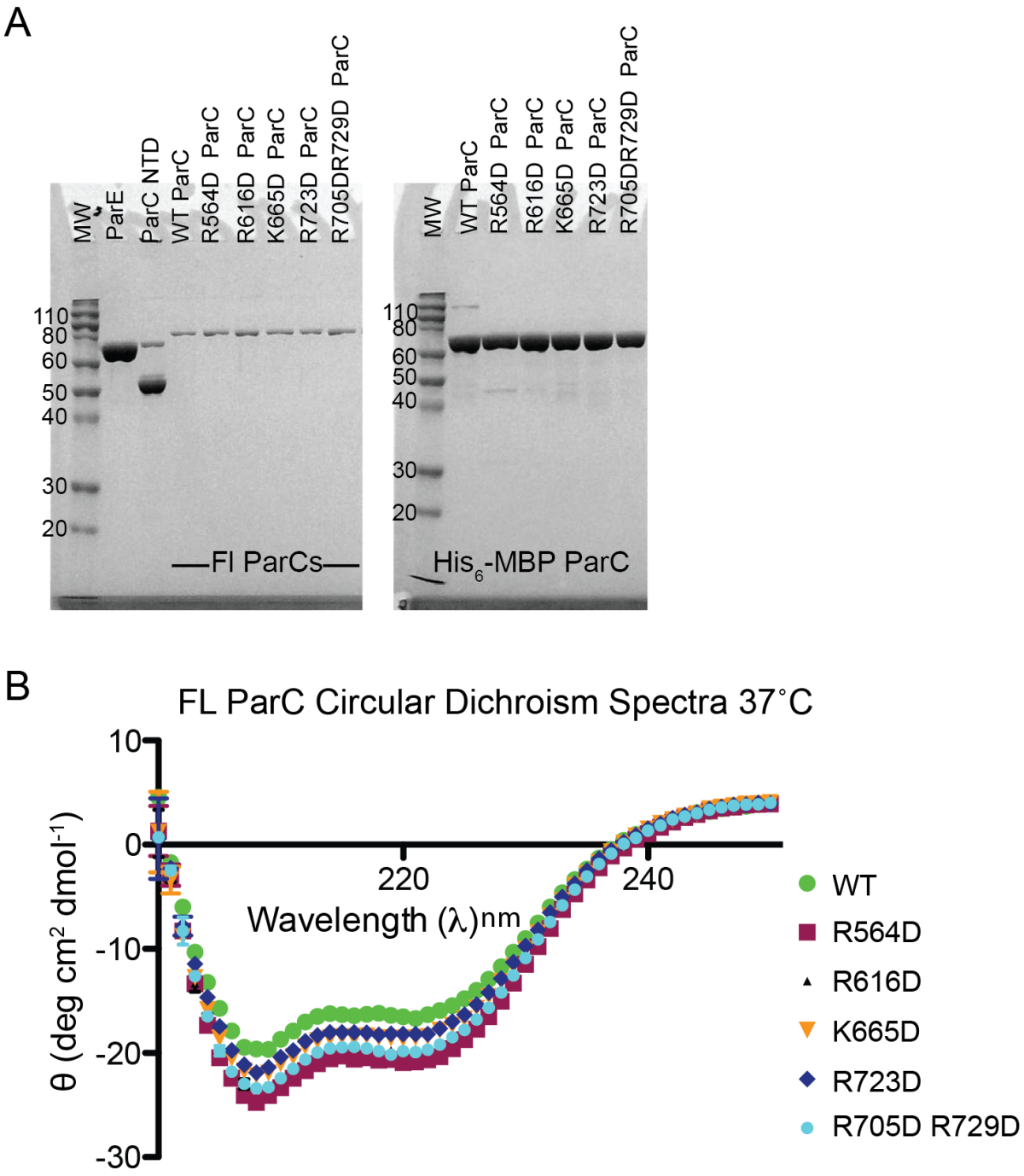

Figure S2.2. Assessment of protein purity of constructs used in this work.
A Protein purity as assessed by SDS-PAGE. Gel was run with ~0.3µg of each protein to show the level of purity after size-exclusion chromatography.
B Circular dichroism spectra of various full-length ParC mutants compared to the WT ParC. Spectra were taken at 37˚C and are similar to spectra taken at 25˚C (not shown).

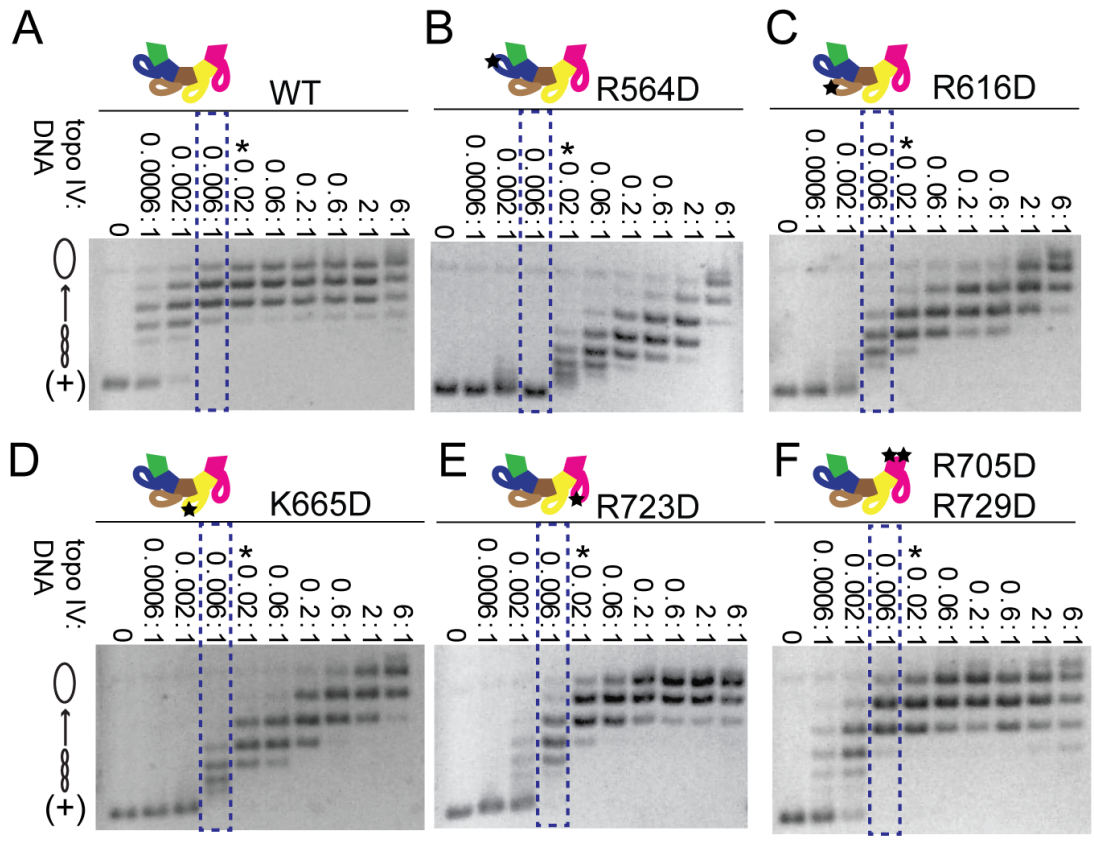

Figure 2.2. General activity of WT and mutant topo IVs on positively-supercoiled DNA substrate.

The constructs assayed are shown in each panel. Each assay proceeded for 10 minutes prior to quenching and contained 7.9nM of a positively-supercoiled plasmid and various concentrations of each topo IV construct (0.005nM-50nM), with the ratio of topo IV to DNA indicated above each gel. A schematic of the topoisomer distribution is illustrated on the left side of the gels. Blue boxes correspond to the enzyme concentration at which WT topo IV removes all positive-supercoils, and reaches its final topoisomer distribution and is shown for reference. Asterisks indicate the concentration of protein used for the positive-supercoil relaxation timecourse (**Fig 2.3**).

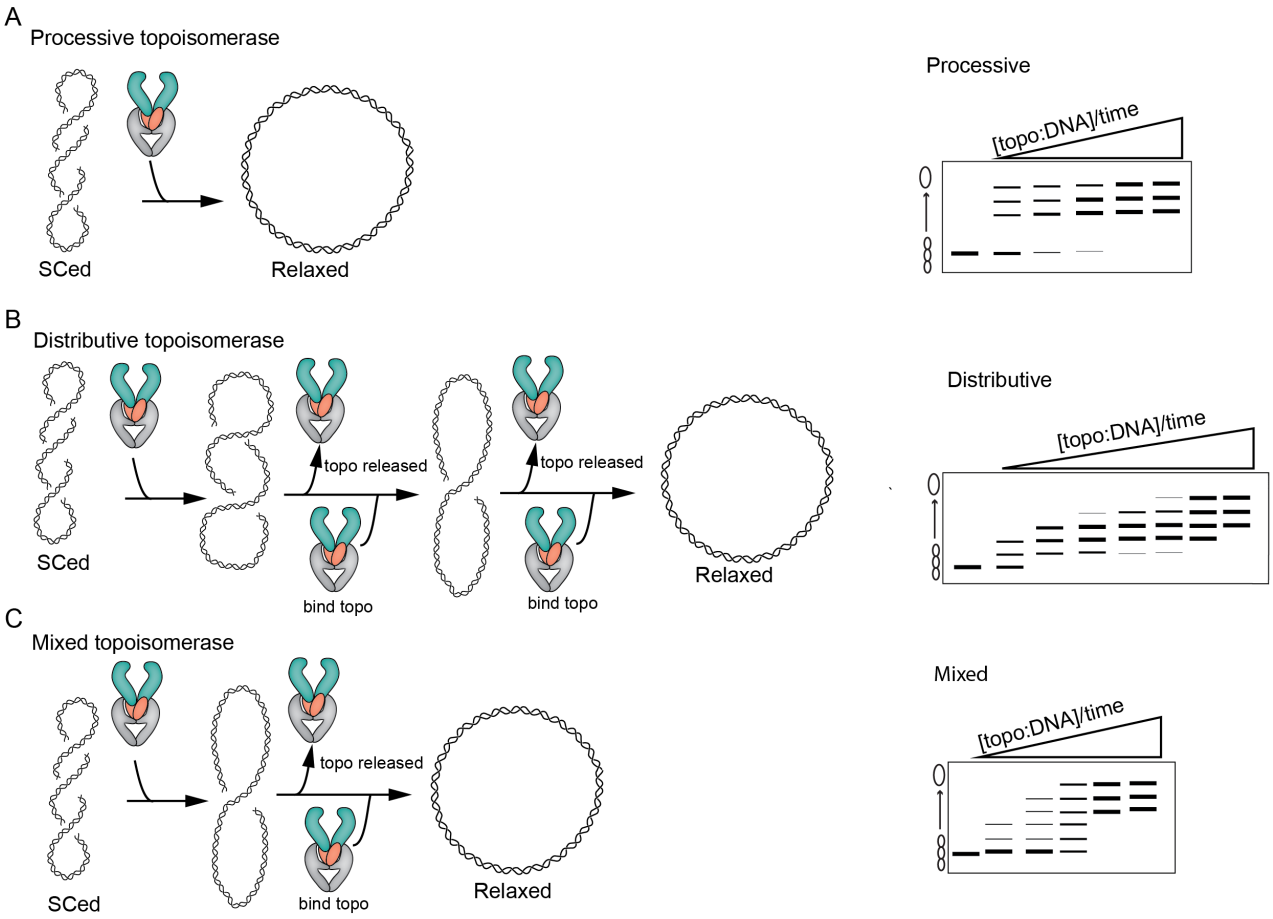

Figure S2.3. Consideration of topoisomerase processivity and distributivity. To observe processivity defects, relaxation experiments are performed at low ionic strength (to prevent rapid dissociation from DNA) and at substoichiometric enzyme-to-DNA concentrations. These conditions favor one topoisomerase binding and working on each DNA in the solution before falling off to bind and act on another DNA. Panels show schematics of processive versus distributive activity. **A**) Highly processive topoisomerases are typified by the conversion of supercoiled substrate into fully relaxed topoisomers with few or no intermediate topoisomers appearing between the two extremes. **B**) If a topoisomerase is highly distributive, the supercoiled substrate initially shifts to a slightly less supercoiled distribution, which moves as a population through all the intermediate topoisomer states before eventually reaching the fully relaxed topoisomer distribution. **C**) In some instances, the topoisomerases can display a blend of moderately distributive behavior, which results in a ladder of topoisomers extending from the supercoiled to the fully relaxed species before the plasmid is fully relaxed.

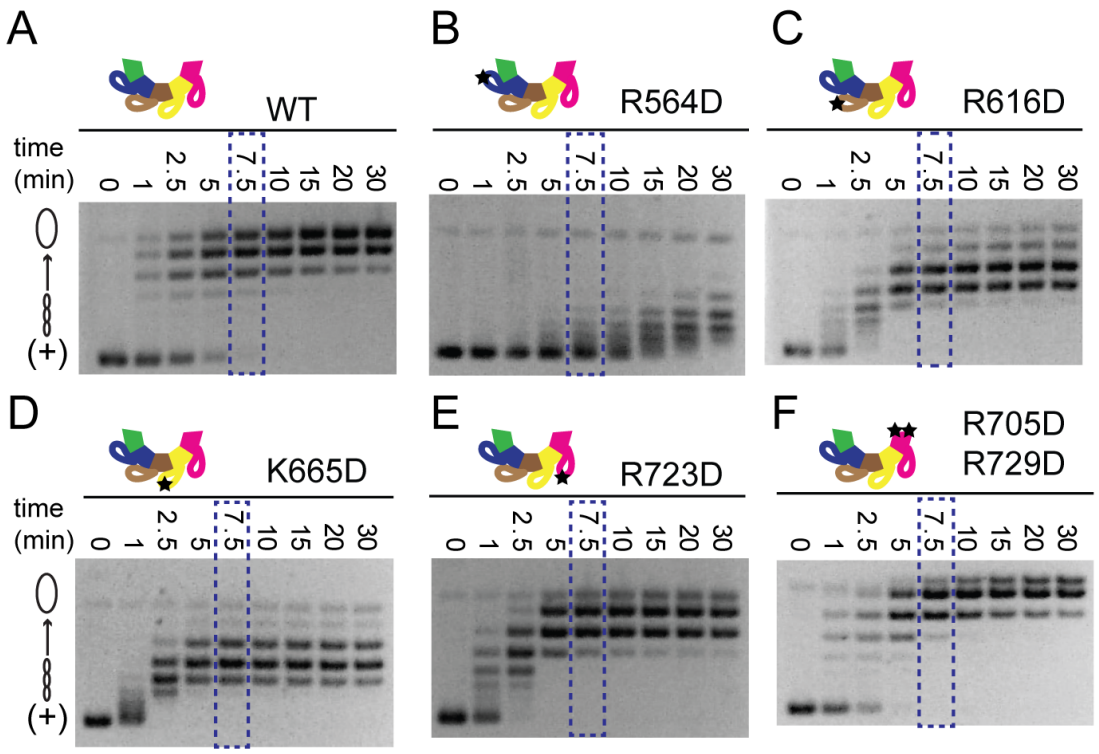

Figure 2.3. Rate of positive-supercoil relaxation by WT and mutant topo IVs. The constructs assayed are shown in each panel. Assays contained one topo IV holoenzyme for every 50 positively-supercoiled plasmid molecules. Samples were quenched at the time points indicated above each gel. The blue box corresponds to the time at which WT topo IV removed all positive supercoils and achieved its final topoisomer distribution and is shown for reference. Topoisomer species are graphically illustrated on the left side of the gels.

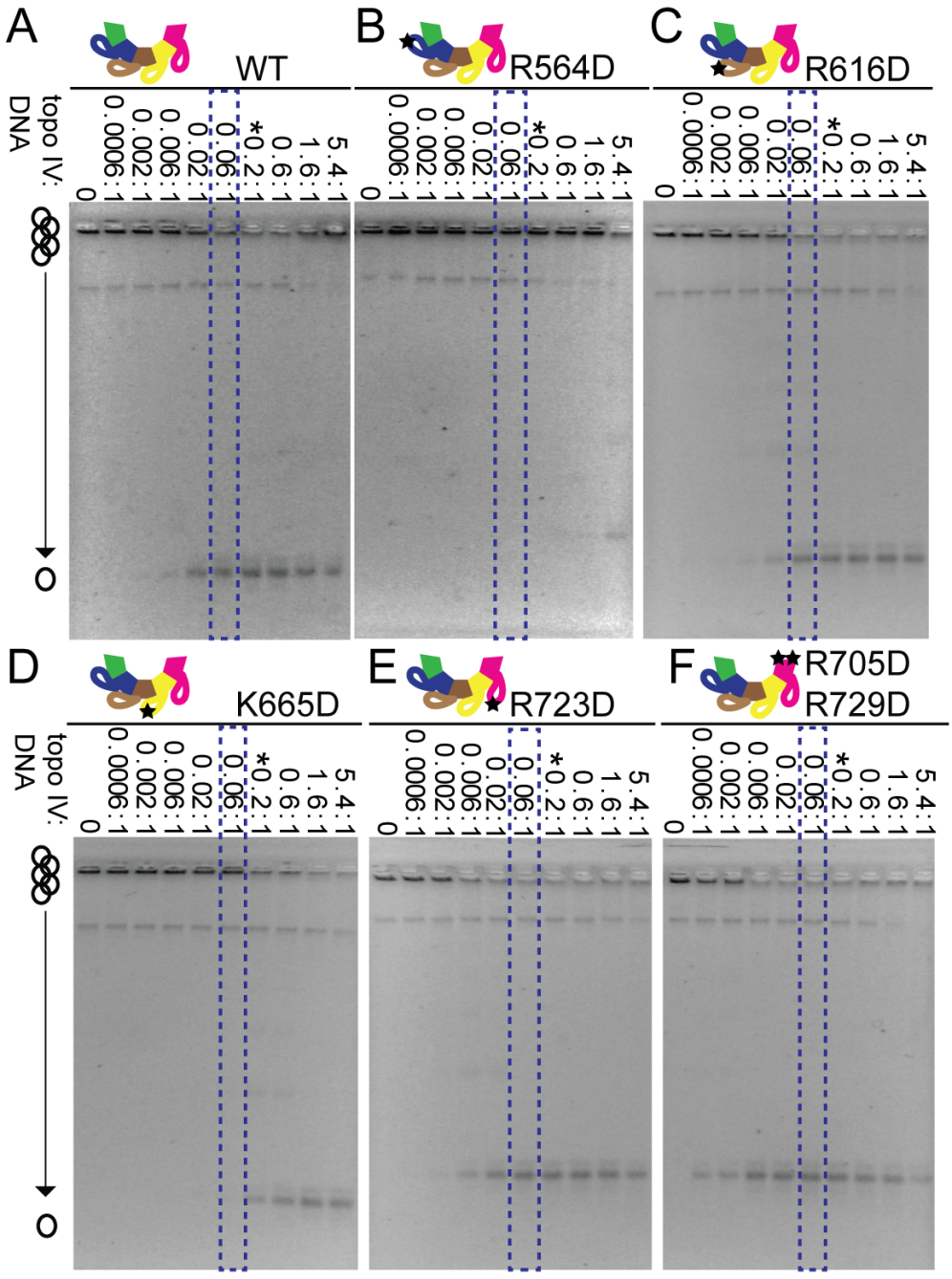

Figure 2.4. General activity of WT and mutant topo IVs on kDNA.
The constructs assayed are shown in each panel. Each assay proceeded for 10 minutes prior to quenching and contained 9.2nM of kDNA and various concentrations of each topo IV construct (0.005nM-50nM), with the ratio of topo IV to DNA indicated above each gel. On the left of each gel, a schematic of the catenated substrate trapped in the wells and the released mini-circles. Blue boxes correspond to the enzyme concentration at which WT topo IV appears to have removed a majority of the catenanes from the kDNA substrate. The asterisk above each gel indicates the concentration at which each topo IV construct was used in time course experiments (**Figure 2.5**).

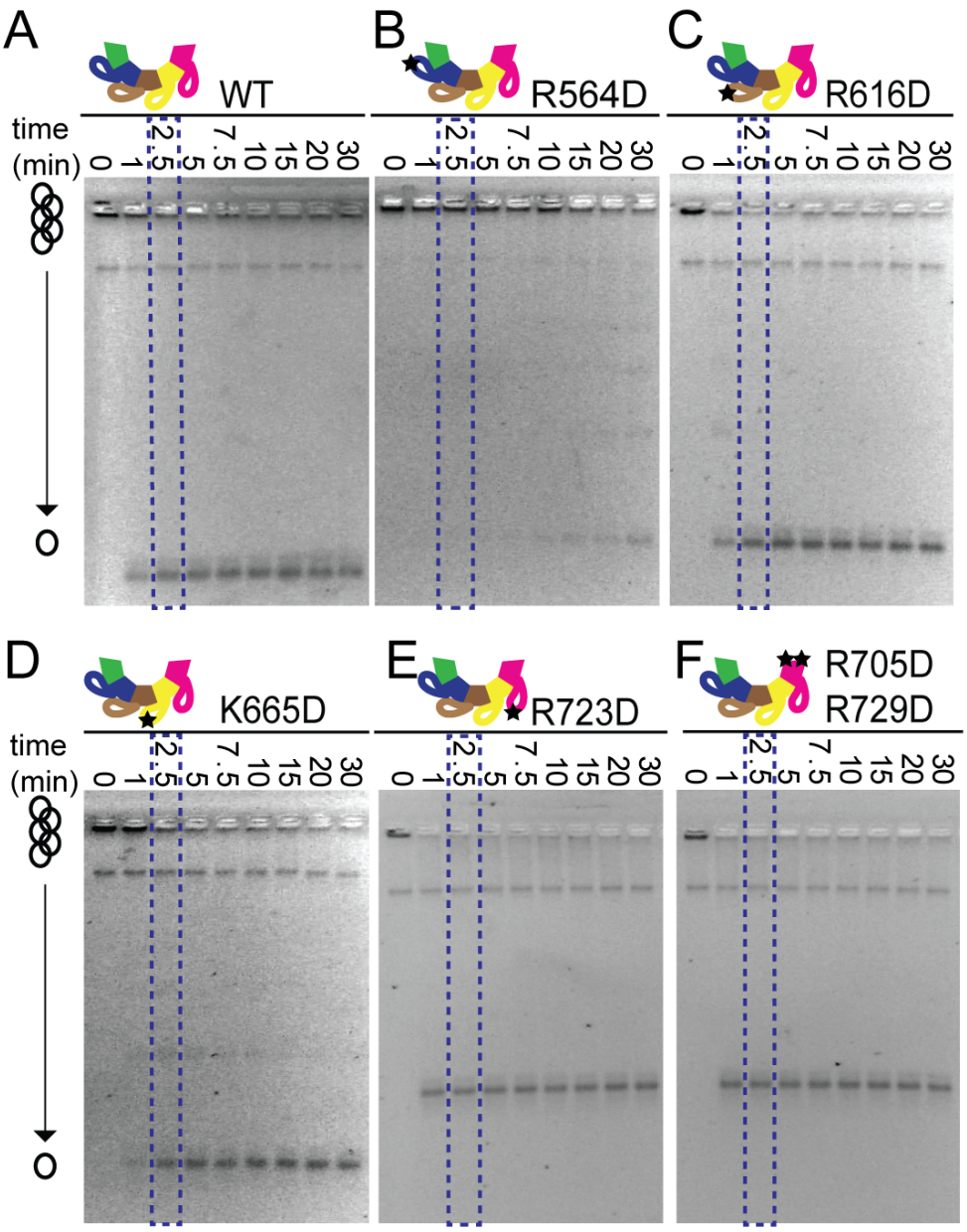

Figure 2.5. Rate of kDNA resolution by WT and mutant topo IVs.
The constructs assayed are shown in each panel. Assays contained approximately 1 topo IV holoenzyme for every 5 kDNA minicircles. Samples were quenched at the time points indicated above each gel. The blue box corresponds to the time at which the WT topo IV enzyme appeared to have removed a majority of the catenanes. Illustrated on the left side of each gel is a schematic of the catenated substrate trapped in the wells and the released mini-circles.

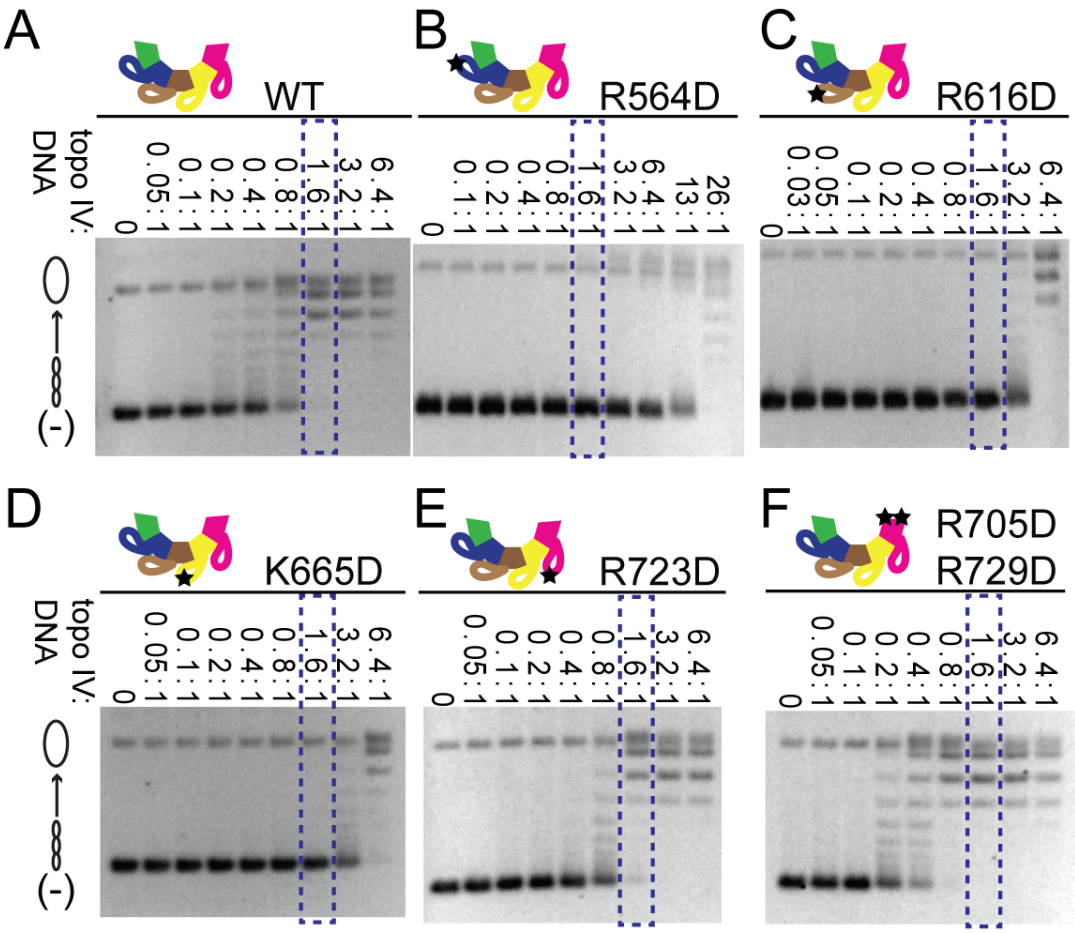

Figure 2.6. General activity of WT and mutant topo IVs on negatively-supercoiled DNA.

The constructs assayed are shown in each panel. Each assay proceeded for 10 minutes prior to quenching and contained 7.9nM of a negatively-supercoiled plasmid and various concentrations of each topo IV construct (0.4nM-50nM). The ratio of topo IV to DNA indicated above each gel. A schematic of the topoisomer distribution is illustrated on the left side of the gels. Blue boxes correspond to the enzyme concentration at which WT topo IV removes all negative-supercoils, and reaches its final topoisomer distribution.

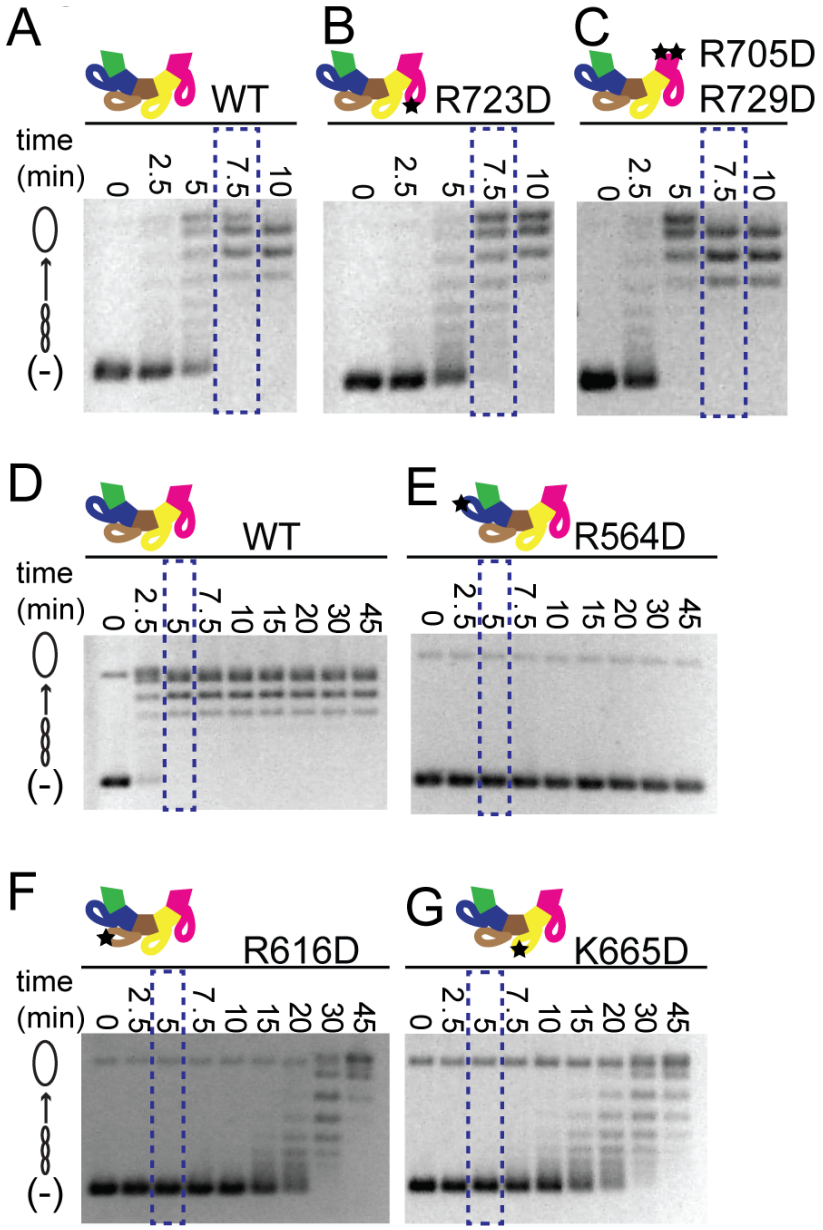

Figure 2.7. Rate of negative-supercoil relaxation by WT and mutant topo IVs. The constructs assayed are shown in each panel. Panels **A-C**: 5nM of WT or mutant topo IV was incubated with 7.9nM of negatively-supercoiled plasmid. Panels **D-G**: 10nM of WT or mutant topo IV was incubated with 7.9nM of negatively-supercoiled plasmid. Samples were quenched at the time points indicated above each gel. The blue box corresponds to the time at which the WT topo IV enzyme removed all negative supercoils and achieved its final topoisomer distribution. Topoisomer species are graphically illustrated on the left side of the gels.

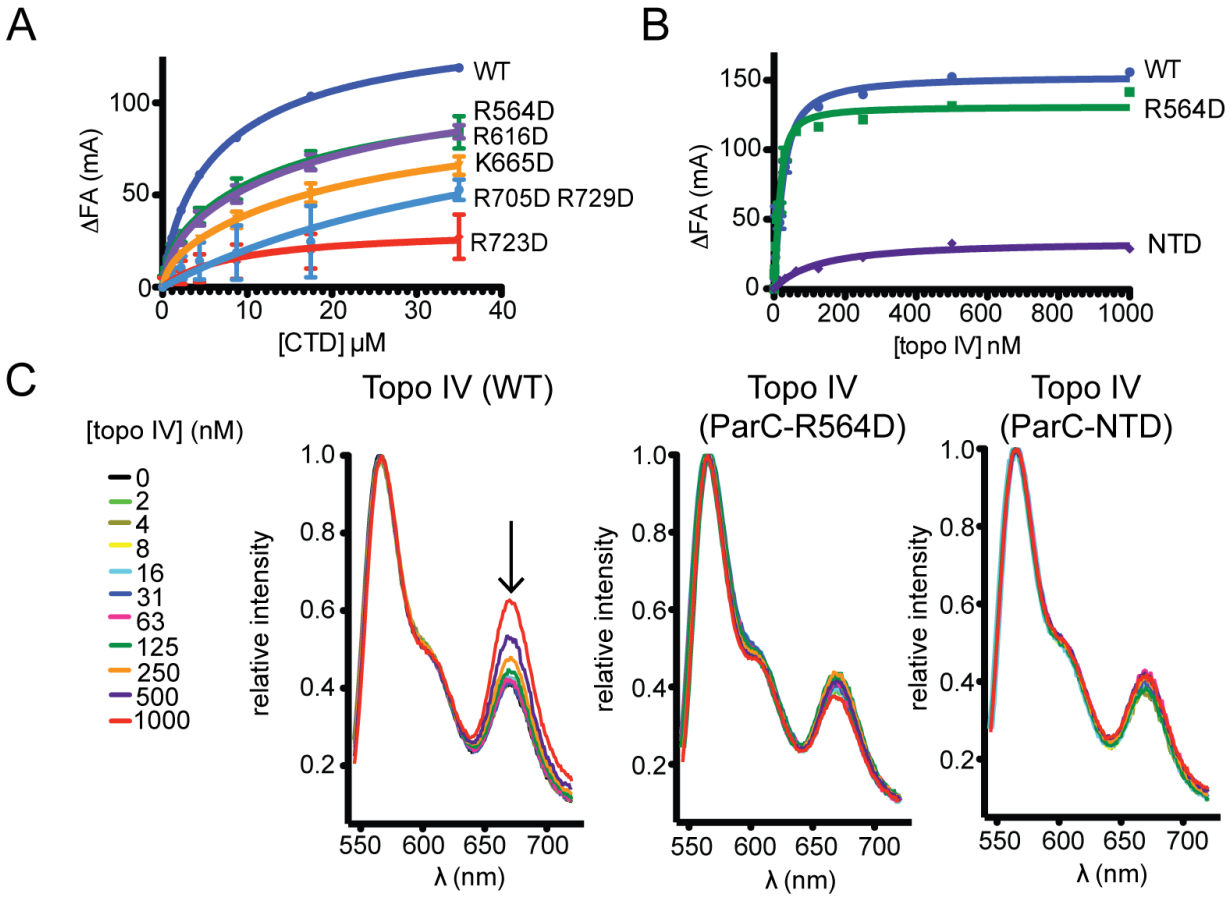

Figure 2.8. DNA binding by the ParC CTD and DNA binding and bending by topo IV.

A DNA binding by WT and mutant MBP-ParC CTD constructs. MBP-ParC CTD was titrated against 20nM of a fluorescein labeled 20mer duplex oligonucleotide, and DNA binding measured as a function of change in fluorescence anisotropy (ΔFA), as measured in millianisotropy units (mA). Error bars correspond to the standard deviation between three replicates. Since the MBP-ParC CTD never achieves fully saturated binding isotherm, only relative dissociation constants can be obtained from this assay ($K_{d,app}$ WT ~5μM; R564D ~13μM; R616D ~14μM; K665D ~26μM; R723D ~113μM; R705D/R729D ~56μM).

B DNA binding by WT topo IV, Arg564Asp ParC topo IV, and NTD-ParC topo IV. Topo IV was titrated against 20nM of a fluorescein labeled 45mer duplex oligonucleotide, and DNA binding was measured as a function of change in fluorescence anisotropy (ΔFA), as measured in millianisotropy units (mA). The $K_{d,app}$ of WT topo IV is 25±5 nM and of R564D topo IV is 15±3nM.

C DNA bending by WT topo IV, Arg564Asp ParC topo IV, and NTD-ParC topo IV. Topo IV was titrated against 20nM of a 45mer duplex, labeled with Cy3 and Cy5. Bending of the oligonucleotide is observed as a change in the relative intensity of the emission spectra of Cy5 (545-720 nm) after excitation of the Cy3 label at 530nm (arrow).

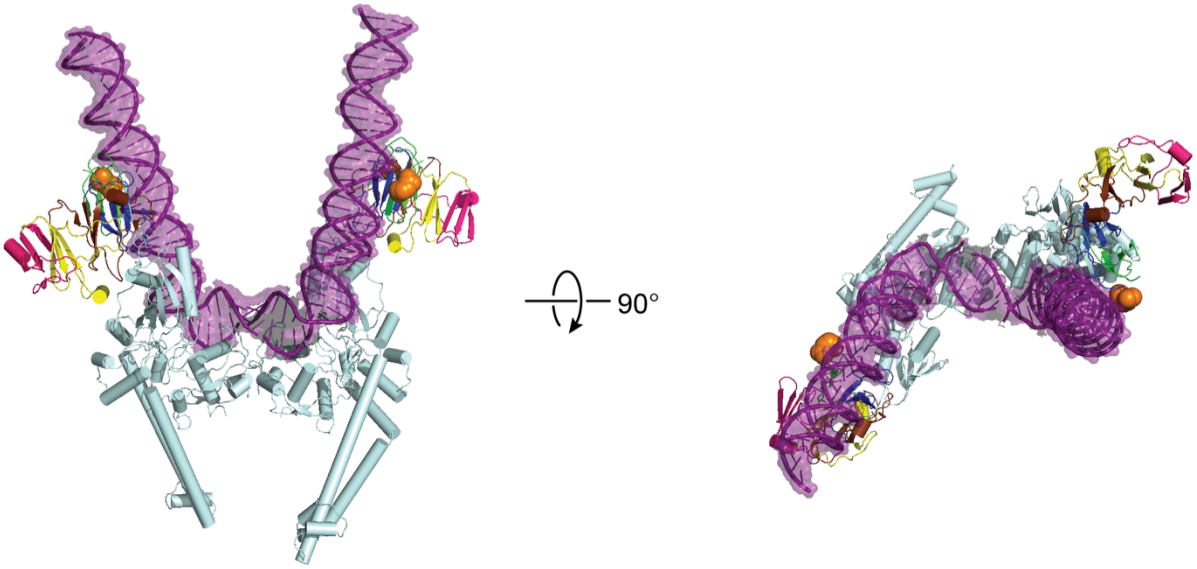

Figure S2.4. Model of G-segment DNA bound to *E. coli* ParC dimer.
The ParC dimer crystal structure (cyan) (PDB id: 1ZVU) was aligned with the yeast topo II enzyme bound to G-segment DNA (2RGR) (purple). The model shows how a G-segment might interact with the CTD of ParC. Residue Arg564 is colored orange and is drawn in sphere representation.

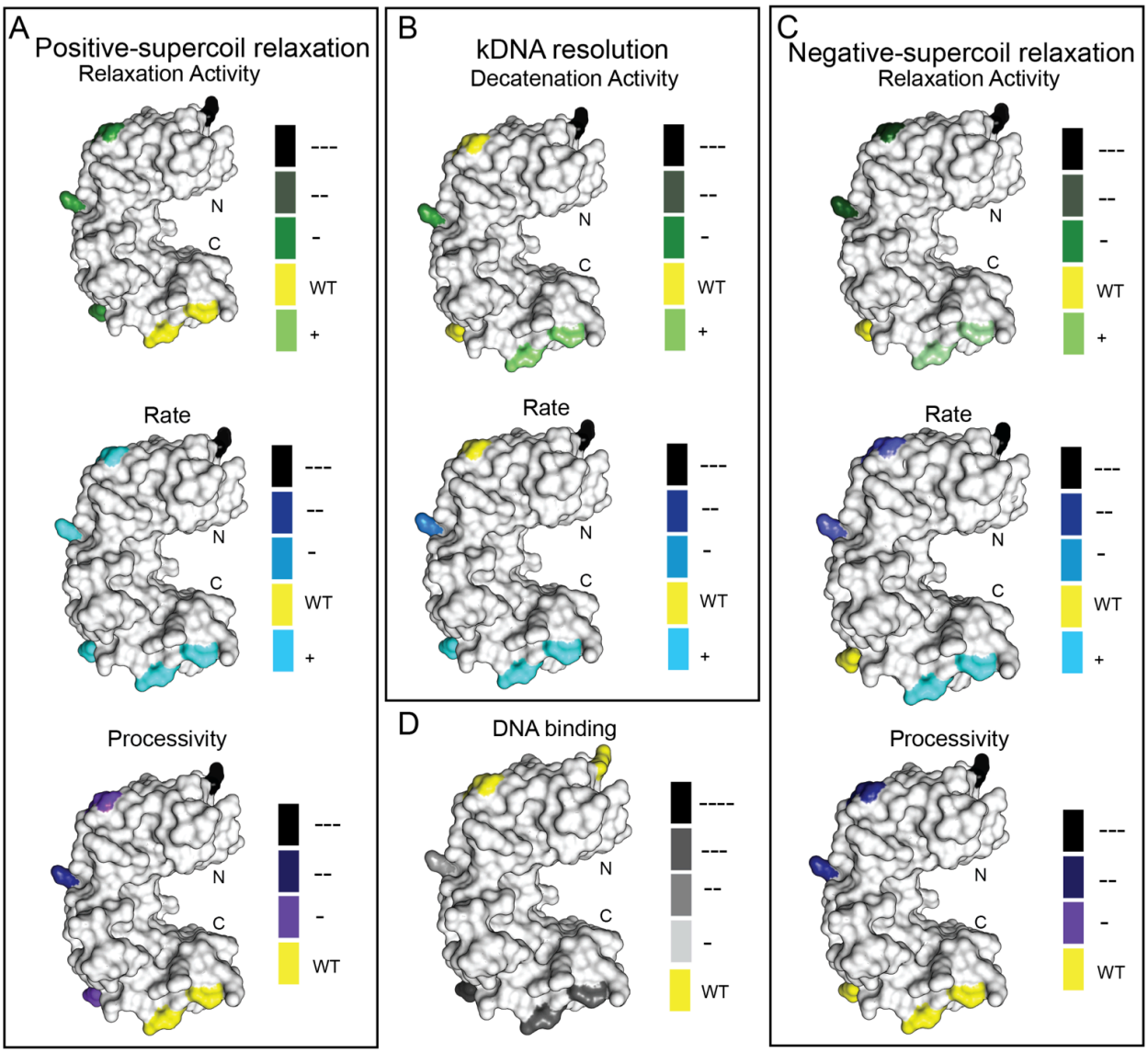

Figure 2.9. Schematic of ParC CTD activities according to residue.
The ParC CTD surface is painted according to various functional parameters (general activity, rate, and processivity) on specific substrates. Panel **A**, positively-supercoiled DNA; **B**, kDNA; **C**, negatively-supercoiled DNA. Panel **D** shows a representative CTD highlighting the effects of mutations on ParC CTD DNA binding. A color key for each activity is found on the right of each CTD.

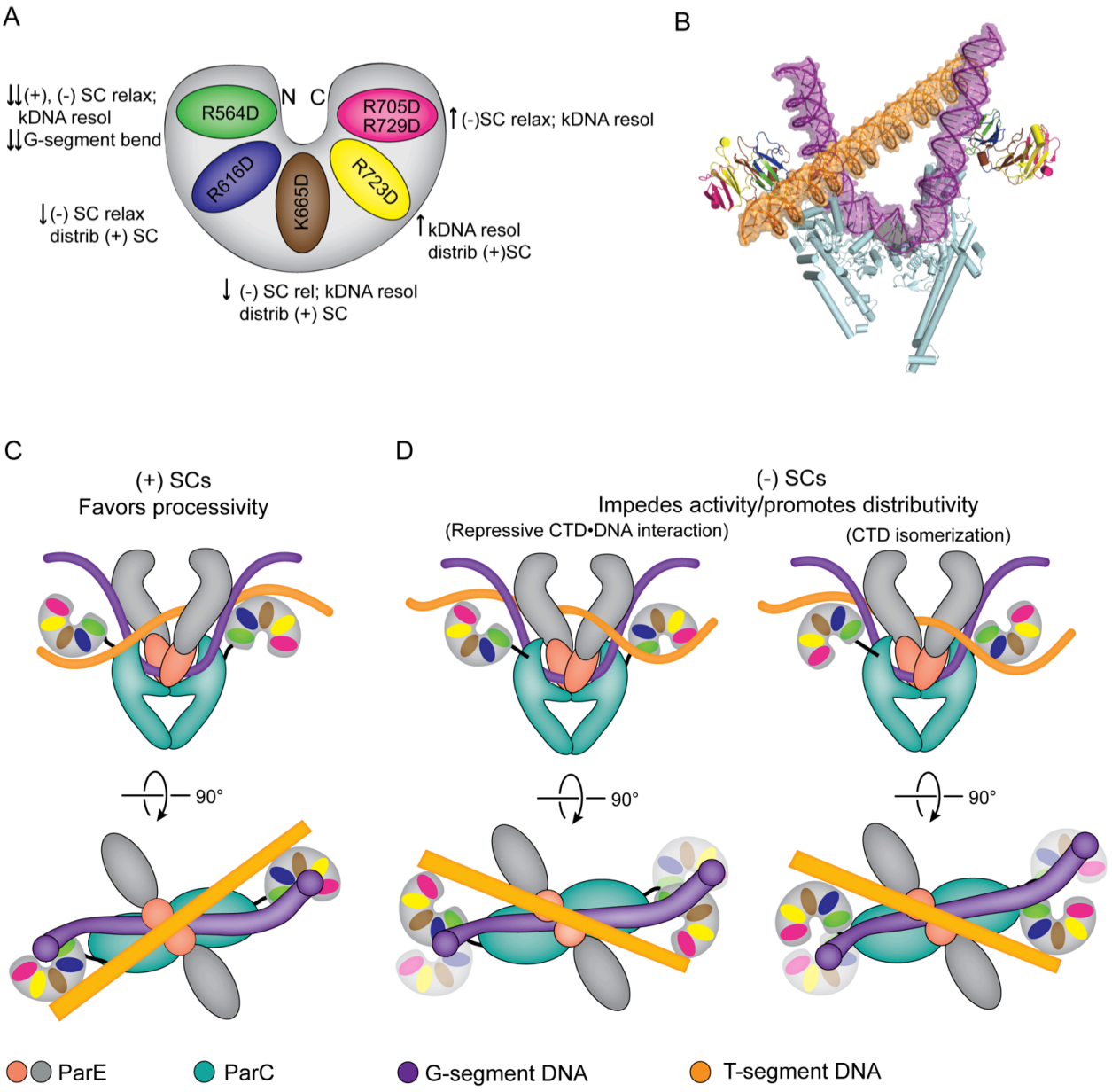

Figure 2.10. The ParC CTD is a DNA topology discrimination element.
A Cartoon summary of the effects resulting from mutating different blades of the ParC CTD. Down arrows indicate that the mutations inhibit (down arrow) topo IV activity on specific substrates, up arrows indicate a stimulating effect. Abbreviations: SC - supercoiled; resol - resolution; distrib. - distributive; relax -relaxation; (+) - positively; (-) - negatively.
B Crystal structure of the ParC dimer (PDB id: 1ZVU) with G-segment DNA (purple) (PDB id: 2RGR) docked into the active site and a T-segment (orange) DNA modeled for perspective.

C Model for topo IV's potential interactions with positively-supercoiled DNA substrates, front and top view. The ParC CTD and the DNA are colored as in panels A and B. The ParC NTD is colored cyan. The N-terminal domain of ParE is colored grey, and the DNA binding C-terminal TOPRIM domain is colored red. DNA is shown associating with surfaces required for processivity and overall enzyme activity.
D Model for topo IV's interactions with negatively-supercoiled DNA substrates, front and top view. A non-productive complex between the fifth blade of the ParC CTD and the T-segment DNA could form on negatively-supercoiled substrate (*left panel*) if the ParC CTDs remain in same rotational orientation as in panel C (illustrated as washed out CTDs), but were to shift positionally away from a subdomain on the ParC NTD known as the tower. To engage the T-segment of a negatively-supercoiled DNA in a catalytically competent manner (*right panel*), the ParC CTD would need to rotate by 180˚ about a flexible linker.

Chapter 3-Structural Basis for the MukB·topoisomerase IV Interaction and its Functional Implications *in vivo*

(Portions of this chapter reproduced from: Vos, SM, Stewart NK, Oakley, MG, and Berger, JM (2013) *The EMBO Journal* **32**, 2950-2962)

INTRODUCTION

Appropriate coordination of DNA replication and chromosome segregation is critical to the maintenance of genetic integrity (Hartwell & Weinert, 1989; Hiraga et al, 1989; Kato et al, 1988; Uhlmann & Nasmyth, 1998; Weinert et al, 1994). In bacteria, replication and chromosome partitioning occur concurrently as a means to apportion progeny with the proper amount of genetic material (Bates & Kleckner, 2005; Joshi et al, 2011; Nielsen et al, 2006; Viollier et al, 2004; Wang et al, 2006c). During replication and segregation, cellular machineries must confront certain physical challenges that arise from DNA's inherently long, intertwined structure. For example, replisome progression generates positive supercoils in front of the advancing fork, as well as precatenanes between newly-replicated sisters (Hiasa & Marians, 1996a; Khodursky et al, 2000; Peter et al, 1998; Postow et al, 2001a; Sogo et al, 1999). Failure to adequately remove replication-dependent supercoils and precatenanes can have significant consequences for the cell, resulting in incomplete DNA replication and improper DNA segregation (Baxter & Diffley, 2008b; Bermejo et al, 2007; Fachinetti et al, 2010; Hardy et al, 2004; Kato et al, 1990; Postow et al, 2001b; Sogo et al, 1999). Deficiencies in chromosome condensation similarly can produce cells with segregation defects, resulting in a high percentage of annucleate cells (Graumann, 2000; Hirano, 2012; Kato et al, 1990; Niki et al, 1991; Wang et al, 2006a).

In Eubacteria, multiple factors aid with accurate condensation and partitioning (Boles et al, 1990; Hardy et al, 2004; Luijsterburg et al, 2008). For example, supercoiling allows close packing of DNA helices that reduces chromosomal volume (Boles et al, 1990; Postow et al, 2004). Proteinaceous factors such as nucleoid-associated proteins (NAPs), topoisomerases, and SMC (structural maintenance of chromosomes) proteins play a similarly key role (Hardy et al, 2004; Luijsterburg et al, 2008). In *E. coli*, topoisomerase (topo) IV uses an ATP-dependent DNA breakage, passage, and rejoining mechanism that can resolve both positive supercoils and catenated DNA structures (Hiasa & Marians, 1996a; Kato et al, 1990; Khodursky et al, 2000; Peng & Marians, 1993b; Peng & Marians, 1993c; Zechiedrich & Cozzarelli, 1995). The *E. coli* SMC homolog, MukB, likewise can effect topological transformations in DNA, primarily by altering DNA writhe (Cui et al, 2008; Petrushenko et al, 2006a).

Recent studies have shown that MukB and topo IV interact physically and that MukB can stimulate the ability of topo IV to relax negatively-supercoiled DNA (Hayama et al, 2013; Hayama & Marians, 2010; Li et al, 2010b). On its own, topo IV operates as a heterotetramer containing two copies of ParE, the ATPase subunit of the enzyme, and two copies of ParC, which binds and cleaves DNA (Kato et al, 1990; Kato et al, 1992; Peng & Marians, 1993c). By comparison, MukB consists of two globular domains – an

ABC-ATPase “head” region and an internal “hinge” element – linked by 50 nm long antiparallel coiled-coil arms (Ku et al, 2009; Li et al, 2010a; Melby et al, 1998; Woo et al, 2009). The interaction between MukB and topo IV has been mapped to the MukB hinge (Li et al, 2010b), which can form a stable dimer (Li et al, 2010a; Li et al, 2009), and the ParC C-terminal domain (CTD) (Hayama & Marians, 2010; Li et al, 2010b), which is monomeric when liberated from its associated N-terminal region (Corbett et al, 2005) (**Fig 3.1A**). At present, the mechanism by which MukB alters topo IV activity, along with the physical interactions that promote complex formation, have not been established. The extent to which topo IV’s association with MukB, as opposed to its strand-passage activity, helps support cell viability is similarly unclear.

To better understand the nature and functional consequences of the MukB-topo IV interaction, we determined the crystal structure of the MukB hinge in complex with the ParC CTD. The structure shows that the CTD and the hinge form a symmetric complex in which a negatively-charged outer surface of MukB associates with a positively-charged patch on the perimeter of the CTD. We find that the hinge alone can specifically stimulate topo IV activity on negatively-supercoiled substrates, and that this stimulation arises through competition for a strong DNA-binding surface on the CTD that otherwise represses the relaxation of negatively-supercoiled DNA. Curiously, the structure of the complex reveals that the mutation responsible for thermal sensitivity in *E. coli* C600*parc1215* cells maps to the surface of the CTD occupied by MukB; complementation studies establish that the strand-passage and MukB-binding functions of topo IV are independent but additive activities that work together to promote cell growth. Geometric considerations of the structure obtained here suggest that topo IV and MukB can assemble into oligomeric arrays, the formation of which may be useful for resolving newly-replicated daughter chromosomes.

RESULTS AND DISCUSSION

Structural characterization of MukB-ParC Interaction

To identify a minimal interaction complex between topo IV and MukB for crystallographic studies, we cloned, purified, and performed pull-down assays with various hinge constructs and the isolated ParC CTD (497-752). The CTD bound to all hinge variants tested, but did not associate with the Ni^{2+} beads or with the coiled-coil arms alone, indicating that the ParC CTD binds directly to the globular core of the hinge region (not shown). The smallest hinge construct identified by this approach (residues 645-804, corresponding to a fragment previously analyzed crystallographically (Ku et al, 2009)) was subsequently used for structural studies.

For screening crystallization conditions, the minimized MukB hinge and the ParC CTD were individually overexpressed and purified from *E. coli*, and then mixed immediately before setting trays. Co-crystals grew in the space group $P2_12_12_1$ and diffracted to 2.3 Å resolution. The structure was solved using a combination of molecular replacement and single-wavelength anomalous dispersion for phasing (**Figs 3.1B, 3.2A**). The final model, which includes residues 497/498-742 of ParC and residues 645-801/804 of MukB, was refined to an R_{work}/R_{free} of 20.4%/24.6% and shows good stereochemistry (**Table 3.1, Materials and Methods**).

Previous studies of the MukB•ParC interaction indicated that two ParC CTDs could bind a single dimer of the MukB hinge (Li et al, 2010b). This binding stoichiometry is recapitulated in the asymmetric unit of the hinge•CTD co-crystals, which contains a single heterotetrameric complex (**Fig 3.1B**). The *E. coli* ParC CTD adopts a crescent-shaped structure composed of five repeating Greek-key folds, or "blades" (**Fig 3.1**). In our structure, the fifth blade of the CTD – the element furthest from the N-terminus of the region – interacts with the hinge. The interface between the hinge and the CTD is small, burying a total surface area of ~690$Å^2$ per protomer. The residues mediating the interaction lie predominantly on loops that connect adjoining secondary structural elements (**Fig 3.2A**), and are highly conserved only in γ-proteobacterial MukB and ParC orthologs (**Fig S3.1**). Surface electrostatic-potential maps show that the negatively-charged hinge of MukB associates with a portion of the positively-charged strip that encircles the outer surface of the ParC CTD (**Fig 3.2B**); these interactions are responsible for the majority of the contacts between the two domains. In particular, a positively-charged string of residues on the CTD comprising residues Lys704, Arg705, and Lys706 interacts with Glu688/Asp691, Asp692/Asp746, and Asp745, respectively, on MukB. Two additional sets of ionic interactions in the structure include crosstalk between Asp692 of MukB and Arg733 of ParC, and between Arg729 of the CTD and hinge residues Glu696, Asp697, and Glu753. Only one hydrophobic residue, Phe701 of MukB, participates in the hinge-CTD interface, where it is coordinated by cation-pi interactions with Arg705 and Arg729 of ParC.

Residues in the MukB•ParC interface are necessary for mutual interactions

The structure of the hinge•CTD complex accounts for previous mutagenesis efforts implicating Glu688, Asp692, Asp697, Asp745, and Glu753 of MukB, and Arg705 and Arg729 of ParC, in the interaction of the two proteins (Hayama et al, 2013; Hayama &

Marians, 2010; Li et al, 2010b). To further probe the contacts seen in the structure, we designed, purified, and performed pull-down assays using other mutations that map to the MukB•ParC interface (**Figs S3.2-S3.3**). In these experiments, a CTD construct bearing an N-terminal, His_6-MBP tag was incubated with Ni^{2+} beads in the presence or absence of the core region of the hinge that bears a portion of the coiled-coil arms (residues 566-863). The wild-type hinge associated with the MBP-tagged CTD but did not associate with the Ni^{2+} beads (**Fig S3.3A**). A CTD double-mutant, Arg705Asp/Arg729Asp (which resembles a previously characterized CTD mutant, Arg705Glu/Arg729Ala (Hayama & Marians, 2010)), likewise behaved as expected, failing to pull-down the MukB hinge. Similar to the MukB Asp692Ala mutation studied previously (Li et al, 2010b), a more severe single point mutant in the hinge, Asp692Phe, again only partially abrogated the interaction with the CTD (**Fig S3.3B**); however, when two additional MukB mutations were added to this substitution (Asp746Arg and Glu753Arg, which should disrupt interactions with residues Arg705, Arg729, and Arg733 of ParC), the hinge completely failed to associate with the MBP-tagged CTD. Together with the original mutagenesis studies (Hayama et al, 2013; Hayama & Marians, 2010; Li et al, 2010b), these data confirm that the residues implicated by our crystal structure are essential for forming the MukB•ParC binding interface.

MukB antagonizes DNA binding by the ParC CTD

The ParC CTD is a DNA-binding domain that helps topo IV differentiate between positively and negatively-supercoiled substrates (Corbett et al, 2005; Vos et al, 2013). The region of the CTD responsible for these activities has been postulated to rely on a positively-charged strip that encircles the CTD (**Fig 3.2B**)(Corbett et al, 2005; Vos et al, 2013). The isolated CTD of ParC has been shown to bind duplex DNA somewhat modestly, with an apparent dissociation constant of ~1μM (Corbett et al, 2004). Because the structure of the complex reported here shows that MukB binds to the outer surface of the ParC CTD, we reasoned that its effect on the activity of topo IV activity could arise by an ability to modulate DNA binding by the ParC CTD directly.

In **Chapter 2**, we found that the behavior of the isolated ParC CTD, which is prone to aggregate over time, could be improved by leaving the domain fused to the MBP tag used for expression and our pull-down assays. To determine how well the MBP-tagged CTD binds DNA, we carried out fluorescence anisotropy experiments using a fluorescein-labeled 20mer duplex oligonucleotide (**Fig 3.3A**). This analysis showed that the MBP-ParC CTD construct binds DNA with an apparent affinity similar to that reported previously for the isolated domain ($K_{d,app} \cong$ 1-2μM) (Corbett et al, 2004). Hence, the MBP fusion does not appear to compromise DNA binding in and of itself.

We next tested whether MukB affects DNA binding by the ParC CTD. Unlike other SMCs, whose hinges can associate with both single- and double-stranded DNA (Chiu et al, 2004; Griese & Hopfner, 2010; Griese et al, 2010; Hirano & Hirano, 2002; Hirano & Hirano, 2006), MukB binds DNA with its ABC-ATPase head domain but not with its hinge (Hayama et al, 2013; Ku et al, 2009; Li et al, 2010a; Woo et al, 2009). Consistent with these data, no association was observed by fluorescence anisotropy when the hinge was incubated with the 20mer duplex DNA in the absence of the CTD (**Fig S3.4A**). By contrast, the presence of the hinge significantly reduced DNA binding

by the MBP-tagged CTD in the same assay (**Fig 3.3A**). To confirm these results, we performed surface plasmon resonance experiments using a sensor chip coated with a biotinylated 20mer oligonucleotide of identical sequence to the one used in the fluorescence anisotropy experiments. DNA was pre-bound with the MBP-ParC CTD construct and then washed with solutions containing a constant concentration of the MBP-ParC CTD (250nM) and various amounts of the MukB hinge. Addition of the MukB hinge resulted in a decrease in response units in a dose-dependent manner (**Fig 3.3B**), suggesting that as with the fluorescence anisotropy results, the MukB hinge competes directly with DNA for binding the ParC CTD.

We next tested whether our MukB hinge mutants could interfere with DNA binding by the CTD. Similar to results obtained for the wild-type hinge, we found that a hinge construct containing the single Asp692Phe substitution, which only weakens the interaction between the two proteins, modestly diminished DNA binding by the CTD (**Fig 3.3A**). By contrast, the triply-substituted hinge (Asp692Phe/Asp746Arg/Glu753Arg), which does not bind to the CTD, did not interfere appreciably with the CTD-DNA association (**Fig 3.3A**). Interestingly, while conducting these studies, we unexpectedly found that the Arg705Asp/Arg729Asp double substitution in the CTD, which maps to the MukB binding site on ParC, is severely compromised for binding DNA, even when MukB is absent (**Fig 3.3C**). In context of the topo IV holoenzyme, the Arg705Asp/Arg729Asp double substitution has a negligible effect on the overall binding of a 42-mer duplex oligonucleotide (~2-fold decrease in binding affinity, **Fig S3.4C**), consistent with recent work indicating that this region of the CTD transiently associates with T-segment DNA (Corbett et al, 2005; Vos et al, 2013). Overall, our results indicate that the MukB-binding interface overlaps with a strong DNA binding site on the ParC CTD, and that the MukB hinge specifically competes with DNA in associating with this surface.

To determine whether the MukB hinge specifically blocks DNA from binding to the CTD of ParC, we next performed DNA fluorescence anisotropy experiments using the analogous C-terminal region from the *E. coli* paralog of topo IV, gyrase. The construct chosen for this work (residues 531-853 of the corresponding GyrA subunit) lacks an autoinhibitory C-terminal tail (Tretter & Berger, 2012), thereby permitting the domain to robustly bind and wrap DNA on its own (Reece & Maxwell, 1991; Ruthenburg et al, 2005; Tretter & Berger, 2012). When the GyrA CTD (531-853) was incubated with the hinge, we observed little effect on DNA binding (**Fig 3.3D, Fig S3.4B,** $K_{d,\,app} > 100$ μM). This result demonstrates that the MukB hinge is specific for blocking DNA binding by the ParC CTD and not for impeding binding by bacterial type IIA topoisomerase CTDs in general.

The MukB hinge stimulates topo IV activity on negatively-supercoiled DNA

It has recently been observed that full-length MukB specifically stimulates the ability of topo IV to relax negatively-supercoiled, but not positively-supercoiled, plasmid substrates (Hayama et al, 2013). Full-length MukB is known to independently alter DNA supercoiling and condensation (Chen et al, 2008; Cui et al, 2008; Petrushenko et al, 2006a), and it has been suggested that MukB stimulates topo IV's activity, at least in part, by altering the topological state of the DNA through which both proteins associate. Evidence for this idea has derived from the observation that a MukB mutant, which can

no longer associate with DNA through its head regions, fails to enhance the relaxation of negatively-supercoiled plasmid substrates by topo IV (Hayama et al, 2013). However, it also has been found that the isolated MukB hinge, which lacks DNA binding activity, can stimulate negative-supercoil relaxation (Li et al, 2010b). This latter result has been interpreted as evidence that MukB might alter topo IV's activity directly.

To better distinguish how MukB impacts topo IV function, we used our structure and collection of mutants to reinvestigate the effects of the isolated MukB hinge on the wild-type topo IV holoenzyme. In designing these studies, we recognized that the MukB•ParC interaction is weak ($K_d \cong 0.5\mu M$) compared to the relative dissociation constants of topo IV and MukB for supercoiled DNA (which are low to subnanomolar) (Charvin et al, 2005; Li et al, 2010b; Petrushenko et al, 2006a); because of this difference, we reasoned that DNA might facilitate the co-association of MukB and topo IV at low protein concentrations, and that in the absence of DNA (or if MukB is unable to bind DNA), higher concentrations would be needed to promote complex formation. To ensure efficient complex formation, positive- and negative-supercoil relaxation experiments were therefore performed in the presence of topo IV and different amounts of the MukB hinge using a topoisomerase concentration (500 nM) near the observed K_d for the hinge•CTD interaction. Since topo IV rapidly catalyzes strand passage events (~2-3/sec)(Charvin et al, 2003; Stone et al, 2003), and is ~20-fold more active on positively-supercoiled substrates than negatively-supercoiled substrates (Charvin et al, 2003; Crisona et al, 2000; Neuman et al, 2009; Stone et al, 2003), both high plasmid concentrations and low temperature were used to slow down the reactions so that experiments conducted in the absence of MukB would only partially go to completion within a measureable timeframe.

In analyzing DNA topoisomers, native-agarose gel electrophoresis is frequently employed to resolve slowly-migrating relaxed plasmid molecules from more rapidly moving supercoiled species. When the products of the topo IV/MukB hinge reactions were monitored by this approach, we found that the isolated hinge domain was able stimulate the relaxation of negatively-supercoiled DNA, with stimulation starting at near-stoichiometric ratios of topo IV and increasing as a function of hinge concentration in a dose-dependent manner (**Fig 3.4A**). Interestingly, the hinge did not stimulate the relaxation of positively-supercoiled DNA by topo IV (**Fig 3.4B, Fig S3.5**). This result indicates that the effect of the hinge on topo IV activity is specific for the handedness of the DNA substrate, a behavior recently reported by Marians and co-workers for full-length MukB (Hayama et al, 2013).

To investigate whether the stimulatory action of the hinge depended on the contacts seen in the crystal structure, we next performed topo IV relaxation experiments using our collection of MukB and ParC interface mutants. We found that the single $MukB^{D692F}$ hinge mutant weakly stimulated topo IV activity, and only at high molar excess (i.e., 160-fold or greater than topo IV) (**Fig 3.4C**). By contrast, the triple $MukB^{D692F/D746R/E753R}$ hinge mutant (which does not associate with the CTD, **Fig S3.3**) failed to stimulate the relaxation of negatively-supercoiled substrates at any of the measured concentrations (**Fig 3.4D**). Together, these data support the proposal that

binding of the MukB hinge to the ParC CTD can directly and specifically fine-tune the activity of topo IV on negatively-supercoiled DNA.

Because MukB appears to compete for a strong DNA binding surface on the CTD (**Fig 3.3C**), the effect of the hinge on topo IV suggested that the activity of the topoisomerase might be naturally repressed on negatively-supercoiled substrates. To test this idea, we examined the concentration-dependent and time-dependent activity of the ParC Arg705Asp/Arg729Asp double mutant compared to the wild-type enzyme. Analysis of the resultant data shows that the activity of the ParC CTD double mutant is elevated with respect to the native enzyme on negatively-supercoiled DNA (**Fig 3.5A**), but that these substitutions have no effect on topo IV function with positively-supercoiled substrates (**Fig 3.5B**). Interestingly, the extent to which the ParC mutations increase the rate of supercoil relaxation approximates the modest degree of stimulation promoted by the MukB hinge alone (~1.5-2-fold, **Fig 3.5C**). These results are consistent with recent findings from our lab showing that different surfaces of the topo IV CTD contribute non-equivalently to the relaxation of positively and negatively-supercoiled DNAs (Vos et al, 2013), and indicate that the MukB hinge exerts its topology-specific effects on topo IV function by binding to and masking an auto-repressive region.

The strand passage and MukB binding functions of topo IV serve distinct but additive roles in the cell

E. coli parC is an essential gene that was discovered in a screen for temperature-sensitive mutants that improperly partitioned sister chromosomes (*E. coli* C600*parC1215*) (Kato et al, 1990; Kato et al, 1988). The temperature sensitivity of the *E. coli* C600*parC1215* strain generally has been attributed to the loss of topo IV decatenation activity at the restrictive temperature (Nurse et al, 2003; Perez-Cheeks et al, 2012; Zechiedrich & Cozzarelli, 1995). However, during the course of our studies, we realized that the mutation responsible for the thermosensitivity of the *E. coli* C600*parC1215* strain, Gly725Asp (Kato et al, 1990), not only resides in the ParC CTD, but actually lies between two residues that bind MukB in our crystal structure (Arg705 and Arg729) (**Fig 3.2A**).

Because Gly725 does not map to a region of topo IV responsible for strand passage, the severe phenotypic consequences arising from its mutation to aspartate raised the question as to whether the topo IV-MukB interaction might play a separable but additive role with the cell's need for a potent DNA decatenase. To test this idea, we used complementation assays to interrogate the activity of topo IV mutations that would be expected to selectively compromise strand passage, MukB binding, or both. *E. coli* C600*parC1215* cells were first grown at 30˚C to mid-log phase, and then shifted to the restrictive temperature (42˚C). Aliquots were removed at various time-points after the shift, serially diluted (20-fold steps), and plated on both rich and minimal media; this scheme allowed us to first impose conditions of fast and slow growth, and then assess the extent to which cells adapted to the restrictive temperature before plating. C600*parC1215* cells bearing a control plasmid encoding the wild-type *parC*$^{+}$ gene were fully competent at both the permissive (30˚C) and restrictive temperatures (42˚C) on both types of growth media (**Figs 3.6, S3.6**). Conversely, cells transformed with the empty vector control were able to grow only at the permissive temperature and showed

no ability to adapt to non-permissive conditions. Together, these data show that the vectors and conditions used for the assay work as shown previously (Lavasani & Hiasa, 2001; Perez-Cheeks et al, 2012), and establish upper and lower limits on the extent of growth seen under complementing and non-complementing conditions.

We next assessed the ability of three different topo IV constructs to complement the C600*parC1215* strain, starting first with cells plated on rich media (**Figs 3.6A, S3.6A**). When transformed with a plasmid expressing the *parC*^{Y120F} allele, which ablates both the catalytic tyrosine and strand passage function of topo IV, cells showed diminished growth at the restrictive temperature, but were nonetheless viable. The *parC*$^{R705D/R729D}$ allele, which contains a disrupted MukB-binding locus, but does not impede topo IV relaxation activity, was also able to partially complement growth at 42˚C. By contrast, when provided with a plasmid that could express only the ParC N-terminal domain (NTD), a construct that both lacks the MukB-binding site entirely and that exhibits only 2-5% of the specific activity of wild-type topo IV (Corbett et al, 2005), cells responded as if they had been transformed with an empty vector, showing an essentially complete loss of growth at the restrictive temperature. Interestingly, when exposed to short, liquid-culture incubations for progressively longer periods of time, cells harboring either the *parC*^{Y120F} or *parC*$^{R705D/R729D}$ genes (but not the *parC*^{NTD} gene) began to lose their temperature sensitivity; sequencing confirmed that neither the plasmids nor the chromosomal loci had reverted in these cells (**Fig S3.6**). Similar phenotypic effects were seen when cells were grown on minimal media (**Fig 3.6B, S3.6**), although the *parC*$^{R705D/R729D}$ allele proved more able to complement the temperature sensitive strain, a result consistent with prior observations showing that MukB is not required for viability when cells are grown under slowly-proliferative conditions (Champion & Higgins, 2007; Niki et al, 1991).

Together, the ParC CTD appears to be required for overall cell viability. Moreover, while the MukB•ParC interaction is not essential in a strict sense, it aids the fitness of rapidly growing cells in a manner that is additive with a need for robust strand passage activity by topo IV. Based on the available biochemical data provided here and by others (Hayama et al, 2013; Hayama & Marians, 2010), it seems likely that an inability to interact with MukB underlies the effect of the Arg705Asp/Arg729Asp CTD mutant *in vivo*. This information, together with the observed partial complementation conferred by the *parC*^{Y120F} gene, in turn suggests that the mutant ParC protein is particularly defective in the C600*parC1215* strain because of a global stability defect in its CTD that leads to both a loss of MukB binding and a diminution of topoisomerase activity. Consistent with this hypothesis, attempts to purify a Gly725Asp ParC mutant have proven unsuccessful due to low expression and aggregation of the protein.

Prospective role of the topo IV•MukB interaction in vivo

Given its role as a key decatenase in *E. coli*, the finding that the strand passage activity *per se* of topo IV is not absolutely essential for cell viability may seem at first surprising. However, other topoisomerases, notably gyrase and topo III, can compensate for loss of topo IV *in vivo*. For example, overexpression of either topo III, a type IA topoisomerase capable of unlinking hemicatenanes (DiGate and Marians 1988; Hiasa, DiGate et al. 1994), or gyrase, a type IIA topoisomerase that negatively-supercoils DNA (Gellert et al,

1976), can complement *parC* or *parE* temperature-sensitive strains (Kato et al, 1992; Lopez et al, 2005; Nurse et al, 2003; Perez-Cheeks et al, 2012; Zechiedrich & Cozzarelli, 1995). By contrast, loss of topo III in the C600*parC1215* temperature sensitive strain results in severe chromosome segregation defects and a near-complete loss of viability at 25˚C, whereas conjoining a *Δtop3* allele with a *parE* temperature-sensitive strain gives rise to cells that exhibit segregation defects at 30˚C but are nonetheless capable of growth (Perez-Cheeks et al, 2012). These results suggest that, in addition to its ability to remove catenanes, the ability of ParC to specifically interact with MukB is one of the essential roles of topo IV. It may be that the phenotype exhibited by the *parE^{ts} Δtop3* strain is less severely compromised because cells still retain the ability to form a ParC•MukB complex even though they have lost their primary decatenase.

If the topo IV•MukB interaction is important to the cell, what purpose might it serve? MukB and topo IV are independently required for the appropriate segregation of sister chromosomes during and after DNA replication (Badrinarayanan et al, 2012a; Niki et al, 1991; Wang et al, 2008), but are not required to complete replicative strand synthesis *per se* (Danilova et al, 2007; Kato et al, 1990; Niki et al, 1991; Wang et al, 2008). The localization of topo IV to precatenanes is thought to aid in the rapid removal of the linkages between newly-replicated DNA strands (Wang et al, 2008); however, additional interactions between the enzyme and MukB could facilitate this process further. In this vein, it is instructive to consider the architecture of what a fully-intact topo IV•MukB complex might look like (**Fig 3.7B**). A typical type IIA topoisomerase holoenzyme is on the order of ~150-200Å in size (Baker et al, 2011; Kirchhausen et al, 1985; Papillon et al, 2013; Schmidt et al, 2012). By comparison, a MukB homodimer forms an extended structure ~500Å long (Melby et al, 1998). Interestingly, docking of the full-length *E. coli* ParC subunits onto a MukB hinge dimer, using the CTDs to guide placement, shows that the spacing of the CTDs on the hinge is too close to permit a single MukB homodimer to simultaneously bind both subunits of a ParC dimer (**Fig 3.7A**). Although the CTD is probably able to change position relative to the central DNA binding channel, it is unclear whether the domain can undergo the extensive movements required to bind MukB in a 2:2 stoichiometry. Moreover, if two CTDs could attain the requisite geometry, their resultant position would occlude the binding sites for G-segment DNA and ParE on ParC, preventing the formation of a catalytically active topo IV holoenzyme. By comparison, the observed positions of the CTD on topo IV can permit co-assembly with MukB to create higher-order chains of the two proteins (**Fig 3.7B**). In such a scheme, were separate MukB•topo IV oligomers to preferentially localize on each of the two sisters, topo IV would be in a position to specifically resolve the links between sisters, thereby favoring appropriate chromosome segregation into daughter cells (**Fig 3.7C**).

Several lines of evidence are consistent with an array type of model. During the initial stages of replication in *E. coli,* sister chromosomes remain associated at the cell center (Bates & Kleckner, 2005; Reyes-Lamothe et al, 2008; Sunako et al, 2001; Wang et al, 2008). After this early phase of cohesion, sister chromosomes move apart, with the *oriC* of each sister relocating to either ¼ or ¾ positions of the cell (Bates & Kleckner, 2005; Joshi et al, 2011; Nielsen et al, 2006; Reyes-Lamothe et al, 2008). Sister

cohesion has been proposed to be mediated by the precatenanes formed between the newly replicated sisters, as a slight overexpression of topo IV drastically reduces the period of sister cohesion (Lesterlin et al, 2012; Wang et al, 2008). In context of a MukB•topo IV oligomer model, the two proteins may associate to ensure that MukB can properly localize to precatenanes during the initial phases of DNA replication, where it subsequently assists in dragging DNA to the ¼ and ¾ positions by an as yet unknown mechanism.

If ParC and MukB are prelocalized to precatenanes generated in the wake of a replication fork, why are these regions not immediately unlinked? Interestingly, ParC is reported to be at least two times more abundant in cells than ParE suggesting that only a subset of ParC is associated with ParE in topo IV heterotetramers (Taniguchi et al, 2010; Wang et al, 2012). ParC and ParE also have been reported to localize to different regions of the cell (Espeli et al, 2003b; Huang et al, 1998; Wang & Shapiro, 2004), and have been proposed to come together at specific times to form an active complex competent for removing supercoils and catenanes. Were such a separation of function to occur, it could make a prospective topo IV•MukB array competent to segregate daughters only at specific points during replication. Consistent with this idea, overexpression of topo IV is toxic and results in both segregation and locus partitioning defects (Lesterlin et al, 2012; Wang et al, 2008). Since MukB and the ParC subunit of topo IV are expressed at similar levels in cells (Badrinarayanan et al, 2012b; Taniguchi et al, 2010; Wang et al, 2012), overexpression of ParC also could disrupt topo IV•MukB chains, thus impeding appropriate chromosome partitioning. Such a mechanism would parallel that proposed for MukE and MukF, which have been suggested to partition MukB between oligomeric $(B_2E_2F)_n$ chains and single $B_2E_4F_4$ complexes depending on the relative stoichiometries of the three proteins (Badrinarayanan et al, 2012b; Petrushenko et al, 2010; Petrushenko et al, 2006b; She et al, 2007; Wang et al, 2006a). In this regard, MukE and MukF, which specially link MukB head domains together (Badrinarayanan et al, 2012b; Woo et al, 2009), could provide a stabilizing anchor to a topo IV•MukB assembly, which would occur through the hinge on the opposite side of the condensin.

One feature of the action of MukB on topo IV not immediately apparent from this model is why the hinge should specifically stimulate negative-supercoil relaxation by topo IV. Interestingly, attempts to abrogate this stimulation – either by using a large molar excess of the hinge or by using hinge heterodimers containing only a single functional ParC binding site (**Fig 3.4A, S3.7**) – were unsuccessful, indicating that the prospective formation of MukB•topo IV oligomers is not responsible for the observed activation. Recent data from our group has shown that distinct surfaces of the ParC CTD contribute differentially to relaxation of supercoiled DNA substrates and the resolution of catenanes (Vos et al, 2013). One potential reason MukB may bind to the fifth blade of the ParC CTD is because alterations to this region do not impair the enzymatic activity of topo IV; as such, the stimulatory effects observed *in vitro* may simply be a fortuitous byproduct of the interaction. Alternatively, during rapid DNA replication, MukB could stimulate topo IV to specifically remove negative supercoils that form behind the replisome in the leading sister strand (supercoils cannot form in the

lagging strand due to the gaps between the Okazaki fragments) (**Fig S3.8**). Future studies will be required to determine whether large-scale MukB•topo IV oligomers do indeed form on DNA and how such complexes might help facilitate daughter chromosome disentanglement and appropriate partitioning.

MATERIALS AND METHODS

Cloning of MukB and ParC Constructs for Crystallography and Biochemistry
Cloning of the ParC CTD (497-752), full-length ParC (1-752), full-length ParE (1-630), the ParC NTD (1-482)(Corbett et al, 2005), the His6-MBP-ParC CTD (Vos et al, 2013), and MukB (645-804) have been described previously (Li et al, 2010b). Mutations were made by QuikChange (Agilent).

Protein Expression and Purification
For a detailed protein purification protocol for E. coli ParE, ParC, MukB (566-863) and the His_6-MBP-ParC CTD, see **Appendix 5.**
MukB (645-804) and ParC CTD (497-752) were over-expressed in *E. coli* BL21codon-plus (DE3) RIL cells (Stratagene). To produce selenomethionine deriviatized ParC CTD, cells were grown at 37°C in M9 minimal media (Sambrook & Russell, 2001) supplemented with 1µg/ml thiamine to an OD600 of 0.4-0.5. Protein expression was then induced with 0.5mM isopropyl β-D-1-thiogalactopyranoside (IPTG), while methionine production was repressed by adding 58.25 mg/L (leucine, isoleucine, valine), 116.75mg/L (phenylalanine, lysine, threonine), and 87.5 mg/L (selenomethionine) to the media (Van Duyne et al, 1993). Cells were grown for an additional 3 h at 37°C, harvested by centrifugation, and resuspended in buffer A800 (10% glycerol, 20mM Tris-HCl pH 7.9, 800mM NaCl, 30 mM imidazole pH 8.0, 2mM β-mercaptoethanol (BME), 1µg/mL pepstatin A, 1µg/mL leupeptin, and 1mM phenyl methylsulfonyl fluoride(PMSF)); resuspended cells were drop-frozen into liquid nitrogen, and stored at -80°C prior to purification. MukB (645-804) protein expression was induced at 37°C by adding 0.5mM IPTG to 2xYT liquid media cultures after cells had grown to an OD600 of 0.4-0.5. After induction, cells were grown at 37°C for an additional 3-4 h, centrifuged, resuspended in buffer A800, drop-frozen in liquid nitrogen, and stored at -80°C prior to purification. MukB (645-804) contains no methionine residues, and thus was not grown in the presence of selenomethionine.

For purification, cells first were thawed, lysed by sonication, and centrifuged. Clarified lysates were applied to HiTrap Ni^{2+} columns (5 mL) (GE) and washed extensively with buffer A800. MukB (645-804) and the ParC CTD were eluted in buffer B800 (10% (v/v) glycerol, 20mM Tris-HCl pH 7.9, 800mM NaCl, 300 mM imidazole pH 8.0, 2mM BME, 1µg/mL pepstatin A, 1µg/mL leupeptin, and 1mM PMSF) and concentrated by centrifugation (Millipore Amicon Ultra MWCO 10). To remove His_6 tags, the proteins were dialyzed overnight at 4°C against A800 in the presence of 1mg His_6-tagged TEV protease (MacroLab, UC Berkeley). The proteins were then loaded on HiTrap Ni^{2+}columns equilibrated in A800 to isolate tag-less proteins and retain tagged proteins and TEV protease on the column. All proteins were concentrated and applied separately to a S-200 gel filtration column (GE) equilibrated and run in 800mM KCl, 20mM Tris-HCl pH 7.9, 0.5mM tris(2-carboxyethyl)phosphine (TCEP), and 10% (v/v) glycerol. Peak fractions were run on SDS-PAGE to confirm purity, pooled, and concentrated by centrifugation (Mllipore Amicon Ultra MWCO 10).

Cloning, expression, and purification of the E. coli GyrA CTD (531-853)
The truncated E. coli GyrA CTD (531-853) was expressed and purified as previously described (Tretter & Berger, 2012).

MukB (566-863) Heterodimer Purification
For purification, cells were thawed, lysed by sonication, and centrifuged. Clarified lysates were applied to HiTrap Ni^{2+} columns (5mL) (GE) and washed extensively with A800. The column was washed further with A400. Proteins were eluted onto a 10mL amylose column (New England BioLabs) in B400. The amylose column was washed in 400mM NaCl, 20mM Tris-HCl pH 7.9, 10% (v/v) glycerol, 2mM BME, 1µg/mL pepstatin A, 1µg/mL leupeptin, and 1mM PMSF, and proteins were eluted in 400mM NaCl, 20mM Tris-HCl pH 7.9, 10% (v/v) glycerol, 100mM maltose, 2mM BME, 1µg/mL pepstatin A, 1µg/mL leupeptin and concentrated by centrifugation. MukB (566-863) heterodimer constructs were dialyzed against A400 in the presence of 1mg His_6-TEV protease for 16 hours at 4°C. To remove tagged heterodimer constructs and TEV protease, the heterodimer was run over a HiTrap Ni^{2+} column (5mL) (GE) and an amylose column (New England Biolabs) in tandem in buffer A400. The heterodimer was then concentrated by centrifugation (Millipore Amicon Ultra MWCO 30) and run over a S-300 size exclusion column (GE) in SE buffer. Peak fractions were collected and concentrated, and protein purity assessed by SDS-PAGE followed by Coomassie staining. The MukB hinge heterodimer was dialyzed for 16 h at 4°C against 40% (v/v) glycerol, 50mM Tris-HCl pH 7.9, 150mM potassium glutamate, 6mM $MgCl_2$ and 2mM BME, and then flash frozen and stored at -80°C.

Crystallography and Data Collection
For crystallography, the selenomethionine-labeled ParC CTD (residues 487-752) and MukB hinge (residues 645-804) were dialyzed separately at 15-20 mg/mL concentration each for 16 h at 4°C against 100mM KCl, 20mM Tris-HCl pH 7.9, and 0.5mM TCEP. The hinge and CTD were then mixed at equimolar ratios immediately before setting trays. Crystals were grown at 18°C in hanging drop format by combining 1µL of well solution (212.5mM lithium citrate tribasic tetrahydrate, 20% PEG 3350) with 1µL of the hinge/CTD mix. Crystals generally formed within 24 hours and were cryoprotected by adding a solution containing the protein buffer, well solution, and 30% PEG 400 directly to the drop. After cryoprotection, the crystals were immediately looped and flash frozen in liquid nitrogen.

Diffraction data sets (two remote, two peak) were collected from a single crystal at Beamline 8.3.1 at the Advanced Light Source at Lawrence Berkeley National Laboratory (MacDowell et al, 2004). Data were indexed and scaled with ELVES and HKL2000, revealing that the unit cell belongs to the space group $P2_12_12_1$ (Holton & Alber, 2004; Otwinowski & Minor, 1997). Phase calculations were performed with PHENIX AutoSOL (Terwilliger et al, 2009), using a combination of single-wavelength anomalous dispersion and molecular replacement with the ParC CTD (PDB ID 1ZVT) the MukB hinge (PDB ID 3IBP) as search models. Manual building was performed with COOT (Emsley et al, 2010) and the complete hinge•CTD heterotetramer model refined with PHENIX (Adams et al, 2010). TLS parameters were analyzed by the TLSMD server,

which generated 24 groups for use in the late stages of refinement (Painter & Merritt, 2006). The final model was refined to an R_{work}/R_{free} of 20.4%/24.6%, with Molprobibity analysis showing that 98.5% of residues reside in favored Ramachandran space and one residue occupies a disallowed region (0.13%) (Chen et al, 2010). The atomic structure and coordinate files have been deposited with the Protein Data Bank (ID 4MN4). Figures were prepared with PyMol (DeLano, 2002).

DNA Binding Assays

A randomly generated, 20bp annealed duplex oligonucleotide (5'-l56-FAMl-TTAGGCGTAAACCTCCATGC-3' and 5'-AATCCGCATTTGGAGGTACG-3', where l56-FAMl indicates the position of a carboxyfluorescein dye used for analysis) was purchased from Integrated DNA Technologies (IDT) and resuspended in water (50% G/C content, T_m = 50°C). All proteins were diluted on ice in protein dilution buffer (300mM potassium glutamate, 20mM Tris-HCl pH 7.5, 10% glycerol, and 0.05mg/mL bovine serum albumen (BSA)). The assay contained 4µL of the His_6-MBP ParC CTD (0.01-10µM) mixed with either 4µL of the MukB hinge (aa 566-863,10µM) or 4µL protein dilution buffer and 20nM of the fluorescently-labeled 20mer oligonucleotide. DNA and proteins were initially incubated on ice in the dark for 10 min, after which they were diluted to the final assay volume (80µL) and kept at room temperature in the dark for 10 min (final assay conditions: 2.4mM DTT, 20mM Tris-HCl pH 7.5, 10% (v/v) glycerol, 1mM $MgCl_2$, 0.05mg/mL BSA, 30mM potassium glutamate). Measurements were made with a Perkin Elmer Victor 3V 1420 multilabel plate reader at 535nm. Data points are the average of three independent experiments and all points are normalized to wells that did not contain protein. Data were plotted in GraphPad Prism Version 5 using the following single-site binding equation:

$$y = Bmax\left(\frac{([x] + [L] + K_{d,app}) - \sqrt{([x] + [L] + K_{d,app})^2 - 4([x] \bullet [L])}}{2 \bullet [L]}\right)$$

where B_{max} is the maximum specific binding, L is the DNA concentration, x is the His_6-MBP ParC CTD concentration, and $K_{d,\ app}$ is the apparent dissociation constant for His_6-MBP ParC CTD and DNA (Kenakin, 1993; Lundblad et al, 1996; Swillens, 1995). DNA binding experiments with the *E. coli* GyrA CTD (531-853) were performed in an identical manner to those described for the His_6-MBP ParC CTD.

Surface Plasmon Resonance

All surface plasmon resonance experiments were performed on a Biacore 2000 instrument (GE), using a 20mer duplex of identical sequence to that used in the fluorescent anisotropy study, but bearing a 5' carboxy biotin label instead of fluorescein. Biotinylated oligonucleotides were diluted in 300mM NaCl to a final concentration of 1 nM, and 50µL of the solution was injected over a Strepavidin coated sensor chip (Sensor Chip SA (GE)) at a rate of 5µL/min. The chip was then washed in Wash Buffer (100 µL 50mM Tris-HCl pH 7.5, 40mM potassium glutamate, 1mM $MgCl_2$, 2mM dithiothreitol (DTT), and 0.005% (v/v) Tween-20 (Sigma-Aldrich)) at 100 µL/min. The His_6-MBP ParC CTD was serially diluted (10-fold dilution series) to 250nM in Wash

Buffer and the protein solution (50 µL) was added to the chip at a flow rate of 100µL/min. Then solutions containing the His_6-MBP ParC CTD and various concentrations of MukB (566-863) were mixed in Wash Buffer and 100µL was flowed over the sensor chip at 100µl/min. The chip was then washed with 100µL Wash Buffer at a rate of 100µL/min. To remove protein and regenerate the chip, 10µL of a 1M NaCl solution was flowed over the chip prior to flowing more His_6-MBP ParC CTD and solutions containing the His_6-MBP ParC:MukB hinge mixtures. All data were graphed in GraphPad Prism Version 5 and normalized to a lane containing DNA but no protein.

DNA Supercoil Relaxation Assays

Topo IV heterotetramers were formed by adding equimolar ParE and ParC to a final concentration of 40µM in dilution buffer (150mM potassium glutamate, 50mM Tris-HCl pH 7.9, 10% glycerol, 6mM $MgCl_2$) and incubating on ice for 10 min. The tetramer was then serially diluted (2-fold steps) to 5µM in dilution buffer. Topo IV (2µL) was added to serially-diluted (half-log dilution steps) MukB (566-863) (2µL) in dilution buffer or added to dilution buffer alone (2µL). The proteins were then incubated together on ice for 10 min. Supercoiled pSG483 plasmid DNA (500nM final concentration) was added to the protein mixture (2-4µL) and the assay was incubated at 25°C for 5 minutes. The resulting mixtures were then diluted to 18µL and were incubated at 25°C/15°C (negative/positive supercoil relaxation) for another 5 min prior to initiating the topo IV reaction with 2µL of 2mM (final) ATP pH 7.5. The final reaction (20µL) contained 30mM potassium glutamate, 1% (v/v) glycerol, 10mM DTT, 1mM spermidine, 10µg/mL BSA, 50mM Tris-HCl pH 7.9, 6mM $MgCl_2$, and 2mM ATP pH 7.5. Samples (3µL) were quenched at various time points (15 s -10 min) with 2µL stop buffer (100mM EDTA, 10% SDS (w/v)). Samples were then diluted with water (145 µL). Sucrose loading dye was added to 10 µL of each diluted sample and each sample was run for 6-18 h on 1% (w/v) TAE agarose gels (40mM sodium acetate, 50mM Tris-HCl pH 7.9, 1mM EDTA pH 8.0) at 2-2.5 volts/cm. To visualize the DNA, gels were stained with 0.5µg/mL ethidium bromide in TAE buffer for 20 min, destained in TAE buffer for 30 min, and exposed to UV transillumination. Positive-supercoil relaxation gels have an altered topoisomer distribution due to the low temperature used in the positive-supercoil relaxation experiments. This effect is also observed when topo IV relaxes negatively-supercoiled DNA substrates at low temperature (15˚C) (**Fig S3.9**)(Depew & Wang, 1975).

Temperature sensitive complementation assays

The C600*ParC1215* strain was a generous gift of Hiroshi Hiasa (Kato et al, 1990; Kato et al, 1988; Lavasani & Hiasa, 2001). ParC constructs were cloned into a modified pET28b vector with a ligation independent cloning site (Doyle, 2005). The C600*ParC1215* strain was complemented by leaky expression from T7 promoter containing rescue plasmids as previously described (Lavasani & Hiasa, 2001). Cells were transformed and plated on 2xYT or M9 minimal media supplemented with 2% (w/v) glucose (Sambrook & Russell, 2001) and grown at 30˚C. M9 minimal media was made with M9 salts, 0.2% (v/v) glucose, 1mM $MgSO_4$ 1µg/ml thiamine, 116.75mg/L threonine, 58.25 mg/L leucine, and 100 µM $CaCl_2$. Several colonies were picked to start 5mL overnight liquid cultures grown in 2% (w/v) glucose. Overnight cultures were then

used to inoculate duplicate 50 mL liquid cultures containing either 2xYT or M9 minimal media and incubated at 30°C. When cells reached an OD_{600} of 0.3±0.05, duplicate liquid media cultures were split so that one remained at the permissive temperature (30°C) while the other was shifted to the nonpermissive temperature (42°C). Cells were adapted to the new temperature for 30 minutes, after which cells were grown for an additional 4 h with time points taken at 30, 60, 150, 310 min post-temperature shift. Cells were serially diluted after normalization, plated, and grown at 30°C and 42°C to assess survival resulting from leaky expression for each time point. For all plating dilutions, cells were normalized to the culture with the lowest OD_{600} at the 0 min time point.

At the time of the temperature shift, OD_{600nm} readings were taken for each liquid culture. Samples taken from the liquid cultures for plating 30, 60, 120, and 270 minutes post temperature shift were mixed with the appropriate volume of fresh media (final volume 100µL) to achieve the relative cell density of the culture with the lowest OD_{600nm} at the time of the temperature shift. This regime ensures that differences observed in the assay are not due to variance in cell density at the beginning of the experiment but rather to changes in the viability of the cells grown at the restrictive temperature over time.

Complementation of the *C600parC1215* strain was mediated by leaky expression from T7 promoter driven pET28b rescue plasmids. The C600*parC1215* strain does not encode a T7 RNA polymerase, thus transcription of rescue plasmids is achieved by promiscuous activity of the endogenous *E. coli* RNA polymerase (Rosenberg et al, 1987; Wiggs et al, 1979). It is unknown how many copies of each ParC transcript are produced by leaky expression, but it is likely that there are more copies of the transcript originating from the rescue plasmid than that of the endogenous promoter (there ~ 30-40 rescue plasmids per cell) (Held et al, 2003). Although it is possible that hybrid topo IV enzymes composed of the endogenous (Gly725Asp ParC) and the rescue plasmid ParC form at the permissive temperature, these hybrids likely do not account for the partial complementation phenotype we observe with the *parC*^{Y120F} rescue plasmid at the restrictive temperature. Attempts to purify the Gly725Asp ParC have found that the protein is poorly expressed and largely aggregated. This *in vitro* behavior suggests that the G725D mutation in the ParC CTD destabilizes the entire ParC protein, likely prohibiting its ability to fold properly and associate with other factors. See **Appendix 1** for more details.

DNA binding experiments with the topo IV holoenzyme

Two strands of DNA with a strong topo II DNA cleavage site were obtained from IDT and annealed as previously described by Dong and Berger, 2007 (Dong & Berger, 2007; Mueller-Planitz & Herschlag, 2007).

One strand contained a 5'-fluorescein dye:

5'--I56-FAMI-CTATCCGAGGATGACGATGCGCGCATCGTCATACAGCGAATG - 3'.
The other has the sequence:
5'- CATTCGCTGTATGACGATGCGCGCATCGTCATCCTCGGATAG - 3'.

Fluorescence-anisotropy based DNA binding experiments with this substrate and topo IV were carried out as described in **Chapter 2**.

Pull-down Assays

His_6-MBP ParC CTD constructs (10μM) were bound to 50μL of Ni NTA agarose resin (Qiagen) in the presence or absence of the MukB hinge (566-863) constructs (10μM) in binding buffer (20mM Tris-HCl pH 7.9, 50mM potassium glutamate, and 30mM imidazole pH 8.0)(final assay volume, 100μL). Proteins were co-incubated on the resin for 15 minutes at room temperature prior to washing the resin three times in 200μL binding buffer to remove unbound protein from the resin. The proteins were eluted from the resin in 60μL elution buffer (20mM Tris-HCl pH 7.9, 50mM potassium glutamate, and 500mM imidazole pH 8.0). The washes (10μL) and elutions (10μL) were run on 10% SDS-PAGE and stained with Coomassie blue.

Table 3.1. Crystallography Statistics.

Data Collection	**Remote**	**Peak**
Resolution (Å)	49.97-2.3	50-3.1
Wavelength (Å)	1.1	0.979648
Space Group	P212121	P212121
Unit cell dimensions (a, b, c) (Å)	49.76, 103.67,186.59	49.713, 103.633, 186.537
Unit cell angles (α, β, γ) (°)	90, 90, 90	90, 90, 90
I/σ (last shell)	17.0 (2.78)	15.0 (4.68)
R_{merge} (last shell) (%)	6.2 (39.4)	12.2 (34.2)
Completeness (last shell) (%)	98.1 (88.5)	99.3 (100)
Redundancy	3.8 (2.8)	4.3 (4.3)
Unique Reflections	44001	18525
Number of Sites		18
Fig of Merit		0.37
Refinement		
Resolution (Å)	49.974-2.3	
No. of reflections	43079	
R_{work} (%) (last shell)	20.4(25.4)	
R_{free} (%) (last shell)	24.6(31.5)	
Structure and Stereochemistry		
No. atoms	6684	
Protein	6335	
Water	349	
B factor (Å^2)		
Protein	20.0	
Water	33.5	
r.m.s.d. bond lengths (Å)	0.002	
r.m.s.d. bond angles (°)	0.552	
Ramachandran Plot (%)		
Favored Region	98.1	
Allowed Region	1.7	
Outliers	0.1	

$R_{merge} = {}_{hkli}I_i(hkl)\ I(hkl) / {}_{hkli}I_i(hkl)$, where $I_i(hkl)$ is the intensity of an observation and I(hkl)is the mean value for its unique reflection. Summations cover all reflections.

$R_{work} = {}_{hkl}\ F_{obs}\ k\ F_{calc} /{}_{hkl}\ F_{obs}$. R_{free} was as per R_{work}, but with the reflections excluded from refinement. The R_{free} set was chosen using default parameters in PHENIX (Adams et al, 2010).

Ramachandran Plot categories were defined by Molprobity (Chen et al, 2010).

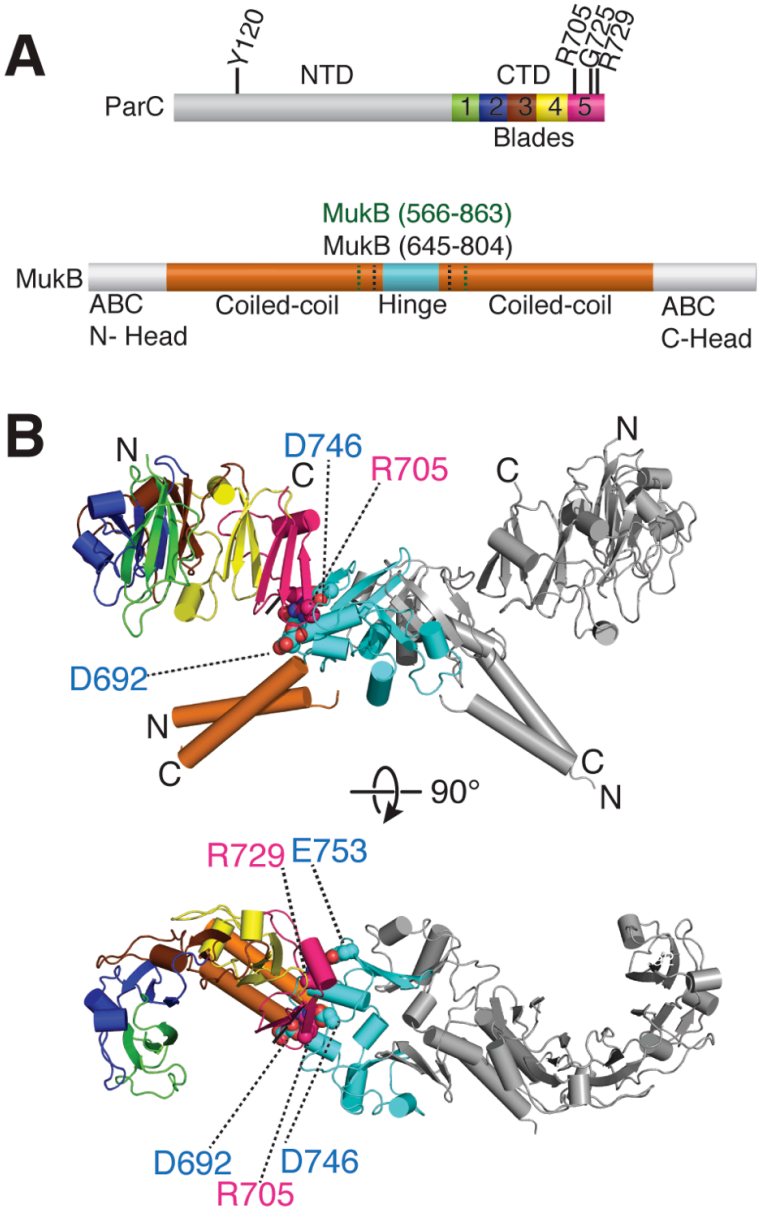

Figure 3.1. Structure of a MukB hinge·topo IV complex.
A Primary structure and domain organization of *E. coli* ParC and MukB. A subset of the ParC residues addressed in this study are labeled on the primary structure. MukB hinge constructs (aa 566-863 (green), aa 645-804 (black)) used here are also denoted. Different subdomain repeats of the CTD (termed “blades”) are colored rainbow.
B Crystal structure of the hinge•CTD heterotetramer in cartoon representation. Coloring for one MukB hinge and ParC CTD is as per panel (A), with dimer related protomer colored gray. Residues mutated and assayed in this study are depicted as spheres and labeled.

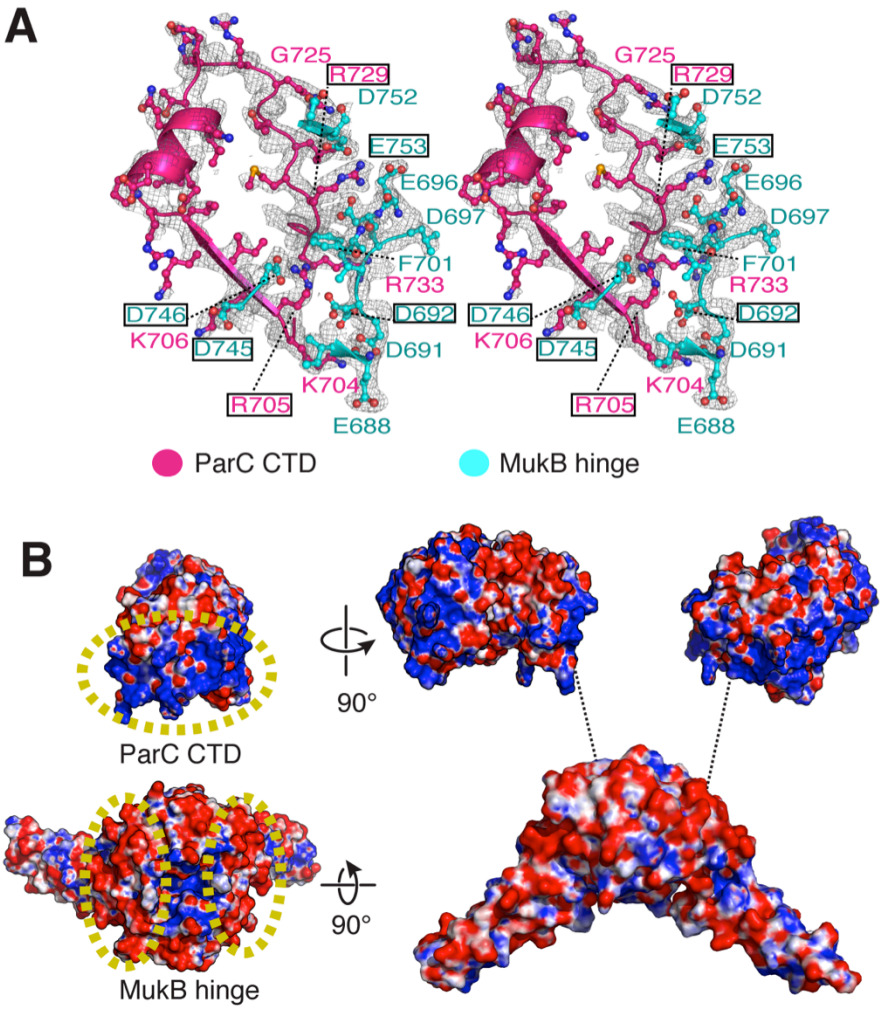

Figure 3.2. The hinge•CTD interaction is predominantly electrostatic.
A Stereo representation of MukB hinge (cyan)•ParC CTD (pink) interface shown with a $2F_o$-F_c map contoured at 1σ. Interacting residues are labeled; boxed residues were mutated and assayed in this study.
B Electrostatic potential map of the MukB•ParC interaction surfaces. On the left, a single ParC CTD and MukB hinge dimer are colored according to surface charge (blue for positive, red for negative). The interacting surfaces of MukB and ParC are demarcated by yellow, dashed ovals. On the right, an exploded view of the hinge•CTD complex is shown.

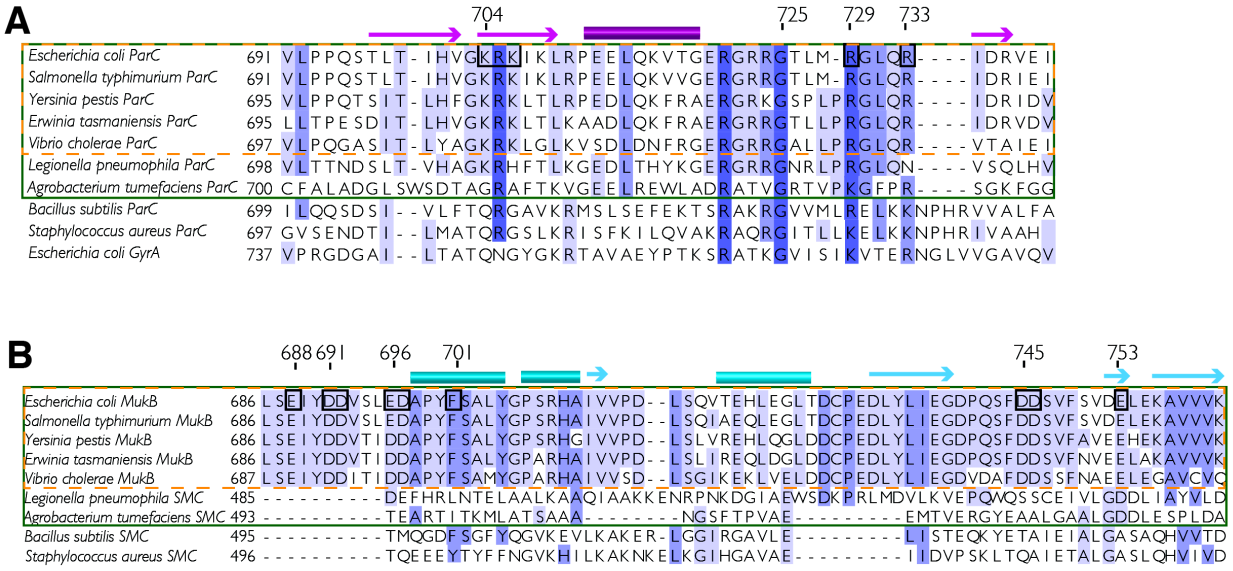

Figure S3.1. Sequence alignments of the interacting regions between MukB and ParC.

Residues are colored according to percent identity, with dark blue corresponding to highly conserved residues and white indicating no conservation. Selected ParC, MukB, and SMC proteins were aligned using MAFFT(Katoh et al, 2009). Alignment figures were made in Jalview (Waterhouse et al, 2009). γ-proteobacteria are indicated by the green box. γ-proteobacteria encoding MukB are highlighted by the orange box. Secondary structural elements are shown as arrows (β-strands) and rectangles (α-helices).

A *E. coli* ParC CTD residues involved in binding MukB are bordered by black boxes and numbered above the alignment. The homologous region of *E. coli* GyrA is shown for comparison.

B Alignment of various bacterial MukB and SMC proteins. MukB residues that interact with ParC are bordered by black boxes and are numbered above the alignment.

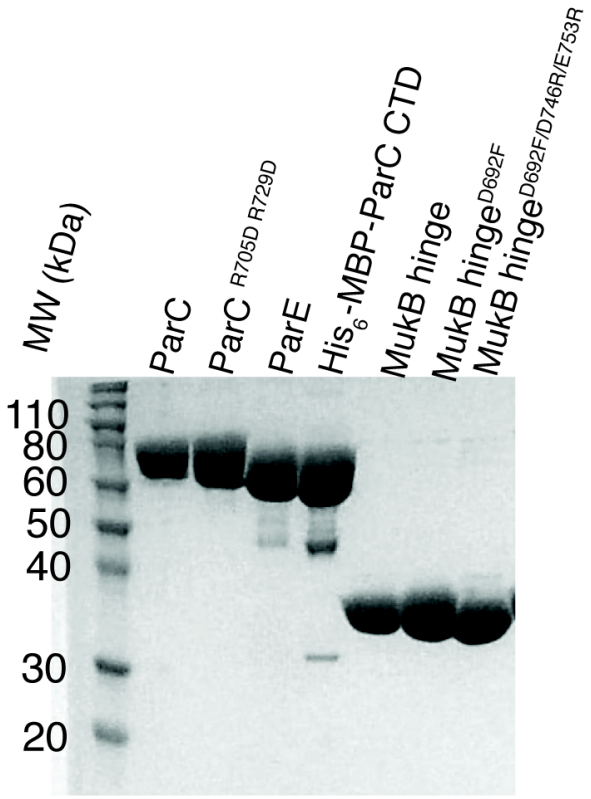

Figure S3.2.Purity levels of proteins used in this chapter.
All proteins were purified as described in **Materials and Methods.** Here 0.3µg of each protein construct was run on 10% SDS PAGE to assess purity. The His_6-MBP-ParC CTD construct retained a small amount of His_6-MBP and Par CTD that derive from background cleavage of the linker joining the two proteins during purification.

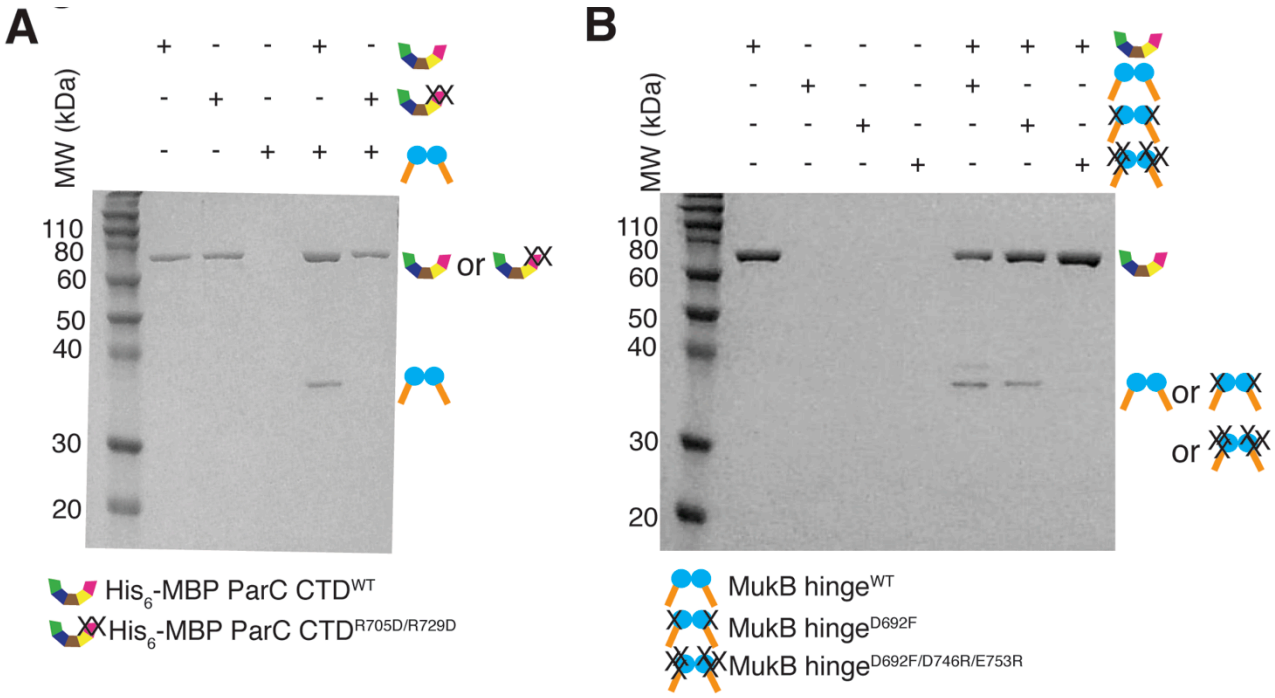

Figure S3.3.
Interacting residues between MukB and ParC were mutated and assayed for their ability to form a stable hinge•CTD complex. Constructs used in each pull-down are shown above their respective wells. Pictograms on the right of each gel indicate where the His_6-MBP-ParC CTD and the MukB hinge (566-863) constructs migrate.
A The WT and Arg705Asp/Arg729Asp His_6-MBP-ParC CTD were tested for their ability to pull-down the WT MukB hinge (566-863).
B Mutant MukB hinge constructs (indicated below the gel) were tested for their ability to pull-down with the WT His_6-MBP-ParC CTD construct.

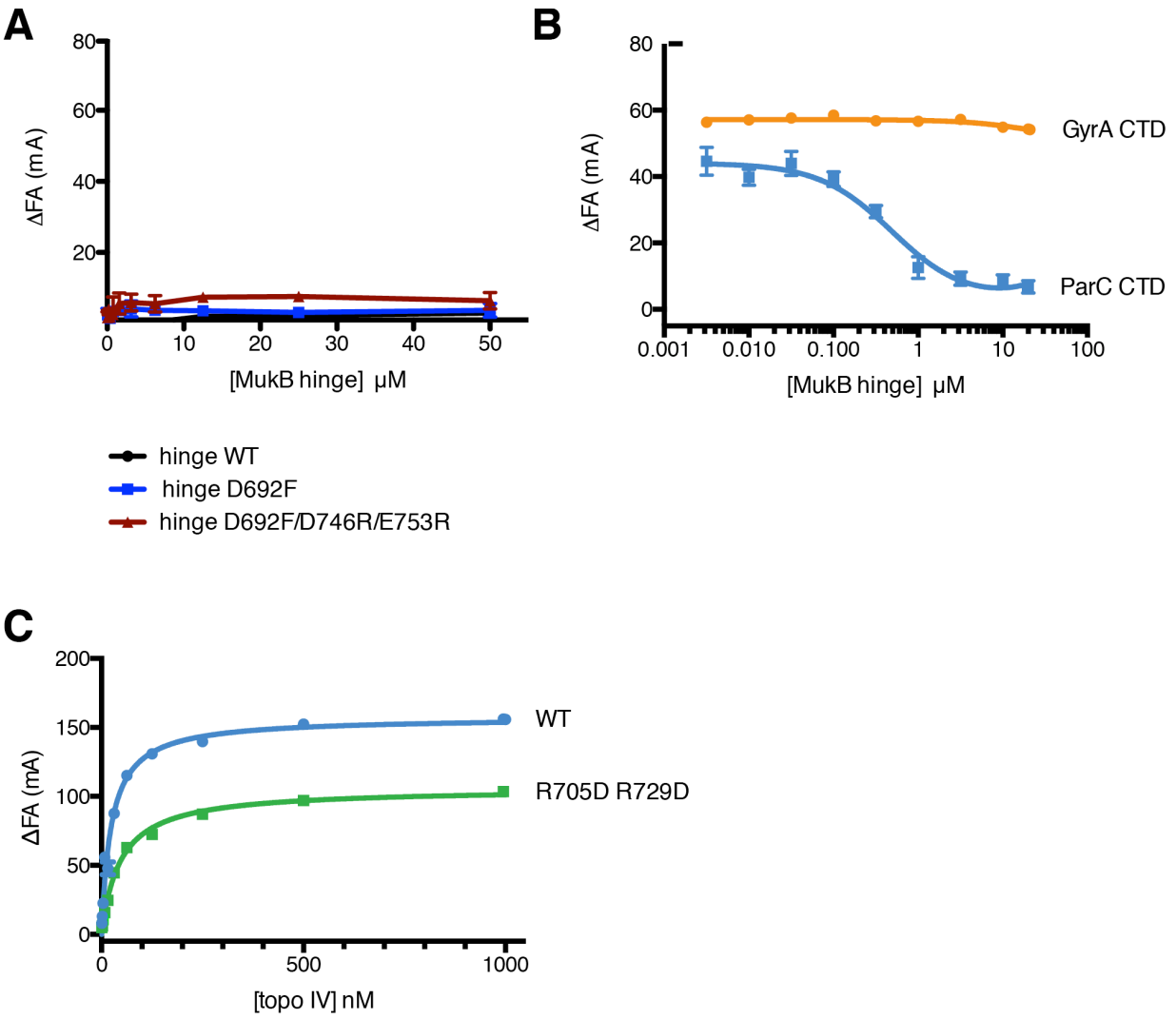

Figure S3.4.
DNA binding monitored as a function of change in fluorescence anisotropy (ΔFA), as measured in millianisotropy units (mA). The DNA substrate used for panels A and B corresponds to that used in **Fig 3.3**. Panel C used a fluorescently-labeled 42mer dsDNA substrate described in **Materials and Methods**.
A The MukB hinge (residues 566-863) shows little affinity for DNA. Titrations compared the MukB hinge WT (black), Asp692Phe mutant (blue), and the Asp692Phe/Asp746Arg/Glu753Arg mutant (maroon). Values are normalized to control reactions containing no protein.
B The MukB hinge specifically inhibits DNA binding to the ParC CTD. WT MukB hinge (566-863) was titrated against 5μM of the MBP-ParC CTD (blue) or the GyrA CTD (aa 531-853) (orange) in the presence of a fluorescently-labeled 20mer DNA (20 nM). Values are normalized to control reactions containing no protein. $K_{d,app}$ of the MBP-ParC CTD for the MukB hinge is ~0.5μM ±0.18 and >100μM for the GyrA CTD.

C DNA binding by WT (blue) and ParC Arg705Asp Arg729Asp (green) topo IV as measured by change in fluorescence anisotropy. Values are normalized to control reactions containing no protein. $K_{d,app}$ of WT topo IV for the DNA substrate is ~24±3.1and ~46.6±3.4 for the Arg705Asp/Arg729Asp mutant.

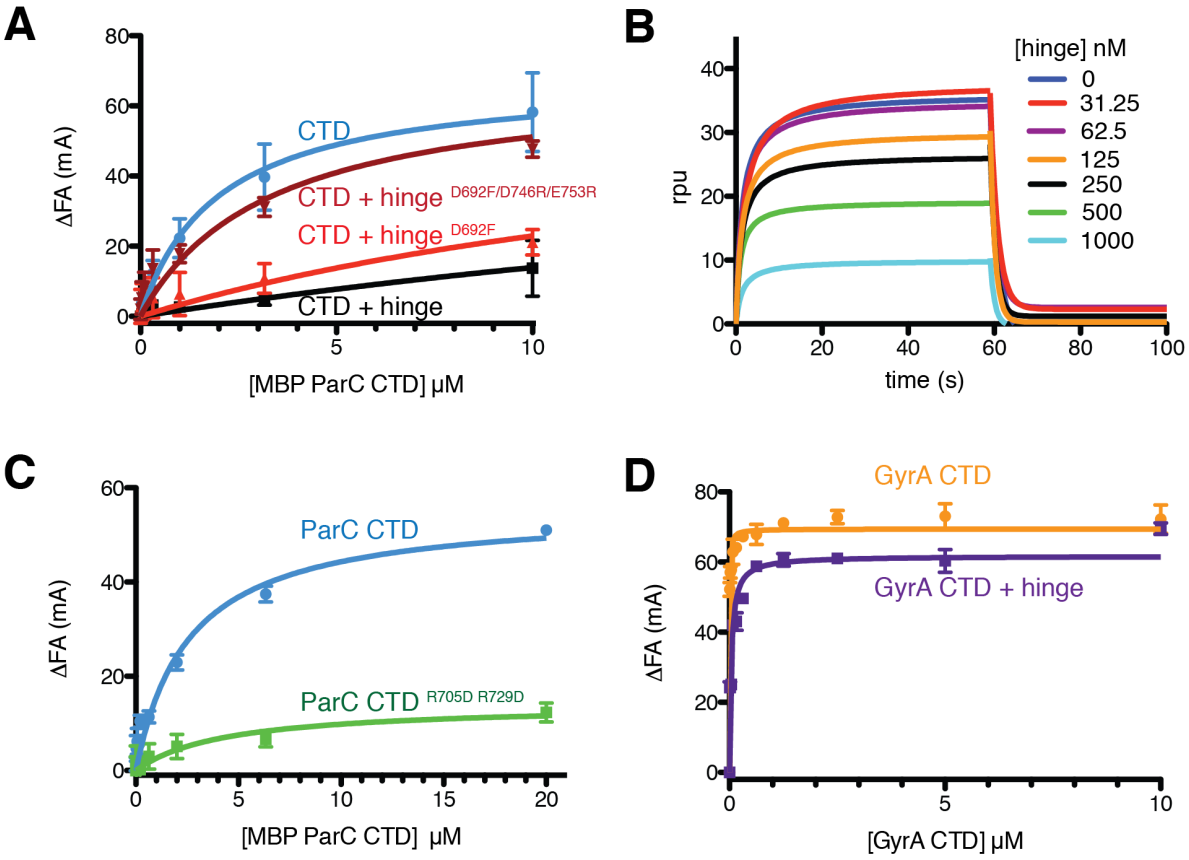

Figure 3.3. The hinge prevents the ParC, but not GyrA CTD from binding DNA.
A Binding of the MBP-ParC CTD to a 20 nM of a fluorescently labeled 20mer duplex oligonucleotide (20nM), as monitored by relative change (ΔFA) in fluorescence anisotropy (millianisotropy units – mA). Data correspond to titrations with MBP-ParC CTD (CTD) alone, or with 10μM of the WT MukB hinge, the Asp692Phe mutant, or the Asp692Phe/Asp746Arg/Glu753Arg mutant. See also **Fig S3.4**.
B DNA binding by the MBP-tagged CTD as monitored by surface plasmon resonance in the presence of different hinge concentrations. The y-axis indicates changes in response units (rpu) due to protein association with the DNA bound sensor chip. The DNA substrate is identical in sequence to the DNA substrate utilized in the fluorescence anisotropy experiments.
C DNA binding by the MBP-ParC CTD$^{R705D/R729D}$ mutant as determined by fluorescence anisotropy. Substrate is the same as in panel (A).
D DNA binding by the tailless *E. coli* GyrA CTD (aa 531-853) construct as determined by fluorescence anisotropy in the presence and absence of the MukB hinge (10μM). Substrate is the same as in panel (A). See also **Fig S3.4**.

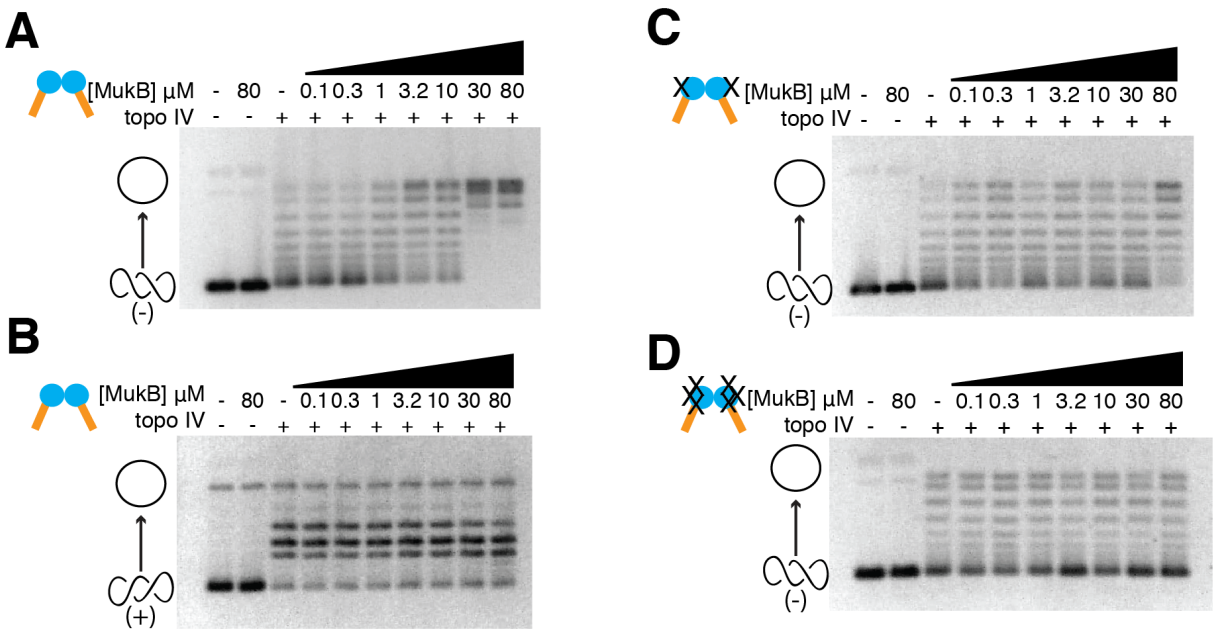

Figure 3.4. The hinge activates topo IV on negatively-supercoiled but not positively-supercoiled DNA.
All panels show the relaxation of supercoiled pSG483 plasmid substrate by an equimolar amount of topo IV (500 nM). Negatively-supercoiled substrates were used for panels A, C, and D. Panel B shows the results for positively-supercoiled substrate. In each instance, reactions were quenched midway to prevent full relaxation of the DNA by topo IV alone, so as to determine any effects of MukB (see **Fig S3.5** for corresponding activity time course). Different panels compare different MukB hinge constructs: **A** and **B** – WT MukB hinge; **C** – Asp692Phe hinge mutant; **D** – AspD692Phe/AspD746Arg/Asp753Arg hinge mutant. Cartoon representations of topoisomer states are shown on the left side of the gels, (open circle – relaxed species; intertwined circles – supercoiled species).

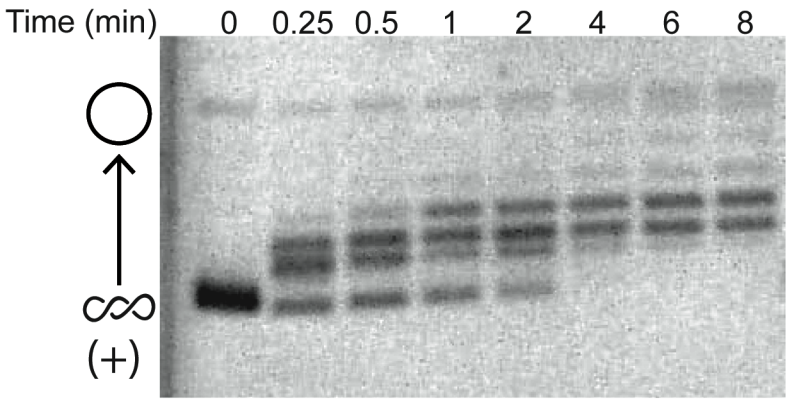

Figure S3.5.
Positive-supercoil relaxation time course with WT topo IV, performed at 15˚C with 500nM positively-supercoiled pSG483 plasmid substrate and 500nM topo IV. This experiment shows that the reaction has not yet gone to completion at 2 min (the time point used for the assay shown in **Fig. 3.4C**). A cartoon representation of topoisomer states is shown on the left side of the gel (open circle – relaxed species, intertwined circles – supercoiled species).

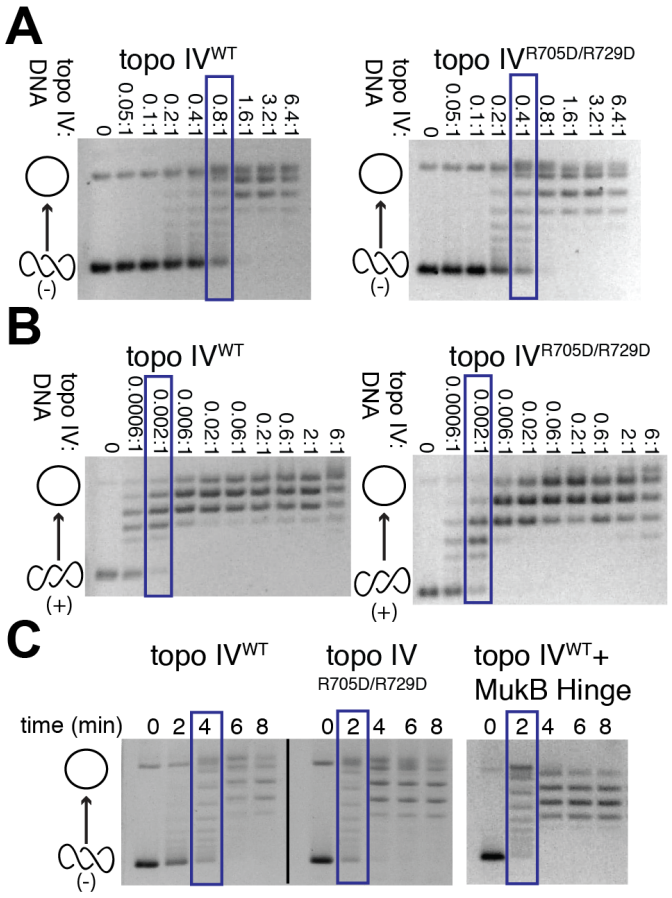

Figure 3.5. The hinge masks a DNA-binding site on the CTD that autorepresses the relaxation of negatively-supercoiled DNA.

Native gels show the relaxation of either negatively- or positively-supercoiled pSG483 plasmid substrates by WT topo IV or by Arg705Asp/Arg729Asp topo IV (which does not bind MukB). Cartoon representations of topoisomer states are shown on the left side of the gels (open circle – relaxed species, intertwined circles – supercoiled species). Blue boxes indicate protein concentration or time point at which topo IV has relaxed approximately half the supercoiled substrate. Gels are representative of at least three independent replicates from three different protein topo IV preparations.

A Enzyme titrations showing that mutation of the MukB binding site on the ParC CTD leads to elevated relaxation activity on negatively-supercoiled DNA. The molar ratio of enzyme:DNA is indicated above each gel (reactions contained 7.9nM supercoiled plasmid).

B Enzyme titrations showing that mutation of the MukB binding site on the ParC CTD does not affect the relaxation of positively-supercoiled DNA. The molar ratio of enzyme:DNA is indicated above each gel (reactions contained 7.9nM supercoiled plasmid).

C Rates of negative-supercoil relaxation are similarly stimulated by either the Arg705Asp/Arg729Asp ParC mutation or binding of the MukB hinge. Reactions contain 500 nM plasmid DNA and 500 nM of either WT or mutant topo IV (500nM), together with the presence or absence of 10μM of the MukB hinge.

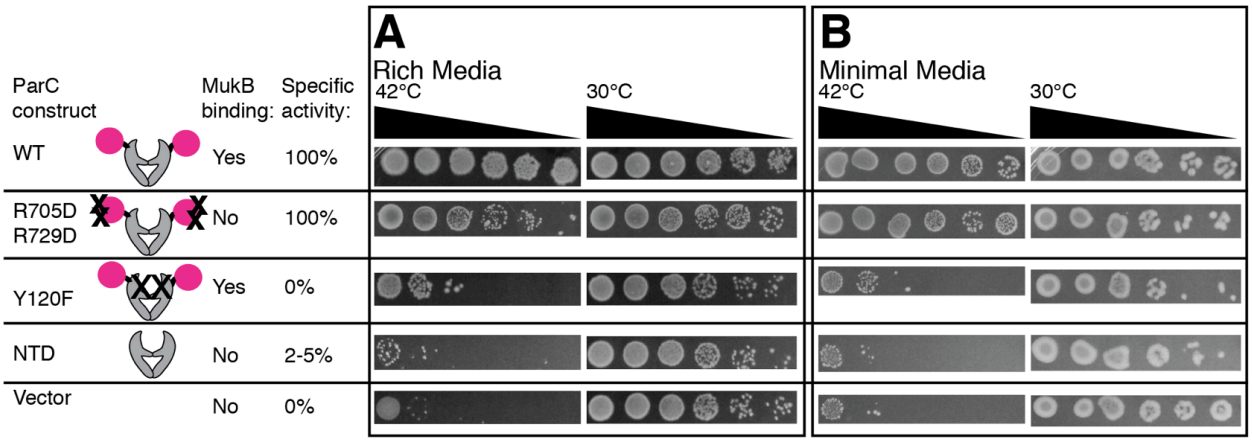

Figure 3.6. The strand passage activity of topo IV and its ability to bind MukB are separable and contribute additively to cell growth.
Complementation assays of the *C600parc1215* strain are shown grown at 42˚C on rich (**A**) and minimal (**B**) media. Spotted cultures correspond to 20-fold dilution series taken one hour after liquid cultures were shifted to the restrictive temperature. For plating, cells were normalized to the culture with the lowest OD_{600nm} at the time of the temperature shift ($OD_{600nm} \approx 0.3$). Cartoons of ParC constructs assayed, and their specific activity relative to WT and their ability to bind MukB, are illustrated next to each row. Dilutions of cells grown at the permissive temperature (30˚C) are shown to the right of cells grown at the restrictive temperature. Time points taken from cultures at time points 30 minutes to 270 minutes after the temperature shift are shown in **Fig S3.6**.

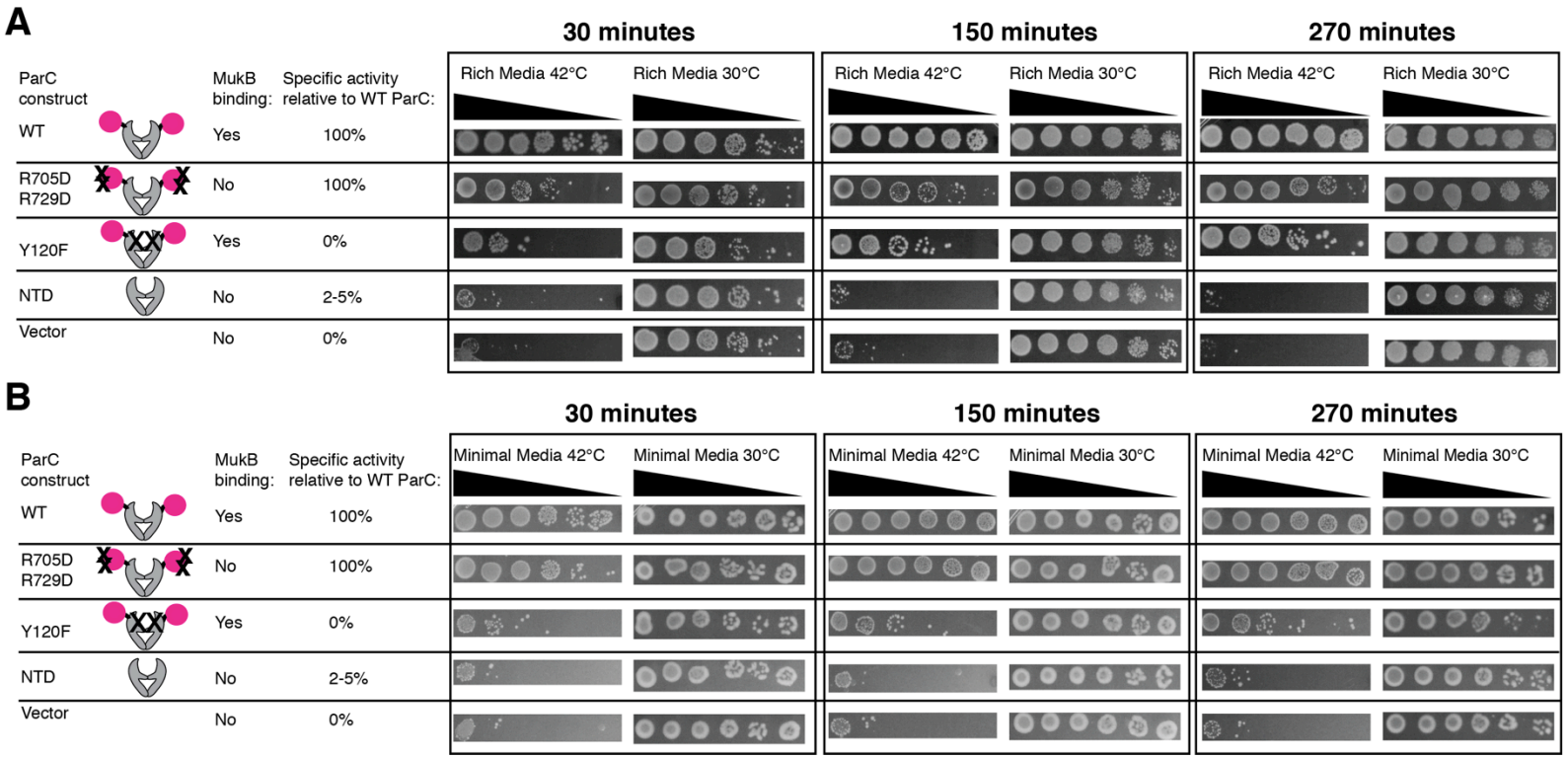

Figure S3.6.
Complementation of the ParC *C600parc1215* temperature sensitive strain after adapting to the non-permissive temperature for different periods of time in liquid culture prior to plating on (**A**) rich media or (**B**) minimal media. Spotted cultures correspond to 20-fold dilution series (black triangles) taken 30 minutes (right boxes), 150 minutes (middle boxes) or 270 minutes (left boxes) after the temperature shift. For plating, cells were normalized to the culture with the lowest OD_{600nm} at the time of the temperature shift ($OD_{600nm} \approx 0.3$) (see **Materials and Methods** for additional details). Cartoons of ParC constructs assayed, their specific activity relative to WT ParC and their ability to bind MukB are illustrated on the left of each row. Dilutions of cells grown at the permissive temperature (30˚C) are to the right of cells grown at the restrictive temperature.

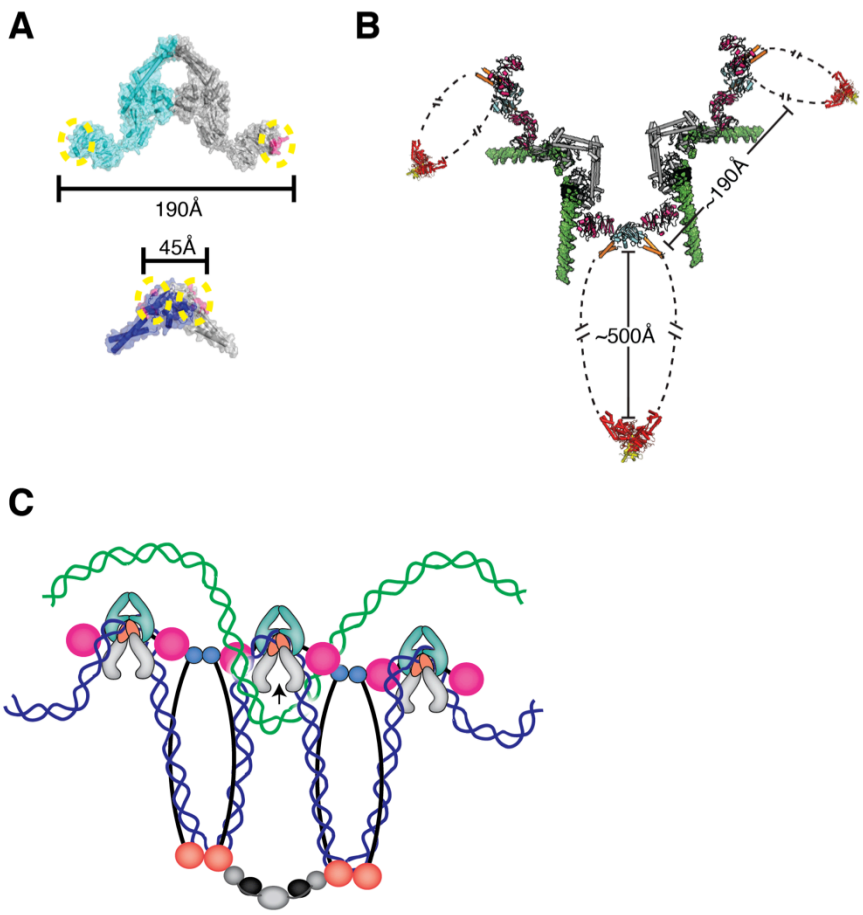

Figure 3.7. Physical considerations for the formation of higher-order MukB•ParC oligomers.
A The geometry of the MukB•topo IV interaction does not favor intradimeric complex formation. *Upper* – MukB binding sites (magenta with dotted yellow circles) are marked on the crystal structure of the *E. coli* ParC dimer (cyan and grey) (PDB ID: IZVU). *Lower* – The ParC binding sites (magenta with dotted yellow circles) are marked on the crystal structure of the *E. coli* MukB hinge dimer (navy blue and gray) (PDB ID: 3IBP). The distances between binding sites are shown in ångströms.
B The geometry of the MukB•topo IV interaction permits formation of oligomeric arrays. The ParC CTD (pink)•MukB hinge (cyan) coiled-coil arms (orange) structure determined here is shown docked onto with the full-length *E. coli* ParC crystal structure (grey) (PDB ID: IZVU), modeled with a docked G-segment DNA (green) (superposed from PDB ID: 2RGR). For perspective, the *Haemophilus ducreyi* MukB head domain (red) in complex with MukF (yellow) (PDB ID: 3EUJ) also is shown. Distances between subunits and domains are labeled.
C Prospective functional role of a MukB•ParC oligomeric array. Oligomers of MukB and ParC form through the hinge (cyan)•CTD (pink) interaction; MukB oligomers are further stabilized by interactions of their head domains with

accessory proteins, MukE (black) and MukF (gray). If MukB and ParC engage the same newly-replicated sister chromosome (blue) through DNA bending and looping, then the array predisposes topo IV to remove catenated crossovers formed with the corresponding sister chromosome (green).

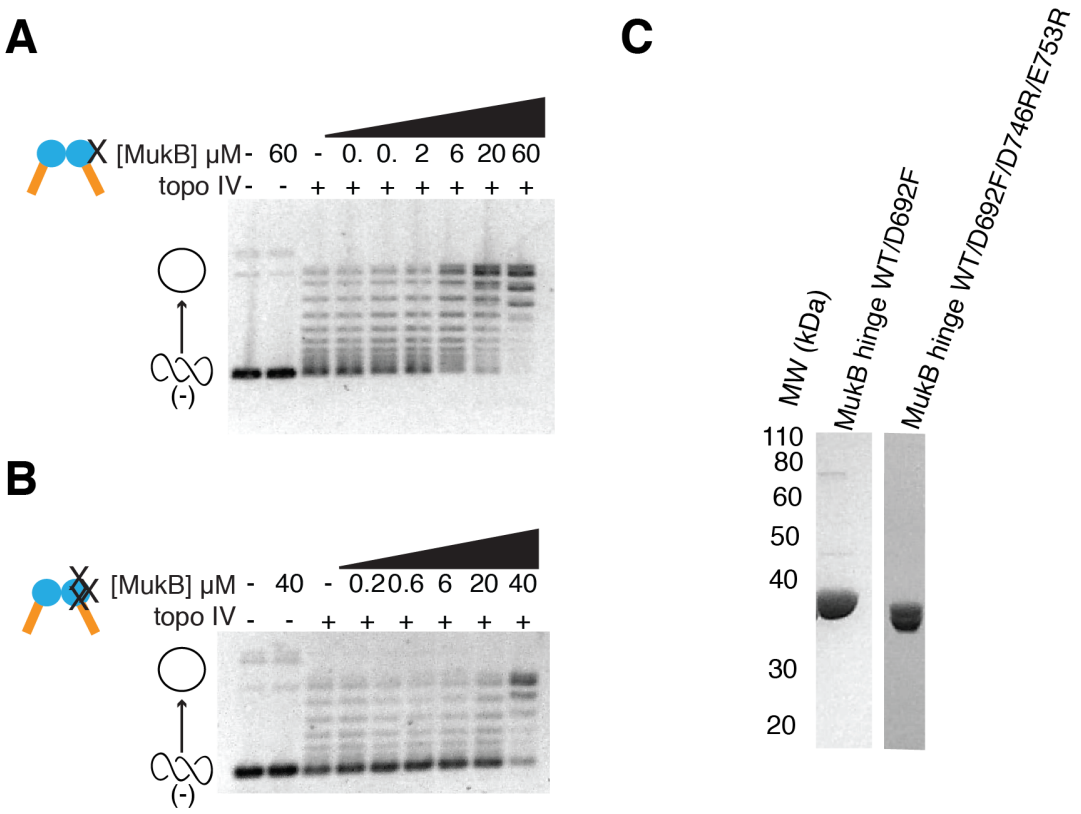

Figure S3.7. MukB-dependent stimulation of topo IV does not depend on higher-order oligomer formation.
To test whether the formation of higher-order topo IV•MukB arrays might underlie the observed stimulatory effect of the hinge, we incubated topo IV with negatively-supercoiled DNA in the presence of a large molar excess of the hinge. In this experiment, the concentration of topo IV was set near its dissociation constant for the hinge (500 nM) to permit robust complex formation, and balanced by an equimolar ratio of DNA to partition ~1-2 copies of the enzyme to each plasmid molecule. The hinge concentration was then increased to more than a 100-fold molar excess over the amount of topo IV present in the reaction to favor the binding of each topo IV holoenzyme to two separate hinge dimers and thereby preclude the formation of higher-order ParC•MukB oligomers. Inspection of the resultant relaxation products showed that the hinge still stimulated topo IV activity on negatively-supercoiled DNA even when present in such an overabundance (**Fig 3.4A**), indicating that the formation of a higher-order MukB•topo IV oligomer does not underpin the stimulatory effects arising from the interaction of the two proteins.

To further test whether the oligomerization of topo IV by MukB might play a role in stimulating negative supercoil relaxation, we set out to completely disrupt the formation of higher-order arrays by purifying a MukB hinge

heterodimer containing one wild-type subunit and one ParC binding-deficient mutant subunit. Both a single (D692F) and triple interface mutant (D692F/D746R/E753R) were tested; the MukB hinge forms a stable dimer in solution (Li et al, 2010; Li et al, 2009), allowing us to purify heterodimers away from homodimers by using differential affinity chromatography (See **Materials and Methods**). As with the super-stoichiometric assay, we found that both hinge heterodimers stimulated topo IV activity at concentrations roughly two-fold higher than those required for stimulation by the wild-type MukB hinge homodimer, a value consistent with the 50% reduction in the available number of ParC binding sites present in the constructs (compare the 10 and 30 μM lanes in **Fig 3.4A** to the 20μM and 60μM lanes, respectively, in panels **A** and **B** here). Together, these data indicate that while the geometry of the MukB•topo IV interaction should favor the formation of higher-order complexes (**Fig 3.7**), these oligomers are not necessary to stimulate topo IV function. Instead, the action exhibited by MukB appears to derive specifically from the ability of its hinge to mask an autorepressive site on the ParC CTD.

Panels A and B) Heterodimer titrations. Topo IV (500nM) was incubated with various concentrations of a MukB hinge heterodimer (WT•Asp692Phe or WT•Asp692Phe/Asp746Arg/Glu753Arg) and 500nM of negatively-supercoiled plasmid pSG483. Topoisomer states are represented graphically on the left side of the gel. The maximal protein concentration tested was limited to 40μM due to low yields for the heterodimer complex.

Panel C) Purity of MukB hinge heterodimers. Here 0.3μg of each protein construct was run on 10% SDS PAGE to confirm purity. MukB hinge refers to the MukB (566-863). MW positions are labeled on the left side of the gel. Note that the MukB hinge D692F/D746R/E753R runs slightly faster than the WT hinge, likely due to a difference in relative charge (**Fig S3.2**); in the WT•D692F/D746R/E753R hinge heterodimer construct, the protein appears as a doublet.

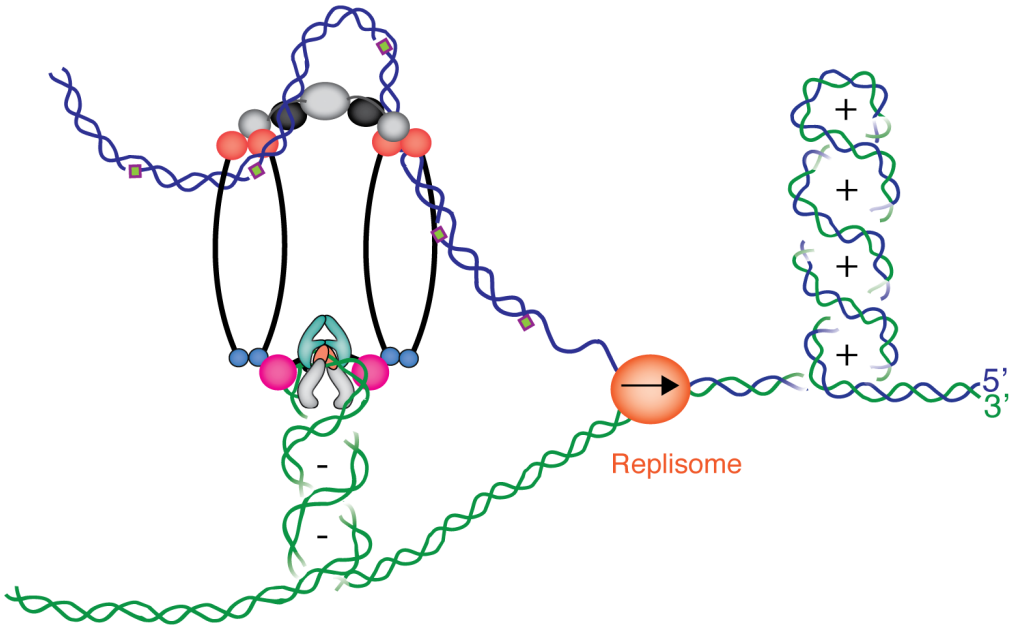

Figure S3.8. Alternative prospective role for MukB·topo IV interaction. During DNA replication, negative supercoils can form behind the replisome (orange) in the leading DNA strand (green), but not in the lagging strand (blue) due to gaps between the Okazaki fragments (purple and green boxes indicate RNA primers). Association of MukB (hinge sky blue, head domain red, coiled-coil arms black) with topo IV (ParC cyan, ParC CTD magenta, ParE gray) on the leading strand could stimulate topo IV to preferentially dissipate these negative supercoils by masking its autorepressive site for this substrate on the CTD.

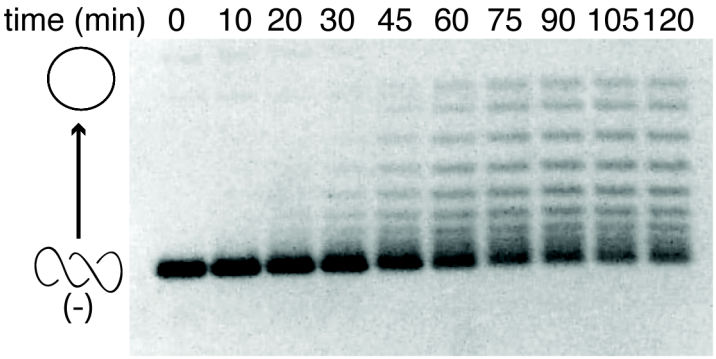

Figure S3.9.
Relaxation of negatively-supercoiled DNA at 15°C. Positive supercoil relaxation experiments performed at 15˚C in the presence of topo IV have a topoisomer distribution closer to supercoiled (see **Fig 4B**). When topo IV (500nM) is incubated with negatively-supercoiled DNA (500nM) at 15˚C, a similar shift in topoisomer distribution is observed.

Chapter 4- Novel Gyrase Control Mechanism Revealed by Co-Crystal Structure of *Escherichia coli* Gyrase bound to the Proteinaceous Inhibitor YacG

Introduction

The ability to rapidly alter the production and activity of proteins associated with housekeeping and proliferative processes is essential to allow cells to respond to environmental and developmental cues. Appropriate regulation of gene expression and cell growth can occur through variety of mechanisms such as transcription factors and RNAi (Castel & Martienssen, 2013; de Nadal *et al*, 2011).

Although difficult to monitor directly, chromosome topology is similarly known to play a central part in homeotic control and response pathways (Dorman *et al*, 1990; Sonnenschein *et al*, 2011; Stewart *et al*, 1990; King *et al*, 2013; Pedersen *et al*, 2012; Merino *et al*, 1993). The topological state of chromosomes is maintained by a variety of factors, including DNA bending and wrapping proteins and the ability of DNA supercoil upon itself in response to over and undertwisting (Luijsterburg *et al*, 2008). Topoisomerases are a ubiquitous class of enzyme that play a particularly key role in controlling topological status, supporting essential DNA transactions such as replication, transcription, and repair (Vos *et al*, 2011). Topoisomerases alter supercoiling levels and can resolve chromosomal tangles by transiently breaking, moving, and rejoining different DNA segments with respect to each other (Schoeffler & Berger, 2008). In turn, topoisomerase expression level and activity are reciprocally influenced by the extent of supercoiling in the genome and the metabolic status of the cell (Menzel & Gellert, 1983; Schneider *et al*, 1999; Tse-Dinh & Beran, 1988; Rovinskiy *et al*, 2012; Champion & Higgins, 2007; Kouzine *et al*, 2013; Naughton *et al*, 2013; Hsieh *et al*, 1991; van Workum *et al*, 1996). Due to their central role in aiding the proper flow of genetic information, and to their ability to transiently create DNA nicks and breaks, topoisomerases have served as the successful targets of a number of cell-killing agents, often with great therapeutic benefit (Nitiss, 2009a; Pommier *et al*, 2010; Collin *et al*, 2011).

Because the DNA substrates for topoisomerases frequently bear distinctive biophysical properties and/or shapes (Schoeffler & Berger, 2008), it has frequently been assumed that topoisomerases are generally “stand-alone” actors that rely on the topological state of DNA to direct their time and place of work. However, many studies have called this assumption into question, instead showing that in cells, topoisomerases are actually subject to multiple levels of control (Vos *et al*, 2011), including condensin-like proteins (Li *et al*, 2010; Hayama & Marians, 2010; Bhat *et al*, 1996), anti-toxin toxin components (Bernard & Couturier, 1992; Vizán *et al*, 1991), post-translational modification machineries (Takahashi, 2005; Díaz-Martínez *et al*, 2006; Azuma *et al*, 2005),

and chromatin remodeling complexes (Dykhuizen *et al*, 2013; Varga-Weisz *et al*, 1997). At present, it has yet to be established how a majority of these factors directly modulate topoisomerase activity. How these control mechanisms are in turn more broadly integrated with feedback systems that use changes in topoisomerase function to fine-tune transcriptional output as a means to alter metabolic state or respond to the cellular environment is similarly unknown.

In bacteria, both transcription and the initiation of DNA replication are highly sensitive to the steady-state levels of DNA underwinding or overwinding present in the cell (Drlica, 1992; Champion & Higgins, 2007; Baker *et al*, 1986; Freiesleben & Rasmussen, 1992). This steady-state is determined in part by two topoisomerases, topo I and gyrase (Sternglanz *et al*, 1981; Zechiedrich *et al*, 2000; DiNardo *et al*, 1982; Pruss *et al*, 1982), which counterbalance other by either adding (gyrase) or subtracting (topo I) negative supercoils to and from DNA (Gellert *et al*, 1976; Wang, 1971).-To date, a number of distinct proteins and pharmaceutical agents have been discovered that either generally inhibit gyrase to in response to specific toxins or environmental cues or that trap gyrase in a covalent complex with DNA to directly induce cell death (Collin *et al*, 2011). While significant strides have been made in understanding how small-molecule inhibitors interfere with topoisomerase function (Pommier *et al*, 2010; Pommier, 2013), how proteinaceous inhibitors of these enzymes exert specific agonistic or inhibitory effects remains a frontier question.

Here we have determined how one newly-discovered protein, YacG, inhibits gyrase directly. YacG is a member of the treble clef and FCS zinc finger motif families (Grishin, 2001; Ramelot *et al*, 2002; Krishna *et al*, 2003; Lechtenberg *et al*, 2009) that mediate diverse functions including protein•protein (Fox *et al*, 1999) and nucleic acid interactions (Grishin, 2001; Krishna *et al*, 2003). Using x-ray crystallography, we show that the zinc-finger domain of YacG prevents DNA binding by gyrase by both remodeling a key loop associated with resistance to fluoroquinolones, a highly successful class of antibacterial agent, and occluding the enzyme's principal DNA binding site. At the same time, the extreme C-terminus of YacG forms an extended tail that unexpectedly associates with region of gyrase found to serve as the binding locus for a recently discovered gyrase inhibitor, GSK299423 (Bax *et al*, 2010). Biochemical experiments confirm the importance of the interactions seen structurally to YacG binding and function, and further show inhibition by YacG is specific to its cognate gyrase. We find that a C-terminal peptide encompassing both binding epitopes of YacG is sufficient to inhibit gyrase, while small-angle x-ray scattering experiments indicate that YacG further remodels the gyrase holoenzyme to enforce closure of is distal ATPase regions. Bioinformatic analyses of *yacG* and its neighboring genes across bacterial species suggest that the YacG protein regulates gyrase, and thereby supercoiling-dependent transcriptional and replicative events, in response to specific metabolic signals linked to cell growth. Together, our work defines a novel protein-based mechanism for regulating gyrase that may be of use in the development of new classes of small-molecule

gyrase inhibitors, and further provides a framework for understanding how bacteria can control topoisomerases in response to specific cellular demands.

RESULTS

YacG preferentially binds to the C-terminus of GyrB

Gyrase is heterotetrameric ($GyrA_2$•$GyrB_2$) enzyme that uses three, reversibly-associable dimer interfaces (or "gates") to coordinate the transient, ATP-dependent breakage of one DNA duplex and the passage of a second duplex through the break. YacG is a member of the treble clef and FCS zinc finger motif families (Grishin, 2001; Ramelot *et al*, 2002; Krishna *et al*, 2003; Lechtenberg *et al*, 2009) that mediate diverse functions including protein•protein (Fox *et al*, 1999) and nucleic acid interactions (Grishin, 2001; Krishna *et al*, 2003). To determine how *E. coli* YacG and gyrase interact, we cloned, purified, and performed fluorescence anisotropy-based binding experiments with various gyrase constructs and a fluorescently-labeled construct of the inhibitor. Consistent with a previous limited-proteolysis study suggesting that YacG binds primarily to the C-terminus of GyrB (Sengupta & Nagaraja, 2008), we observed that YacG associated robustly with the full-length gyrase tetramer, the individual GyrB subunit, and the isolated TOPRIM domain of GyrB ($K_{d,app}$~ 32.26-44.1±5.5-13.6nM) (**Fig 4.1A, 4.1B**). By contrast, no change in anisotropy was evident when YacG was incubated with the GyrB ATPase domain. Tests using GyrB•GyrA fusion protein (GyrBA) that lacks both an auxiliary C-terminal domain of GyrA and the GyrB ATPase domain (**Fig 4.1A**), but that is still capable of binding and cleaving DNA (Schoeffler *et al*, 2010), showed YacG could bind this construct with an affinity similar to that of the full-length gyrase tetramer ($Kd_{,app}$ 25±6.5nM). This construct, which had been crystallized previously (Schoeffler *et al*, 2010), was subsequently used for follow-up structural studies.

Determination of a binary YacG•Gyrase crystal structure

To crystallize an *E. coli* YacG•GyrBA complex, the two proteins were firth overexpressed and purified separately from each other, and then mixed together upon setting trays (**Fig S4.1**). Following crystallization by hanging-drop vapor diffusion and the collection of diffraction data, the structure was solved by molecular replacement (MR) using the previously reported apo structure of the *E. coli* GyrBA fusion as a search model (Schoeffler *et al*, 2010). Inspection of the resultant MR maps revealed strong difference density associated with each GyrBA dimer that could accommodate two copies of YacG. For the purposes of refinement, strong anisotropy evident in the diffraction data was accounted for by applying an ellipsoidal truncation to the structure factors (Strong *et al*, 2006). Following several rounds of rebuilding, refinement stabilized at an R_{work}/R_{free} of 23.0/27.8% for the resolution range of 3.5-3.3-3.15Å (**Table 4.1**). The final model contains nearly all regions of four copies of GyrBA and YacG present in the asymmetric unit, with the exception of a single GyrB "insert" domain (**Fig 4.1A**) in each GyrBA homodimer that was too disordered to model.

YacG binds to GyrB and GyrA to remodel and occlude the DNA binding groove of gyrase

Inspection of the GyrBA•YacG complex reveals that the inhibitor recognizes gyrase by a bipartite mechanism. The dominant contacts are formed by the globular zinc-finger domain of YacG, which nestles against the GyrB TOPRIM fold on the portion of the domain that faces the enzyme's principal DNA binding groove (**Figs 4.1C**). YacG primarily associates with the TOPRIM region using its lone α-helix and a ten amino-acid linker that connects the helix to the two β-strands of the zinc-binding motif. Specific contacts between YacG and GyrB include residues Trp18 and Pro26 with Tyr515, residues Asp36, Lys30, Gln33 with amino acids Arg516, Asp481 and Gln517, and residue Ile47 with His505, Leu509, Phe777, and Leu780 (**Fig 4.2A, 4.2B**).

One particularly notable interaction between YacG and GyrB derives from the C-terminal α-helix of the inhibitor, a region that previous NMR studies had shown to be unstructured in the apo protein (PDB ID:1LV3) (Ramelot *et al*, 2002) (**Fig 4.2B**). This element, which is ordered in the structure of the complex, allows Trp40 of YacG to dock into a hydrophobic pocket on GyrB composed of residues Met461, Leu509, Phe513, Phe777, and the aliphatic arm of Arg516 (**Fig 4.2A**). Trp40 is invariant in all YacG proteins, while the GyrB hydrophobic pocket is well conserved in all corresponding GyrB counterparts, suggesting that the interaction is important to the binding affinity of the two proteins (**Figs S4.2, S4.3**). Consistent with this idea, using phylogenetic and biochemical studies, we found that gyrases which derive from bacteria that lack YacG (such as *Mycobacterium smegmatis*) have a slightly altered suite of amino acids in their respective TOPRIM domains and are not inhibited by *E. coli* YacG (**Fig S4.4**).

The association of YacG with gyrase induces reciprocal conformational changes within GyrB, particularly within a loop on the TOPRIM domain (residues 446-464) that is linked to quinolone resistance (the so-called "QRDR" motif, corresponding to residues 426-464 in *E. coli* (Piton *et al*, 2010; Yoshida *et al*, 1991)) (**Fig S4.2**). The QRDR loop is unstructured in almost all type IIA topoisomerases in the absence of DNA (Fu *et al*, 2009; Schoeffler *et al*, 2010; Piton *et al*, 2010) (**Fig 4.2C**), but becomes ordered and visible when DNA is present (**Fig 4.2D**) (Laponogov *et al*, 2013; Wendorff *et al*, 2012; Schmidt *et al*, 2010; Wohlkonig *et al*, 2010; Bax *et al*, 2010; Dong & Berger, 2007; Laponogov *et al*, 2010). Ordering of the QRDR loop through DNA binding masks the hydrophobic pocket occupied by Trp40 of YacG, whereas the pocket is exposed when the loop is unstructured. In the YacG•GyrBA co-crystal structure, the QRDR loop is ordered, but takes on a conformation not seen previously, projecting over the gyrase active site (**Fig 4.2E**). Modeling of various DNA-bound type IIA topoisomerases onto the YacG•GyrBA structure indicates that the rearrangement of the QRDR loop induced by the binding of YacG would sterically clash with a bound DNA (**Fig 4.2F**).

The orientation of YacG on the GyrB TOPRIM fold also orients the inhibitor's C-terminus toward the DNA cleavage center of gyrase (**Fig 4.3**).

Although one copy of the YacG zinc-finger domain is seen to associate with each GyrBA dimer (**Fig 4.1C**), only a single YacG C-terminus is visible in the tetrameric complex. In the case of the more ordered YacG C-terminal tail, this region binds asymmetrically to GyrA, across the dyad that relates the winged-helix domains (WHD) of the two GyrA protomers with one another; the extended conformation and placement of the ordered tail excludes the tail of its dimer-related YacG partner from occupying the same site. Surprisingly, the position of the ordered YacG tail allows Trp59 of the protein to dock into a pocket between the GyrA WHDs that was recently shown to be a binding site for a newly discovered small-molecule inhibitor of gyrase, GSK299423 (**Fig 4.3**) (Bax *et al*, 2010).

YacG•GyrB interactions are required for inhibition of DNA supercoiling by gyrase

To establish whether the specific contacts observed in the YacG•GyrBA model are important for YacG's biochemical function, we designed, cloned, and purified several *E. coli* YacG mutants based on the structure, and tested the activities of these altered constructs against *E. coli* gyrase. Given its conservation and prominence in the YacG-GyrB interface, Trp40 was mutated to a smaller residue (valine). Using amino acid sequence conservation and contacts evident from the structure, we also constructed three different truncations of the YacG C-terminus (residues Δ40-65, Δ46-65, and Δ52-65) (**Figs S4.1-S4.3**).

To establish whether the specific contacts seen in our structure are important for the activity of YacG in general, we next used fluorescence anisotropy to look at the ability of different YacG mutants to compete prebound (fluorescently-labeled) wild-type YacG off of gyrase. As a control, unlabeled wild-type YacG proved readily able to compete with the binding of the labeled wild-type inhibitor to gyrase (**Fig 4.4A**) ($K_{i,app}$=0.36±0.12 μM). Removal of the C-terminal tail of YacG up to residue 52 only marginally reduced the ability of the protein to compete with wild-type YacG ($K_{i,app=}$0.96±0.16 μM); however, further tail truncations greatly reduced ($YacG^{\Delta 46-65}$; $K_{i,app=}$9.14±3.8 μM) or completely abrogated ($YacG^{\Delta 40-65}$) competition (**Fig 4.4A**). The $YacG^{Trp40Val}$ mutant behaved similarly to the most severe truncation tested, showing essentially no ability compete wild-type YacG from gyrase. Together, these data corroborate our structural observations, indicating that the C-terminal region of YacG, Trp40 in particular, is required for efficient inhibition by the protein.

We next used native agarose gels to examine the effect of our panel of wild and mutant YacG proteins on gyrase's principal activity, the ATP-dependent introduction of negative supercoils into DNA (Gellert *et al*, 1976). As reported previously (Sengupta & Nagaraja, 2008), the addition of wild-type YacG inhibited gyrase supercoiling activity in a dose-dependent manner (**Fig 4.4B**), with gyrase supercoiling DNA ~50% less effectively at a concentration of 300nM YacG and not all at ~3μM YacG. The YacG construct bearing the least severe truncation (Δ52-65) inhibited gyrase in a manner comparable to wild-type YacG (**Fig 4.4C**), while the intermediate C-terminal truncation (Δ46-65) was ~3 fold less effective at inhibiting supercoiling activity (**Fig 4.4D**). By comparison, mutation of Trp40 to

valine, or the removal of residues 40-65, resulted in YacG proteins that had little (if any) discernable effect on supercoiling by gyrase (**Figs 4.4E, 4.4F**). These data support the premise that Trp40 and the portion of the YacG tail that binds GyrB are important for YacG function, and that the contribution of these elements to gyrase inhibition masks any benefits that might be afforded by the additional contacts seen between YacG's extreme C-terminus and GyrA.

YacG physically blocks DNA binding to gyrase

Based on the observed binding position of YacG on GyrB and GyrA (**Figs 4.1C, 4.2**), our structure suggested that YacG would inhibit gyrase by sterically blocking the topoisomerase's principal DNA-binding site. To test this model directly, we assessed the effects of our panel of YacG mutants on the DNA affinity of gyrase using fluorescence anisotropy. To specifically examine the effects of YacG on the binding of duplexes that associate with gyrase's DNA cleavage center, we formed gyrase tetramers from full-length GyrB and a truncation of GyrA that lacks an auxiliary C-terminal DNA binding and wrapping domain (gyrase$^{\Delta CTD}$). Using a FITC-labeled, 37mer duplex DNA (20nM) sufficiently long to span gyrase's central DNA-binding site, we found that our gyrase$^{\Delta CTD}$ construct could bind this substrate with a $K_{d,app}$ of ~64±9 nM (**Fig 4.4G**), a value close to that of the wild-type gyrase ($K_{d,app}$=58±4 nM, **Fig 4.4G**). Consistent with previous studies (Hiasa & Shea, 2000), we found that the interaction of gyrase$^{\Delta CTD}$ with DNA was highly salt sensitive, necessitating the use of a relatively low salt concentration (30mM potassium glutamate) in the assay (**Fig S4.6A**).

We next titrated YacG against a fixed amount of gyrase$^{\Delta CTD}$ and the FITC-labeled 37mer DNA (20nM), using an excess of the topoisomerase compared to DNA (500 vs. 20 nM) to ensure that all substrate was bound in the reaction. In agreement with previous EMSA experiments (Sengupta & Nagaraja, 2008), the addition of YacG resulted in a dose-dependent decrease in DNA association by gyrase ($K_{i,app}$=35±11 nM) (**Fig 4.4H**). Replicates of the experiment performed in the absence of gyrase$^{\Delta CTD}$ resulted in no observable change in anisotropy, indicating that YacG did not associate with DNA itself (**Fig S4.6B**). When gyrase$^{\Delta CTD}$ was incubated with the least severe YacG truncation (Δ52-65), we observed binding inhibition that was comparable to that seen for wild-type YacG ($K_{i,\ app}$=31±14 nM). By contrast, the more moderate truncation mutant, YacG$^{\Delta 46\text{-}65}$, was only partially able to prevent DNA from binding to gyrase ($K_{i,\ app}$=199±35 nM), while both the most severe YacG truncation (Δ40-65) and YacG^{Trp40Val} were both unable to compete DNA off of the enzyme (**Fig 4.4H**). Together with the placement and effect of YacG on the structure of GyrB (**Fig 4.1C, 4.2F**), these data indicate that YacG operates by sterically preventing DNA from binding to gyrase, and that Trp40 in particular is a so-call "hotspot" residue (Clackson & Wells, 1995), providing key support for the YacG-gyrase interaction.

The isolated C-terminus of YacG is sufficient for inhibiting gyrase

Given the essential role the C-terminus of YacG appears to play for the activity of the inhibitor, we were curious as to whether this region alone might be sufficient

to inhibit gyrase. To test this idea, we assessed whether peptides corresponding to residues 40-52 and 40-65 of YacG could compete with DNA binding to the enzyme. Different concentrations of both YacG peptides were titrated against both gyrase$^{\Delta CTD}$ (500nM) and the labeled 37mer duplex used in the previous DNA binding experiments, while changes in fluorescence anisotropy were monitored at the emission maximum for the associated FITC dye. Notably, we found that whereas the shorter YacG$^{40-52}$ peptide had no effect on the gyrase DNA complex, the entirety of the YacG$^{40-65}$ C-terminus was sufficient to compete gyrase off of DNA in a dose-dependent manner ($K_{i,\ app}$=93±10 μM), (**Fig 4.5A**). Analysis of both peptides in DNA supercoiling reactions followed a similar trend, with only the longer YacG$^{40-65}$ peptide proving capable of blocking gyrase activity (**Fig 4.5B, 4.5C**). Together, these data show that the isolated C-terminus of YacG is both necessary and sufficient to prevent gyrase from associating with and supercoiling DNA, albeit with lower efficiency compared to the full-length protein. Interestingly, although YacG inhibits gyrase with near wild-type efficacy when its C-terminus is truncated after residue 51 (**Fig 4.2B, Fig 4.4A-C, 4.4H**), the C-terminal peptide alone required the remaining 13 amino acids (residues 53-65) to block gyrase function. This result indicates that the C-terminal interactions formed between YacG and GyrA aids in the action of the protein against gyrase, but that these contributions are largely masked by more dominant contacts between the body of YacG and GyrB, Trp40 in particular.

YacG appears to induce ATPase domain closure in the gyrase holoenzyme

In addition to blocking DNA binding, *E. coli* YacG has been reported to diminish the basal (DNA-free) ATPase activity of gyrase (Sengupta & Nagaraja, 2008). As the YacG•GyrBA complex imaged here lacks the ATPase domain of GyrB (**Fig 4.1A**), an explanation for this effect was not immediately evident from the structure. To determine whether YacG might have some additional effect on the organization or architecture of the gyrase holoenzyme, we therefore modeled our structure onto previously crystallized, near-full-length crystallographic structures of type IIA topoisomerases from *S. cerevisiae (*topo II) (PDB ID: 4FGH) (Schmidt *et al*, 2012) and *S. pneumoniae (*topo IV) (PDB ID: 4I3H)(Laponogov *et al*, 2013), which together exhibit closed and open conformations of the ATPase gate, respectively. Inspection of the resultant models suggested that YacG binding to the TOPRIM fold GyrB might allow the protein to interact with the ATPase domains when they are closed and thereby potentially interfere with their reopening to impede ATP turnover.

To test the idea that YacG might globally affect the conformation of the gyrase holoenzyme, we analyzed the solution structure of gyrase$^{\Delta CTD}$ in the presence and absence of YacG by small-angle X-ray scattering (SAXS); the CTDs of GyrA were removed so as to avoid complications from their reported positional mobility (Kirchhausen *et al*, 1985; Papillon *et al*, 2013; Costenaro *et al*, 2005; Baker *et al*, 2011). Scattering data obtained for gyrase$^{\Delta CTD}$ in the absence of YacG showed that the protein adopted an extended conformation with a significantly greater R_g value than that seen for samples prepared with YacG ($R_{g,}$

$_{gyrase}$ = 90.3±1.7 vs. $R_{g,\ gyrase•YacG}$ = 62.8±2.7) (**Fig 4.6A, S4.7**). In the presence of the non-hydrolyzable ATP analogue AMPPNP, gyrase$^{\Delta CTD}$ alone underwent a further contraction (R_g = 76.0±0.5) (**Fig 4.6A, S4.7**), consistent with the known ability of this nucleotide to promote closure of the GyrB GHKL ATPase domains (Wigley *et al*, 1991; Brino *et al*, 2000; Ali *et al*, 1993); however, when YacG was added, the hydrodynamic radius of the complex shrank even further (R_g = 59.2±2.4) (**Fig 4.6A, S4.7**). Together, these data demonstrate that YacG has a compacting effect on gyrase, inducing global conformational changes that inhibit the relative mobility of the enzyme.

To further define the action of YacG on the gyrase holoenzyme, we calculated 3D *ab initio* volumes from SAXS data collected with gyrase, YacG, and AMPPMP (attempts to produce 3D volumes with gyrase and AMPPNP alone failed to converge on any one subset of solution volumes, indicating that complex retained significant conformational heterogeneity). One volume in particular that arose frequently from random-seeded calculations exhibited an elongated “arrow” docking of the YacG•GyrBA complex and the gyrase ATPase domains into this volume revealed that it could readily accommodate a composite model in which the ATP- and DNA-binding-and-cleavage regions of gyrase assume a fully-dimerized conformation most similar to that seen in the AMPPNP- and DNA-bound crystal structure of yeast topo II (Schmidt *et al*, 2012) (**Fig 4.6B**). Together with the observed changes in R_g, this finding indicates that upon binding to the DNA-gate of gyrase, YacG can further interact with and stabilize the association of the enzyme’s ATPase domains as part of its inhibitory action.

Discussion

Although frequently considered to be relatively independent actors, multiple lines of evidence have shown that topoisomerases are actually subject to a wide number of cellular control mechanisms, ranging from protein-protein interactions to post-translational modifications (Nitiss, 2009b; Vos *et al*, 2011). However, how the vast majority of these regulatory systems operate is not understood.

YacG is a recently-identified protein that represses the supercoiling activity of DNA gyrase *in vitro* (Sengupta & Nagaraja, 2008a). To understand how YacG interferes with gyrase function, we determined the co-crystal structure of a minimal gyrase fusion construct comprising the central DNA-binding-and-cleavage region of the enzyme bound to the full-length inhibitor. The structure reveals that YacG binds to both the GyrB and GyrA subunits of gyrase, remodeling a loop associated with fluoroquinolone resistance (the "QRDR") to occlude gyrase's central DNA-binding groove (the "DNA-gate"). The observed restructuring of the QRDR region is mediated by interactions between the C-terminus of YacG and a hydrophobic pocket on GyrB that is surface exposed in the absence of DNA. Biochemical experiments confirm that contacts observed between the C-terminus of YacG and GyrB are required for binding of the inhibitor to gyrase and for the subsequent YacG-dependent inhibition of both DNA binding and strand passage by the enzyme. Interestingly, we find that the C-terminal region alone is both necessary and sufficient to inhibit gyrase-dependent supercoiling and DNA binding, provided that the extreme termini of YacG is present to engage a small pocket formed on the surface of GyrA when the region is dimerized. Moreover, using SAXs, we show that YacG helps compact gyrase by stabilizing a dimerized state of the N-terminal GHL ATPase domains of GyrB. This latter result helps explain the inhibitory effect YacG has on the basal ATPase rate of gyrase, and highlights the action of a multifaceted inhibitor that exploits several binding surfaces on gyrase to achieve its function.

Taken together, the present study provides the first high-resolution insights into how a protein-based inhibitor can associate with a catalytically-functional type II topoisomerase to regulate its biochemical activity. The manner by which YacG acts in turn establishes a new mechanistic approach for the control of gyrase by an endogenous cellular protein. In this scheme, two copies of YacG would each first bind to the TOPRIM fold of a pair of GyrB subunits in the gyrase holoenzyme in absence of DNA. Binding, mediated in large part by an invariant tryptophan, would subsequently remodel the QRDR loop of both GyrB protomers, blocking access the principal DNA-binding-and-cleavage center of the enzyme (**Fig 4.7A**). Once bound, the orientation of YacG would allow the extended C-terminus of one YacG protomer to engage the GyrA portion of gyrase's nucleolytic center, in part by positioning a second tryptophan into small binding pocket in the region; the binding mechanism of this latter tryptophan (Trp59), which occupies the same region as a recently discovered small molecule

inhibitor of gyrase, GSK299423, suggests that the drug may exploit a natural inhibitory locus on the enzyme. Once YacG has stably bound gyrase in the presence of ATP, the zinc-binding domain of the inhibitor would interfere with ATPase domain dissociation, thereby stabilizing a dimerized form of the region. Given that full-length gyrase binds to long DNAs much more tightly than to YacG (0.2nM (Higgins & Cozzarelli, 1982; Morrison *et al*, 1980) vs. ~30nM (**Fig 4.1B**), respectively), this mechanism would appear well-suited to sequestering gyrase from engaging DNA, rather than to promoting its dissociation from DNA once already bound (**Fig 4.7**).

One key issues that remains to be addressed is the role of YacG *in vivo*. Gyrase is an essential enzyme required for both DNA replication and transcription, and is targeted by both proteinaceous and pharmaceutical agents (Collin *et al*, 2011). Proteinaceous inhibitors of bacterial gyrases can be divided into two broad classes, those found typically in plasmid borne toxin-antitoxin systems and those that inhibit DNA binding by gyrase. Antitoxin-toxin proteins and peptides such as CcdB(Bernard & Couturier, 1992), ParE (Jiang *et al*, 2002; Yuan *et al*, 2010), and Microcin B17(Vizán *et al*, 1991) trap Gyrase in a covalent cleavage state if their respective antitoxin is absent, resulting in the formation of double-strand DNA breaks and rapid cell death. Conversely, proteins that prevent gyrase from binding DNA, such as the pentapeptide repeat proteins Mpfa/Qnr or the glutamate racemase MurI, have been proposed to protect cells from the toxic effects of fluoroquinolones by sequestering gyrase from DNA (Sengupta & Nagaraja, 2008b; Sengupta *et al*, 2008; Hegde *et al*, 2005; Hashimi *et al*, 2007). While YacG would appear to fall into the second class of proteinaceous inhibitor, to date it has not been implicated in fluoroquinolone resistance.

If YacG is not involved in drug resistance, what then what purpose does it serve to the cell? Based on a survey of existing bacterial genomes, we propose that normal YacG may be a regulator of cell growth in response to metabolic stress. The rationale for this idea comes from our observation that YacG is frequently found downstream of an essential metabolic protein, dephospho-CoA kinase (CoaE), and in a few instances even appears to be fused to CoaE as part of a single polypeptide (**Fig S4.3**). CoaE is the last enzyme in the coenzyme A (CoA) biosynthetic pathway, and acts by adding phosphate to the 3' ribose moiety of dephospho-CoA. Since CoaE and YacG appear to be part of the same operon, conditions result in transcription of CoaE could also produce YacG.

One instance where co-transcription of YacG and CoaE may be useful is during fatty acid biosynthesis. During this process, CoA is utilized as precursor to produce fatty acids required for cells to grow in size (Yao *et al*, 2012). Interestingly, the amount of DNA in an *E. coli* cell is proportional to the mass of the cell, and DNA replication initiation is restricted until cells reach an appropriate size size:DNA ratio (Donachie, 1969; Hill *et al*, 2012; Donachie *et al*, 1976). When cells require more CoA synthesis to make fatty acids, YacG expression could inhibit DNA replication by suppressing gyrase, thereby preventing cells from reaching a sufficiently negative level of superhelical density (which is

required for origin melting (Baker *et al*, 1986; Freiesleben & Rasmussen, 1992)) until the appropriate size :DNA ratio is reached. The YacG-dependent sequestration of gyrase away from the DNA would also serve to rapidly alter transcription, which (like replication) is also highly sensitive to supercoiling status. Consistent with a role in controlling cell growth, when *E. coli* cells possessing a non-functional *yacG* allele are given sub-lethal doses of a fatty acid elongation inhibitor cerulenin, they grow better than the isogeneic wild-type strain at all concentrations tested (Nichols *et al*, 2011). This latter finding suggests that if the CoA biosynthetic pathway is upregulated in response to reduced fatty acid availability, then co-expression of YacG could act to inhibit DNA replication until cells produce enough fatty acids to grow to an appropriate size where replication is now desired. Consistent with this idea, in *B. subtilis,* an organism that does not encode YacG, the cell size:DNA ratio does not influence replication initiation (Hill *et al*, 2012)

Control of gyrase through metabolic means is not unprecedented. The supercoiling activity of gyrase has been found to be sensitive to the relative ratio of ADP and ATP concentrations *in vivo* (Westerhoff *et al*, 1988; Hsieh *et al*, 1991). Gyrase also has been found to be inhibited by the glutamate racemase MurI (Sengupta & Nagaraja, 2008b; Sengupta *et al*, 2006; Ashiuchi *et al*, 2002), which converts L-glutamate to D-glutamate for synthesis of peptidoglycan components of the cell wall. It is unknown why MurI inhibits Gyrase, but the protein appears to do so by again preventing the enzyme from associating with DNA(Sengupta *et al*, 2006); whether inhibition is direct, as we find for YacG, or allosteric in nature is not known. Regardless, this finding indicates that MurI may serve as another means to link cell wall synthesis to the control of transcription and DNA replication by restricting gyrase function and, together with the available data on YacG, suggests that gyrase inhibition could prove to be a key cell-cycle dependent means to regulate DNA replication and transcription in response to nutrient availability. Future studies will be necessary to test these ideas further.

MATERIALS AND METHODS

Cloning of YacG, GyrA, and GyrB constructs

Full-length *E. coli* GyrA and GyrB, $GyrA_{\Delta CTD}$ (1-522), and the GyrBA fusion construct were cloned as previously described (Schoeffler *et al*, 2010). The YacG coding region was amplified from a previously described construct (Sengupta & Nagaraja, 2008) and inserted into a modified pET28b plasmid behind an N-terminal, hexa-histidine (His6)/maltose-binding protein (MBP) tag followed by a tobacco etch virus (TEV) cleavage site. The coding regions of *M. smegmatis* GyrA (1-842), GyrB (1-675) and the *E. coli* GyrB ATPase domain (1-393) and TOPRIM domains (320-804) were amplified from genomic DNA and inserted into modified pET28b plasmids behind an N-terminal hexa-histidine tag followed by a TEV protease cleavage site. Truncations were made by 'Round-the-horn' PCR and mutations were introduced by site directed mutagenesis using QuikChange (Stratagene).

Protein expression and purification

All proteins were overexpressed in *E. coli* in BL21(DE3)RIL cells. Cells were grown at 37˚C and protein expression was induced by adding 0.5mM IPTG when cells reached an OD_{600nm} ~0.3. After induction, cells were grown for 3-4 hours at 37˚C and were harvested by centrifugation. Cell pellets were resuspended in buffer A800 (800mM NaCl, 20mM Tris-HCl pH 7.9, 30mM imidazole pH 8.0, 0.5mM TCEP, 10% (v/v) glycerol, 5µM $ZnCl_2$), snap frozen in liquid nitrogen, and stored at -80˚C prior to protein purification.

For protein purification, cells were thawed, lysed by sonication, and centrifuged. Clarified lysates were passed over 5mL Ni^{2+} HiTrap columns (GE) equilibrated in A800. Columns were washed in A800 followed by A400 (400mM NaCl, 20mM Tris-HCl pH 7.9, 30mM imidazole pH 8.0, 0.5mM TCEP, 10% (v/v) glycerol, 5µM $ZnCl_2$). All constructs, except GyrB, were eluted from the column in B400 (400mM NaCl, 20mM Tris-HCl pH7.9, 30mM imidazole pH 8.0, 0.5mM TCEP, 10% (v/v) glycerol, 5µM $ZnCl_2$) and concentrated by centrifugation (Millipore Amicon 30 MWCO). Nickel columns bound with GyrB were exchanged into A50 (50mM NaCl, 20mM Tris-HCl pH 7.9, 30mM imidazole pH 8.0, 0.5mM TCEP, 10% (v/v) glycerol, 5µM $ZnCl_2$) prior to eluting the protein from the column in B50 (50mM NaCl, 20mM Tris-HCl pH7.9, 30mM imidazole pH 8.0, 0.5mM TCEP, 10% (v/v) glycerol, 5µM $ZnCl_2$) directly onto a 5mL Hi-Trap Q (GE) anion exchange column equilibrated in B50. Buffer C50 was then applied to the Q column (50mM NaCl, 20mM Tris-HCl pH7.9, 0.5mM TCEP, 10% (v/v) glycerol, 5µM $ZnCl_2$) and GyrB was eluted from the column by a stepwise gradient from buffer C50 into buffer D500 (500mM NaCl, 20mM Tris-HCl pH7.9, 0.5mM TCEP, 10% (v/v) glycerol, 5µM $ZnCl_2$) and concentrated by centrifugation (Millipore Amicon 30 MWCO). Proteins were then mixed with 1mg His_6-TEV protease (Kapust & Waugh, 1999) and dialyzed against A400 in Slide-A-Lyzers (Pierce, 10 MWCO for gyrase constructs, 3.5 MWCO for YacG) for 16 h at 4˚C. The cleavage reactions were then applied to 5mL Hi-Trap Ni^{2+}columns equilibrated in

A400, which bound residual tagged protein and His_6-TEV protease while allowing cleaved proteins to pass through the column. Proteins from the flow-through were concentrated by centrifugation (Millipore Amicon, 30 MWCO for gyrase constructs, 3 MWCO for YacG) and applied to either an S-200 (YacG) or S-300 (Gyrase) (GE) columns equilibrated in SE500 (500mM KCl, 20mM Tris-HCl pH 7.9, 10% (v/v) glycerol, 0.5mM TCEP, 5μM $ZnCl_2$). Peak fractions were run on SDS-PAGE to confirm purity, pooled and concentrated by centrifugation. Protein concentration was measured by absorbance at 280nm as described by Edelhoch (Edelhoch, 1967). Proteins utilized for biochemistry were stored in a final buffer containing 500mM KCl, 30% (v/v) glycerol, 20mM Tris-HCl pH 7.9, 0.5mM TCEP, and 5μM $ZnCl_2$.

N-terminal Labeling of YacG

Purified YacG (500μL, 165μM) was exchanged into amine labeling buffer (25mM HEPES pH 7.5, 10% (v/v) glycerol, 5μM $ZnCl_2$, 200mM KCl, and 1mM TCEP, final pH of solution was 7.0) by centrifugation; the neutral pH favors labeling of the amino terminus of proteins over surface lysines by several orders of magnitude (Sélo *et al*, 1996). The protein was concentrated to a final volume of 350μL (final concentration 226μM). AlexaFluor 488 Carboxylic acid, 2,3,5,6 Tetrafluorophenyl Ester 5 isomer (Life Technologies) (1mg) was dissolved in 20μL DMSO. The dye (20μL) was added to the concentrated protein and the reaction was incubated at 4˚C, rocking, for 1 hour. Unreacted dye was quenched by adding 20μL of 1M L-lysine dissolved in 20mM Tris-HCl pH 7.5 and incubating the reaction at 25˚C for 30 minutes. Free dye was separated from dye-protein conjugates using a 10mL PD-10 desalting column (GE) equilibrated in amine labeling buffer. Protein was exchanged into a final solution containing 500mM KCl, 30% (v/v) glycerol, 20mM Tris-HCl pH7.9, 0.5mM TCEP, 5μM $ZnCl_2$, by centrifugation and was snap frozen in liquid nitrogen, and stored at -80˚C. The final concentration of the protein was 156μM.

Binding experiments with N-terminally labeled YacG and gyrase

Purified gyrase subunits and domains were thawed and dialyzed against protein dilution buffer (150mM potassium glutamate, 10% (v/v) glycerol, 5μM $ZnCl_2$, and 25mM Tris-HCl pH 7.9) at 4˚C for 16 h. Gyrase tetramers were formed by incubating equimolar concentrations of GyrA and GyrB on ice for 15 min (40μM, final tetramer concentration). For serial dilutions, reconstituted gyrase, individual subunits, and domains were sequentially diluted in 2-fold steps in protein dilution buffer. N-terminally labeled YacG was diluted to 500nM (labeled protein) in protein dilution buffer. N-terminally labeled YacG (8μL) and reconstituted gyrase, gyrase subunits, and gyrase domains (8μL) were mixed and incubated on ice for 10 min. The reaction was then brought up to a final volume of 80μL in a final solution containing 120mM potassium glutamate, 0.12mg/mL bovine serum albumin (BSA), 6μM $ZnCl_2$, 12% (v/v) glycerol, and 30mM Tris-HCl pH 7.9 and incubated at 25˚C in the dark for 10 min (a physiological salt concentration of 120mM potassium glutamate was used to reduce non-specific interactions

between the proteins). The final concentration of labeled YacG in each reach reaction was 50nM. Measurements were made with a Perkin Elmer Victor 3V 1420 multilabel plate reader at 535nm. Data points are the average of three independent experiments and all points are normalized to wells that did not contain reconstituted gyrase, gyrase subunits, or gyrase domains. Data were plotted in GraphPad Prism Version 6 using the following single-site binding equation:

$$y = Bmax\left(\frac{\left([x] + [L] + K_{d,app}\right) - \sqrt{([x] + [L] + K_{d,app})^2 - 4([x] \bullet [L])}}{2 \bullet [L]}\right)$$

where B_{max} is the maximum specific binding, L is the labeled YacG concentration, x is the gyrase concentration, and $K_{d,\,app}$ is the apparent dissociation constant (Kenakin, 1993; Swillens, 1995; Lundblad *et al*, 1996).

For competition assays, YacG constructs were dialyzed against protein dilution buffer at 4˚C for 16hrs. Gyrase tetramers were reconstituted as described above (500nM final tetramer) (4μL) and were mixed with N-terminally labeled WT YacG (50nM final) (4μL) and various non-labeled YacG constructs (8μL). Assays were then performed as described above for the labeled YacG and gyrase subunits and domains. Data were plotted in GraphPad Prism Version 6 using an exact expression for competitive binding between two ligands described by Wang (Wang, 1995).

Crystallization

For crystallography, freshly purified YacG and GyrBA were dialyzed separately at concentrations of 3-6mg/mL and 20-30mg/mL, respectively against 100mM KCl, 20mM Tris-HCl pH 7.9, and 1mM TCEP at 4˚C for 16hrs. YacG and GyrBA were mixed immediately after dialysis in ratios 1:1, 4:1, 8:1 and 16:1, respectively, at a final concentration of 15mg/mL complex. The YacG•GyrBA mixes were then mixed 1:1 with well solution containing 8.3% (w/v) PEG 3350, 30mM sodium cacodylate pH 5.0, 40mM potassium thiocynate, 30mM spermidine, and 2.5µM $ZnCl_2$ and co-crystallized by vapor diffusion. Crystals appeared after 24 h and continued to grow over the course of six days. Drops containing crystals were exchanged into a solution containing 25% (v/v) 1,2 propane diol, 50mM KCl, 10mM Tris-HCl pH 7.9, 0.5mM TCEP, 4.7% (w/v) PEG 3350, 15mM sodium cacodylate pH 5.0, 20mM potassium thiocynate, 15mM spermidine, 1.25μM $ZnCl_2$, harvested in nylon micro-loops (Hampton Research), and snap frozen in liquid nitrogen. Diffraction data were collected at Beamline 8.3.1 at the Lawrence Berkeley National Laboratory Advanced Light Source from a single crystal (MacDowell *et al*, 2004), and integrated and scaled using MOSFLM (Leslie & Powell, 2007). Strong anisotropy in the data was addressed by applying ellipsoidal truncation to the structure factors (Strong *et al*, 2006), which resulted in a resolution of 3.5-3.3-3.15Å (along the h, k, and l directions, respectively) for the purposes of refinement. The structure was solved by molecular replacement using PHENIX (Afonine *et al*, 2012), with a truncated *E. coli* GyrBA dimer (corresponding to a $GyrB^{\Delta ATPase}$•$GyrA^{\Delta CTD}$ fusion construct obtained from a

previously published structure, PDB ID: 3NUH (Schoeffler *et al*, 2010)) as a search model. Refinement and model building were performed with PHENIX and COOT (Afonine *et al*, 2012; Emsley *et al*, 2010). Despite the presence of four GyrBA-YacG heterodimers in the asymmetric unit, best results were achieved without the use of non-crystallographic symmetry restraints or averaging, likely due to modest, differential flexing within and between subdomains in the complex. On several occasions, we found it advantageous to use deformed elastic networks (DEN) refinement in conjunction with simulated-annealing composite omit maps to aid in building the more difficult parts of the model (Schröder *et al*, 2010); these steps were carried out using CNS (Brunger *et al*, 1998). All crystallography figures were made in PyMol (PyMol). The structure will be deposited in the Protein Data Bank. The final data collection and refinement statistics are summarized in **Table 4.1**.

SAXS Sample Preparation and Data Collection

Fresh, non-frozen preparations of GyrA$^{\Delta CTD}$, full-length GyrB, and wild-type YacG were exchanged into SAXS buffer (100mM KCl, 20mM Tris-HCl pH7.9, 5% (v/v) glycerol, 100µM TCEP, 5µM $ZnCl_2$, 6mM $MgCl_2$) by buffer exchange and reconcenration. Individual subunits, reconstituted gyrase$^{\Delta CTD}$, and gyrase$^{\Delta CTD}$•YacG complexes were diluted to 7.5mg/mL and run over a Superose-6 (GE) column equilibrated in SAXS buffer at 25˚C. Fractions were collected and examined by SDS-PAGE to isolate samples that contained full complexes. Samples were stored at 4˚C 24-48 h prior to SAXS experiments. SAXS experiments were performed at the SSRL Beamline 4-2. Samples were spun prior to each experiment to remove aggregated protein. For experiments performed in the presence of AMP-PNP, the buffer alone control and protein samples were incubated at RT for 1 hour with 1mM AMP-PNP before analysis by SAXS. Data were collected as a series of one-second exposures, which were subsequently averaged. Subtraction of buffer scattering (using the buffer from Superose-6 elution) was then applied to yield the final scattering curves. Raw data were processed on-site using SasTool (SSRL). Subsequent data analyses were carried out in the ATSAS package (Petoukhov *et al*, 2007), using PRIMUS for visualization and analysis of scattering curves (Konarev *et al*, 2003), AUTORG for R_gs estimation (Petoukhov *et al*, 2007), AUTOPOROD for molecular weight estimates obtained from Porod volumes (Petoukhov *et al*, 2007), and DAMMIN for a*b initio* 3-D modeling using 2-fold symmetry constraints. Results of 20 independent refinement runs were clustered and averaged using DAMCLUST (Volkov & Svergun, 2003). Despite the rigorous approach, only one conformation could be found for gyrase$^{\Delta CTD}$•YacG•AMPPNP complex, while 3D reconstruction failed altogether for all other samples, indicating that only the nucleotide-bound and inhibited gyrase was sufficiently immobile to allow 3D modeling by SAXS. Model fitting and rendering of SAXS envelopes was done with UCSF Chimera (Pettersen *et al*, 2004).

Preparation of relaxed plasmid substrate
Negatively-supercoiled pSG483 (2927bp), a pBluescript SK derivative with a NB.BbVCI nicking site, was prepared from *E. coli* using a maxiprep kit (Machery-Nagel). To produce relaxed DNA, the plasmid was nicked with NB.BbVCI (New England Biolabs) and religated with T4 DNA ligase (New England Biolabs). DNA was purified by phenol chloroform extraction followed by ethanol precipitation. Purified DNA was resuspended in water and stored at -80˚C.

DNA supercoiling assays
Gyrase holoenzyme was formed on ice by incubating equimolar amounts of GyrA and GyrB (40µM final concentration tetramer) for 10 min. Gyrase was then serially diluted in protein dilution buffer (2-3 fold steps in 150mM potassium glutamate, 25 mM Tris-HCl pH 7.9, 10% (v/v) glycerol, 5μM $ZnCl_2$ and 2.5mM $MgCl_2$) and mixed with protein dilution buffer (3μL) at 4˚C for 5 min. Reactions were brought up to a volume of 27μL in a final buffer containing 0.1mg/mL BSA, 10% glycerol, 0.5mM TCEP, 5.5mM $MgCl_2$, 5μM $ZnCl_2$, 30mM Tris-HCl pH7.9, 120mM potassium glutamate, and 2mM ATP pH 7.5, after which the mixture was incubated at 25˚C for 10 min. To initiate the reaction, 3μL of relaxed pSG483 (5nM final concentration) was mixed with gyrase and incubated at 30˚C for 4 min. Reactions were quenched by the addition of 2% (w/v) SDS and 20mM EDTA pH 8.0 (final concentrations). Sucrose loading dye was then added to the samples, which were then run on 1% (w/v) TAE agarose gels (40mM sodium acetate, 50mM Tris-HCl pH 7.9, 1mM EDTA pH 8.0) for 6-15 h at 2-2.5 volts/cm. For visualization, gels were stained with 0.5µg/ml ethidium bromide in 1% TAE buffer for 20 min, then destained in 1% TAE buffer for 30 minutes and exposed to UV transillumination. For experiments performed with YacG, the gyrase heterotetramer (1nM final in assay) was mixed with various concentrations of YacG instead of protein dilution buffer. All other experimental parameters are identical to those utilized in the enzyme titration experiments. All gel-based experiments were performed independently at least three times.

DNA binding assays
A pre-annealed 37bp oligonucleotide (5'-TAA AGT CTA GAG ACA CGC ATA GTC AAT GAC GGA GTT A-3' and 5'-56-FAM-TAA CTC CGT CAT TGA CTA TGC GTG TCT CTA GAC TTT A-3', where 56-FAM indicates the position of a carboxyfluorescein dye for visualization) was purchased from Integrated DNA Technologies and resuspended in water. YacG constructs were dialyzed against a buffer containing 150mM potassium glutamate, 25mM Tris-HCl pH 7.9, 10% (v/v) glycerol, 5μM $ZnCl_2$ and 0.5% PEG 20000 at 4˚C for 16 h prior to performing competition experiments. Gyrase and gyrase$^{\Delta CTD}$ holoenzymes were formed on ice by incubating equimolar amounts of GyrA/GyrA$^{\Delta CTD}$ and GyrB (final concentration tetramer 20µM) for 10 min. Gyrase and gyrase$^{\Delta CTD}$ were serially diluted in 2-fold steps in DNA binding buffer (150mM potassium glutamate, 25mM Tris-HCl pH 7.9, 10% (v/v) glycerol, 5μM $ZnCl_2$). Gyrase and gyrase$^{\Delta CTD}$ were mixed (8μL) with DNA binding buffer (8μL) and incubated on ice for 5 min. The

assay was then brought up to a final volume of 80μL and contained 10% (v/v) glycerol, 6μM $ZnCl_2$, 0.05mg/mL BSA, 1mM $MgCl_2$, 0.5mM TCEP, 30mM potassium glutamate, 30mM Tris-HCl pH 7.9 and 20nM of the 37bp FAM-labeled oligonucleotide. Reactions were incubated at 25˚C for 10 min in the dark, after which measurements and graphing were performed as described for the YacG binding assays. Assays containing YacG used 500nM gyrase or gyrase$^{\Delta CTD}$ and a titration of YacG and were otherwise performed in an identical manner to that described for the gyrase and gyrase$^{\Delta CTD}$ DNA-binding titration experiments. Data were plotted in GraphPad Prism Version 6 using an exact expression for competitive binding between two ligands as described by Wang (Wang, 1995).

YacG C-terminal Peptides

Peptides corresponding to residues 40-52 and 40-65 of *E. coli* YacG were purchased from Elim Biopharmaceuticals Inc and were resuspended in 150mM potassium glutamate, 10% (v/v) glycerol, 25mM Tris-HCl pH 7.9, 5μM $ZnCl_2$ at a concentration of 10mM and stored at -80˚C. DNA binding and supercoiling assays performed with the peptides and either gyrase$^{\Delta CTD}$ or gyrase were performed in an identical manner to those that contained the zinc-binding domain of YacG.

Circular Dichroism

The solution behavior of purified YacG mutants were assessed by circular dichroism (CD) and found to produce spectra nearly identical to the wild-type protein, indicating that these constructs were properly folded. The one exception was the Trp40Asp mutant, which showed a somewhat aberrant spectrum compared to native YacG and was hence omitted from further analysis (**Fig S4.1B**). For collecting CD data, Aliquots of WT and mutant YacG were thawed and dialyzed overnight at 4˚C against a buffer containing 100mM KCl, 5mM Tris-HCl pH 7.9, and 5μM $ZnCl_2$. After dialysis, the proteins were diluted to a final concentration of 0.33mg/ml. CD spectra were taken at 25˚C with an Aviv model 410 Circular Dichroism Spectrophotometer in a 1cm pathlength cuvette. Data were obtained from 250-200nm, at 1nm intervals. Each point is averaged over 5 seconds and each read was performed three times. All points were normalized to a buffer control.

TABLE 4.1 Data Collection and Refinement statistics.

Data Collection	
Resolution (Å)	80-3.15
Wavelength (Å)	1.1
Space Group	P212121
Unit cell dimensions (a, b, c) (Å)	107.3, 114.5, 462.1
Unit cell angles (α, β, γ) (°)	90, 90, 90
I/σ (last shell)	5.5 (0.4)
R_{merge} (last shell)	0.13 (3.66)*
R_{pim} (last shell)	0.073 (2.06)*
Completeness (last shell) (%)	99.9 (100)
Redundancy	4.1
Unique Reflections	99506

Refinement	
Resolution (Å)	70-3.5/3.3/3.15
No. of reflections	87696
R_{work} (%) (last shell)	23.0 (48.6)
R_{free} (%) (last shell)	27.8 (47.3)

Structure and Stereochemistry	
No. atoms	54893
Protein	54888
Water	0
<u>B factor (Å^2)</u>	
Protein	108.24
r.m.s.d. bond lengths (Å)	0.005
r.m.s.d. bond angles (°)	0.886
<u>Ramachandran Plot (%)</u>	
Favored Region	93.5
Allowed Region	5.9
Outliers	0.65

*Prior to performing ellipsoidal truncation to correct for anisotropy in the data.

$R_{merge} = {}_{hkli}|I_i(hkl) - I(hkl)| / {}_{hkli}I_i(hkl)$, where $I_i(hkl)$ is the intensity of an observation and I(hkl)is the mean value for its unique reflection. Summations cover all reflections.

$R_{work} = {}_{hkl}|F_{obs} - k F_{calc}| / {}_{hkl}F_{obs}$. R_{free} was as per R_{work}, but with the reflections excluded from refinement. The R_{free} set was chosen using default parameters in PHENIX (Adams et al, 2010).

Ramachandran Plot categories were defined by Molprobity (Chen et al, 2010).

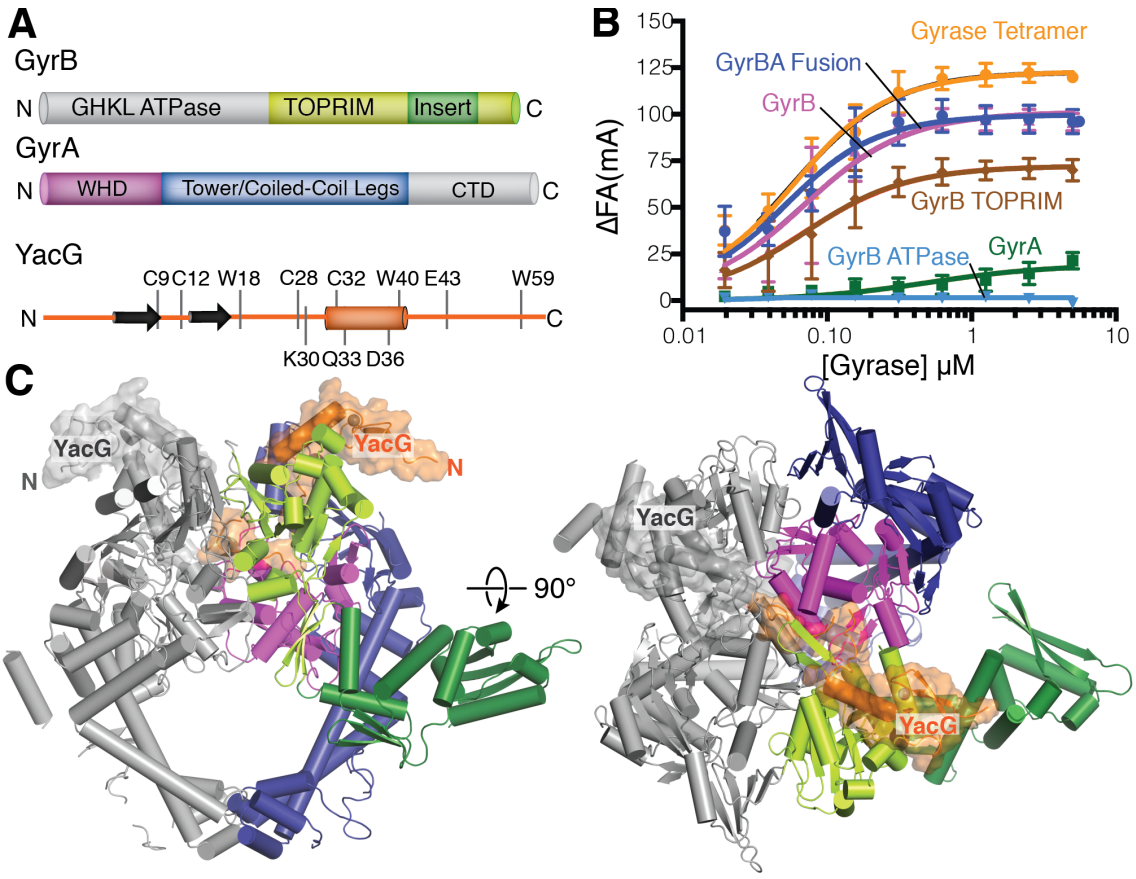

Figure 4.1. Structure of the YacG·Gyrase complex.

A Domain organization and primary structure of gyrase (GyrA, GyrB) and YacG. Cysteines involved in zinc coordination and residues addressed in this study are marked on the primary structure of YacG.

B YacG association with *E. coli* gyrase domains, subunits, and the holoenzyme as measured by fluorescence anisotropy. Gyrase components were titrated against Alexa-Fluor 488 labeled YacG (50nM labeled) and binding was monitored as a change in (ΔFA) fluorescence anisotropy (mill-anisotropy units (ma)). Concentrations on the X-axis correspond to monomers of gyrase. Each data point is representative of three independent experiments.

C Overview of YacG•GyrBA crystal structure in cartoon depiction. One of two GyrBA dimers found in the asymmetric unit. One protomer is colored grey for contrast and all other domains are colored as in A. YacG is shown as a surface for contrast (orange). One insert domain (grey) per GyrBA dimer is not observed. This figure and all other crystallography figures were made in PyMol (PyMol).

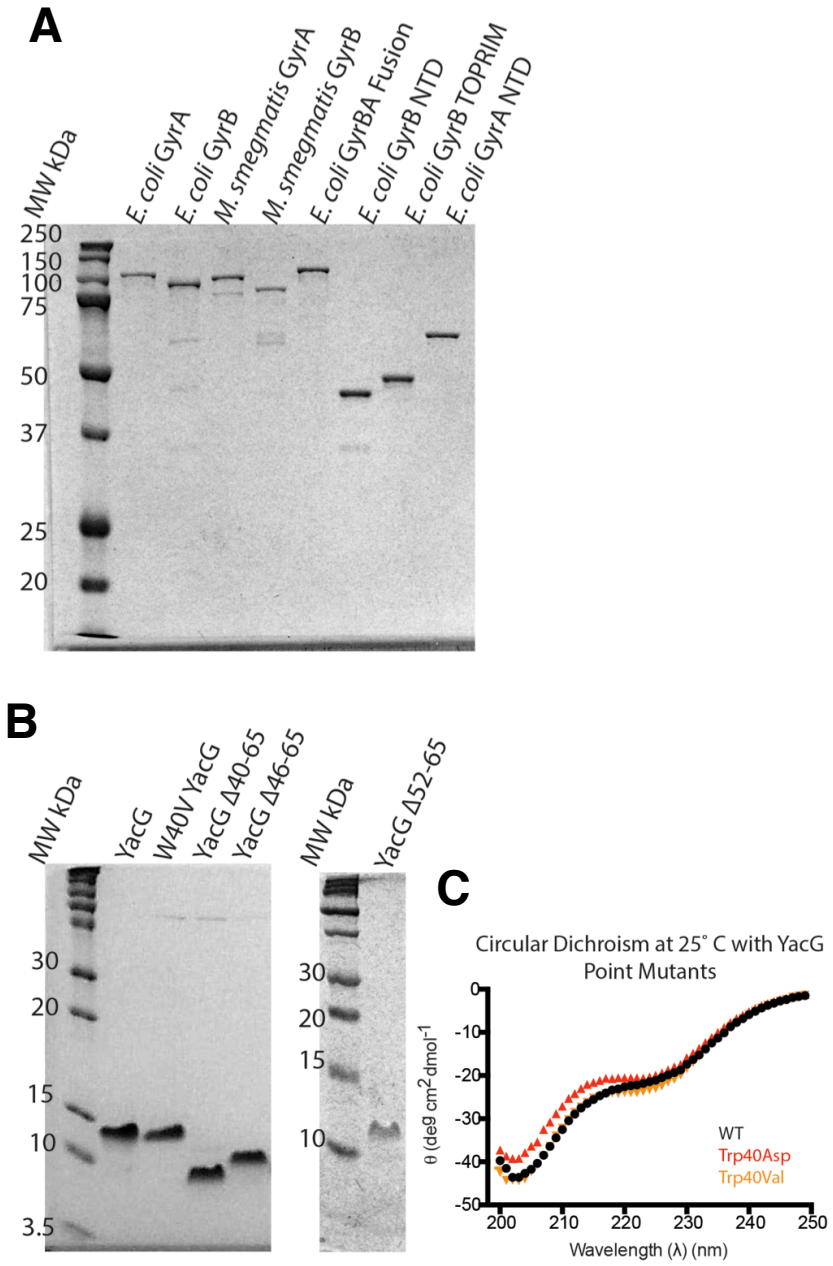

Figure S4.1. Protein purity and solution behavior.

A Protein purity of gyrase subunits and domains as assessed by SDS-PAGE (10%), 0.1μg each construct. Gels stained with Coomassie Blue.

B Protein purity of YacG constructs as assessed by SDS-PAGE (15%), 0.6μg each construct. Gels stained with Coomassie Blue.

C Circular dichroism spectra measured for YacG and YacG mutants at 25˚C.

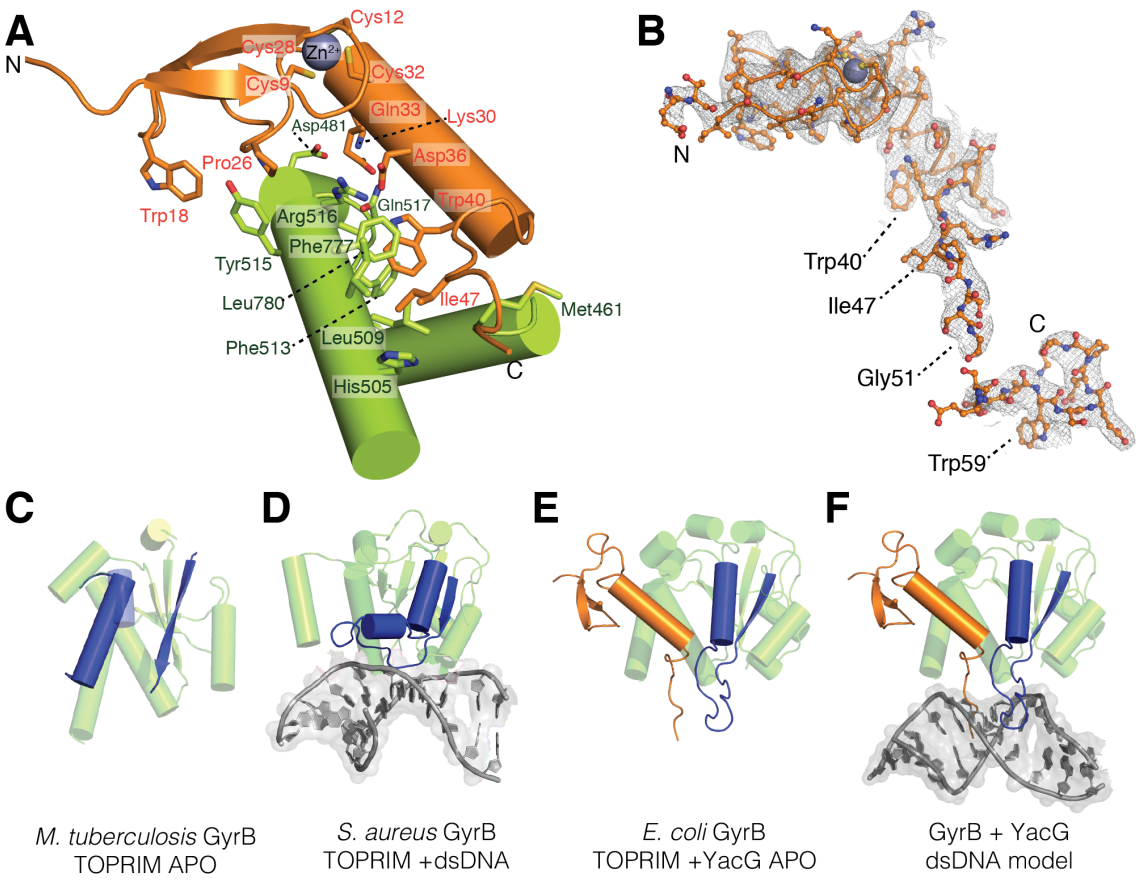

Figure 4.2. YacG remodels the TOPRIM domain of GyrB.

A Close-up of YacG interaction (orange) with GyrB TOPRIM core (green). Zinc ion is colored grey. Interacting side chains are depicted as sticks.

B $2F_o$-F_C map of YacG contoured at 1σ. Backbone drawn in stick representation.

C The TOPRIM QRDR loop is not observed in the absence of a DNA substrate. *M. tuberculosis* GyrB TOPRIM domain (green) crystallized in the absence of DNA (PDB ID: 2ZJT).

D In the presence of a gate-segment DNA (grey), the QRDR loop (blue) pinned against the GyrB TOPRIM (green) *S. aureus* GyrB crystallized with DNA (PDB ID: 2XCS).

E *E. coli* GyrB TOPRIM (green) bound to YacG (orange). QRDR loop visible (blue) and projects over the active site of the gyrase enzyme.

F Identical to panel E., with modeled gate segment DNA (dsDNA) from panel D. The position of the QRDR loop in YacG bound gyrase clashes with the modeled DNA.

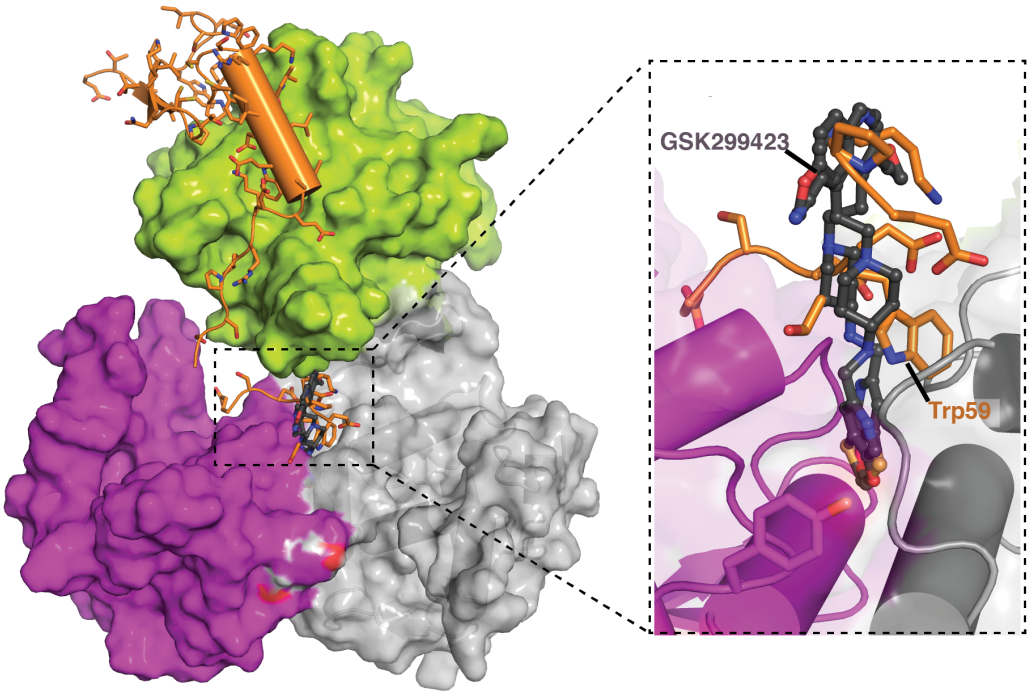

Figure 4.3. The C-terminus of YacG occupies the same region as a novel gyrase inhibitor.
YacG (orange) C-terminus drops from TOPRIM core (green) into GyrA active site (magenta). QRDR loop is shown in blue. Inset- C-terminal tryptophan (Trp59) of YacG binds same region of GyrA as gyrase inhibitor GSK299423 (teal) (PDB ID: 2XCS). The active site tyrosine of GyrA (Tyr 122) is indicated and is ~10Å away from Trp59 of YacG.

Figure S4.2. Sequence alignment of the YacG binding region of various GyrB proteins.

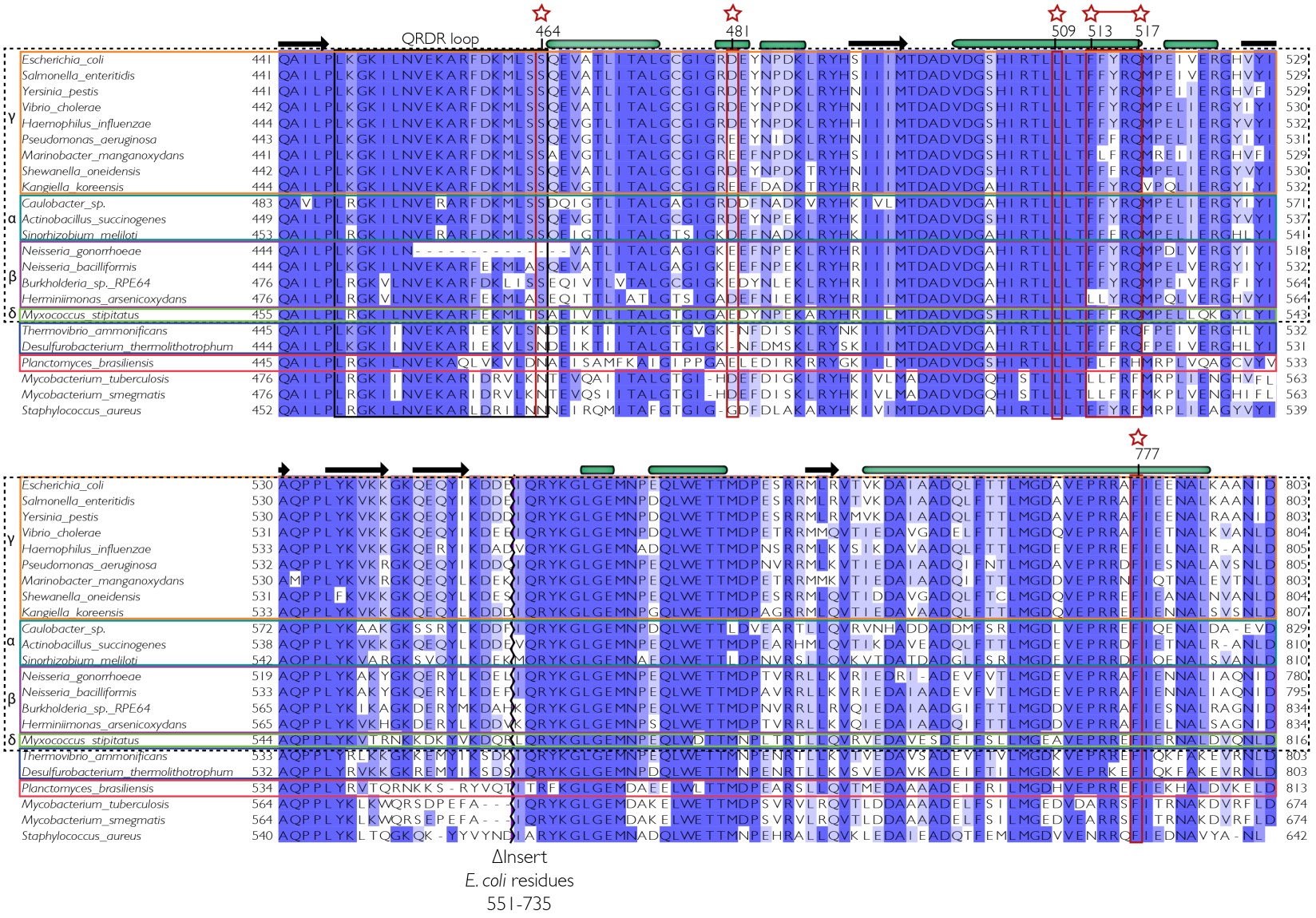

Figure S4.2. Sequence alignment of the YacG binding region of various GyrB proteins.
Horizontal colored boxes correspond to organisms that encode YacG. Dotted box demarcates proteobacteria with horizontal colored boxes corresponding to alpha (cerulean), beta (lilac), delta (green), gamma (orange) classes of the proteobacterial phylum. The other colored horizontal boxes correspond to the phyla Aquificae (navy blue) and Planctomycetes (hot pink). Secondary structural elements are shown above the alignment as arrows (beta strands) and elongated teal ovals (alpha helices). *E. coli* GyrB residues that bind YacG in are outlined in red and starred above the alignment. The insert domain of GyrB was removed from the alignment, since YacG does not associate with this region. Figure was made in JALVIEW (Waterhouse et al, 2009).

Figure S4.3. Sequence alignment of select YacG proteins

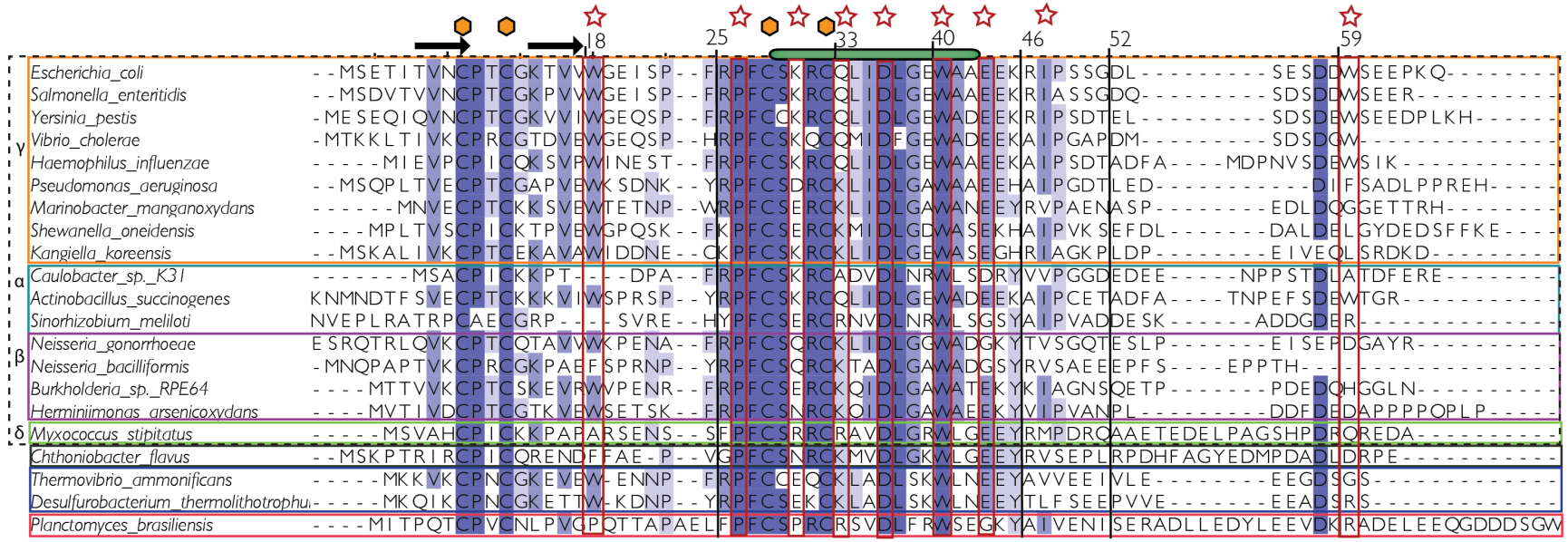

Operon Structure

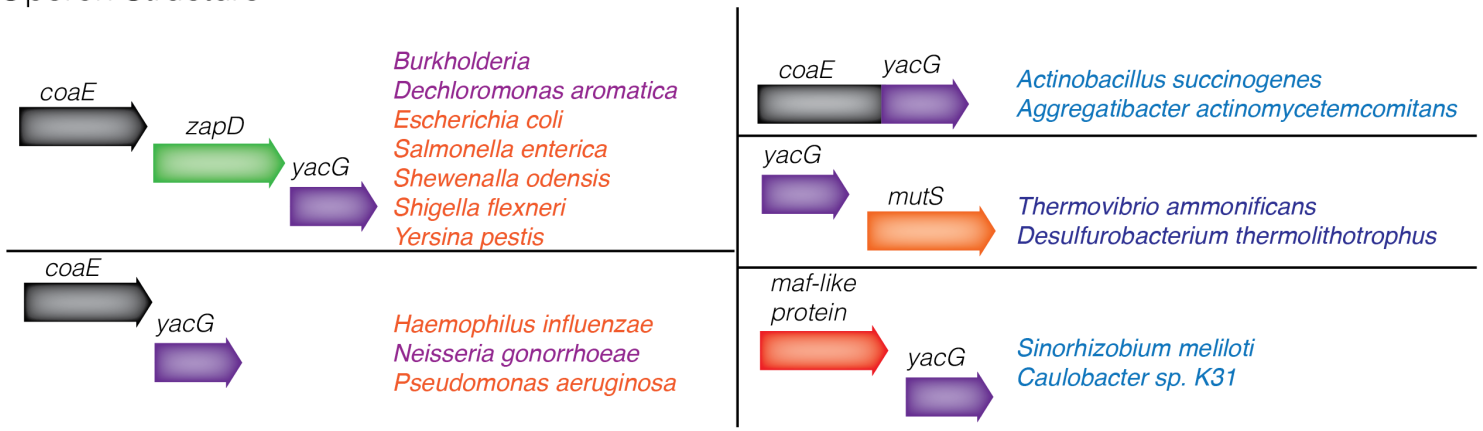

Figure S4.3. Sequence alignment of select YacG proteins.
Top: Dotted box demarcates the proteobacteria with horizontal colored boxes corresponding to alpha (cerulean), beta (lilac), delta (green), gamma (orange) classes of the proteobacterial phylum. The other colored horizontal boxes correspond to the phyla Aquificae (navy blue) and Planctomycetes (hot pink). Secondary structural elements are shown above the alignment as arrows (beta strands) and elongated teal ovals (alpha helices). Yellow hexagons indicate positions of cysteines required for zinc coordination. *E. coli* YacG residues that interact with GyrB/GyrA are boxed in red and starred above the alignment. Figure was made in JALVIEW (Waterhouse et al, 2009). Bottom: Various structures of YacG containing operons. Species with indicated operon structures are listed to the right of each operon.

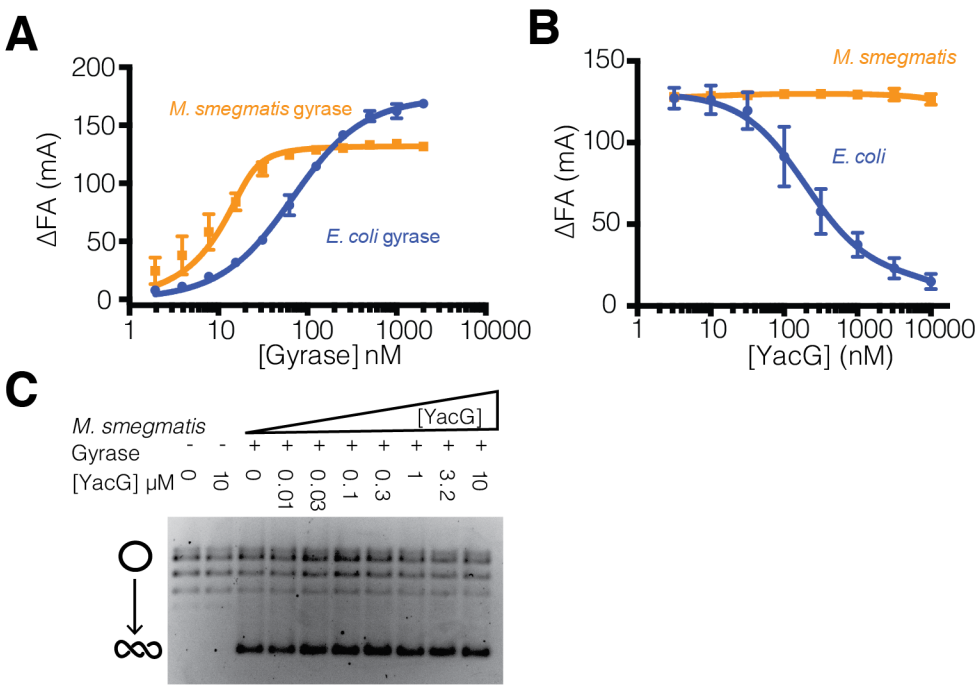

Figure S4.4 YacG is a narrow-spectrum inhibitor of bacterial gyrases
In surveying bacterial genomes available in the databases, we found that YacG and its homologs are present in all classes of proteobacteria, as well as in certain other bacterial phyla such as *Planctomycetes* and *Aquificiae* (**Fig S4.3**). By contrast, organisms such as *B. subtilis*, *M. smegmatis, and M. tuberculosis* do not encode a YacG homolog. Consistent with this absence, some of the TOPRIM residues that contact YacG differ between bacteria that encode YacG and those that lack the gene; for example, *M. smegmatis* and *M. tuberculosis* GyrB have a phenylalanine in place of Gln517 and a leucine in place of Phe513 (numbering according to *E. coli*) (**Fig S4.2**). These differences suggest that gyrases of bacterial species outside of those that possess YacG likely are not susceptible to inhibition by the protein.

To test that idea that YacG acts specifically against only certain gyrases, we examined whether *E. coli* YacG could inhibit various activities of *Mycobacterium smegmatis* gyrase. *E. coli* YacG has been reported to interfere with the binding of its cognate gyrase to DNA (Sengupta & Nagaraja, 2008). To assess the effects of YacG on DNA binding by a non-cognate gyrase, we used a FITC-labeled, 37mer duplex DNA substrate and quantitated changes in relative affinity by fluorescence anisotropy. As controls, *M. smegmatis* and *E. coli* gyrase tetramers were first assembled and separately titrated in varying concentrations against a fixed amount of labeled DNA in the absence of YacG (20 nM); under our assay conditions, *M. smegmatis* gyrase bound DNA approximately 35-fold more tightly ($K_{d,app}$ = 1.5±0.61 nM) than *E. coli* gyrase ($K_{d,\ app}$ 57.3±2.6 nM) (**Fig S4.4A**). We next titrated different amounts of *E. coli* YacG against both full-length *M. smegmatis* and *E. coli* gyrase in the presence of the labeled 37-mer

oligonucleotide, using conditions where the DNA was completely bound by the enzyme (500nM gyrase, a 25-fold molar excess). We observed that while YacG had no effect on DNA binding by the *M. smegmatis* gyrase holoenzyme, the *E. coli* holoenzyme showed a clear dose-dependent reduction in DNA binding as YacG levels were increased (**Fig S4.4B**).

By contrast, YacG showed no ability to inhibit supercoiling by *M. smegmatis* gyrase (**Fig S4.4C**). Together with our DNA binding study, these data indicate that YacG is not a general gyrase inhibitor, likely due to naturally-occurring differences in the YacG-binding site of GyrB and GyrA of other species.

A DNA binding by full-length *M. smegmatis* and *E. coli* Gyrase. Gyrase tetramers were titrated a 37mer FITC labeled DNA (20nM). DNA binding was monitored as a function of change in fluorescence anisotropy as measured in milli-anisotropy units (mA).

B DNA binding by full-length *M. smegmatis* and *E. coli* Gyrase in the presence of *E. coli* YacG.

C DNA supercoiling by *M. smegmatis* gyrase (1nM) in the presence of YacG and a relaxed plasmid substrate (5nM) at 30˚C. Compare to *E. coli* enzyme in **Fig 4.4B**. Reactions were quenched after 30 min, run on 1% TAE agarose gels, and visualized by ethidium bromide staining. Cartoons to the left of each gel represent relaxed (open circles) and negatively-supercoiled (intertwined circles) products. Each experiment was performed at least 3 times. See **Fig S4.5** for specific activity of *E. coli* and *M. smegmatis* gyrase enzymes and 4 min timepoint for *M. smegmatis* gyrase with YacG.

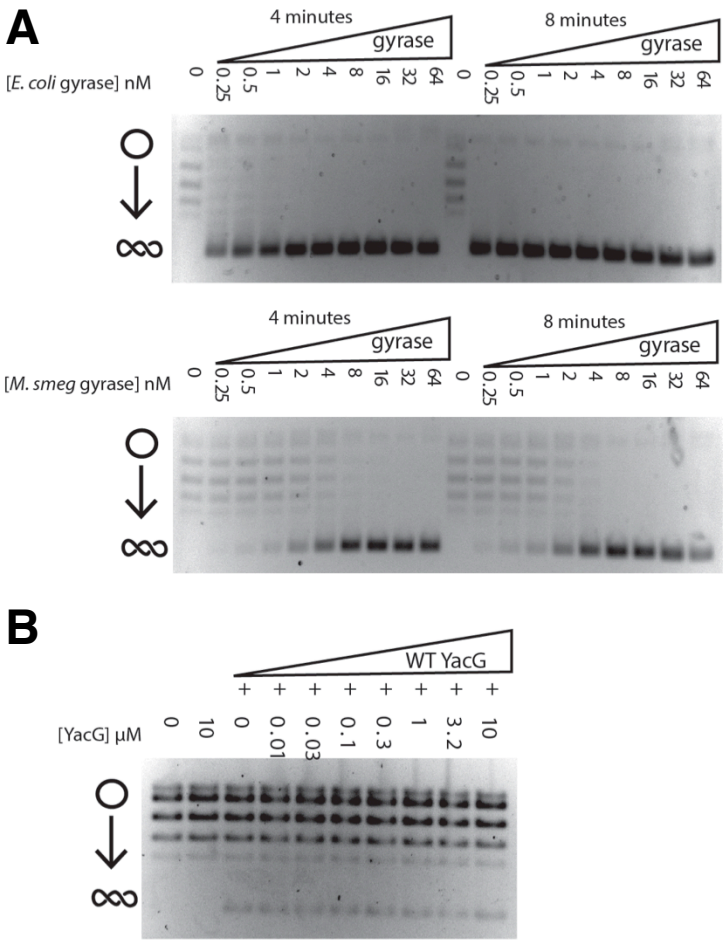

Figure S4.5. Measure of gyrase specific activity.
A Measure of specific activity of *E. coli* (top) and *M. smegmatis* (bottom) gyrase on relaxed plasmid DNA (5nM). Gyrase was titrated and incubated with relaxed plasmid substrate for 4 or 8 minutes. Reactions were quenched and run on 1% TAE gels to assess the extent of supercoiling. A cartoon is shown on the left of the gels to illustrate where the relaxed (open circle) and supercoiled (intertwined circles) topoisomers run in the gel matrix.
B Similar to **Fig 4.4D**, *M. smegmatis* gyrase (1nM) was incubated with various concentrations of YacG and the extent of gyrase supercoiling was assessed. The reactions shown on this gel were quenched 4 minutes after adding DNA. A cartoon is shown on the left of the gels to illustrate where the relaxed (open circle) and supercoiled (intertwined circles) topoisomers run in the gel matrix.

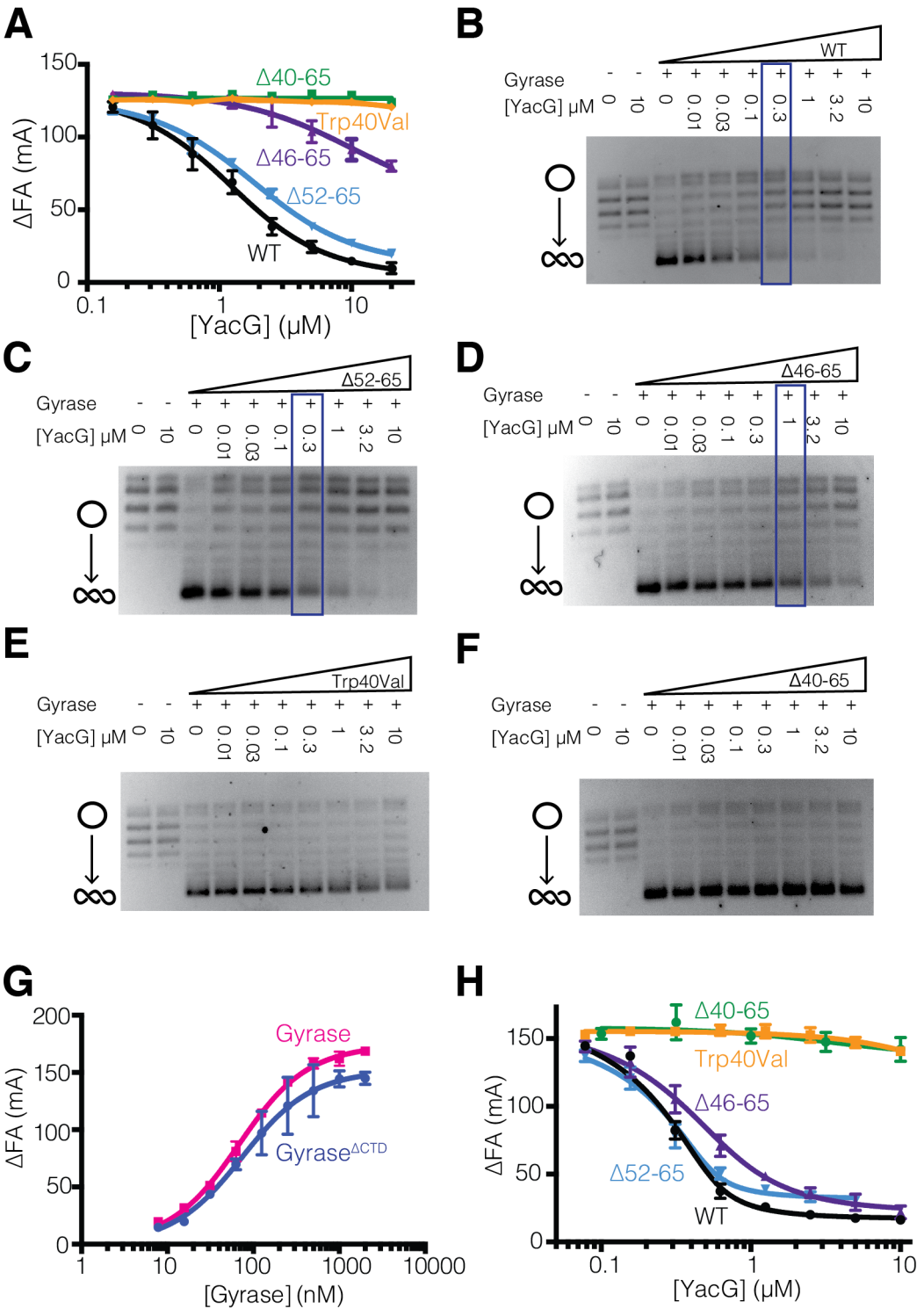
A
150
100
50
0
ΔFA (mA)
0.1
1
10
[YacG] (μM)
Δ40-65
Trp40Val
Δ46-65
Δ52-65
WT
B
WT
Gyrase
[YacG] μM
0
10
0
0.01
0.03
0.1
0.3
1
3.2
10
C
Δ52-65
D
Δ46-65
E
Trp40Val
F
Δ40-65
G
200
150
100
50
0
ΔFA (mA)
1
10
100
1000
10000
[Gyrase] (nM)
Gyrase
GyraseΔCTD
H
Δ40-65
Trp40Val
Δ46-65
Δ52-65
WT

Figure 4.4. YacG C-terminal region is required for gyrase inhibition.
A Binding assay to assess the ability of YacG tail truncation mutants to compete WT N-terminal Alexa fluor 488 labeled YacG (50nM) from gyrase (750nM). YacG truncation mutants were titrated and competition was observed as a change in fluorescence anisotropy (ΔFA) as measured in milli-anisotropy units (mA). Each data point corresponds to the average of three independent experiments.
B-E DNA supercoiling assay to assess the activity of *E. coli* gyrase in the presence of various YacG constructs. YacG constructs were titrated against gyrase (1 nM) and a relaxed plasmid substrate (5nM). Reactions proceeded for 4 minutes at 30˚C before quenching. Products were run on 1% (w/v) agarose gels and visualized by ethidium bromide staining. Cartoons to the left of each gel represent relaxed (open circles) and negatively-supercoiled (intertwined circles) topoisomers. The blue boxes correspond to the YacG concentration at which gyrase supercoils half as effectively as the gyrase alone sample. Gels are representative of at least 3 independent replicate experiments. B. WT YacG C. Δ52-65 YacG D. Δ46-65 YacG E. Trp40Val F. Δ40-65 YacG. Also see **Fig S4.5**.
F DNA binding by Gyrase$^{\Delta CTD}$ (magenta) and full-length gyrase (blue). Gyrase was titrated into a solution containing a labeled duplex 37mer DNA (20nM) and 30mM potassium glutamate. DNA binding was monitored as the change in fluorescence anisotropy (ΔFA)(mill-anisotropy units (ma)). DNA binding by Gyrase$^{\Delta CTD}$ is salt dependent (see **Fig S4.6A**).
G YacG constructs were titrated against Gyrase$^{\Delta CTD}$(500nM) incubated with the same 37mer DNA substrate used in G. DNA binding was monitored as the change in fluorescence anisotropy (ΔFA)(mill-anisotropy units (ma)). YacG does not bind DNA independently (see **Fig S4.6B**). Each data point corresponds to the average of three independent experiments.

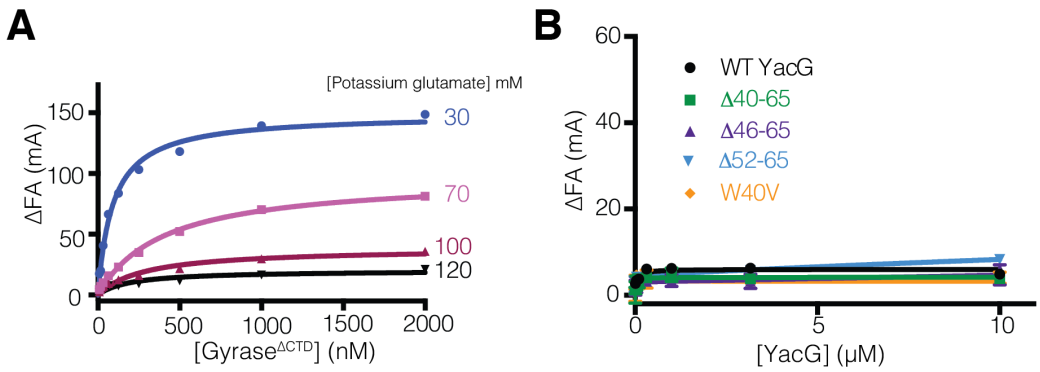

Figure S4.6

A DNA binding by Gyrase$^{\Delta CTD}$ is salt dependent. Gyrase$^{\Delta CTD}$ was titrated as in (A) against the labeled 37mer DNA (20nM). The final reactions contained different concentrations of potassium glutamate. DNA binding was monitored as a function of change in fluorescence anisotropy as measured in mill-anisotropy units (mA). Salt concentrations are in millimolar and found to the right of each curve.

B YacG does not bind short, linear DNA substrates. YacG constructs were titrated against the labeled 37mer DNA (20nM) used in (A). The reactions contained 30mM potassium glutamate and DNA binding was monitored as a change in fluorescence anisotropy as measured in mill-anisotropy units (mA).

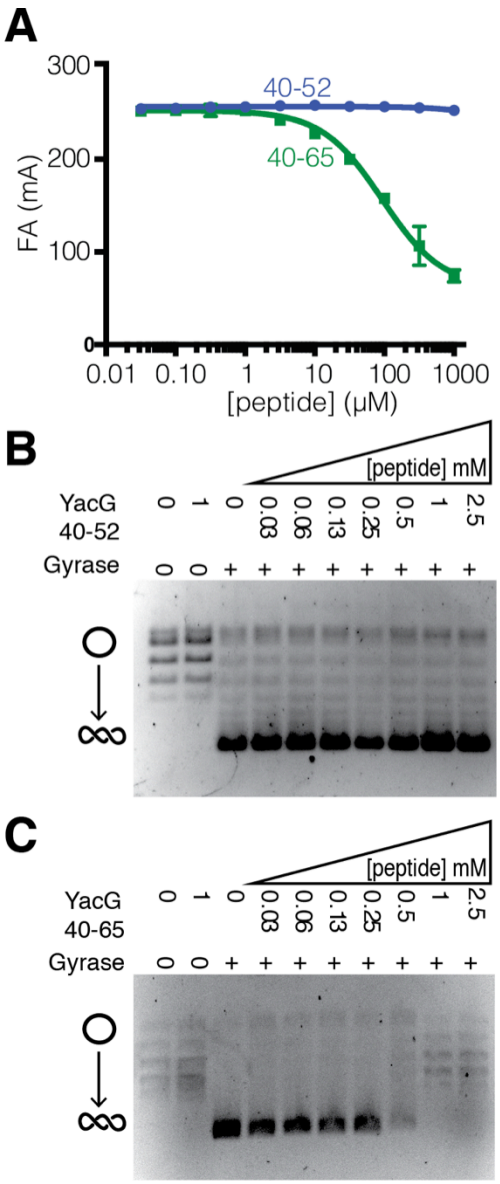

Figure 4.5. C-terminal YacG peptide is sufficient to inhibit gyrase.
A DNA binding by gyrase$_{\Delta CTD}$ (500nM) with identical FITC labeled 37mer DNA substrate used in **Figs 4.4A, 4.4B, 4.5F** with titration of YacG C-terminal peptides aa 40-52 and aa 40-65. DNA binding was monitored as a function of fluorescence anisotropy as measured in milli-anisotropy units (mA). Error bars correspond to 3 independent replicates.
B –C DNA supercoiling by *E. coli* gyrase (1nM) in the presence of YacG C-terminal peptides and a relaxed plasmid substrate (5nM). Reactions proceeded for 4 minutes at 30˚C before quenching. Products were run on 1% agarose gels and visualized by ethidium bromide and imaged. Cartoons to the left of each gel represent relaxed (open circles) and negatively-supercoiled (intertwined circles) products. **B** aa 40-52 peptide, **C** aa 40-65 peptide.

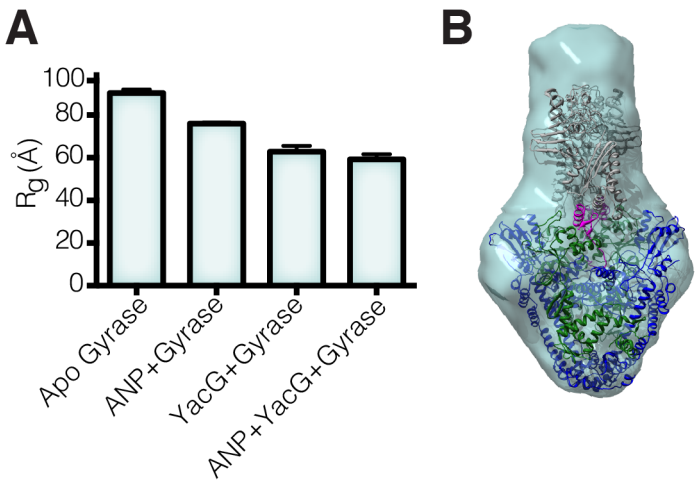

Figure 4.6. YacG may induce closure of the GyrB N-terminal ATPase.
A Radius of gyration as measured by SAXS with Gyrase$^{\Delta CTD}$ and Gyrase$^{\Delta CTD}$•YacG in the presence and absence of 1mM AMP-PNP. For corresponding Guinier plots, see **Fig S4.7**.
B Representative *ab initio* model obtained from SAXS data collected from the Gyrase$^{\Delta CTD}$•YacG complex in the presence of AMP-PNP (2-fold symmetry was applied obtain shape). Gyrase$^{\Delta CTD}$ crystal structure was modeled after the yeast holoenzyme crystal structure (PDB ID: 4GFH) and colored as in **Fig 4.1A**. Figure made in UCSF Chimera(Pettersen *et al*, 2004).

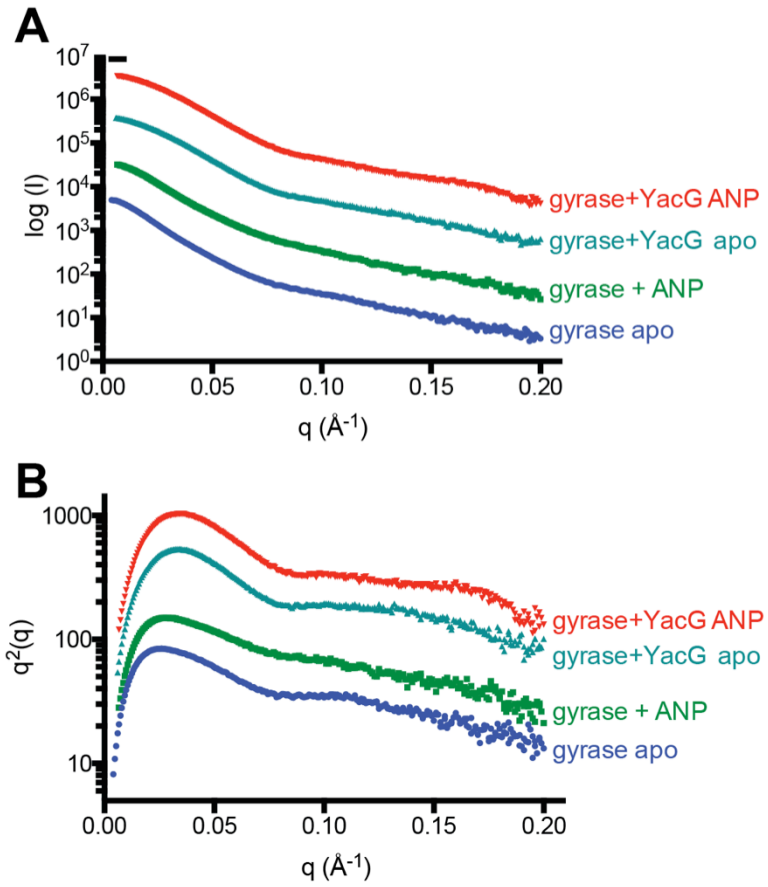

Figure S4.7. Samples used for SAXS analysis are not aggregated.
A Guinier plot of SAXS data collected with Gyrase$^{\Delta CTD}$ in the presence and absence of YacG and AMP-PNP (ANP).
B Kratky plot of SAXS data collected with Gyrase$^{\Delta CTD}$ in the presence and absence of YacG and AMP-PNP (ANP).

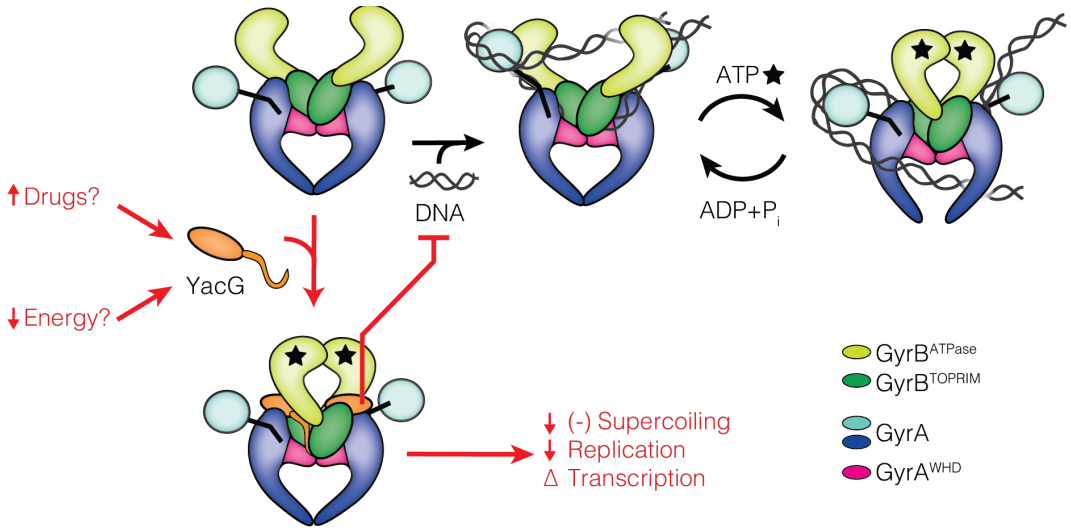

Figure 4.7. Model for gyrase inhibition by YacG.
Gyrase and YacG domains colored as in **Fig 4.1A**. Gyrase introduces negative supercoils into DNA (upper) in the presence of ATP. In response to stress, cells may upregulate YacG expression to slow growth. YacG binding to gyrase would prohibit the enzyme from binding DNA by remodeling the QRDR loops on the GyrB TOPRIM and enforce closure of GHKL ATPase gate (lower). Inactivation of gyrase would reduce the amount of negative supercoiling in the genome, changing the transcriptional profile of the cell and inhibit DNA replication initiation, leading to a period of cellular quiescence.

Chapter 5–Conclusions and Future Directions

Topoisomerases are key effectors of chromosome topology, however, it is largely unknown how cells integrate topoisomerase function into larger feedback systems. Many of the mechanisms that permit these enzymes to resolve topological challenges by transiently cleaving and passing DNA segments through each other have been elucidated. Additionally, numerous small molecule inhibitors have been developed to exploit the topoisomerase catalytic cycle for significant therapeutic gain. Because topoisomerases have biophysical and structural features that favor action on specific DNA substrates, it has been thought that these distinctions drive localization and activity in cells. Recent work has called this notion into question as multiple factors and modifications have been reported to affect topoisomerases (**Chapter 1**). It remains largely unknown how these modifications and factors influence topoisomerase activity and localization and how these factors connect topoisomerases to the cellular status. To begin to understand ways cells control topoisomerase action, I have defined some of the regulation mechanisms used by *Escherichia coli* to govern its two type IIA topoisomerases, gyrase and topo IV.

Substrate discrimination by topo IV

Topo IV preferentially acts on positively-supercoiled and catenated substrates over those that are negatively-supercoiled (Crisona *et al*, 2000; Neuman *et al*, 2009; Charvin *et al*, 2003; Stone *et al*, 2003). It was previously shown that the CTD of the topo IV ParC subunit assists in substrate discrimination. It was subsequently hypothesized that a positively-charged strip that encircles the domain is responsible for engaging various DNA substrates (Corbett *et al*, 2005). To address this idea, I used mutagenesis and biochemical experiments to assess the importance of highly-conserved, positively-charged residues on the surface of the domain for substrate engagement. These experiments reveal that the ParC CTD regulates topo IV substrate discrimination by binding distinct DNA substrates on specific surfaces (**Chapter 2**). I also identified an autorepressive site that impedes activity on negatively-supercoiled and catenated substrates and another site that assists in bending G-segment DNAs. Finally, this study resolves a conflict in the field concerning the recognition of positively- and negatively-supercoiled substrates by topo IV. Early single molecule studies proposed that topo IV discriminates between distinct DNA topologies by recognizing different chiral juxtapositions between G- and T- segment DNAs in the topo IV active site (Stone et al, 2003). Subsequent experiments, however, revealed that topo IV has no preference for cross-over angle and instead suggested that enhanced processivity on positively-supercoiled substrates drives the observed substrate preference of topo IV. The data presented here suggest that topo IV can read specific DNA crossovers, but that this occurs outside of the enzyme's active site, where it then influences strand passage efficiency and processivity.

Although this work provides a detailed understanding of how distinct DNA substrates associate with the CTD of ParC, it does not directly establish how T-segment DNA associates with the domain in context of the topo IV holoenzyme. Future work should address the juxtaposition of the T-segment relative to the G-segment in the holoenzyme, perhaps through structural or biophysical techniques such as crosslinking. Such experiments will require special considerations as the ParC CTD has a modest affinity for DNA and the topo IV holoenzyme appears to have no sequence specificity.

Interaction between topo IV and the condensin homolog MukB

Efficient chromosome partitioning in *E. coli* requires topo IV and a γ-proteobacterial condensin homolog, MukB (**Chapter 3**). Previous studies showed that MukB and topo IV physically interact and that MukB stimulates the action of the topo IV on negatively-supercoiled substrates (Hayama & Marians, 2010), (Hayama *et al*, 2013; Li *et al*, 2010). To understand the basis of the MukB•topo IV interaction, I solved 2.3Å crystal structure of a minimal MukB•topo IV complex. The structure shows that a domain of MukB known as the hinge associates with the outer positively-charged strip that encircles the CTD of ParC. Biochemical experiments reveal that MukB stimulates topo IV action on negatively-supercoiled substrates by competing DNA from the strong, autorepressive DNA binding site identified in **Chapter 2**. Genetic complementation experiments suggest topo IV is essential in cells for both its topoisomerase activity and its interaction with MukB. Finally, the steric positioning of MukB and ParC in the crystal structure indicates that the proteins cannot interact intradimerically; however, the proteins may form protein arrays, providing a framework for MukB and topo IV collaboration during chromosome segregation and partitioning (**Chapter 3**).

Future work should address whether MukB and topo IV form higher-order structures. The affinity of MukB for topo IV is modest (0.5-1μM) and salt sensitive, likely making it difficult to visualize higher-order associations without crosslinking or otherwise stabilizing. It is also unknown how topo IV affects MukB function. Other SMCs such as cohesin are thought to open their hinge domains to engage DNA substrates (Gruber *et al*, 2006; Chan *et al*, 2012). It is unknown whether MukB can open its hinge and if topo IV stimulates this action. By placing FRET probes on the domain, it may be possible to observe the dynamics of hinge opening and determine whether the ParC CTD or the topo IV holoenzyme stimulate this action. Finally, several studies have implicated genetic and physical interactions between eukaryotic type IIA topoisomerases and SMCs(Baxter *et al*, 2011; Baxter & Aragón, 2012; Tapia-Alveal *et al*, 2010) or related SMC proteins(Aguilar & Davidson, 2005; Bhat *et al*, 1996; Bhalla *et al*, 2002). Further study is required to determine if direct physical interactions between topoisomerases and SMCs or SMC related proteins aid in appropriate chromosome condensation and segregation in eukaryotes.

Inhibition of gyrase by YacG

Gyrase is a key modulator of chromosome topology in bacteria and is necessary for DNA replication initiation and transcription. Several proteins endogenous to *E. coli* have been reported to inhibit gyrase function; however, it is unknown how these proteins modulate enzyme function. To address this issue, we solved a structure of a gyrase assembly, bound to its inhibitor, YacG. YacG remodels a loop associated with fluoroquinolone resistance to disrupt DNA association with gyrase and surprisingly, also associates with a region of gyrase that is involved in engaging a novel gyrase inhibitor, GSK299423(Bax *et al*, 2010). Biochemical experiments confirm the functional significance of interactions we observe in our structure and further show that a peptide fragment of YacG is sufficient to inhibit gyrase function. Bioinformatic analysis of *yacG* and its neighboring genes suggests that the YacG protein may inhibit gyrase function in response to specific metabolic needs, thus affecting DNA replication initiation and the transcriptional profile of the cell. This work provides a novel protein-based mechanism for inhibiting gyrase that may prove useful for the development of small-molecule inhibitors of gyrase and for integrating topoisomerase function with the metabolic status of the cell.

It is unknown what role YacG serves *in vivo.* Others have suggested that YacG protects cells from fluoroquinolones by sequestering gyrase from DNA. However, to date there is no evidence that YacG provides a growth advantage to cells faced with fluoroquinolones or that YacG is involved in persistor cell formation after fluoroquinolone exposure (Amato *et al*, 2013). In my preliminary attempts to study YacG function *in vivo*, I generated a *kan::yacG* MG1655 K-12 *E. coli* strain. I then compared growth of the deletion strain to the isogenic WT strain in a commercially available screen with ~1900 conditions that include various antiproliferative agents and nutrient sources. The screen yielded a number of interesting results that suggest in the absence of YacG cells may grow better in the presence of DNA damaging agents such as nitrofurantoin and hydroxylamine and cell wall damaging agents such as Compound 48/80 and Poly-L-Lysine. Colistin sulfate, another cell wall damaging agent, appears have a greater impact on growth for the *kan::yacG* strain than the WT strain. These results may indicate that expression of YacG is differentially regulated in response to specific cells stresses. Although tantalizing, these results require further validation.

Since YacG is a non-essential gene, it may be possible to obtain information about its function *in vivo* through a classic genetic synthetic lethal screen. Such a screen would involve generating transposon libraries from a *spec::yacG* and isogenic WT strains grown in various conditions (ie glucose depleted media or in the presence of fatty acid synthesis inhibitor cerulenin). Sequencing the resulting strains will provide a list of genes and operons that can be disrupted by the transposon and not affect growth. Genes or operons that are targeted in the WT strain but not in the deletion strain will provide a number of candidate genes whose function may be involved in pathways that are parallel or similar to that of YacG.

Finally, future efforts should re-examine the physical interaction between the glutamate racemase, MurI, and gyrase. It is suggested that MurI inhibits various bacterial gyrases from supercoiling DNA(Sengupta *et al*, 2006; Sengupta & Nagaraja, 2008b; Ashiuchi *et al*, 2002), by preventing the enzyme from associating with DNA (Sengupta *et al*, 2006). Since MurI is involved in cell wall biogenesis, it may provide a way to link the metabolic state of the cell to the topological state of the bacterial chromosome.

Other future directions

The work presented in this dissertation provides a glimpse into the mechanistic underpinnings that underlie regulation of the bacterial type IIA topoisomerases, topo IV and gyrase. Certainly many other modifications and interactions direct topoisomerase action but remain to be described. Pull-down/mass spectrometry screens with various prokaryotic and eukaryotic topoisomerase subunits or domains may identify novel binding partners for future structural and biochemical studies. Additionally, future studies should examine post-translational modification of eukaryotic topoisomerases to determine how these changes affect enzyme function, stability and localization. Many putative topoisomerase binding partners warrant further investigation, and may provide a greater understanding of how topoisomerases are manipulated in response to specific cellular signals (**Table 1.1**). For instance, it may be interesting to investigate the reported interactions between gyrase and the thioredoxins TrxA/C and the transcription repressor MarR (Li et al 2004; Domian and Levy 2010). These interactions are suggested to link cellular state to transcriptional output by altering gyrase activity (TrxA/C) or by sequestering the binding partner from DNA (MarR). The field of topoisomerase regulation remains a frontier area of study and will surely yield many exciting and novel surprises to those who investigate these incredible enzymes and their binding partners in the future.

References

Abdurashidova G, Radulescu S, Sandoval O, Zahariev S, Danailov MB, Demidovich A, Santamaria L, Biamonti G, Riva S, Falaschi A (2007) Functional interactions of DNA topoisomerases with a human replication origin. *EMBO J* **26:** 998-1009

Adams DE, Shekhtman EM, Zechiedrich EL, Schmid MB, Cozzarelli NR (1992) The role of topoisomerase IV in partitioning bacterial replicons and the structure of catenated intermediates in DNA replication. *Cell* **71:** 277-288

Adams PD, Afonine PV, Bunkoczi G, Chen VB, Davis IW, Echols N, Headd JJ, Hung LW, Kapral GJ, Grosse-Kunstleve RW, McCoy AJ, Moriarty NW, Oeffner R, Read RJ, Richardson DC, Richardson JS, Terwilliger TC, Zwart PH (2010) PHENIX: a comprehensive Python-based system for macromolecular structure solution. *Acta Crystallogr D Biol Crystallogr* **66:** 213-221

Afonine PV, Grosse-Kunstleve RW, Echols N, Headd JJ, Moriarty NW, Mustyakimov M, Terwilliger TC, Urzhumtsev A, Zwart PH & Adams PD (2012) Towards automated crystallographic structure refinement with phenix.refine. *Acta Crystallogr. D Biol. Crystallogr.* **68:** 352–367

Aguilar C & Davidson C (2005) Topoisomerase II Suppresses the Temperature Sensitivity of Saccharomyces cerevisiae pds5 Mutants, but not the Defect in Sister Chromatid Cohesion. *Cell Cycle* **4:** 1294–1304

Ali JA, Jackson AP, Howells AJ & Maxwell A (1993) The 43-kilodalton N-terminal fragment of the DNA gyrase B protein hydrolyzes ATP and binds coumarin drugs. *Biochemistry* **32:** 2717–2724

Amato SM, Orman MA & Brynildsen MP (2013) Metabolic Control of Persister Formation in Escherichia coli. *Mol Cell*

Anderson VE, Gootz T, Osheroff N (1998) Topoisomerase IV Catalysis and the Mechanism of Quinolone Action. *J Biol Chem* **273:** 17879-17885

Aravind L, Leipe DD, Koonin EV (1998) Toprim--a conserved catalytic domain in type IA and II topoisomerases, DnaG-type primases, OLD family nucleases and RecR proteins. *Nucleic Acids Res* **26:** 4205-4213

Ashiuchi M, Kuwana E, Komatsu K, Soda K, Misono H (2003) Differences in effects on DNA gyrase activity between two glutamate racemases of Bacillus subtilis, the poly-γ-glutamate synthesis-linking Glr enzyme and the YrpC (MurI) isozyme. *FEMS Microbiol Lett* **223:** 221-225

Ashiuchi M, Kuwana E, Yamamoto T, Komatsu K, Soda K & Misono H (2002)

Glutamate racemase is an endogenous DNA gyrase inhibitor. *J Biol Chem* **277:** 39070–39073

Azuma Y, Arnaoutov A, Anan T & Dasso M (2005) PIASy mediates SUMO-2 conjugation of Topoisomerase-II on mitotic chromosomes. *EMBO J* **24:** 2172–2182

Bachant J, Alcasabas A, Blat Y, Kleckner N, Elledge SJ (2002) The SUMO-1 isopeptidase Smt4 is linked to centromeric cohesion through SUMO-1 modification of DNA topoisomerase II. *Mol Cell* **9:** 1169-1182

Badrinarayanan A, Lesterlin C, Reyes-Lamothe R, Sherratt D (2012a) The Escherichia coli SMC complex, MukBEF, shapes nucleoid organization independently of DNA replication. *J Bacteriol* **194:** 4669-4676

Badrinarayanan A, Reyes-Lamothe R, Uphoff S, Leake MC, Sherratt DJ (2012b) In vivo architecture and action of bacterial structural maintenance of chromosome proteins. *Science* **338:** 528-531

Baker NM, Weigand S, Maar-Mathias S, Mondragon A (2011) Solution structures of DNA-bound gyrase. *Nucleic Acids Res* **39:** 755-766

Baker TA, Sekimizu K, Funnell BE & Kornberg A (1986) Extensive unwinding of the plasmid template during staged enzymatic initiation of DNA replication from the origin of the Escherichia coli chromosome. *Cell*

Bates D, Kleckner N (2005) Chromosome and replisome dynamics in E. coli: loss of sister cohesion triggers global chromosome movement and mediates chromosome segregation. *Cell* **121:** 899-911

Baudat F, Manova K, Yuen JP, Jasin M, Keeney S (2000) Chromosome synapsis defects and sexually dimorphic meiotic progression in mice lacking Spo11. *Mol Cell* **6:** 989-998

Bax BD, Chan PF, Eggleston DS, Fosberry A, Gentry DR, Gorrec F, Giordano I, Hann MM, Hennessy A, Hibbs M, Huang J, Jones E, Jones J, Brown KK, Lewis CJ, May EW, Saunders MR, Singh O, Spitzfaden CE, Shen C, Shillings A, Theobald AF, Wohlkonig A, Pearson ND, Gwynn MN (2010) Type IIA topoisomerase inhibition by a new class of antibacterial agents. *Nature* **466:** 935-940

Baxter J & Aragón L (2012) A model for chromosome condensation based on the interplay between condensin and topoisomerase II. *Trends Genet* **28:** 110–117

Baxter J, Diffley JF (2008a) Topoisomerase II inactivation prevents the completion of DNA replication in budding yeast. *Mol Cell* **30:** 790-802

Baxter J, Diffley JFX (2008b) Topoisomerase II inactivation prevents the completion of DNA replication in budding yeast. *Mol Cell* **30:** 790-802

Baxter J, Sen N, Martinez VL, De Carandini MEM, Schvartzman JB, Diffley JFX, Aragon L (2011) Positive Supercoiling of Mitotic DNA Drives Decatenation by Topoisomerase II in Eukaryotes. *Science* **331:** 1328-1332

Belova GI, Prasad R, Kozyavkin SA, Lake JA, Wilson SH, Slesarev AI (2001) A type IB topoisomerase with DNA repair activities. *Proc Natl Acad Sci USA* **98:** 6015-6020

Berger JM, Fass D, Wang JC, Harrison SC (1998) Structural similarities between topoisomerases that cleave one or both DNA strands. *Proc Natl Acad Sci U S A* **95:** 7876-7881

Bergerat A, de Massy B, Gadelle D, Varoutas PC, Nicolas A, Forterre P (1997) An atypical topoisomerase II from Archaea with implications for meiotic recombination. *Nature* **386:** 414-417

Bergerat A, Gadelle D, Forterre P (1994) Purification of a DNA topoisomerase II from the hyperthermophilic archaeon Sulfolobus shibatae. A thermostable enzyme with both bacterial and eucaryal features. *J Biol Chem* **269:** 27663-27669

Bermejo R, Doksani Y, Capra T, Katou YM, Tanaka H, Shirahige K, Foiani M (2007) Top1- and Top2-mediated topological transitions at replication forks ensure fork progression and stability and prevent DNA damage checkpoint activation. *Genes Dev* **21:** 1921-1936

Bernard P, Couturier M (1992) Cell killing by the F plasmid CcdB protein involves poisoning of DNA-topoisomerase II complexes. *J Mol Biol* **226:** 735-745

Bhalla N, Biggins S, Murray AW (2002) Mutation of YCS4, a budding yeast condensin subunit, affects mitotic and nonmitotic chromosome behavior. *Mol Biol Cell* **13:** 632-645

Bhat MA, Philp AV, Glover DM, Bellen HJ (1996) Chromatid segregation at anaphase requires the barren product, a novel chromosome-associated protein that interacts with Topoisomerase II. *Cell* **87:** 1103-1114

Bigot S, Marians KJ (2010) DNA chirality-dependent stimulation of topoisomerase IV activity by the C-terminal AAA+ domain of FtsK. *Nucleic Acids Res* **38:** 3031-3040

Blot N, Mavathur R, Geertz M, Travers A, Muskhelishvili G (2006) Homeostatic regulation of supercoiling sensitivity coordinates transcription of the bacterial genome. *EMBO Rep* **7:** 710-715

Boles TC, White JH, Cozzarelli NR (1990) Structure of plectonemically supercoiled DNA. *J Mol Biol* **213:** 931-951

Breuer C, Stacey NJ, West CE, Zhao Y, Chory J, Tsukaya H, Azumi Y, Maxwell A, Roberts K, Sugimoto-Shirasu K (2007) BIN4, a novel component of the plant DNA topoisomerase VI complex, is required for endoreduplication in Arabidopsis. *Plant Cell* **19:** 3655-3668

Brill SJ, DiNardo S, Voelkel-Meiman K, Sternglanz R (1987) Need for DNA topoisomerase activity as a swivel for DNA replication for transcription of ribosomal RNA. *Nature* **326:** 414-416

Brino L, Urzhumtsev A, Mousli M, Bronner C, Mitschler A, Oudet P & Moras D (2000) Dimerization of Escherichia coli DNA-gyrase B provides a structural mechanism for activating the ATPase catalytic center. *J Biol Chem* **275:** 9468–9475

Brochier-Armanet C, Forterre P (2007) Widespread distribution of archaeal reverse gyrase in thermophilic bacteria suggests a complex history of vertical inheritance and lateral gene transfers. *Archaea* **2:** 83-93

Brown PO, Cozzarelli NR (1979) A sign inversion mechanism for enzymatic supercoiling of DNA. *Science* **206:** 1081-1083

Brown PO, Cozzarelli NR (1981) Catenation and knotting of duplex DNA by type 1 topoisomerases: a mechanistic parallel with type 2 topoisomerases. *Proc Natl Acad Sci USA* **78:** 843-847

Brunger AT, Adams PD, Clore GM, DeLano WL, Gros P, Grosse-Kunstleve RW, Jiang J-S, Kuszewski J, Nilges M & Pannu NS (1998) Crystallography & NMR system: A new software suite for macromolecular structure determination. *Acta Crystallogr. D Biol. Crystallogr.* **54:** 905–921

Castel SE & Martienssen RA (2013) RNA interference in the nucleus: roles for small RNAs in transcription, epigenetics and beyond. *Nat Rev Genet* **14:** 100–112

Cejka P, Cannavo E, Polaczek P, Masuda-Sasa T, Pokharel S, Campbell JL, Kowalczykowski SC (2010) DNA end resection by Dna2-Sgs1-RPA and its stimulation by Top3-Rmi1 and Mre11-Rad50-Xrs2. *Nature* **467:** 112-116

Champion K, Higgins NP (2007) Growth rate toxicity phenotypes and homeostatic supercoil control differentiate Escherichia coli from Salmonella enterica serovar Typhimurium. *J Bacteriol* **189:** 5839-5849

Champoux J, Been M (1980) Topoisomerases and the swivel problem. *Mechanistic studies of DNA replication and recombination: ICN-UCLA symposia on molecular and cellular biology***:** 809-815

Champoux JJ, Dulbecco R (1972) An activity from mammalian cells that untwists superhelical DNA--a possible swivel for DNA replication (polyoma-ethidium bromide-mouse-embryo cells-dye binding assay). *Proc Natl Acad Sci USA* **69:** 143-146

Chan KL, North PS, Hickson ID (2007) BLM is required for faithful chromosome segregation and its localization defines a class of ultrafine anaphase bridges. *EMBO J* **26:** 3397-3409

Chan K-L, Roig MB, Hu B, Beckouët F, Metson J & Nasmyth K (2012) Cohesin's DNA Exit Gate Is Distinct from Its Entrance Gate and Is Regulated by Acetylation. *Cell* **150**: 961-974

Chang M, Bellaoui M, Zhang C, Desai R, Morozov P, Delgado-Cruzata L, Rothstein R, Freyer GA, Boone C, Brown GW (2005) RMI1/NCE4, a suppressor of genome instability, encodes a member of the RecQ helicase/Topo III complex. *EMBO J* **24:** 2024-2033

Charbonnier F, Forterre P (1994) Comparison of plasmid DNA topology among mesophilic and thermophilic eubacteria and archaebacteria. *J Bacteriol* **176:** 1251-1259

Charvin G, Bensimon D, Croquette V (2003) Single-molecule study of DNA unlinking by eukaryotic and prokaryotic type-II topoisomerases. *Proc Natl Acad Sci USA* **100:** 9820-9825

Charvin G, Strick TR, Bensimon D, Croquette V (2005) Topoisomerase IV bends and overtwists DNA upon binding. *Biophys J* **89:** 384-392

Chatterji M, Sengupta S, Nagaraja V (2003) Chromosomally encoded gyrase inhibitor GyrI protects Escherichia coli against DNA-damaging agents. *Arch Microbiol* **180:** 339-346

Chen N, Zinchenko AA, Yoshikawa Y, Araki S, Adachi S, Yamazoe M, Hiraga S, Yoshikawa K (2008) ATP-induced shrinkage of DNA with MukB protein and the MukBEF complex of Escherichia coli. *J Bacteriol* **190:** 3731-3737

Chen VB, Arendall WB, 3rd, Headd JJ, Keedy DA, Immormino RM, Kapral GJ, Murray LW, Richardson JS, Richardson DC (2010) MolProbity: all-atom structure validation for macromolecular crystallography. *Acta Crystallogr D Biol Crystallogr* **66:** 12-21

Cheng B, Annamalai T, Sorokin E, Abrenica M, Aedo S, Tse-Dinh YC (2009) Asp-to-Asn substitution at the first position of the DxD TOPRIM motif of recombinant bacterial topoisomerase I is extremely lethal to E. coli. *J Mol Biol* **385:** 558-567

Cheng B, Zhu CX, Ji C, Ahumada A, Tse-Dinh YC (2003) Direct interaction between Escherichia coli RNA polymerase and the zinc ribbon domains of DNA topoisomerase I. *J Biol Chem* **278:** 30705-30710

Cheng C, Kussie P, Pavletich N, Shuman S (1998) Conservation of Structure and Mechanism between Eukaryotic Topoisomerase I and Site-Specific Recombinases. *Cell* **92:** 841-850

Chiu A, Revenkova E, Jessberger R (2004) DNA interaction and dimerization of eukaryotic SMC hinge domains. *J Biol Chem* **279:** 26233-26242

Choudhary C, Kumar C, Gnad F, Nielsen ML, Rehman M, Walther TC, Olsen JV, Mann M (2009) Lysine acetylation targets protein complexes and co-regulates major cellular functions. *Science* **325:** 834-840

Classen S, Olland S, Berger JM (2003) Structure of the topoisomerase II ATPase region and its mechanism of inhibition by the chemotherapeutic agent ICRF-187. *Proc Natl Acad Sci USA* **100:** 10629-10634

Cliby WA (2002) S Phase and G2 Arrests Induced by Topoisomerase I Poisons Are Dependent on ATR Kinase Function. *J Biol Chem* **277:** 1599-1606

Coelho PA, Queiroz-Machado J, Carmo AM, Moutinho-Pereira S, Maiato H, Sunkel CE (2008) Dual role of topoisomerase II in centromere resolution and aurora B activity. *PLoS Biol* **6:** e207

Collin F, Karkare S & Maxwell A (2011) Exploiting bacterial DNA gyrase as a drug target: current state and perspectives. *Appl Microbiol Biotechnol* **92:** 479–497

Confalonieri F, Elie C, Nadal M, de La Tour C, Forterre P, Duguet M (1993) Reverse gyrase: a helicase-like domain and a type I topoisomerase in the same polypeptide. *Proc Natl Acad Sci USA* **90:** 4753-4757

Corbett KD, Benedetti P, Berger JM (2007) Holoenzyme assembly and ATP-mediated conformational dynamics of topoisomerase VI. *Nat Struct Mol Biol* **14:** 611-619

Corbett KD, Berger JM (2003) Structure of the topoisomerase VI-B subunit: implications for type II topoisomerase mechanism and evolution. *EMBO J* **22:** 151-163

Corbett KD, Berger JM (2006) Structural basis for topoisomerase VI inhibition by the anti-Hsp90 drug radicicol. *Nucleic Acids Res* **34:** 4269-4277

Corbett KD, Schoeffler AJ, Thomsen ND, Berger JM (2005) The structural basis for substrate specificity in DNA topoisomerase IV. *J Mol Biol* **351:** 545-561

Corbett KD, Shultzaberger RK, Berger JM (2004) The C-terminal domain of DNA gyrase A adopts a DNA-bending beta-pinwheel fold. *Proc Natl Acad Sci USA* **101:** 7293-7298

Cortes Ledesma F, El Khamisy SF, Zuma MC, Osborn K, Caldecott KW (2009) A human 5'-tyrosyl DNA phosphodiesterase that repairs topoisomerase-mediated DNA damage. *Nature* **461:** 674-678

Costenaro L, Grossmann JG, Ebel C, Maxwell A (2005) Small-angle X-ray scattering reveals the solution structure of the full-length DNA gyrase a subunit. *Structure* **13:** 287-296

Crisona NJ, Strick TR, Bensimon D, Croquette V, Cozzarelli NR (2000) Preferential relaxation of positively supercoiled DNA by E. coli topoisomerase IV in single-molecule and ensemble measurements. *Genes Dev* **14:** 2881-2892

Crozat E, Grainge I (2010) FtsK DNA translocase: the fast motor that knows where it's going. *Chembiochem* **11:** 2232-2243

Cui Y, Petrushenko ZM, Rybenkov VV (2008) MukB acts as a macromolecular clamp in DNA condensation. *Nat Struct Mol Biol* **15:** 411-418

Danilova O, Reyes-Lamothe R, Pinskaya M, Sherratt D, Possoz C (2007) MukB colocalizes with the oriC region and is required for organization of the two Escherichia coli chromosome arms into separate cell halves. *Mol Microbiol* **65:** 1485-1492

Datsenko KA (2000) One-step inactivation of chromosomal genes in Escherichia coli K-12 using PCR products. *Proc Natl Acad Sci USA* **97:** 6640–6645

Datta A, Jinks-Robertson S (1995) Association of increased spontaneous mutation rates with high levels of transcription in yeast. *Science* **268:** 1616-1619

Datta K, LiCata VJ (2003) Thermodynamics of the binding of Thermus aquaticus DNA polymerase to primed-template DNA. *Nucleic Acids Res* **31:** 5590-5597

Dawlaty MM, Malureanu L, Jeganathan KB, Kao E, Sustmann C, Tahk S, Shuai K, Grosschedl R, van Deursen JM (2008) Resolution of sister centromeres requires RanBP2-mediated SUMOylation of topoisomerase IIalpha. *Cell* **133:** 103-115

Déclais AC, Marsault J, Confalonieri F, de La Tour CB, Duguet M (2000) Reverse gyrase, the two domains intimately cooperate to promote positive supercoiling. *J Biol Chem* **275:** 19498-19504

DeLano WL (2002) The PyMOL Molecular Graphics System. (http://www.pymol.org).

de Nadal E, Ammerer G & Posas F (2011) Controlling gene expression in response to stress. *Nat Rev Genet*

Desai SD, Liu LF, Vazquez-Abad D, D'Arpa P (1997) Ubiquitin-dependent destruction of topoisomerase I is stimulated by the antitumor drug camptothecin. *J Biol Chem* **272:** 24159-24164

Desai SD, Zhang H, Rodriguez-Bauman A, Yang J-M, Wu X, Gounder MK, Rubin EH, Liu LF (2003) Transcription-dependent degradation of topoisomerase I-DNA covalent complexes. *Mol Cell Biol* **23:** 2341-2350

Deweese JE, Osheroff N (2009) Coordinating the Two Protomer Active Sites of Human Topoisomerase IIα: Nicks as Topoisomerase II Poisons *Biochemistry* **48:** 1439-1441

DiGate RJ, Marians KJ (1988) Identification of a potent decatenating enzyme from Escherichia coli. *J Biol Chem* **263:** 13366-13373

DiNardo S, Voelkel K, Sternglanz R (1984) DNA topoisomerase II mutant of Saccharomyces cerevisiae: topoisomerase II is required for segregation of daughter molecules at the termination of DNA replication. *Proc Natl Acad Sci USA* **81:** 2616-2620

DiNardo S, Voelkel KA, Sternglanz R & Reynolds AE (1982) Escherichia coli DNA topoisomerase I mutants have compensatory mutations in DNA gyrase genes. *Cell*

Díaz-Martínez LA, Giménez-Abián JF, Azuma Y, Guacci V, Giménez-Martín G, Lanier LM & Clarke DJ (2006) PIASgamma is required for faithful chromosome segregation in human cells. *PLoS ONE* **1:** e53

Domain F, Levy SB (2010) GyrA Interacts with MarR To Reduce Repression of the marRAB Operon in Escherichia coli. *J Bacteriol* **192:** 942-948

Donachie WD (1969) Control of cell division in Escherichia coli: experiments with thymine starvation. *J Bacteriol* **100:** 260–268

Donachie WD, Begg KJ & Vicente M (1976) Cell length, cell growth and cell division. *Nature* **264:** 328–333

Dong KC, Berger JM (2007) Structural basis for gate-DNA recognition and bending by type IIA topoisomerases. *Nature* **450:** 1201-1205

Dorman CJ, Ni Bhriain N & Higgins CF (1990) DNA supercoiling and environmental regulation of virulence gene expression in Shigella flexneri. *Nature* **344:** 789–792

Doyle SA (2005) High-throughput cloning for proteomics research. *Methods Mol Biol* **310:** 107-113

Drlica K (1992) Control of bacterial DNA supercoiling. *Mol Microbiol* **6:** 425–433

Drolet M, Bi X, Liu LF (1994) Hypernegative supercoiling of the DNA template during transcription elongation in vitro. *J Biol Chem* **269:** 2068

Drolet M, Phoenix P, Menzel R, Massé E, Liu LF, Crouch RJ (1995) Overexpression of RNase H partially complements the growth defect of an Escherichia coli delta topA mutant: R-loop formation is a major problem in the absence of DNA topoisomerase I. *Proc Natl Acad Sci USA* **92:** 3526

Durand-Dubief M, Persson J, Norman U, Hartsuiker E, Ekwall K (2010) Topoisomerase I regulates open chromatin and controls gene expression in vivo. *EMBO J* **29:** 2126-2134

Dykhuizen EC, Hargreaves DC, Miller EL, Cui K, Korshunov A, Kool M, Pfister S, Cho YJ, Zhao K, Crabtree GR (2013) BAF complexes facilitate decatenation of DNA by topoisomerase IIalpha. *Nature* **497:** 624-627

Edelhoch H (1967) Spectroscopic determination of tryptophan and tyrosine in proteins. *Biochemistry* **6:** 1948–1954

Edwards MJ, Flatman RH, Mitchenall LA, Stevenson CE, Le TB, Clarke TA, McKay AR, Fiedler HP, Buttner MJ, Lawson DM, Maxwell A (2009) A crystal structure of the bifunctional antibiotic simocyclinone D8, bound to DNA gyrase. *Science* **326:** 1415-1418

Emsley P, Lohkamp B, Scott WG, Cowtan K (2010) Features and development of Coot. *Acta Crystallogr D Biol Crystallogr* **66:** 486-501

Espeli O, Lee C, Marians KJ (2003a) A physical and functional interaction between Escherichia coli FtsK and topoisomerase IV. *J Biol Chem* **278:** 44639-44644

Espeli O, Levine C, Hassing H, Marians KJ (2003b) Temporal regulation of topoisomerase IV activity in E. coli. *Mol Cell* **11:** 189-201

Fachinetti D, Bermejo R, Cocito A, Minardi S, Katou Y, Kanoh Y, Shirahige K, Azvolinsky A, Zakian VA, Foiani M (2010) Replication termination at eukaryotic chromosomes is mediated by Top2 and occurs at genomic loci containing pausing elements. *Mol Cell* **39:** 595-605

Forterre P (2006) DNA topoisomerase V: a new fold of mysterious origin. *Trends Biotechnol* **24:** 245-247

Forterre P, Gribaldo S, Gadelle D, Serre MC (2007) Origin and evolution of DNA topoisomerases. *Biochimie* **89:** 427-446

Forterre P, Mirambeau G, Jaxel C, Nadal M, Duguet M (1985) High positive supercoiling in vitro catalyzed by an ATP and polyethylene glycol-stimulated topoisomerase from Sulfolobus acidocaldarius. *EMBO J* **4:** 2123-2128

Fox AH, Liew C, Holmes M, Kowalski K, Mackay J & Crossley M (1999) Transcriptional cofactors of the FOG family interact with GATA proteins by means of multiple zinc fingers. *EMBO J* **18:** 2812–2822

Freiesleben Von U & Rasmussen KV (1992) The level of supercoiling affects the regulation of DNA replication in Escherichia coli. *Research in Microbiology* **143:** 655–663

Frohlich RF, Veigaard C, Andersen FF, Mcclendon AK, Gentry AC, Andersen AH, Osheroff N, Stevnsner T, Knudsen BR (2007) Tryptophane-205 of human topoisomerase I is essential for camptothecin inhibition of negative but not positive supercoil removal. *Nucleic Acids Res* **35:** 6170-6180

Fu G, Wu J, Liu W, Zhu D, Hu Y, Deng J, Zhang X-E, Bi L & Wang D-C (2009) Crystal structure of DNA gyrase B' domain sheds lights on the mechanism for T-segment navigation. *Nucleic Acids Res* **37:** 5908–5916

Gadelle D, Filée J, Buhler C, Forterre P (2003) Phylogenomics of type II DNA topoisomerases. *Bioessays* **25:** 232-242

Gangloff S, Mcdonald J, Bendixen C, Arthur L, Rothstein R (1994) The yeast type I topoisomerase Top3 interacts with Sgs1, a DNA helicase homolog: a potential eukaryotic reverse gyrase. *Mol Cell Biol* **14:** 8391-8398

Gellert M, Mizuuchi K, O'Dea MH, Nash HA (1976) DNA gyrase: an enzyme that introduces superhelical turns into DNA. *Proc Natl Acad Sci USA* **73:** 3872-3876

Goto T, Wang JC (1982) Yeast DNA topoisomerase II. An ATP-dependent type II topoisomerase that catalyzes the catenation, decatenation, unknotting, and relaxation of double-stranded DNA rings. *J Biol Chem* **257:** 5866-5872

Graumann PL (2000) Bacillus subtilis SMC is required for proper arrangement of the chromosome and for efficient segregation of replication termini but not for bipolar movement of newly duplicated origin regions. *J Bacteriol* **182:** 6463-6471

Griese JJ, Hopfner KP (2010) Structure and DNA-binding activity of the Pyrococcus furiosus SMC protein hinge domain. *Proteins* **79**: 558-568

Griese JJ, Witte G, Hopfner KP (2010) Structure and DNA binding activity of the mouse condensin hinge domain highlight common and diverse features of SMC proteins. *Nucleic Acids Res* **38**: 3454-3465

Grishin NV (2001) Treble clef finger--a functionally diverse zinc-binding structural motif. *Nucleic Acids Res* **29:** 1703–1714

Gruber S, Arumugam P, Katou Y, Kuglitsch D, Helmhart W, Shirahige K & Nasmyth K (2006) Evidence that loading of cohesin onto chromosomes involves opening of its SMC hinge. *Cell* **127:** 523–537

Hardin AH, Sarkar SK, Seol Y, Liou GF, Osheroff N, Neuman KC (2011) Direct measurement of DNA bending by type IIA topoisomerases: implications for non-equilibrium topology simplification. *Nucleic Acids Res* **39:** 5729-5743

Hardy CD, Crisona NJ, Stone MD, Cozzarelli NR (2004) Disentangling DNA during replication: a tale of two strands. *Philos Trans R Soc London [Biol]* **359:** 39-47

Harmon FG, Brockman JP, Kowalczykowski SC (2003) RecQ helicase stimulates both DNA catenation and changes in DNA topology by topoisomerase III. *J Biol Chem* **278:** 42668-42678

Harmon FG, DiGate RJ, Kowalczykowski SC (1999) RecQ helicase and topoisomerase III comprise a novel DNA strand passage function: a conserved mechanism for control of DNA recombination. *Mol Cell* **3:** 611-620

Hartsuiker E, Mizuno K, Molnar M, Kohli J, Ohta K, Carr AM (2009) Ctp1CtIP and Rad32Mre11 nuclease activity are required for Rec12Spo11 removal, but Rec12Spo11 removal is dispensable for other MRN-dependent meiotic functions. *Mol Cell Biol* **29:** 1671-1681

Hartung F, Angelis KJ, Meister A, Schubert I, Melzer M, Puchta H (2002) An archaebacterial topoisomerase homolog not present in other eukaryotes is indispensable for cell proliferation of plants. *Curr Biol* **12:** 1787-1791

Hartwell LH, Weinert TA (1989) Checkpoints: controls that ensure the order of cell cycle events. *Science* **246:** 629-634

Hashimi S, Wall M, Smith A, Maxwell A, Birch R (2007) The Phytotoxin Albicidin is a Novel Inhibitor of DNA Gyrase. *Antimicrob Agents and Chemother* **51:** 181

Hayama R, Bahng S, Karasu ME, Marians KJ (2013) The MukB-ParC Interaction Affects Intramolecular, not Intermolecular, Activities of Topoisomerase IV. *J Biol Chem* **288:** 7653-7661

Hayama R, Marians KJ (2010) Physical and functional interaction between the condensin MukB and the decatenase topoisomerase IV in Escherichia coli. *Proc Natl Acad Sci USA* **107:** 18826-18831

Hegde S, Vetting M, Roderick S, Mitchenall L, Maxwell A, Takiff H, Blanchard J (2005) A fluoroquinolone resistance protein from Mycobacterium tuberculosis that mimics DNA. *Science* **308:** 1480-1483

Heyduk T, Lee JC (1990) Application of fluorescence energy transfer and polarization to monitor Escherichia coli cAMP receptor protein and lac promoter interaction. *Proc Natl Acad Sci USA* **87:** 1744-1748

Hiasa H, DiGate RJ, Marians KJ (1994) Decatenating activity of Escherichia coli DNA gyrase and topoisomerases I and III during oriC and pBR322 DNA replication in vitro. *J Biol Chem* **269:** 2093-2099

Hiasa H, Marians KJ (1994) Topoisomerase IV can support oriC DNA replication in vitro. *J Biol Chem* **269:** 16371-16375

Hiasa H, Marians KJ (1996a) Two distinct modes of strand unlinking during θ-type DNA replication. *J Biol Chem* **271:** 21529

Hiasa H, Marians KJ (1996b) Two distinct modes of strand unlinking during θ-type DNA replication. *J Biol Chem* **271:** 21529

Hiasa H & Shea ME (2000) DNA gyrase-mediated wrapping of the DNA strand is required for the replication fork arrest by the DNA gyrase-quinolone-DNA ternary complex. *J Biol Chem* **275:** 34780–34786

Higgins NP & Cozzarelli NR (1982) The binding of gyrase to DNA: analysis by retention by nitrocellulose filters. *Nucleic Acids Res* **10:** 6833–6847

Hill NS, Kadoya R, Chattoraj DK & Levin PA (2012) Cell size and the initiation of DNA replication in bacteria. *PLoS Genetics* **8:** e1002549

Hiraga S, Niki H, Ogura T, Ichinose C (1989) Chromosome partitioning in Escherichia coli: novel mutants producing anucleate cells. *J Bacteriol* **171**: 1496-1505

Hirano M, Hirano T (2002) Hinge-mediated dimerization of SMC protein is essential for its dynamic interaction with DNA. *EMBO J* **21:** 5733-5744

Hirano M, Hirano T (2006) Opening closed arms: long-distance activation of SMC ATPase by hinge-DNA interactions. *Mol Cell* **21:** 175-186

Hirano T (2006) At the heart of the chromosome: SMC proteins in action. *Nat Rev Mol Cell Biol* **7:** 311-322

Hirano T (2012) Condensins: universal organizers of chromosomes with diverse functions. *Genes Dev* **26:** 1659-1678

Holm C, Goto T, Wang JC, Botstein D (1985) DNA topoisomerase II is required at the time of mitosis in yeast. *Cell* **41:** 553-563

Holm C, Stearns T, Botstein D (1989) DNA topoisomerase II must act at mitosis to prevent nondisjunction and chromosome breakage. *Mol Cell Biol* **9:** 159

Holton J, Alber T (2004) Automated protein crystal structure determination using ELVES. *Proc Natl Acad Sci USA* **101:** 1537-1542

Hsieh T, Brutlag D (1980) ATP-dependent DNA topoisonmerase from D. melanogaster reversibly catenates duplex DNA rings. *Cell* **21:** 115-125

Hsieh T, Plank JL (2006) Reverse gyrase functions as a DNA renaturase. *J Biol Chem* **281:** 5640

Hsieh TJ, Farh L, Huang WM, Chan NL (2004) Structure of the topoisomerase IV C-terminal domain: a broken beta-propeller implies a role as geometry facilitator in catalysis. *J Biol Chem* **279:** 55587-55593

Hsieh LS, Rouviere-Yaniv J & Drlica K (1991) Bacterial DNA supercoiling and [ATP]/[ADP] ratio: changes associated with salt shock. *J Bacteriol* **173:** 3914–3917

Hsieh TJ, Yen TJ, Lin TS, Chang HT, Huang SY, Hsu CH, Farh L, Chan NL (2010) Twisting of the DNA-binding surface by a beta-strand-bearing proline modulates DNA gyrase activity. *Nucleic Acids Res* **38:** 4173-4181

Hu P, Beresten SF, van Brabant AJ, Ye TZ, Pandolfi PP, Johnson FB, Guarente L, Ellis NA (2001) Evidence for BLM and Topoisomerase IIIalpha interaction in genomic stability. *Hum Mol Genet* **10:** 1287-1298

Huang WM, Libbey JL, van der Hoeven P, Yu SX (1998) Bipolar localization of Bacillus subtilis topoisomerase IV, an enzyme required for chromosome segregation. *Proc Natl Acad Sci USA* **95:** 4652-4657

Ira G, Malkova A, Liberi G, Foiani M, Haber JE (2003) Srs2 and Sgs1-Top3 suppress crossovers during double-strand break repair in yeast. *Cell* **115:** 401-411

Jiang Y, Pogliano J, Helsinki DR & Konieczny I (2002) ParE toxin encoded by the broad-host-range plasmid RK2 is an inhibitor of Escherichia coli gyrase. *Mol Microbiol* **44:** 971–979

Joshi MC, Bourniquel A, Fisher J, Ho BT, Magnan D, Kleckner N, Bates D (2011) Escherichia coli sister chromosome separation includes an abrupt global transition with concomitant release of late-splitting intersister snaps. *Proc Natl Acad Sci USA* **108:** 2765-2770

Joshi MC, Magnan D, Montminy TP, Lies M, Stepankiw N, Bates D (2013) Regulation of Sister Chromosome Cohesion by the Replication Fork Tracking Protein SeqA. *PLoS Genet* **9:** e1003673

Ju BG, Lunyak VV, Perissi V, Garcia-Bassets I, Rose DW, Glass CK, Rosenfeld MG (2006) A topoisomerase IIbeta-mediated dsDNA break required for regulated transcription. *Science* **312:** 1798-1802

Juge F, Fernando C, Fic W, Tazi J (2010) The SR protein B52/SRp55 is required for DNA topoisomerase I recruitment to chromatin, mRNA release and transcription shutdown. *PLoS Genet* **6**

Kaguni JM, Kornberg A (1984) Topoisomerase I confers specificity in enzymatic replication of the Escherichia coli chromosomal origin. *J Biol Chem* **259:** 8578-8583

Kampranis SC, Maxwell A (1996) Conversion of DNA gyrase into a conventional type II topoisomerase. *Proc Natl Acad Sci USA* **93:** 14416-14421

Kang S, Han J, Park J, Skarstad K, HWang D (2003) SeqA protein stimulates the relaxing and decatenating activities of topoisomerase IV. *J Biol Chem* **278:** 48779-48785

Kapoor P, Kumar A, Naik R, Ganguli M, Siddiqi MI, Sahasrabuddhe AA, Gupta CM (2010) Leishmania actin binds and nicks kDNA as well as inhibits decatenation activity of type II topoisomerase. *Nucleic Acids Res* **38:** 3308-3317

Kato J, Nishimura Y, Imamura R, Niki H, Hiraga S, Suzuki H (1990) New topoisomerase essential for chromosome segregation in E. coli. *Cell* **63:** 393-404

Kato J, Nishimura Y, Yamada M, Suzuki H, Hirota Y (1988) Gene organization in the region containing a new gene involved in chromosome partition in Escherichia coli. *J Bacteriol* **170:** 3967-3977

Kato J, Suzuki H, Ikeda H (1992) Purification and characterization of DNA topoisomerase IV in Escherichia coli. *J Biol Chem* **267:** 25676-25684

Keeney S (2008) Spo11 and the formation of DNA double-strand breaks in meiosis. *Genome Dyn Stab* **2:** 81-123

Keeney S, Giroux CN, Kleckner N (1997) Meiosis-specific DNA double-strand breaks are catalyzed by Spo11, a member of a widely conserved protein family. *Cell* **88:** 375-384

Kegel A, Betts-Lindroos H, Kanno T, Jeppsson K, Ström L, Katou Y, Itoh T, Shirahige K, Sjögren C (2011) Chromosome length influences replication-induced topological stress. *Nature* **471:** 392-396

Kenakin TP (1993) *Pharmacologic Analysis of Drug-Receptor Interaction*, 2nd edn. New York: Raven.

Kennedy JA, Daughdrill GW, Schmidt KH (2013) A transient alpha-helical molecular recognition element in the disordered N-terminus of the Sgs1 helicase is critical for chromosome stability and binding of Top3/Rmi1. *Nucleic Acids Res*

Khodursky AB, Peter BJ, Schmid MB, DeRisi J, Botstein D, Brown PO, Cozzarelli NR (2000) Analysis of topoisomerase function in bacterial replication fork movement: use of DNA microarrays. *Proc Natl Acad Sci USA* **97:** 9419-9424

Kikuchi A, Asai K (1984) Reverse gyrase-a topoisomerase which introduces positive superhelical turns into DNA. *Nature* **309:** 677-681

Kim N, Huang SY, Williams JS, Li YC, Clark AB, Cho JE, Kunkel TA, Pommier Y, Jinks-Robertson S (2011) Mutagenic processing of ribonucleotides in DNA by yeast topoisomerase I. *Science* **332:** 1561-1564

Kim RA, Wang JC (1989) Function of DNA topoisomerases as replication swivels in Saccharomyces cerevisiae. *J Mol Biol* **208:** 257-267

Kimura K, Saijo M, Tanaka M, Enomoto T (1996) Phosphorylation-independent stimulation of DNA topoisomerase II alpha activity. *J Biol Chem* **271:** 10990-10995

King IF, Yandava CN, Mabb AM, Hsiao JS, Huang H-S, Pearson BL, Calabrese JM, Starmer J, Parker JS, Magnuson T, Chamberlain SJ, Philpot BD & Zylka MJ (2013) Topoisomerases facilitate transcription of long genes linked to autism. *Nature* **501:** 58–62

Kingma PS, Osheroff N (1997a) Apurinic sites are position-specific topoisomerase II poisons. *J Biol Chem* **272:** 1148-1155

Kingma PS, Osheroff N (1997b) Spontaneous DNA damage stimulates topoisomerase II-mediated DNA cleavage. *J Biol Chem* **272:** 7488-7493

Kirchhausen T, Wang JC, Harrison SC (1985) DNA gyrase and its complexes with DNA: direct observation by electron microscopy. *Cell* **41:** 933-943

Konarev PV, Volkov VV, Sokolova AV, Koch MHJ & Svergun DI (2003) PRIMUS: a Windows PC-based system for small-angle scattering data analysis. *J Appl Crystallogr* **36:** 1277–1282

Koster DA, Croquette V, Dekker C, Shuman S, Dekker NH (2005) Friction and torque govern the relaxation of DNA supercoils by eukaryotic topoisomerase IB. *Nature* **434:** 671-674

Kouzine F, Gupta A, Baranello L, Wojtowicz D, Ben-Aissa K, Liu J, Przytycka TM & Levens D (2013) Transcription-dependent dynamic supercoiling is a short-range genomic force. *Nat Struct Mol Biol* **20:** 396–403

Kowalska-Loth B, Girstun A, Trzcińska AM, Piekiełko-Witkowska A, Staron K (2005) SF2/ASF protein binds to the cap region of human topoisomerase I through two RRM domains. *Biochem Biophys Res Commun* **331:** 398-403

Kramlinger VM, Hiasa H (2006) The "GyrA-box" is required for the ability of DNA gyrase to wrap DNA and catalyze the supercoiling reaction. *J Biol Chem* **281:** 3738-3742

Kreuzer KN & Cozzarelli NR (1979) Escherichia coli mutants thermosensitive for deoxyribonucleic acid gyrase subunit A: effects on deoxyribonucleic acid replication, transcription, and bacteriophage growth. *J Bacteriol* **140:** 424–435

Krishna SS, Majumdar I & Grishin NV (2003) Structural classification of zinc fingers: survey and summary. *Nucleic Acids Res* **31:** 532–550

Krogh BO, Shuman S (2002) A poxvirus-like type IB topoisomerase family in bacteria. *Proc Natl Acad Sci USA* **99:** 1853-1858

Ku B, Lim JH, Shin HC, Shin SY, Oh BH (2009) Crystal structure of the MukB hinge domain with coiled-coil stretches and its functional implications. *Proteins* **78**: 1483-1490

Kurz EU, Leader KB, Kroll DJ, Clark M, Gieseler F (2000) Modulation of human DNA topoisomerase IIalpha function by interaction with 14-3-3epsilon. *J Biol Chem* **275:** 13948-13954

Labourier E, Rossi F, Gallouzi IE, Allemand E, Divita G, Tazi J (1998) Interaction between the N-terminal domain of human DNA topoisomerase I and the arginine-serine domain of its substrate determines phosphorylation of SF2/ASF splicing factor. *Nucleic Acids Res* **26:** 2955-2962

Lanz MA, Klostermeier D (2012) The GyrA-box determines the geometry of DNA bound to gyrase and couples DNA binding to the nucleotide cycle. *Nucleic Acids Res* **40:** 10893-10903

Laponogov I, Pan XS, Veselkov DA, McAuley KE, Fisher LM, Sanderson MR (2010) Structural basis of gate-DNA breakage and resealing by type II topoisomerases. *PLoS One* **5:** e11338

Laponogov I, Veselkov DA, Crevel IMT, Pan X-S, Fisher LM & Sanderson MR (2013) Structure of an 'open' clamp type II topoisomerase-DNA complex provides a mechanism for DNA capture and transport. *Nucleic Acids Res*

Lavasani LS, Hiasa H (2001) A ParE-ParC fusion protein is a functional topoisomerase. *Biochemistry* **40:** 8438-8443

Lechtenberg BC, Allen MD, Rutherford TJ, Freund SMV & Bycroft M (2009) Solution structure of the FCS zinc finger domain of the human polycomb group protein L(3)mbt-like 2. *Protein Science* **18:** 657–661

Lee C, Marians KJ (2013) Characterization of the Nucleoid-associated Protein YejK. *J Biol Chem* (*In Press*)

Lee HO, Davidson JM, Duronio RJ (2009) Endoreplication: polyploidy with purpose. *Genes & Development* **23:** 2461-2477

Lee I, Dong KC, Berger JM (2013) The role of DNA bending in type IIA topoisomerase function. *Nucleic Acids Res*

Lee S, Jung SR, Heo K, Byl JA, Deweese JE, Osheroff N, Hohng S (2012) DNA cleavage and opening reactions of human topoisomerase IIalpha are regulated via Mg2+-mediated dynamic bending of gate-DNA. *Proc Natl Acad Sci USA* **109:** 2925-2930

Leslie AG & Powell HR (2007) Processing Diffraction Data with Mosflm. *Evolving Methods for Macromolecular Crystallography* 245: 41–51

Lesterlin C, Gigant E, Boccard F, Espeli O (2012) Sister chromatid interactions in bacteria revealed by a site-specific recombination assay. *EMBO J* **31:** 3468-3479

Lewis RJ, Singh OM, Smith CV, Skarzynski T, Maxwell A, Wonacott AJ, Wigley DB (1996) The nature of inhibition of DNA gyrase by the coumarins and the cyclothialidines revealed by X-ray crystallography. *EMBO J* **15:** 1412-1420

Li H, Wang Y, Liu X (2008) Plk1-dependent phosphorylation regulates functions of DNA topoisomerase IIα in cell cycle progression. *J Biol Chem* **283:** 6209

Li K, Pasternak C, Härtig E, Haberzettl K, Maxwell A & Klug G (2004) Thioredoxin can influence gene expression by affecting gyrase activity. *Nucleic Acids Res* **32:** 4563–4575

Li W, Ma H (2006) Double-stranded DNA breaks and gene functions in recombination and meiosis. *Cell Res* **16:** 402-412

Li Y, Schoeffler AJ, Berger JM, Oakley MG (2010a) The crystal structure of the hinge domain of the Escherichia coli structural maintenance of chromosomes protein MukB. *J Mol Biol* **395:** 11-19

Li Y, Stewart NK, Berger AJ, Vos S, Schoeffler AJ, Berger JM, Chait BT, Oakley MG (2010b) Escherichia coli condensin MukB stimulates topoisomerase IV activity by a direct physical interaction. *Proc Natl Acad Sci USA* **107:** 18832-18837

Li Y, Weitzel CS, Arnold RJ, Oakley MG (2009) Identification of interacting regions within the coiled coil of the Escherichia coli structural maintenance of chromosomes protein MukB. *J Mol Biol* **391:** 57-73

Lima CD, Wang JC, Mondragón A (1994) Three-dimensional structure of the 67K N-terminal fragment of E. coli DNA topoisomerase I. *Nature* **367:** 138-146

Lin CP, Ban Y, Lyu YL, Liu LF (2009) Proteasome-dependent Processing of Topoisomerase I-DNA Adducts into DNA Double Strand Breaks at Arrested Replication Forks. *J Biol Chem* **284:** 28084-28092

Lippert MJ, Kim N, Cho JE, Larson RP, Schoenly NE, O'Shea SH, Jinks-Robertson S (2011) Role for topoisomerase 1 in transcription-associated mutagenesis in yeast. *Proc Natl Acad Sci USA* **108:** 698-703

Liu L, Liu C (1980) Type II DNA topoisomerases: enzymes that can unknot a topologically knotted DNA molecule via a reversible double-strand break. *Cell*

Liu LF, Liu CC, Alberts BM (1980) Type II DNA topoisomerases: enzymes that can unknot a topologically knotted DNA molecule via a reversible double-strand break. *Cell* **19:** 697-707

Liu LF, Wang JC (1987) Supercoiling of the DNA template during transcription. *Proc Natl Acad Sci USA* **84:** 7024-7027

Lopez CR, Yang S, Deibler RW, Ray SA, Pennington JM, Digate RJ, Hastings PJ, Rosenberg SM, Zechiedrich EL (2005) A role for topoisomerase III in a recombination pathway alternative to RuvABC. *Mol Microbiol* **58:** 80-101

Lotito L, Russo A, Chillemi G, Bueno S, Cavalieri D, Capranico G (2008) Global transcription regulation by DNA topoisomerase I in exponentially growing

Saccharomyces cerevisiae cells: activation of telomere-proximal genes by TOP1 deletion. *J Mol Biol* **377:** 311-322

Lu WJ, Chapo J, Roig I, Abrams JM (2010) Meiotic recombination provokes functional activation of the p53 regulatory network. *Science* **328:** 1278-1281

Luijsterburg MS, White MF, van Driel R, Dame RT (2008) The Major Architects of Chromatin: Architectural Proteins in Bacteria, Archaea and Eukaryotes. *Crit Rev Biochem Mol Biol* **43:** 393-418

Lundblad JR, Laurance M, Goodman RH (1996) Fluorescence polarization analysis of protein-DNA and protein-protein interactions. *Mol Endocrinol* **10:** 607-612

Lyu YL, Lin C-P, Azarova AM, Cai L, Wang JC, Liu LF (2006) Role of Topoisomerase IIβ in the Expression of Developmentally Regulated Genes *Mol Cell Biol* **26:** 7929

MacDowell AA, Celestre RS, Howells M, McKinney W, Krupnick J, Cambie D, Domning EE, Duarte RM, Kelez N, Plate DW, Cork CW, Earnest TN, Dickert J, Meigs G, Ralston C, Holton JM, Alber T, Berger JM, Agard DA, Padmore HA (2004) Suite of three protein crystallography beamlines with single superconducting bend magnet as the source. *J Synchrotron Radiat* **11:** 447-455

Madden KR, Stewart L, Champoux JJ (1995) Preferential binding of human topoisomerase I to superhelical DNA. *EMBO J* **14:** 5399-5409

Maeshima K, Laemmli UK (2003) A two-step scaffolding model for mitotic chromosome assembly. *Dev Cell* **4:** 467-480

Malanga M, Czubaty A, Girstun A, Staron K, Althaus FR (2008) Poly(ADP-ribose) binds to the splicing factor ASF/SF2 and regulates its phosphorylation by DNA topoisomerase I. *J Biol Chem* **283:** 19991-19998

Malik SB, Ramesh MA, Hulstrand AM, Logsdon JM, Jr. (2007) Protist homologs of the meiotic Spo11 gene and topoisomerase VI reveal an evolutionary history of gene duplication and lineage-specific loss. *Mol Biol Evol* **24:** 2827-2841

Mao Y, Desai SD, Liu LF (2000a) SUMO-1 Conjugation to Human DNA Topoisomerase II Isozymes. *J Biol Chem* **275:** 26066-26073

Mao Y, Desai SD, Ting CY, Hwang J, Liu LF (2001) 26 S proteasome-mediated degradation of topoisomerase II cleavable complexes. *J Biol Chem* **276:** 40652-40658

Mao Y, Sun M, Desai SD, Liu LF (2000b) SUMO-1 conjugation to topoisomerase I: a possible repair response to topoisomerase-mediated DNA damage. *Proc Natl Acad Sci USA* **97:** 4046-4051

Marini JC, Miller KG, Englund PT (1980) Decatenation of kinetoplast DNA by topoisomerases. *J Biol Chem* **255:** 4976-4979

Massé E, Drolet M (1999) Relaxation of transcription-induced negative supercoiling is an essential function of Escherichia coli DNA topoisomerase I. *J Biol Chem* **274:** 16654-16658

McClelland M, Sanderson KE, Spieth J, Clifton SW, Latreille P, Courtney L, Porwollik S, Ali J, Dante M, Du F, Hou S, Layman D, Leonard S, Nguyen C, Scott K, Holmes A, Grewal N, Mulvaney E, Ryan E, Sun H, Florea L, Miller W, Stoneking T, Nhan M, Waterston R, Wilson RK (2001) Complete genome sequence of Salmonella enterica serovar Typhimurium LT2. *Nature* **413:** 852-856

McClendon AK, Rodriguez AC, Osheroff N (2005) Human topoisomerase II alpha rapidly relaxes positively supercoiled DNA: implications for enzyme action ahead of replication forks. *J Biol Chem* **280:** 39337-39345

Mcnamara S, Wang H, Hanna N, Miller W (2008) Topoisomerase IIb Negatively Modulates Retinoic Acid Receptor a Function: a Novel Mechanism of Retinoic Acid Resistance. *Mol Cell Biol* **28:** 2066-2077

Melby TE, Ciampaglio CN, Briscoe G, Erickson HP (1998) The symmetrical structure of structural maintenance of chromosomes (SMC) and MukB proteins: long, antiparallel coiled coils, folded at a flexible hinge. *J Cell Biol* **142:** 1595-1604

Menzel R & Gellert M (1983) Regulation of the genes for E. coli DNA gyrase: homeostatic control of DNA supercoiling. *Cell* **34:** 105–113

Merino A, Madden KR, Lane WS, Champoux JJ, Reinberg D (1993) DNA topoisomerase I is involved in both repression and activation of transcription. *Nature* **365:** 227-232

Mizuuchi K, Fisher LM, O'Dea MH, Gellert M (1980) DNA gyrase action involves the introduction of transient double-strand breaks into DNA. *Proc Natl Acad Sci USA* **77:** 1847-1851

Mondal N, Zhang Y, Jonsson Z, Dhar SK, Kannapiran M, Parvin JD (2003) Elongation by RNA polymerase II on chromatin templates requires topoisomerase activity. *Nucleic Acids Res* **31:** 5016-5024

Morrison A, Higgins NP & Cozzarelli NR (1980) Interaction between DNA gyrase and its cleavage site on DNA. *J Biol Chem* **255:** 2211–2219

Mouchel N, Jenkins J (2006) The identification of a functional interaction between PKC and topoisomerase II. *FEBS letters*

Mueller-Planitz F, Herschlag D (2007) DNA topoisomerase II selects DNA cleavage sites based on reactivity rather than binding affinity. *Nucleic Acids Res* **35:** 3764-3773

Naughton C, Avlonitis N, Corless S, Prendergast JG, Mati IK, Eijk PP, Cockroft SL, Bradley M, Ylstra B & Gilbert N (2013) Transcription forms and remodels supercoiling domains unfolding large-scale chromatin structures. *Nat Struct Mol Biol* **20:** 387–395

Neale MJ, Pan J, Keeney S (2005) Endonucleolytic processing of covalent protein-linked double-strand breaks. *Nature* **436:** 1053-1057

Neuman KC, Charvin G, Bensimon D, Croquette V (2009) Mechanisms of chiral discrimination by topoisomerase IV. *Proc Natl Acad Sci USA* **106:** 6986-6991

Nichols MD, DeAngelis K, Keck JL, Berger JM (1999) Structure and function of an archaeal topoisomerase VI subunit with homology to the meiotic recombination factor Spo11. *EMBO J* **18:** 6177-6188

Nielsen HJ, Li Y, Youngren B, Hansen FG, Austin S (2006) Progressive segregation of the Escherichia coli chromosome. *Mol Microbiol* **61:** 383-393

Niimi A, Suka N, Harata M, Kikuchi A, Mizuno S (2001) Co-localization of chicken DNA topoisomerase IIa, but not ß, with sites of DNA replication and possible involvement of a C-terminal region of a through its binding to PCNA. *Chromosoma* **110:** 102-114

Niki H, Jaffé A, Imamura R, Ogura T, Hiraga S (1991) The new gene mukB codes for a 177 kd protein with coiled-coil domains involved in chromosome partitioning of E. coli. *EMBO J* **10:** 183-193

Nitiss JL (2009a) Targeting DNA topoisomerase II in cancer chemotherapy. *Nat Rev Cancer* **9:** 338–350

Nitiss JL (2009b) DNA topoisomerase II and its growing repertoire of biological functions. *Nat Rev Cancer* **9:** 327–337

Nitiss KC, Malik M, He X, White SW, Nitiss JL (2006) Tyrosyl-DNA phosphodiesterase (Tdp1) participates in the repair of Top2-mediated DNA damage. *Proc Natl Acad Sci USA* **103:** 8953-8958

Nichols RJ, Sen S, Choo YJ, Beltrao P, Zietek M, Chaba R, Lee S, Kazmierczak KM, Lee KJ, Wong A, Shales M, Lovett S, Winkler ME, Krogan NJ, Typas A & Gross CA (2011) Phenotypic Landscape of a Bacterial Cell. *Cell* **144:** 143–156

Niu H, Chung WH, Zhu Z, Kwon Y, Zhao W, Chi P, Prakash R, Seong C, Liu D, Lu L, Ira G, Sung P (2010) Mechanism of the ATP-dependent DNA end-resection machinery from Saccharomyces cerevisiae. *Nature* **467:** 108-111

Nurse P, Levine C, Hassing H, Marians KJ (2003) Topoisomerase III can serve as the cellular decatenase in Escherichia coli. *J Biol Chem* **278:** 8653-8660

Nurse P, S B, Mossessova E, Marians KJ (2000) Mutational Analysis of Escherichia coli Topoisomerase IV. II. ATPase NEGATIVE MUTANTS OF ParE INDUCE HYPER-DNA CLEAVAGE. *J Biol Chem* **275:** 4104-4111

Otwinowski Z, Minor W (1997) Processing of X-ray Diffraction Data Collected in Oscillation Mode In *Methods in Enzymology*, Carter CW SR (ed), Vol. 276, Macromolecular Crystallography, part A, pp 307-326. New York: Acadmeic Press

Painter J, Merritt E (2006) TLSMD web server for the generation of multi-group TLS models. *J Appl Cryst* **39:** 109-111

Papillon J, Menetret JF, Batisse C, Helye R, Schultz P, Potier N, Lamour V (2013) Structural insight into negative DNA supercoiling by DNA gyrase, a bacterial type 2A DNA topoisomerase. *Nucleic Acids Res* **41:** 7815-7827

Patel A, Yakovleva L, Shuman S, Mondragón A (2010) Crystal structure of a bacterial topoisomerase IB in complex with DNA reveals a secondary DNA binding site. *Structure* **18:** 725-733

Peciña A, Smith KN, Mézard C, Murakami H, Ohta K, Nicolas A (2002) Targeted stimulation of meiotic recombination. *Cell* **111:** 173-184

Pedersen JM, Fredsoe J, Roedgaard M, Andreasen L, Mundbjerg K, Kruhøffer M, Brinch M, Schierup MH, Bjergbaek L & Andersen AH (2012) DNA Topoisomerases maintain promoters in a state competent for transcriptional activation in Saccharomyces cerevisiae. *PLoS Genetics* **8:** e1003128

Peng H, Marians KJ (1993a) Decatenation activity of topoisomerase IV during oriC and pBR322 DNA replication in vitro. *Proc Natl Acad Sci USA* **90:** 8571-8575

Peng H, Marians KJ (1993b) Decatenation activity of topoisomerase IV during oriC and pBR322 DNA replication in vitro. *Proc Natl Acad Sci USA* **90:** 8571-8575

Peng H, Marians KJ (1993c) Escherichia coli topoisomerase IV. Purification, characterization, subunit structure, and subunit interactions. *J Biol Chem* **268:** 24481-24490

Peng H, Marians KJ (1995) The interaction of Escherichia coli topoisomerase IV with DNA. *J Biol Chem* **270:** 25286-25290

Perez-Cheeks BA, Lee C, Hayama R, Marians KJ (2012) A role for topoisomerase III in Escherichia coli chromosome segregation. *Mol Microbiol*

Perugino G, Valenti A, D'Amaro A, Rossi M, Ciaramella M (2009) Reverse gyrase and genome stability in hyperthermophilic organisms. *Biochem Soc Trans* **37:** 69-73

Peter BJ, Arsuaga J, Breier AM, Khodursky AB, Brown PO & Cozzarelli NR (2004) Genomic transcriptional response to loss of chromosomal supercoiling in Escherichia coli. *Genome Biol.* **5:** R87

Peter BJ, Ullsperger C, Hiasa H, Marians KJ, Cozzarelli NR (1998) The structure of supercoiled intermediates in DNA replication. *Cell* **94:** 819-827

Petoukhov MV, Konarev PV, Kikhney AG & Svergun DI (2007) ATSAS 2.1 - towards automated and web-supported small-angle scattering data analysis. *J Appl Crystallogr* **40:** s223–s228

Petrushenko ZM, Cui Y, She W, Rybenkov VV (2010) Mechanics of DNA bridging by bacterial condensin MukBEF in vitro and in singulo. *EMBO J* **29:** 1126-1135

Petrushenko ZM, Lai CH, Rai R, Rybenkov VV (2006a) DNA reshaping by MukB. Right-handed knotting, left-handed supercoiling. *J Biol Chem* **281:** 4606-4615

Petrushenko ZM, Lai CH, Rybenkov VV (2006b) Antagonistic interactions of kleisins and DNA with bacterial Condensin MukB. *J Biol Chem* **281:** 34208-34217

Pettersen EF, Goddard TD, Huang CC, Couch GS, Greenblatt DM, Meng EC & Ferrin TE (2004) UCSF Chimera--a visualization system for exploratory research and analysis. *J Comput Chem* **25:** 1605–1612

Piton J, Petrella S, Delarue M, André-Leroux G, Jarlier V, Aubry A & Mayer C (2010) Structural Insights into the Quinolone Resistance Mechanism of

Mycobacterium tuberculosis DNA Gyrase. *PLoS ONE* **5:** e12245

Plank JL, Wu J, Hsieh TS (2006) Topoisomerase IIIalpha and Bloom's helicase can resolve a mobile double Holliday junction substrate through convergent branch migration. *Proc Natl Acad Sci USA* **103:** 11118-11123

Plo I, Hernandez H, Kohlhagen G, Lautier D, Pommier Y, Laurent G (2002) Overexpression of the Atypical Protein Kinase C zeta Reduces Topoisomerase II Catalytic Activity, Cleavable Complexes Formation, and Drug-induced Cytotoxicity in Monocytic U937 Leukemia Cells. *J Biol Chem* **277:** 31407-31415

Pommier Y (2013) Drugging Topoisomerases: Lessons and Challenges. *ACS Chem. Biol.* **8:** 82–95

Pommier Y, Leo E, Zhang H & Marchand C (2010) DNA topoisomerases and their poisoning by anticancer and antibacterial drugs. *Chem. Biol.* **17:** 421–433

Postow L, Crisona NJ, Peter BJ, Hardy CD, Cozzarelli NR (2001a) Topological challenges to DNA replication: conformations at the fork. *Proc Natl Acad Sci USA* **98:** 8219-8226

Postow L, Hardy CD, Arsuaga J, Cozzarelli NR (2004) Topological domain structure of the Escherichia coli chromosome. *Gene Dev* **18:** 1766-1779

Postow L, Ullsperger C, Keller RW, Bustamante C, Vologodskii AV, Cozzarelli NR (2001b) Positive torsional strain causes the formation of a four-way junction at replication forks. *J Biol Chem* **276:** 2790-2796

Pouliot JJ, Yao KC, Robertson CA, Nash HA (1999) Yeast gene for a Tyr-DNA phosphodiesterase that repairs topoisomerase I complexes. *Science* **286:** 552-555

Pruss GJ, Manes SH & Drlica K (1982) Escherichia coli DNA topoisomerase I mutants: increased supercoiling is corrected by mutations near gyrase genes. *Cell* **31:** 35–42

PyMol The PyMOL Molecular Graphics System, Version 1.5.0.4 Schrödinger, LLC.

Ramamoorthy M, Tadokoro T, Rybanska I, Ghosh AK, Wersto R, May A, Kulikowicz T, Sykora P, Croteau DL, Bohr VA (2011) RECQL5 cooperates with Topoisomerase II alpha in DNA decatenation and cell cycle progression. *Nucleic Acids Res*

Ramelot TA, Cort JR, Yee AA, Semesi A, Edwards AM, Arrowsmith CH &

Kennedy MA (2002) NMR structure of theEscherichia coli protein YacG: A novel sequence motif in the zinc-finger family of proteins. *Proteins* **49:** 289–293

Rampakakis E, Zannis-Hadjopoulos M (2009) Transient dsDNA breaks during pre-replication complex assembly. *Nucleic Acids Res* **37:** 5714

Ray S, Panova T, Miller G, Volkov A, Porter AC, Russell J, Panov KI, Zomerdijk JC (2013) Topoisomerase IIalpha promotes activation of RNA polymerase I transcription by facilitating pre-initiation complex formation. *Nat Commun* **4:** 1598

Redinbo MR, Stewart L, Kuhn P, Champoux JJ, Hol WG (1998) Crystal structures of human topoisomerase I in covalent and noncovalent complexes with DNA. *Science* **279:** 1504-1513

Reece RJ, Maxwell A (1991) The C-terminal domain of the Escherichia coli DNA gyrase A subunit is a DNA-binding protein. *Nucleic Acids Res* **19:** 1399-1405

Reyes-Lamothe R, Possoz C, Danilova O, Sherratt DJ (2008) Independent positioning and action of Escherichia coli replisomes in live cells. *Cell* **133:** 90-102

Roca J, Wang JC (1992) The capture of a DNA double helix by an ATP-dependent protein clamp: a key step in DNA transport by type II DNA topoisomerases. *Cell* **71:** 833-840

Roca J, Wang JC (1994) DNA transport by a type II DNA topoisomerase: evidence in favor of a two-gate mechanism. *Cell* **77:** 609-616

Roca J, Wang JC (1996) The probabilities of supercoil removal and decatenation by yeast DNA topoisomerase II. *Genes Cells* **1:** 17-27

Rodriguez AC (2002) Studies of a positive supercoiling machine. Nucleotide hydrolysis and a multifunctional "latch" in the mechanism of reverse gyrase. *J Biol Chem* **277:** 29865-29873

Rosa ID, Goffart S, Wurm M, Wiek C, Essmann F, Sobek S, Schroeder P, Zhang H, Krutmann J, Hanenberg H, Schulze-Osthoff K, Mielke C, Pommier Y, Boege F, Christensen MO (2009) Adaptation of topoisomerase I paralogs to nuclear and mitochondrial DNA. *Nucleic Acids Res* **37:** 6414-6428

Rossi F, Labourier E, Forné T, Divita G, Derancourt J, Riou JF, Antoine E, Cathala G, Brunel C, Tazi J (1996) Specific phosphorylation of SR proteins by mammalian DNA topoisomerase I. *Nature* **381:** 80-82

Rovinskiy N, Agbleke AA, Chesnokova O, Pang Z & Higgins NP (2012) Rates of

gyrase supercoiling and transcription elongation control supercoil density in a bacterial chromosome. *PLoS Genetics* **8:** e1002845

Russell B, Bhattacharyya S, Keirsey J, Sandy A, Grierson P, Perchiniak E, Kavecansky J, Acharya S, Groden J (2011) Chromosome breakage is regulated by the interaction of the BLM helicase and topoisomerase IIalpha. *Cancer Res* **71:** 561-571

Ruthenburg AJ, Graybosch DM, Huetsch JC, Verdine GL (2005) A superhelical spiral in the Escherichia coli DNA gyrase A C-terminal domain imparts unidirectional supercoiling bias. *J Biol Chem* **280:** 26177-26184

Ryu H, Furuta M, Kirkpatrick D, Gygi SP, Azuma Y (2010) PIASy-dependent SUMOylation regulates DNA topoisomerase II alpha activity. *J Cell Biol* **191:** 783-794

Sambrook J, Russell DW (2001) *Molecular Cloning: A Laboratory Manual* Third edn. Cold Spring Harbor, New York CSHL Press.

Sawitzke JA, Thomason LC, Costantino N, Bubunenko M, Datta S & Court DL (2007) Recombineering: in vivo genetic engineering in E. coli, S. enterica, and beyond. *Methods in Enzymology* **421:** 171–199

Sayer J, Jerina D, Shuman S (2004) Individual nucleotide bases, not base pairs, are critical for triggering site-specific DNA cleavage by vaccinia topoisomerase. *J Biol Chem*

Schmidt B, Burgin A, Deweese J, Osheroff N, Berger J (2010) A novel and unified two-metal mechanism for DNA cleavage by type II and IA topoisomerases. *Nature* **465:** 641-644

Schmidt BH, Osheroff N, Berger JM (2012) Structure of a topoisomerase II-DNA-nucleotide complex reveals a new control mechanism for ATPase activity. *Nat Struct Mol Biol* **19:** 1147-1154

Schneider R, Travers A, Kutateladze T & Muskhelishvili G (1999) A DNA architectural protein couples cellular physiology and DNA topology in Escherichia coli. *Mol Microbiol* **34:** 953–964

Schoeffler AJ, Berger JM (2008) DNA topoisomerases: harnessing and constraining energy to govern chromosome topology. *Q Rev Biophys* **41:** 41-101

Schoeffler AJ, May AP & Berger JM (2010) A domain insertion in Escherichia coli GyrB adopts a novel fold that plays a critical role in gyrase function. *Nucleic Acids Res* **38:** 7830–7844

Sengupta S, Nagaraja V (2008a) Inhibition of DNA gyrase activity by Mycobacterium smegmatis MurI. *FEMS Microbiol Lett* **279:** 40-47

Sengupta S, Nagaraja V (2008b) YacG from Escherichia coli is a specific endogenous inhibitor of DNA gyrase. *Nucleic Acids Res* **36:** 4310

Sengupta S, Shah M, Nagaraja V (2006) Glutamate racemase from Mycobacterium tuberculosis inhibits DNA gyrase by affecting its DNA-binding. *Nucleic Acids Res* **34:** 5567-5576

Shapiro P, Whalen A, Tolwinski N, Wilsbacher J, Froelich-Ammon S, Garcia M, Osheroff N, Ahn N (1999a) Extracellular Signal-Regulated Kinase Activates Topoisomerase IIα through a Mechanism Independent of Phosphorylation. *Mol Cell Biol* **19:** 3551-3560

Shapiro TA, Klein VA, Englund PT (1999b) Isolation of kinetoplast DNA. *Methods Mol Biol* **94:** 61-67

She W, Wang Q, Mordukhova EA, Rybenkov VV (2007) MukEF Is required for stable association of MukB with the chromosome. *J Bacteriol* **189:** 7062-7068

Singh TR, Ali AM, Busygina V, Raynard S, Fan Q, Du C, Andreassen PR, Sung P, Meetei AR (2008) BLAP18/RMI2, a novel OB-fold-containing protein, is an essential component of the Bloom helicase–double Holliday junction dissolvasome. *Genes Dev* **22:** 2856-2868

Slesarev AI, Stetter KO, Lake JA, Gellert M, Krah R, Kozyavkin SA (1993) DNA topoisomerase V is a relative of eukaryotic topoisomerase I from a hyperthermophilic prokaryote. *Nature* **364:** 735-737

Smith AB, Maxwell A (2006) A strand-passage conformation of DNA gyrase is required to allow the bacterial toxin, CcdB, to access its binding site. *Nucleic Acids Res* **34:** 4667-4676

Sogo JM, Stasiak A, Martínez-Robles ML, Krimer DB, Hernández P, Schvartzman JB (1999) Formation of knots in partially replicated DNA molecules. *J Mol Biol* **286:** 637-643

Sonnenschein N, Geertz M, Muskhelishvili G & Hütt M-T (2011) Analog regulation of metabolic demand. *BMC Syst Biol* **5:** 40

Sordet O, Larochelle S, Nicolas E, Stevens EV, Zhang C, Shokat KM, Fisher RP, Pommier Y (2008) Hyperphosphorylation of RNA Polymerase II in Response to Topoisomerase I Cleavage Complexes and Its Association with Transcription- and BRCA1-dependent Degradation of Topoisomerase I. *J Mol Biol* **381:** 540-549

Staker BL, Hjerrild K, Feese MD, Behnke CA, Burgin AB, Jr., Stewart L (2002) The mechanism of topoisomerase I poisoning by a camptothecin analog. *Proc Natl Acad Sci USA* **99:** 15387-15392

Sternglanz R, DiNardo S, Voelkel K, Nishimura Y, Hirota Y, Becherer K, Zumstein L & Wang J (1981) Mutations in the gene coding for Escherichia coli DNA topoisomerase I affect transcription and transposition. *Proc Natl Acad Sci USA* **78:** 2747

Stewart AF, Herrera RE & Nordheim A (1990) Rapid induction of c-fos transcription reveals quantitative linkage of RNA polymerase II and DNA topoisomerase I enzyme activities. *Cell* **60:** 141–149

Stewart L, Redinbo MR, Qiu X, Hol WG, Champoux JJ (1998) A model for the mechanism of human topoisomerase I. *Science* **279:** 1534-1541

Stone MD, Bryant Z, Crisona NJ, Smith SB, Vologodskii A, Bustamante C, Cozzarelli NR (2003) Chirality sensing by Escherichia coli topoisomerase IV and the mechanism of type II topoisomerases. *Proc Natl Acad Sci USA* **100:** 8654-8659

Strong M, Sawaya MR, Wang S, Phillips M, Cascio D & Eisenberg D (2006) Toward the structural genomics of complexes: crystal structure of a PE/PPE protein complex from Mycobacterium tuberculosis. *Proc Natl Acad Sci USA* **103:** 8060–8065

Stros M, Bacíková A, Polanská E, Stokrová J, Strauss F (2007) HMGB1 interacts with human topoisomerase IIalpha and stimulates its catalytic activity. *Nucleic Acids Res* **35:** 5001-5013

Sugimoto-Shirasu K, Roberts G, Stacey N, McCann M, Maxwell A, Roberts K (2005) RHL1 is an essential component of the plant DNA topoisomerase VI complex and is required for ploidy-dependent cell growth. *Proc Natl Acad Sci USA* **102:** 18736-18741

Sugimoto-Shirasu K, Stacey NJ, Corsar J, Roberts K, McCann MC (2002) DNA Topoisomerase VI Is Essential for Endoreduplication in Arabidopsis. *Curr Biol* **12:** 1782-1786

Sugisaki H, Ray DS (1987) DNA sequence of Crithidia fasciculata kinetoplast minicircles. *Mol Biochem Parasitol* **23:** 253-263

Sunako Y, Onogi T, Hiraga S (2001) Sister chromosome cohesion of Escherichia coli. *Mol Microbiol* **42:** 1233-1241

Suski C, Marians KJ (2008) Resolution of converging replication forks by RecQ and topoisomerase III. *Mol Cell* **30:** 779-789

Swillens S (1995) Interpretation of binding curves obtained with high receptor concentrations: practical aid for computer analysis. *Mol Pharmacol* **47:** 1197-1203

Tadesse S, Mascarenhas J, Koesters B, Hasilik A, Graumann PL (2005) Genetic interaction of the SMC complex with topoisomerase IV in Bacillus subtilis. *Microbiology* **151:** 1-9

Takahashi T, Burguiere-Slezak G, Van der Kemp PA, Boiteux S (2011) Topoisomerase 1 provokes the formation of short deletions in repeated sequences upon high transcription in Saccharomyces cerevisiae. *Proc Natl Acad Sci USA* **108:** 692-697

Takahashi Y (2005) SIZ1/SIZ2 Control of Chromosome Transmission Fidelity Is Mediated by the Sumoylation of Topoisomerase II. *Genetics* **172:** 783-794

Taneja B, Patel A, Slesarev A, Mondragon A (2006) Structure of the N-terminal fragment of topoisomerase V reveals a new family of topoisomerases. *EMBO J* **25:** 398-408

Taneja B, Schnurr B, Slesarev A, Marko JF, Mondragón A (2007) Topoisomerase V relaxes supercoiled DNA by a constrained swiveling mechanism. *Proc Natl Acad Sci USA* **104:** 14670-14675

Taniguchi Y, Choi PJ, Li GW, Chen H, Babu M, Hearn J, Emili A, Xie XS (2010) Quantifying E. coli Proteome and Transcriptome with Single-Molecule Sensitivity in Single Cells. *Science* **329:** 533-538

Tapia-Alveal C, Outwin EA, Trempolec N, Dziadkowiec D, Murray JM & O'Connell MJ (2010) SMC complexes and topoisomerase II work together so that sister chromatids can work apart. *Cell Cycle* **9:** 2065–2070

Terwilliger TC, Adams PD, Read RJ, McCoy AJ, Moriarty NW, Grosse-Kunstleve RW, Afonine PV, Zwart PH, Hung LW (2009) Decision-making in structure solution using Bayesian estimates of map quality: the PHENIX AutoSol wizard. *Acta Crystallogr D Biol Crystallogr* **65:** 582-601

Tran J, Jacoby G, Hooper D (2005) Interaction of the plasmid-encoded quinolone resistance protein Qnr with Escherichia coli DNA gyrase. *Antimicrob Agents Chemother* **49:** 118-125

Treszezamsky AD, Kachnic LA, Feng Z, Zhang J, Tokadjian C, Powell SN (2007) BRCA1- and BRCA2-Deficient Cells Are Sensitive to Etoposide-Induced DNA Double-Strand Breaks via Topoisomerase II. *Cancer Res* **67:** 7078-7081

Tretter EM, Berger JM (2012) Mechanisms for Defining Supercoiling Set Point of DNA Gyrase Orthologs: I. A NONCONSERVED ACIDIC C-TERMINAL TAIL MODULATES ESCHERICHIA COLI GYRASE ACTIVITY. *J Biol Chem* **287:** 18636-18644

Tretter EM, Lerman JC, Berger JM (2010) A naturally chimeric type IIA topoisomerase in Aquifex aeolicus highlights an evolutionary path for the emergence of functional paralogs. *Proc Natl Acad Sci USA* **107:** 22055-22059

Tsai FT, Singh OM, Skarzynski T, Wonacott AJ, Weston S, Tucker A, Pauptit RA, Breeze AL, Poyser JP, O'Brien R, Ladbury JE, Wigley DB (1997) The high-resolution crystal structure of a 24-kDa gyrase B fragment from E. coli complexed with one of the most potent coumarin inhibitors, clorobiocin. *Proteins* **28:** 41-52

Tsai SC, Valkov N, Yang WM, Gump J, Sullivan D, Seto E (2000) Histone deacetylase interacts directly with DNA topoisomerase II. *Nat Genet* **26:** 349-353

Tse-Dinh Y-C & Beran RK (1988) Multiple promoters for transcription of the Escherichia coli DNA topoisomerase I gene and their regulation by DNA supercoiling. *J Mol Biol* **202:** 735–742

Tse YC, Kirkegaard K, Wang JC (1980) Covalent bonds between protein and DNA. Formation of phosphotyrosine linkage between certain DNA topoisomerases and DNA. *J Biol Chem* **255:** 5560-5565

Tuduri S, Crabbe L, Conti C, Tourriere H, Holtgreve-Grez H, Jauch A, Pantesco V, De Vos J, Thomas A, Theillet C, Pommier Y, Tazi J, Coquelle A, Pasero P (2009) Topoisomerase I suppresses genomic instability by preventing interference between replication and transcription. *Nat Cell Biol* **11:** 1315-1324

Uemura T, Ohkura H, Adachi Y, Morino K, Shiozaki K, Yanagida M (1987) DNA topoisomerase II is required for condensation and separation of mitotic chromosomes in S. pombe. *Cell* **50:** 917-925

Uemura T, Tanagida M (1986) Mitotic spindle pulls but fails to separate chromosomes in type II DNA topoisomerase mutants: uncoordinated mitosis. *EMBO J* **5:** 1003-1010

Uemura T, Yanagida M (1984) Isolation of type I and II DNA topoisomerase mutants from fission yeast: single and double mutants show different phenotypes in cell growth and chromatin organization. *EMBO J* **3:** 1737-1744

Uhlmann F, Nasmyth K (1998) Cohesion between sister chromatids must be established during DNA replication. *Curr Biol* **8:** 1095-1101

Ullsperger C, Cozzarelli NR (1996) Contrasting enzymatic activities of topoisomerase IV and DNA gyrase from Escherichia coli. *J Biol Chem* **271:** 31549-31555

Valjavec-Gratian M, Henderson TA, Hill TM (2005) Tus-mediated arrest of DNA replication in Escherichia coli is modulated by DNA supercoiling. *Mol Microbiol* **58:** 758-773

van Workum M, van Dooren SJ, Oldenburg N, Molenaar D, Jensen PR, Snoep JL & Westerhoff HV (1996) DNA supercoiling depends on the phosphorylation potential in Escherichia coli. *Mol Microbiol* **20:** 351–360

Varga-Weisz PD, Wilm M, Bonte E, Dumas K, Mann M, Becker PB (1997) Chromatin-remodelling factor CHRAC contains the ATPases ISWI and topoisomerase II. *Nature* **388:** 598-602

Viollier PH, Thanbichler M, McGrath PT, West L, Meewan M, McAdams HH, Shapiro L (2004) Rapid and sequential movement of individual chromosomal loci to specific subcellular locations during bacterial DNA replication. *Proc Natl Acad Sci USA* **101:** 9257-9262

Vizán J, Hernández-Chico C, del Castillo I, Moreno F (1991) The peptide antibiotic microcin B17 induces double-strand cleavage of DNA mediated by E. coli DNA gyrase. *EMBO J* **10:** 467-476

Volkov VV & Svergun DI (2003) Uniqueness of ab initio shape determination in small-angle scattering. *J Appl Crystallogr* **36:** 860–864

Vologodskii AV, Zhang W, Rybenkov VV, Podtelezhnikov AA, Subramanian D, Griffith JD, Cozzarelli NR (2001) Mechanism of topology simplification by type II DNA topoisomerases. *Proc Natl Acad Sci USA* **98:** 3045

Vos SM, Lee I, Berger JM (2013) Distinct Regions of the *Escherchia coli* Par C C-terminal Domain are Required for Substrate Discrimination by Topoisomerase IV. *J Mol Biol* **425:** 3029-3045

Vos SM, Tretter EM, Schmidt BH & Berger JM (2011) All tangled up: how cells direct, manage and exploit topoisomerase function. *Nat Rev Mol Cell Biol* **12:** 827–841

Wallis JW, Chrebet G, Brodsky G, Rolfe M, Rothstein R (1989) A hyper-recombination mutation in S. cerevisiae identifies a novel eukaryotic topoisomerase. *Cell* **58:** 409-419

Wang JC (1971) Interaction between DNA and an Escherichia coli protein omega. *J Mol Biol* **55:** 523-533

Wang M, Weiss M, Simonovic M, Haertinger G, Schrimpf SP, Hengartner MO, von Mering C (2012) PaxDb, a database of protein abundance averages across all three domains of life. *Mol Cell Proteomics* **11:** 492-500

Wang Q, Mordukhova EA, Edwards AL, Rybenkov VV (2006a) Chromosome condensation in the absence of the non-SMC subunits of MukBEF. *J Bacteriol* **188:** 4431-4441

Wang S, West L, Shapiro L (2006b) The Bifunctional FtsK Protein Mediates Chromosome Partitioning and Cell Division in Caulobacter. *J Bacteriol* **188:** 1497

Wang SC, Shapiro L (2004) The topoisomerase IV ParC subunit colocalizes with the Caulobacter replisome and is required for polar localization of replication origins. *Proc Natl Acad Sci USA* **101:** 9251-9256

Wang X, Lesterlin C, Reyes-Lamothe R, Ball G, Sherratt DJ (2011) Replication and segregation of an Escherichia coli chromosome with two replication origins. *Proc Natl Acad Sci USA* **108:** E243-250

Wang X, Liu X, Possoz C, Sherratt DJ (2006c) The two Escherichia coli chromosome arms locate to separate cell halves. *Genes Dev* **20:** 1727-1731

Wang X, Reyes-Lamothe R, Sherratt DJ (2008) Modulation of Escherichia coli sister chromosome cohesion by topoisomerase IV. *Genes Dev* **22:** 2426-2433

Wang Y, Knudsen BR, Bjergbaek L, Westergaard O, Andersen AH (1999) Stimulated activity of human topoisomerases IIalpha and IIbeta on RNA-containing substrates. *J Biol Chem* **274:** 22839-22846

Wang ZX (1995) An exact mathematical expression for describing competitive binding of two different ligands to a protein molecule. *FEBS Lett* **360:** 111–114

Ward D, Newton A (1997) Requirement of topoisomerase IV parC and parE genes for cell cycle progression and developmental regulation in Caulobacter crescentus. *Mol Microbiol* **26:** 897-910

Waterhouse, A., Procter, J., Martin, D., Clamp, M. & Barton, G (2009) Jalview Version 2--a multiple sequence alignment editor and analysis workbench.

Bioinformatics **25**, 1189-1191

Watt PM, Louis EJ, Borts RH, Hickson ID (1995) Sgs1: A eukaryotic homolog of E. coil RecQ that interacts with topoisomerase II in vivo and is required for faithful chromosome segregation. *Cell* **81:** 253-260

Weinert TA, Kiser GL, Hartwell LH (1994) Mitotic checkpoint genes in budding yeast and the dependence of mitosis on DNA replication and repair. *Genes Dev* **8:** 652-665

Wells NJ, Addison CM, Fry AM, Ganapathi R, Hickson ID (1994) Serine 1524 is a major site of phosphorylation on human topoisomerase II alpha protein in vivo and is a substrate for casein kinase II in vitro. *J Biol Chem* **269:** 29746-29751

Wendorff TJ, Schmidt BH, Heslop P, Austin CA, Berger JM (2012) The Structure of DNA-Bound Human Topoisomerase II Alpha: Conformational Mechanisms for Coordinating Inter-Subunit Interactions with DNA Cleavage. *J Mol Biol* **424:** 109-124

Westerhoff HV, O'Dea MH, Maxwell A & Gellert M (1988) DNA supercoiling by DNA gyrase. A static head analysis. *Cell Biophys* **12:** 157–181

Wigley DB, Davies GJ, Dodson EJ, Maxwell A & Dodson G (1991) Crystal structure of an N-terminal fragment of the DNA gyrase B protein. *Nature* **351:** 624–629

Woese CR, Kandler O & Wheelis ML (1990) Towards a natural system of organisms: proposal for the domains Archaea, Bacteria, and Eucarya. *Proc Natl Acad Sci USA* **87:** 4576–4579

Wohlkonig A, Chan PF, Fosberry AP, Homes P, Huang J, Kranz M, Leydon VR, Miles TJ, Pearson ND, Perera RL, Shillings AJ, Gwynn MN, Bax BD (2010) Structural basis of quinolone inhibition of type IIA topoisomerases and target-mediated resistance. *Nat Struct Mol Biol* **17:** 1152-1153

Woo JS, Lim JH, Shin HC, Suh MK, Ku B, Lee KH, Joo K, Robinson H, Lee J, Park SY, Ha NC, Oh BH (2009) Structural studies of a bacterial condensin complex reveal ATP-dependent disruption of intersubunit interactions. *Cell* **136:** 85-96

Wu CC, Li TK, Farh L, Lin LY, Lin TS, Yu YJ, Yen TJ, Chiang CW, Chan NL (2011) Structural basis of type II topoisomerase inhibition by the anticancer drug etoposide. *Science* **333:** 459-462

Wu HY, Shyy SH, Wang JC, Liu LF (1988) Transcription generates positively and negatively supercoiled domains in the template. *Cell* **53:** 433-440

Wu L, Hickson ID (2003) The Bloom's syndrome helicase suppresses crossing over during homologous recombination. *Nature* **426:** 870-874

Xiao H, Mao Y, Desai SD, Zhou N, Ting C-Y, Hwang J, Liu LF (2003) The topoisomerase IIbeta circular clamp arrests transcription and signals a 26S proteasome pathway. *Proc Natl Acad Sci USA* **100:** 3239-3244

Xu D, Guo R, Sobeck A, Bachrati CZ, Yang J, Enomoto T, Brown GW, Hoatlin ME, Hickson ID, Wang W (2008) RMI, a new OB-fold complex essential for Bloom syndrome protein to maintain genome stability. *Genes Dev* **22:** 2843

Xu D, Shen W, Guo R, Xue Y, Peng W, Sima J, Yang J, Sharov A, Srikantan S, Yang J, Fox D, 3rd, Qian Y, Martindale JL, Piao Y, Machamer J, Joshi SR, Mohanty S, Shaw AC, Lloyd TE, Brown GW, Ko MS, Gorospe M, Zou S, Wang W (2013) Top3beta is an RNA topoisomerase that works with fragile X syndrome protein to promote synapse formation. *Nat Neurosci* **16:** 1238-1247

Yang L, Wold MS, Li JJ, Kelly TJ, Liu LF (1987) Roles of DNA topoisomerases in simian virus 40 DNA replication in vitro. *Proc Natl Acad Sci USA* **84:** 950-954

Yang X, Li W, Prescott ED, Burden SJ, Wang JC (2000) DNA topoisomerase IIbeta and neural development. *Science* **287:** 131-134

Yin Y, Cheong H, Friedrichsen D, Zhao Y, Hu J, Mora-Garcia S, Chory J (2002) A crucial role for the putative Arabidopsis topoisomerase VI in plant growth and development. *Proc Natl Acad Sci USA* **99:** 10191

Yao Z, Davis RM, Kishony R, Kahne D & Ruiz N (2012) Regulation of cell size in response to nutrient availability by fatty acid biosynthesis in Escherichia coli. *Proc Natl Acad Sci USA* **109:** E2561–8

Yoshida H, Bogaki M, Nakamura M, Yamanaka LM & Nakamura S (1991) Quinolone resistance-determining region in the DNA gyrase gyrB gene of Escherichia coli. *Antimicrob Agents Chemother* **35:** 1647–1650

Yuan J, Sterckx Y, Mitchenall LA, Maxwell A, Loris R & Waldor MK (2010) Vibrio cholerae ParE2 poisons DNA gyrase via a mechanism distinct from other gyrase inhibitors. *J Biol Chem* **285:** 40397–40408

Zechiedrich E, Cozzarelli N (1995) Roles of topoisomerase IV and DNA gyrase in DNA unlinking during replication in Escherichia coli. *Genes Dev* **9:** 2859

Zechiedrich EL, Khodursky AB, Bachellier S, Schneider R, Chen D, Lilley DM, Cozzarelli NR (2000) Roles of topoisomerases in maintaining steady-state DNA supercoiling in Escherichia coli. *J Biol Chem* **275:** 8103-8113

Zeng Z, Cortes-Ledesma F, El Khamisy SF, Caldecott KW TDP2/TTRAP is the major 5'-tyrosyl DNA phosphodiesterase activity in vertebrate cells and is critical for cellular resistance to topoisomerase II-induced DNA Damage. *J Biol Chem* **286:** 403-409

Zhang H, Pommier Y (2008) Mitochondrial Topoisomerase I Sites in the Regulatory D-Loop Region of Mitochondrial DNA †. *Biochemistry* **47:** 11196-11203

Appendix 1:Temperature sensitive complementation experiments in the *parC1215* C600 *E. coli* strain using leaky expression

The *parC1215* C600 *E. coli* strain possesses a temperature sensitive mutation in *parC* (Gly725Asp). The strain is poorly behaved and requires special treatment for successful experiments. This protocol describes how to perform complementation assays in this strain by leaky expression from a T7 RNA polymerase promoter.

Materials

parC1215 C600 *E. coli* glycerol stock (in Seychelle's glycerol stocks)
Sterile 1.5mL eppendorf tubes
2M $CaCl_2$
1M HEPES pH 6.7
4M KCl
$MnCl_2$
Autoclaved SOB media
2M $MgCl_2$
3X 2L Baffled flasks
DMSO
LB plates
temperature controlled incubator and shaker (18˚C and 42˚C)
Multi-channel pipettes (200μL and 20μL 8-channel)
Corning Costar 3799 round bottom 96-well plates

Making Competent Cells (protocol adapted from Mary Coons)

1. Day 1: Streak out *parC1215* C600 on an LB plates with no selection. Incubate plates at 30˚C.
2. Day 2: Autoclave 3, 2L baffled flasks with 250mL of SOB media. Store media at room temperature. Inoculate an overnight 5mL SOB culture with one colony. Grow cells at 30˚C.
3. Day 3: Inoculate SOB media prepared on day 2 with 0.25, 0.5, or 1mL of the overnight *parC1215* C600 culture. Grow cells at 18˚C until they reach OD_{600} of 0.6.
    a. Make 1x Inoue Buffer (250mL).
        i. Mix 2.5mL of 1M HEPES pH 6.7, 15.62mL of 4M KCl, and 1.87mL of 2M $CaCl_2$ in 150mL $_{dd}H_2O$. Adjust the pH to 6.7.
        ii. Add 2.72g $MnCl_2$ and bring up to a final volume of 250mL. Filter sterilize (0.22μ filter) and store at 4˚C.
    b. Autoclave 1.5 mL eppendorf tubes, 2, 500mL bottles for the Sorvall GS3 rotor, and 200μL pipette tips. Store at 4˚C.

c. Chill the GS3 rotor in the cold room. Must be chilled for at least 1hr prior to use.

4. Day 4: When cells reach OD_{600} of 0.6, pour into pre-chilled 500mL Sorvall GS3 bottle. Incubate on ice for 10 minutes. Then, spin the cells for 10 minutes at 3000xg (4k rpm for GS3 rotor) at 4˚C.
    a. Pour off supernatant. Place pelleted cells on ice and gently resuspend in 1X Inoue Buffer (perform in cold room if possible).
    b. Incubate suspension on ice for 10 minutes.
    c. Spin the cells for 10 minutes at 3000xg (4k rpm for GS3 rotor) at 4˚C.
    d. Pour off supernatent. Gently resuspend in 10mL 1x Inoue Buffer on ice.
    e. Add 700μL DMSO dropwise to the cells and gently swirl cells. Incubate suspension on ice for 10 minutes.
    f. Aliquot cells in pre-chilled1.5mL eppendorf tubes (100μL per tube) in the cold room. Snap freeze cells in liquid nitrogen and store at -80˚C prior to use.
    g. Perform test transformation (see protocol below) to assess transformation ability and potential contamination. *parC1215* C600 prepared in this manner should remain competent for >3 years.

Transformation

1. Remove one tube of competent cells for each transformation from -80˚C stock and place on ice. Add plasmid (50-100ng) and incubate on ice for 25 minutes.
2. Heat shock cells at 42˚C for 45 seconds. Remove and return to ice for two minutes.
3. Add cells to 1mL of SOB media with no antibiotic selection. Outgrow cells at 30˚C for 2-3 hours.
4. After outgrowth, remove cells from culture tubes and spin at 4K in sterile 1.5mL eppendorf tubes. Remove most of the supernatant and resuspend in 100μL SOB. Plate on appropriate selection LB plates with 2% (w/v) glucose. Grow at 30˚C overnight.
5. Colonies will take ~18 hours to appear and will be very small. Once colonies form, remove plates from 30˚C incubator and store at 4˚C until ready to inoculate overnight cultures.

Experiment

1. Inoculate 5mL of LB +2% (w/v) glucose in culture tubes with 1-2 colonies from transformation plates with appropriate selection. Grow overnights at 30˚C.

2. The following morning, inoculate 25-50mL of desired media (ie 2xYT/M9 Minimal Media, etc) with 1:1000 dilution of cells. Grow with antibiotic selection but not in the presence of glucose.
3. Grow cells at 30˚C until OD_{600} ~ 0.3. At this time, take OD readings for all cultures and record. Transfer cultures that will be grown at the restrictive to a prewarmed shaker at the restrictive temperature (42˚C).
4. Begin taking samples 30 minutes after the temperature shift. This allows the cells to fully adapt to the restrictive temperature. Cells taken at time points earlier than 30 minutes will not show the full penetrance of the *parC1215* severe temperature sensitivity mutation.
5. For plating, remove 100μL of each culture at the restrictive and permissive temperatures. Normalize cultures to the OD_{600} of the culture with the lowest OD_{600} at the time of the temperature shift by diluting each sample with fresh media (100μL final volume). (
    a. ie OD_{600} at time of temperature shift of $parC^{WT}$ = 0.33, $parC^{497\text{-}752}$ =0.25. For plating dilutions, add 75.76μL $parC^{WT}$ cells to 24.24μL media to achieve a similar concentration of the $parC^{497\text{-}752}$ containing cells.
6. Serially dilute cells in 10-20 fold dilutions, with 5-6 total serial dilutions. Perform dilutions in sterile round bottom 96-well plate. (Note: 20-fold dilutions usually work best).
7. Use frogger or multi-channel (5μL) to spot cells on plate with appropriate antibiotic selection and media composition. Allow plates to fully dry before transferring to incubator at the restrictive or permissive temperature.

Appendix 2:Recombineering in *Escherichia coli* using λ Red

(Modified from Datsenko and Wanner 2000 *PNAS* (Datsenko, 2000))

Materials:
Escherichia coli strains:
MG1655 K-12 with pKD46 plasmid or BW25113 with pKD46 plasmid
Obtained from Coli Genetic Stock Center, Yale University
pKD46 markers: *repA101*(ts), *araBp-gam-bet-exo*, *oriR101*, *bla*(Amp^r)
Sterile 70% (v/v) glycerol
20%(w/v) L-arabinose
SOB media
Autoclaved MilliQ water
Autoclaved 1.5 mL Eppendorf tubes
Autoclaved pipette tips
Electroporation cuvettes (BioRad, 0.1cm width)
BioRad Electroporator
LB Agarose plates with appropriate selection
Plasmid with Kan^r $SacB^s$ genes or other double selection marker (in Seychelle's clone archive)
50mL Falcon tubes
Qiagen Dnaeasy Blood and Tissue Kit

E. coli usually degrade exogenous linear DNA products, thus hampering homologous recombination reactions in cells. λ Red recombination overcomes this challenge through the action of 3 phage λ proteins that are encoded on an arabinose inducible plasmid (pKD46): 1. Gam inhibits RecBCD to protect linear DNA from degradation, 2. Exo a 5'->3' exonuclease that protects one DNA strand while chewing the other back 3. Bet which performs the homologous recombination reaction after binding to and protecting the ssDNA region made by Exo (See Sawitizke *et al*., 2007 *Methods in Enzymology* for a review (Sawitzke *et al*, 2007)).

Design and amplify a PCR product to target specific genomic locus
For efficient recombination, PCR products should have 50-100bp homology outside of the target region in the genome. I have had the most success with 70bp homology. Ensure that homology regions are not similar to other regions of the genome. If there is significant similarity, make constructs with a longer region of homology to prevent recombination in an undesired genomic locus. Design sequencing primers that are at least 50-100bps outside of the region that is targeted by the PCR product and verify that these primers do not have significant homology to other regions of the genome. If inserting an antibiotic cassette in the

genome, ensure that it is not Amp^r, since this is the selection used to maintain the λ-red plasmid.

If removing a gene to insert another gene, it is usually beneficial to use a double-selection marker. For example, an antibiotic cassette linked to the *Bacillus subtilis sacB* gene provides a selection and counter-selection marker (SacB prevents *E. coli* from growing on sucrose media). After the recombination reaction, the cells are plated on with antibiotic selection. Potential recombinants will grow on the antibiotic but will fail to grow on media with 10% (w/v) sucrose. This scheme assists in selecting successful recombinants and not those cells that have gained resistance to the antibiotic cassette. It also permits selection of potential recombinants arising from subsequent recombination reactions when the double selection cassette is removed. Successful recombinants will grow on sucrose but not on the antibiotic selection media.

PCR reaction to produce linear product for recombination

PCR Mix (150µL mix split into 3x50 µL reactions)
3µL F primer 100µM
3µL R primer 100µM
15µL Pfu (II) Ultra polymerase buffer
3µL Pfu (II) Ultra polymerase
7µL DMSO
50-100ng DNA template
H_20 to 150 µL

PCR Program
1-95˚C 4 min
2- 94˚C 45”
3- Gradient 55˚C, 57˚C, 60˚C 1 min (3 different tubes at each temp)
4- 72˚C 5 min (can be extended for longer genes)
5- Go back to 2 and repeat 29X.
6- 72˚C 10min
7- 4˚C ∞

Gel extract DNAs of the appropriate length and verify that product is correct by sequencing. Final DNA concentration should be 100-500ng/µL with a total volume of at least 20µL. Store at -20˚C.

Recombination Reaction

1. Day 1: Streak out *E. coli* cells that possess pKD46 plasmid on an LB carbenicillin plate from the glycerol stock. The pKD46 plasmid is

temperature sensitive and cells will loose the plasmid at temperatures over 30˚C. Grow streaked cells at 30˚C overnight.

2. Day 2: Make 250-1000 mL SOB media. Autoclave tubes, pipette tips, and 2L baffled flasks. Store a sterile 100mL bottle of autoclaved MilliQ water at 4˚C.
2. Day 2: Remove the plate streaked with the *E. coli* strain possessing the pKD46 plasmid and store at 4˚C until the evening. In the evening, inoculate 5mLs of SOB with a single colony with ampicillin selection.
3. Day 3: Inoculate 250mLs of SOB in a baffled 2L flask with 2.5 mLs of overnight culture. Grow cells shaking (~220rpm) at 30˚C.
4. When cells reach OD_{600} 0.5-0.6, add 2.5mL 20%(w/v) L-arabinose (0.2% (w/v) final concentration) to the culture. Arabinose induces expression of λ-red proteins, which are highly toxic to the cells if expressed for extended periods of time. Grow cells for 30 minutes after addition of arabinose at 30˚C.
5. Transfer cells to 50mL falcon tubes (You only need 1-2 50mL tubes of cells). Incubate cells on ice for 20 minutes.
6. Spin cells for 7 minutes at 4K in Sorvall Legend Tabletop centrifuge. Carefully remove supernatant.
7. Resuspend cells in 1mL sterile, ice-cold H_2O. Then add additional 30mL of H_2O stepwise (2-5mLs at a time, gently swirling).
8. Spin cells for 7 minutes at 4K in Sorvall Legend Tabletop centrifuge. Carefully remove supernatant.
9. Carefully resuspend cells in 1mL sterile, ice-cold H_2O. Transfer cells to sterile 1.5mL eppendorf tube.
10. Spin cells in tabletop microfuge at 4˚C for 30 seconds. Carefully remove supernatant.
11. Resuspend cells in 1mL H_2O.
12. Aliquot cells in sterile 1.5mL eppendorf tubes (50-100µLs of cells per tube).
13. Add linear PCR product to cells (try several different DNA concentrations ranging from 100ng-1µg). Incubate cells and DNA on ice for 10 minutes. At this time, pre-chill BioRad electroporation cuvettes. As a control, electroporate a plasmid DNA with the same antibiotic resistance as the linear antibiotic cassette into one aliquot of cells (100ng).
14. Transfer cells to BioRad electroporation cuvettes (0.1cm width). Be careful to not introduce air bubbles to the cells.
15. Set electroporator to 25µF, 200Ω, and 1.8KV/cm. Wipe outside of electroporation cuvette with Kimwipe to remove condensation.
16. Place in electroporation cuvette holder, and electroporate. Place electroporated cells on ice.
17. Add 1mL of SOB media directly to cuvette. Gently resuspend cells in cuvette and transfer to a culture tube.

18. Outgrow cells at 30˚C for 3 hours. Remove cells from culture tube, gently spin (4K for 5 minutes), and plate all cells on appropriate selection media (include Amp if you intend on performing additional recombinations with your strain).
19. Day 4: Colonies should appear early the next day. Cells electroporated with plasmid DNA should have many more colonies than those with linear DNAs.
20. Streak 3-10 colonies onto appropriate selective media(s) at 30˚C. Note: if using double selection, streak colonies on antibiotic media and media with secondary selection.
21. Day 5: Inoculate LB or SOB (5mL) liquid media cultures with colonies that grow on appropriate media after streaking. Grow under appropriate selection at 30˚C.

    Note: It is critical to grow the cells at 30˚C if another recombination step is required to obtain the strain of interest. Growing cells at higher temperatures will cause the cells to expel the λ Red plasmid (pKD46).
22. Day 6: Save 500µLs of overnight culture. Add 500µL sterile 70%(v/v) glycerol and flash freeze in a cryo tube. Store at -80˚C. Remove 2mLs of the remaining overnight culture, extract genomic DNA (Qiagen Dnaeasy Blood and Tissue Kit works well for this). Follow kit directions for gram negative bacteria.
23. Perform a PCR with the extracted DNA and primers outside of the locus of interest. Gel extract DNA products of the appropriate size and submit for sequencing.
24. Day 7: If the cassette integrated appropriately into the locus, steps 1-23 can be repeated to perform another round of recombination or the λ Red plasmid can be cured from the strain.

Curing E. coli strains of λ Red Plasmid

1. Streak cells from recombineered glycerol stock on appropriate media. Grow at 37˚C.
2. Select a single colony to inoculate 5mLs of LB or 2xYT media. Grow cells at 37˚C or 42˚C during the day. Plate 50µL on carbenicillin LB plates (200*µ*g/mL). Grow cells on plate at 37˚C. Inoculate another 5mL culture with 5 µLs of the culture that was grown throughout the day. Grow overnight at 37˚C or 42˚C.
3. Repeat step 2 until few (10) or no colonies appear on carbenicillin LB plates. Save glycerol stocks from each saturated culture until the plasmid is lost (usually within 2-days. The MG1655 strain is more resistant to losing the plasmid, so you may have to perform several rounds to cure the strain).

Appendix 3: 2-D Gel Electrophoresis to Determine Plasmid Linking Number and σ

(Protocol adapted from Kevin Jude)

Materials
10x TPE Buffer pH 7.9 at 4˚C, 1L final volume
360mM Tris base 43.6g
300mM NaH_2PO_4 46.8g
10mM EDTA 20mL 0.5M pH 8.0

Chloroquine (10mg/mL stock), dissolved in water, stored in foil at 4˚C
Netropsin
Ethidium bromide
ATP pH 7.5 (200mM)
TE buffer

Generate Topoisomer Ladder
To determine the σ (superhelical density) of a plasmid, the linking number of the substrate must be first determined. Two different ways of obtaining the linking number are presented below.

Nick-Ligate-Ethidium Bromide Technique
This technique only works for plasmids that possess a nicking site for an enzyme such as Nb.BbvCI. If the plasmid of interest does not possess a nicking site, use the topo IV technique.
1. Use maxi-prep kit to prepare plasmid of interest with a nicking site.
2. Prepare nicked substrate by incubating 150μg of plasmid with 15μL of appropriate nicking enzyme in designated buffer. Incubate reaction at 37˚C for 4 hrs. Run quick 1% (w/v) TAE agarose gel with ethidium bromide (5μg/mL) and 10μL of reaction to assess progress of the reaction. If all DNA is nicked, proceed to next step, otherwise, incubate reaction overnight until all DNA is nicked.
3. Heat inactivate nicking enzyme at 80˚C for 20 minutes.
4. Add 1-2μg of nicked DNA to 10 1.5mL eppendorf tubes. Titrate ethidium bromide. Add ethidium bromide to eppendorf tubes so that the final ethidium bromide concentration spans 0-9μM (final concentration) in a 30μL reaction volume. Add T4 ligase buffer, 2mM ATP (final concentration) and 1μL T4 ligase to each tube. Bring up to 30μL by adding water.
5. Incubate reactions at room temperature for 75 minutes.
6. Add 170μL TE buffer to each reaction. Perform phenol: chloroform extraction. Recover DNA by ethanol precipitation.
7. Resuspend each reaction in 15μL TE buffer. Combine reactions. Measure DNA concentration.

8. Run 1% (w/v) agarose TAE gel (medium gel, 150mL) 36V, 15 hours with 10ng of sample to assess quality of topoisomer ladder. Post stain with ethidium bromide (5μg/mL) for 20 minutes in TAE buffer. Destain for 30 minutes. Visualize by UV transillumination. An example of a good distribution is provided in **Fig A.1**.

Topo IV Technique

This technique takes advantage of *E. coli* topo IV's ability to relax negative and positive supercoiled substrates. For this assay, use WT topo IV for negative supercoil relaxation and the Arg616Asp ParC mutant for positive supercoil relaxation to produce a ladder of topoisomer bands (distributive activity on respective substrates)(Vos *et al*, 2013).

1. Form topo IV tetramers on ice by incubating equimolar ParE and ParC for 10 minutes (20-40μM final tetramer concentration).
2. Serially dilute in protein dilution buffer (10% (v/v) glycerol, 300mM potassium glutamate, 50mM Tris-HCl pH 7.9, and 6mM $MgCl_2$) in 2-fold steps to 5μM tetramer.
3. Add 5μL of 5μM topo IV tetramer to 45μL of protein dilution buffer. For experiments with negatively-supercoiled substrates, dilute in 2-fold steps to 3nM topo IV. For experiments with positively-supercoiled substrates, dilute in half log steps to 0.05nM topo IV.
4. Mix 8μL of topo IV (500-3nM or 500-0.05nM) with 8μL of 150ng/μL negatively or positively supercoiled DNA, respectively. Incubate on ice for 5 minutes. Add 40μL 2X buffer (100mM Tris-HCl pH 7.9, 20μg/mL BSA, 20mM DTT, 2mM spermidine, 12mM $MgCl_2$) and 8μL water. Incubate at RT for 5 minutes. Transfer reactions to 37˚C.
5. Add 8μL ATP (20nM diluted in water) and incubate at 37˚C for 10 minutes.
6. Quench reactions by adding 1% (w/v) SDS and 10mM EDTA pH 8.0 (final concentrations).
7. Run 1% (w/v) TAE (50mM Tris-HCl pH 7.9, 40mM sodium acetate, 1mM EDTA pH 8.0) gel with 10μL of each reaction to assess extent of relaxation. Use medium size gel box (150mL gel) at 36V for 15 hours. Store the remainder of reach reaction at 4˚C overnight.
8. Post stain with ethidium bromide (5 μg/mL) for 20 minutes in TAE buffer. Destain for 30 minutes. Visualize by UV transillumination.
9. Pool appropriate reactions as determined by gel. A representative gel is shown (**Fig A.1**).
10. Use PCR clean up kit to remove topo IV from pooled fractions. Elute from column in TE buffer (~35μL at a final concentration of 100ng/μL).

Preparing, Running, and Visualizing DNA on a 2-D gel

This protocol is designed for a Hoefer SUB20 Maxi Submarine Gel Electrophoresis unit.

1. Prepare a 250mL 1.2% (v/v) agarose TPE gel. Cool gel to 50˚C in a water bath and pour into caster. Prepare with a circular 1-well comb.

2. Once gel has set, transfer gel apparatus and gel to 4˚C. Equilibrate for at least 1 hour prior to running samples. Running buffer (1xTPE) should also be chilled.
3. Prepare sample for gel by adding 6x sucrose DNA loading buffer (final DNA concentration should be ~1μg in 15μL). Load 18μL of sample into circular well.
4. Run gel at 4˚C, 70V with buffer recirculation for 18 hours.
5. Remove gel from apparatus. Remove bottom 2cm of gel with a razor blade.
6. For samples prepared by the nick-ligate method or from negatively-supercoiled substrates, soak gel in 1xTPE (0.5L) with 3-30μg chloroquine at RT. The concentration of chloroquine required depends on the sigma of the plasmid and is derived empirically. Soak for 1hour, shaking, then exchange buffer. Repeat 3 times.
7. For positively-supercoiled samples, soak gel in TPE (0.5L) with 13μM netropsin. Soak for 1 hour, shaking, then exchange buffer. Repeat 3 times.
8. Make 1xTPE running buffer with appropriate concentration of chloroquine or netropsin. Chill buffer, gel apparatus, and gel for at least 1 hour.
9. Rotate gel 90˚ from previous position in gel apparatus. Use the trimmed bottom and loading well as a guide.
10. Run gel at 4˚C for 18hrs at 70V with buffer recirculation.
11. Remove gel from apparatus and soak in TPE buffer (0.5L) for 0.5-1hr at RT shaking.
12. Remove TPE buffer. Add ethidium bromide (5μg/mL) to fresh 1xTPE buffer and stain gel for 30 minutes at room temperature shaking.
13. Destain gel for 30-60minutes in 1xTPE buffer (0.5mL). Visualize by UV transillumination. The gel is fragile and large, so handle with care. Representative 2-D gels for positively- and negatively-supercoiled pSG483 are shown (**Fig A.2**).

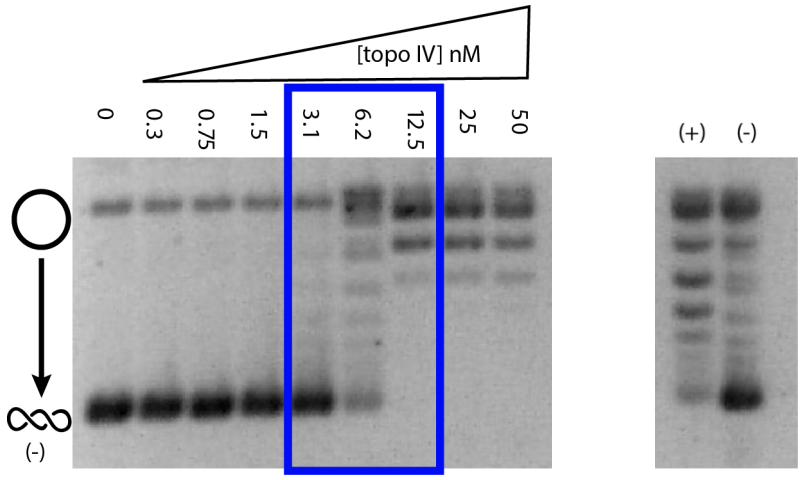

Figure A.1 Selecting samples with appropriate topoisomer distribution for 2-D gel analysis.
Left: Titration of Topo IV with a negatively supercoiled plasmid. Blue box indicates samples pooled for analysis by 2D gel electrophoresis.
Right: Pooled reactions of positively- and negatively-supercoiled topoisomers of pSG483 produced by incubating the plasmid with Topo IV. This gel shows a good topoisomer distribution required for obtaining the linking number from a 2-D gel.

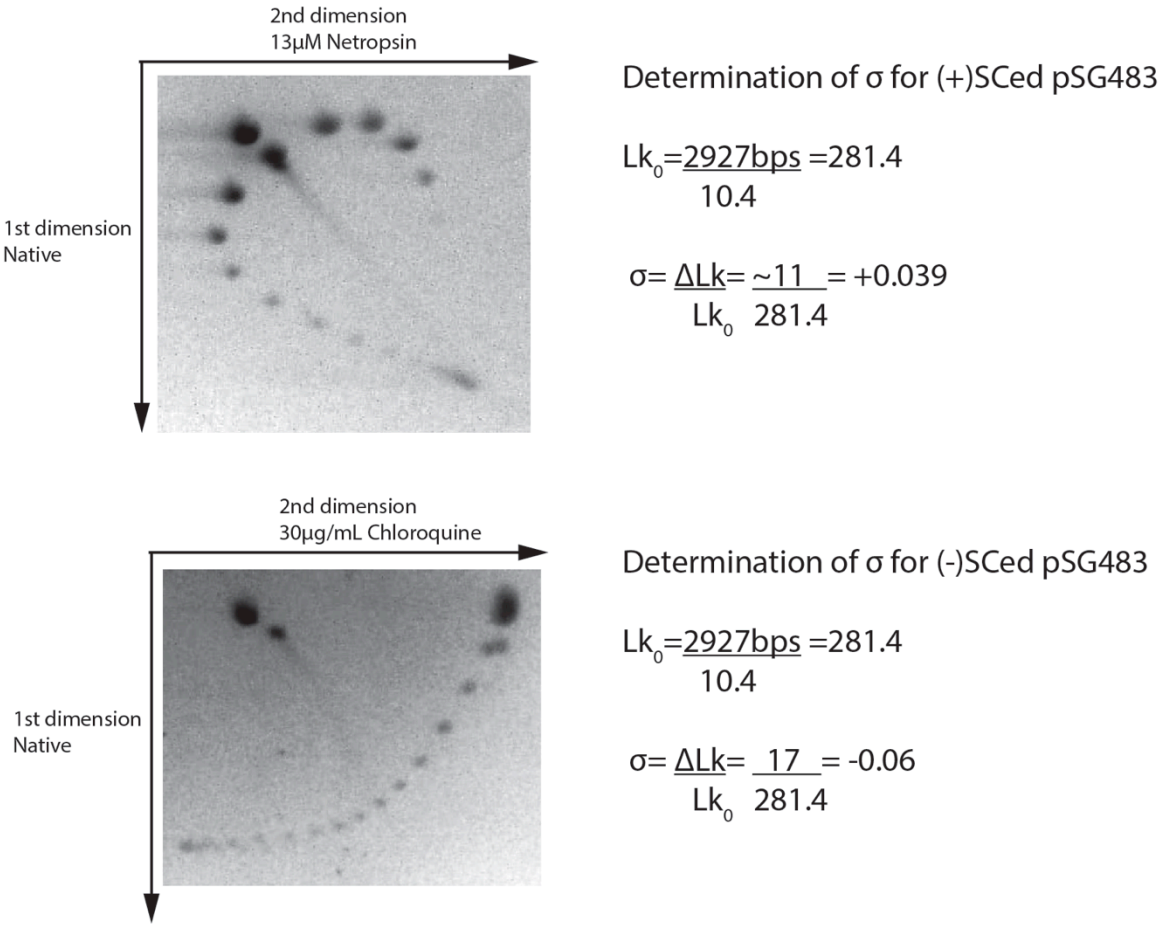

Figure A.2. Representative 2-D gels.
Run with positively (upper) and negatively (bottom) topoisomers. Calculation of σ is illustrated to the left of each gel.

Appendix 4: Round-the-Horn Site Directed Mutagenesis

(Modified from OpenWetWare protocol by Sean Moore)

This is an alternative technique for site directed mutagenesis. It is useful for generating truncations and large deletions. Primers flanking the region of interest anneal in opposing directions. For single mutations, the 3' end of one primer contains the mutation. The primer going in the opposing directions starts ('5 end) directly after the mutation. The 3' end of each primer is phosphorylated, either by PNK treatment or by purchasing pre-phosphorylated primers. After PCR, the linear product is ligated by T4 DNA ligase to produce a circular substrate that can be transformed into *E. coli*. A scheme of the procedure is provided in **Fig A.3**.

Materials
T4 DNA ligase (New England Biolabs)
ATP pH 7.5 (200mM)
$MgSO_4$ 50mM
PNK
PNK buffer
DpnI (New England Biolabs)
Pfu(II)Ultra DNA Polymerase (Novagen)
Pfu(II)Ultra DNA Polymerase buffer (Novagen)
dNTPs (2.5mM)
Plasmid DNA of interest

Procedure
Design appropriate primers with a Tm between 55-60˚C. Primers can be ordered pre-phosphorylated or can be phosphorylated as described below.

Primer phosphorylation
37.5 µL Water
5 µL PNK buffer
1 µL $MgSO_4$ (50mM)
2.5 µL primer (200µM)
1 µL ATP pH 7.5 (200mM)
1 µL PNK

Incubate the reaction at 37˚C for 1 hour. Heat kill at 95˚C for 5 minutes.

PCR
39 µL Water
5 µL 10x DNA polymerase buffer
1.5 µL primer 1 (10 µM)
1.5 µL primer 2 (10 µM)

5 µL dNTPs (2.5mM)
1 µL DNA (50ng)
1 µL Pfu(II) Ultra DNA Polymerase (or other favorite DNA Polymerase)

PCR Program

1. 98˚C 1min
2. 96˚C 30s
3. 58˚C 30s
4. 72˚C 7min
5. Repeat to 2 25x
6. 18˚C 1 min
7. 4˚C ∞

1. After PCR, add 1μL DpnI and incubate at 37˚C for one hour to digest mother plasmid.
2. Run entire PCR reaction on a 1% (w/v) agarose EtBr TAE with a ladder.
3. Excise the properly sized band and gel extract product. Elute with 20μL water.

Ligation Reaction

4 µL gel extracted vector
1 µL T4 DNA Ligase
1 µL 10mM ATP pH 7.5
0.5 µL T4 DNA Ligase
3.5 µL Water

1. Ligate for 4-16 hours at RT.
2. Transform 5 µL of ligation mixture into *E. coli* Xl-1 Blue cells. Incubate cells on ice for 20min. Heat shock at 42˚C for 45s. Chill on ice for 2min. Add cells to 1mL LB medium and outgrow for 1.5 hours at 37˚C. For a negative control, transform 5μL of unligated PCR product.
3. Add cells/media to 1.5mL eppendorf and spin in tabletop centrifuge (4k for 5 minutes). Remove media and resuspend cells gently in 100μL fresh media. Plate entire volume on media with appropriate selection.
4. Grow cells at 37˚C for ~16 hours.
5. Pick three colonies for miniprepping and sequencing and grow overnight in 5mL culture.
6. Mini-prep entire culture. Store DNA products at -20˚C and submit for sequencing.

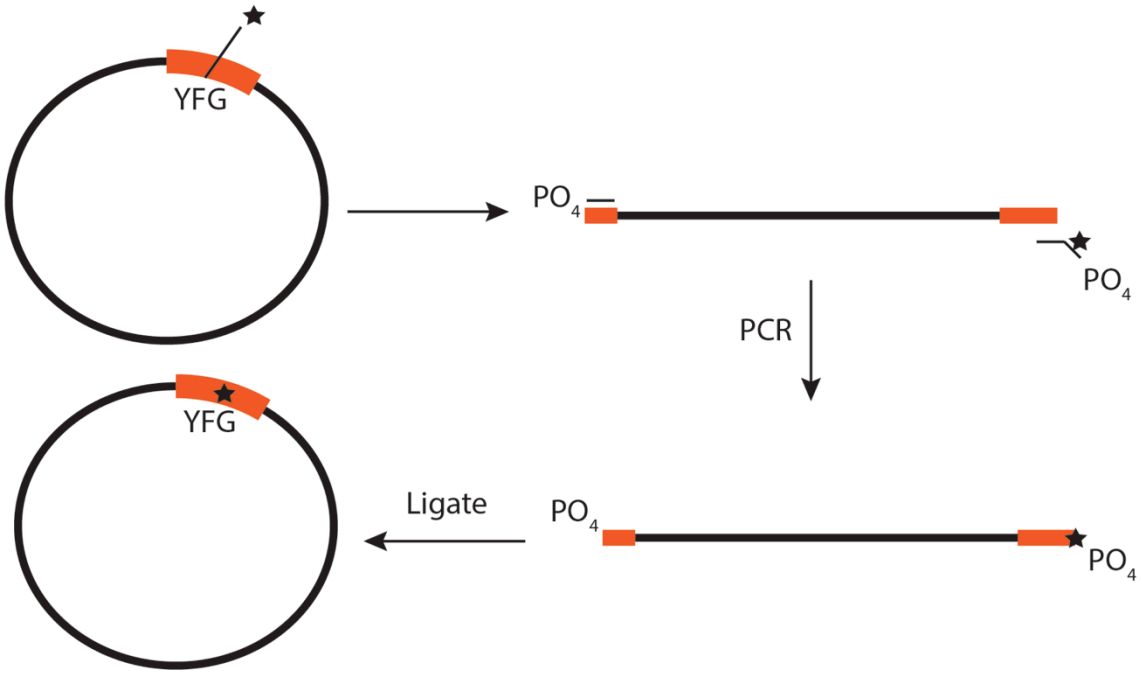

Fig A.3. General scheme of Round-the-Horn site directed mutagenesis. Starting with your favorite gene (YFG, orange) in the plasmid of interest (black), design primers that abut the region that will be mutated. One primer should contain the mutation to be introduced (star). Primers should be phosphorylated. After PCR, a linear product is obtained and is ligated to produce a circular product that can be transformed.

Appendix 5: Expression and Purification of *E. coli* ParC, ParE, His_6-MBP-ParC CTD, and MukB (566-863)

Materials
2xYT media
34 mg/mL kanamycin
30 mg/mL chloramphenicol
2L baffled flasks
Sterile 1.5mL eppendorf tubes
2x Protein Loading Buffer
1M Tris-HCl pH7.9
4M NaCl
3M KCl
Reducing agent (BME or TCEP)
Glycerol
LB plates with 34μg/mL chloramphenicol and 30μg/mL kanamycin
5mL Ni^{2+} Hi-Trap columns (GE)
Sterile 10mL serological pipettes
Filtered (0.2μ) ddH_2O
20% (v/v) ethanol
Peristaltic pump tubing (optional)
Peristaltic pump (optional)
S-300 column (GE)
Amylose resin (New England BioLabs) (His_6-MBP-ParC only)
Maltose (His_6-MBP-ParC only)

Expression
Day 1
Transform *E. coli* ParE, ParC or His_6-MBP-ParC CTD (all in pET28b background) into BL21(DE3) RIL cells.

a. Add 50-100ng of plasmid to 100μL cells.
b. Incubate cells and DNA on ice for 20 minutes.
c. Heat shock at 42˚C for 45s.
d. Return to ice for 2 minutes.
e. Add 1mL 2xYT or LB media to cells and transfer to sterile culture tube. Grow cells at 37˚C for 1 hour.
f. Remove 100μL of cells and spread on LB plate with 34μg/mL chloramphenicol and 30μg/mL kanamycin. Incubate plate at 37˚C overnight.

Day 2
Remove plate(s) from incubator and store at 4˚C until evening.

a. Autoclave 2xYT media in 2L baffled flasks. Cool.
b. Prepare 250mL A800 buffer (**Table A.1**). Do not add reducing agent or protease inhibitors. Chill at 4˚C.

c. Inoculate 50-75mL 2xYT media in sterile 250mL culture flask with several colonies from transformation plate and 34μg/mL chloramphenicol and 30μg/mL kanamycin. Incubate cells, shaking (220rpm) at 37˚C overnight.
d. Prewarm 2xYT media prepared in (a) overnight (37˚C).

Day 3

a. Remove starter culture from 37˚C incubator.
b. Add antibiotics to media in 2L baffled flasks (34μg/mL chloramphenicol and 30μg/mL kanamycin, final)
c. Inoculate media with 10mL of overnight culture. Grow cells at 37˚C, shaking (220 rpm). Measure OD_{600} every thirty minutes after inoculation. When cells reach OD_{600} 0.4-0.5, induce protein expression by adding 0.5mM IPTG (usually 1.5-2hrs after inoculation).
    i. Take 1mL of cells prior to induction for a gel "pre-induction sample". Store at -20˚C.
d. Grow cells for 3-4 hrs after inoculation at 37˚C, shaking.
e. Transfer cells to 1L centrifuge tubes and balance.
f. Spin cells for 15 min at 15k, 4˚C in Avanti. While cells are spinning, add protease inhibitors and reducing agent to the A800 buffer prepared in step (b) of Day 2.
g. Decant media from cell pellet. Place centrifuge bottles on ice. Add 10-20mL buffer A800 to pelleted cells and gently swirl.
h. Pipette cells gently with a sterile 10mL serological pipette. Avoid adding air bubbles to the cell. Continue to swirl/pipette until cells and buffer are homogenously mixed.
i. Add resuspended cells to another bottle containing pelleted cells. Avoid adding extra A800 for resuspension as greater volumes will make subsequent purification steps cumbersome. Continue until all cell pellets are resuspended in A800. If cells will be stored, continue with step j. If used immediately for purification, proceed to Protein Purification steps.
j. Pour liquid nitrogen in dog bowl. Add resuspended cell mixture to liquid nitrogen drop wise (should look like Dip N' Dots).
k. Gently decant pellets into a 50mL falcon tube with a funnel. Store cell pellets at -80˚C.

Protein Purification (FL ParE, FL ParC)

Pre-Day 1

a. Prepare all buffers described in **Table A.1**. Store at 4˚C. Do not add protease inhibitors or reducing agent at this time.

Day 1

a. Add protease inhibitors and reducing agent to buffers A-D (C and D are for His_6-MBP-ParC CTD only). Filter sterilize (0.2μ) and store at 4˚C.

b. Charge Ni^{2+} columns for protein preparation. I prefer to use a peristaltic pump in the cold room to charge and equilibrate the columns. This procedure can also be performed on an FPLC. (CV= column volume(s))
    i. Run 5CV of filtered ddH_2O over the column(s) at a rate of 1mL/min.
    ii. Apply 5CV Acidic Salt Buffer (**Table A.1**) to the column(s).
    iii. Apply 0.5CV Nickel Sulfate Buffer (**Table A.1**) to the column(s). Collect flow through.
    iv. Rinse column with 5CV Acidic Salt Buffer (**Table A.1**) to remove unbound Ni^{2+}. Collect flow through and dispose of in appropriate waste bin.
    v. Apply 1CV buffer B400 (**Table A.1**) to remove weakly bound Ni^{2+}.
    vi. Equilibrate column(s) in A800 (5CV). Store columns at 4˚C.
c. Remove cells from -80˚C and defrost at 25˚C or in a beaker with warm water. When cells are almost fully melted, transfer to metal beaker on ice.
d. Once cells are fully melted on ice, sonicate cells. Do not use the microtip because it will not shear DNA sufficiently. (Proteins bound to long DNA segments will destroy nickel columns and prevent isolation of the protein).
    i. 5.5mW, 15s pulse, 2 minute pauses between pulses. 3 pulses for 2-3L of cells, 4 pulses for 6L.
e. Transfer lysate to SS34 tube. Balance.
f. Spin lysate in Sorvall SS34 rotor for 30 minutes, 15k, 4˚C.
g. Pour clarified lysate into a 50mL Falcon tube on ice.
    i. Save 10μL of the clarified lysate and a fraction of the pelleted material for a gel. Add SDS-PAGE loading buffer to the samples and store at -20˚C.
h. Apply clarified lysate to charged 5mL Ni^{2+} Hi-Trap column. This can be done on an FPLC or with a peristaltic pump (flow rate~1mL/min).
i. Wash column with Buffer A800 until protein is no longer detected (<100mAU reading with FPLC UV detector or when 10μL of column flow through added to 90μL Bradford reagent no longer turns blue).
j. Stop flow and change lines to Buffer A400. Wash column for at least 5CV or until protein is no longer detected (<100mAU reading with FPLC UV detector or when 10μL of column flow trough added to 90μL Bradford reagent no longer turns blue). (For preparations of His_6-MBP-ParC, continue with steps **Protein Purification (His_6-MBP-ParC)**).
k. Stop flow and change lines to Buffer B400. Collect fractions.
l. Pool fractions containing protein and concentrate by centrifugation until protein volume is ≤ 2mL. (Amicon 30 MWCO concentrators, balanced, in Sorvall Legend Tabletop Centrifuge, 4k, 4˚C).
m. Prepare 0.5-3mL Slide-A-Lyzer cassettes.
    i. Equilibrate cassette in ddH_2O for 10min.

ii. Add 1mg of His_6-TEV protease to the concentrated protein. Mix gently.
iii. Inject protein/protease into Slide-A-Lyzer cassette and place in beaker with 0.5-1L of Buffer A400.
iv. Dialyze overnight at 4˚C, stirring.

n. Equilibrate S-300 column.
i. Apply 150mL ddH_2O to column at 0.5 mL/min followed by 150mL Buffer SE400. Equilibration takes 10hrs.

o. Strip and re-charge 5mL Ni^{2+} Hi-Trap columns.
i. Apply 5CV ddH_2O to the column(s).
ii. Apply 5CV Stripping Buffer (**Table A.1**).
iii. Wash with 5CV ddH_2O.
iv. Repeat steps (b).ii.-v. Final equilibration buffer is buffer A400.

Day 2

a. Remove protein from Slide-A-Lyzer cassette and transfer to 1.5-2mL eppendorf tube.
b. Apply protein to re-charged 5mL Ni^{2+} Hi-Trap. Collect fractions.
c. Run A400 over the column. Collect fractions. Uncleaved protein and TEV protease remain bound to the column while the cleaved protein of interest does not associate with the column.
d. Pool fractions containing protein and concentrate by centrifugation. (Millipore Amicon 30 MWCO concentrators, balanced, spin in Sorvall Legend Tabletop Centrifuge, 4k, 4˚C).
e. Apply B400 to column to elute TEV protease and uncleaved protein. Collect fractions. Save 10μL of protein containing fraction for a gel to assess cleavage efficiency. Store at -20˚C.
f. When protein is concentrated to a volume of ≤ 2mL, remove from concentrator and transfer to a 2.0mL eppendorf tube. Spin in cold room for 10 minutes at 14k in tabletop centrifuge to remove aggregates. This should be done immediately before applying protein to the S-300 column.
g. Apply protein to S-300 column equilibrated in SE400. Collect fractions. (ParE elutes between ~60-75mL, ParC elutes between ~50-65mL, His_6-MBP-ParC CTD elutes between ~65-80mL).
h. Assess fraction purity by SDS-PAGE (10% 19:1 Bis:acrylamide). Also run saved fractions at this time (preinduction sample, clarified lysate, pelleted fraction, uncleaved protein (5μL of these samples is usually sufficient)).
i. Pool appropriate fractions and concentrate by centrifugation (≤500μL).
j. Add storage buffer (**Table A.1**)(final 2 protein:1 storage buffer, 30% (v/v) glycerol). Measure protein concentration by absorption at 280nm using the method of Edelhoch (Edelhoch, 1967). Aliquot protein (10-20μL) and store at -80˚C. Assess protein activity.
k. Strip and store 5mL Ni^{2+} Hi-Trap columns.
i. Apply 5CV ddH_2O to the column(s).

ii. Apply 5CV Stripping Buffer (**Table A.2**).
iii. Wash with 5CV ddH_2O.
iv. Apply 5CV 0.5M NaOH.
v. Wash with 5CV ddH_2O.
vi. Exchange column into 20% ethanol (~5CV). Store columns at 4˚C.

Protein Purification (His_6-MBP-ParC)

Pre-day 1

a. Equilibrate S-300 column (step n protein purification day 1 for FL ParE and ParC).
b. Pack a 10mL amylose column (New England Biolabs). Equilibrate in A400. Store at 4˚C.

Day 1

a. After completing step (j) of day 1 of the protein purification for FL ParC, ParE, place amylose column in line with the Ni^{2+} Hi-Trap column.
b. Apply 50mL B400 to the column series. Collect flow through in the event there is more protein in the sample than the amylose column can effectively bind.
c. Take Ni^{2+} Hi-Trap column out of line. Wash amylose column in C400 (50mL).
d. Elute protein from amylose column in D400. Collect fractions. Pool peak fractions and concentrate by centrifugation. (Millipore Amicon 30 MWCO concentrators, balanced, spin in Sorvall Legend Tabletop Centrifuge, 4k, 4˚C).
e. When protein volume is ≤2mL, apply to S-300 column equilibrated in SE400. Proceed with Purification of FL ParC, ParE Day 2, step (f).

Buffer	A800	A400	B400	C400	D400	SE400	Storage
NaCl	800mM	400mM	400mM	400mM	400mM	———	———
KCl	———	———	———	———	———	400mM	400mM
Glycerol (v/v)	10%	10%	10%	10%	10%	10%	70%
Tris-HCl pH 7.9	20mM	20mM	20mM	20mM	20mM	20mM	20mM
Imidazole pH 8.0	30mM	30mM	500mM	———	———	———	———
Maltose	———	———	———	———	100mM	———	———
BME	2mM	2mM	2mM	2mM	2mM	2mM	2mM
Leupeptin	1μg/mL	1μg/mL	1μg/mL	1μg/mL	1μg/mL	1μg/mL	———
Pepstatin A	1μg/mL	1μg/mL	1μg/mL	1μg/mL	1μg/mL	1μg/mL	———
PMSF	1mM	1mM	1mM	1mM	1mM	1mM	———

Table A.1
Purification buffer compositions for preparation of *E. coli* ParC, ParE and His_6-MBP-ParC CTD.

Stripping Buffer	**Nickel Sulfate Buffer**	**Acidic Salt Buffer**
0.5M NaCl	0.2M $NiSO_4$	0.5M NaCl pH 3.0
50mM EDTA pH 8.0		

Table A.2 Buffers for charging nickel columns.
All of these buffers should be filter sterilized (2μ) prior to applying to the column(s).

Appendix 6: Overexpression and Purification of *A. fulgidus* Reverse Gyrase

(Protocol modified from Rodriguez, AC 2002 *JBC*)

Protein Overexpression

Day 1

1. Prepare 3L 2xYT media. Autoclave in 2L baffled flasks. Store at room temperature.
2. Transform *A. fulgidus* into *E. coli* C41(DE3) cells. The plasmid confers ampicillin resistance. Note: this plasmid **will not** transform into other commonly used expression strains such as *E. coli* Bl21(DE3)RIL.
    i. After outgrowth, add 50μL of freshly transformed cells to 50-75mL 2xYT cultures with carbenicillin (200μg/mL final) or ampicillin (100μg/mL final). Incubate culture at 37˚C overnight, shaking (220 rpm).
    ii. Warm 2xYT media prepared in step 1. Incubate at 37˚C.

Day 2

1. Inoculate 2xYT media in baffled flasks with 10mL of overnight culture. Add ampicillin to cultures (final concentration 100μg/mL). Grow cells at 37˚C shaking, 220rpm. Check OD_{600} every 30 minutes.
2. When cells reach OD_{600} 0.6, reduce temperature to 18˚C and induce protein expression by adding 05.mM IPTG (final) to the media. Grow cells for an additional 16 hrs shaking.

Day 3

1. Harvest cells. Pour cells into 1L plastic bottles for Avanti. Balance and incubate on ice. Spin for 15min, 4k, 4˚C.
2. Decant media from cells and place pellets on ice.
3. Resuspend pellets in chilled Buffer A (**Table A.3**)
4. Freeze drop-wise and store at -80˚C until protein is purified.

Protein Purification

Pre-day 1

1. Prepare buffers in **Table A.3**. Do not add protease inhibitors or reducing agent at this time. Chill buffers at 4˚C.
2. Filter 1L of ddH_2O and SE buffer (add reducing agent and protease inhbitors) (0.2μ filter). Equilibrate S-300 column (150mL ddH_2O followed by 150mL SE buffer (**Table A.3**)).

Day 1

1. Thaw cells at RT. Before cells are fully thawed, transfer to metal beaker on ice.

2. Once cells are fully thawed, sonicate 3x, 15s bursts 5.5mW, 2min rests between bursts.
3. Pour lysate into SS34 tube. Balance and spin in SS34 rotor for 30 minutes at 15k.
4. Add protease inhibitors and filter Buffer A and Buffer B (**Table A.3**).
5. Prepare a 5mL Ni^{2+} Hi-Trap column as described on pg. 187 (b) for the preparation of ParE and ParC.
6. Pour clarified lysate in 50mL falcon tube. Apply lysate to prepared 5mL Ni^{2+} Hi-Trap column.
7. Wash 5mL Ni^{2+} Hi-Trap column with Buffer A until no protein is observed to flow through (mAU ≤100 or Bradford reagent no longer turns blue when 10μL protein is added to 90μL of the reagent).
8. Elute protein from column in Buffer B.
9. Pool protein containing fractions and concentrate by centrifugation (Millipore Amicon 30 MWCO, 4K, 4˚C). Add $MgCl_2$ to the protein to a final concentration of 10mM to maintain solubility during centrifugation. Alternatively, NaCl can be added to 1M (final concentration).
10. When protein volume is less than 2mL, remove from concentrator and transfer to a 2.0mL eppendorf tube. Spin in cold room for 10minutes at 14k in tabletop centrifuge to remove protein aggregates.
11. Apply to S-300 column prepared on Pre-day 1. Collect fractions and run in Buffer SE.
12. Pool peak fractions and concentrate by centrifugation (Millipore Amicon 30 MWCO, 4K, 4˚C). (Reverse gyrase usually elutes between 50-60mL from S-300, MW~121300). Add chilled protein storage buffer (2:1, 30% (v/v) final glycerol concentration). Determine protein concentration, aliquot, flash freeze in liquid nitrogen, and store at -80˚C.

Table A.3 Protein Purification Buffers for Reverse Gyrase Preparation

	Buffer A	**Buffer B**	**SE Buffer**
Tris-HCl pH 7.9	50mM	50mM	50mM
NaCl	800mM	800mM	200mM
Imidazole pH 8.0	10mM	300mM	10mM
Glycerol (v/v)	10%	10%	10%
Sodium Azide (w/v)	–	–	0.02%
PMSF	1mM	1mM	1mM
Leupeptin	1μg/mL	1μg/mL	1μg/mL
Pepstatin A	1μg/mL	1μg/mL	1μg/mL

Appendix 7: Production of Positively-Supercoiled Plasmid DNA using *A. fulgidus* Reverse Gyrase

Test specific activity of reverse gyrase preparation

Materials

Negatively-supercoiled plasmid substrate
200mM ATP pH 7.0
Tris-HCl pH 7.9
NaCl
$MgCl_2$
Thermocycler or 95˚C heat block
Stop Buffer (100mM EDTA/10% (w/v) SDS solution)
10M Ammonium acetate
6X Sucrose loading dye
TAE Buffer
Agarose

Method

1. Serially dilute reverse gyrase protein in SE Buffer (**Table A.3**). Serial dilution should range from 8μM to 0.25μM (final concentration in 100μL reaction volume). Usually 5-6 different concentrations covering this range will be sufficient to assess activity.
2. Mix together the following on ice in 100μL PCR tube for each reverse gyrase concentration:
    a. 5μg negatively-supercoiled plasmid DNA
    b. 5μL Reverse gyrase (serial dilution)
    c. 2mM ATP
    d. 10mM NaCl
    e. 10mM $MgCl_2$
    f. 50mM Tris-HCl pH 7.9
3. Prepare plate with 3μL stop buffer for each protein concentration and time point that will be taken.
4. Remove tubes from ice and place in thermocycler or heat block pre-heated to 95˚C. Remove 7.5μL of each reaction at time 0, 15s, 30s, 1min, 3min, and 6min and mix with stop buffer prepared in step 3.
5. To assess enzyme activity, add 6X Sucrose-DNA loading dye to samples and run 10μL on a 1% TAE gel (50mM Tris-HCl pH 7.9, 40mM sodium acetate, 1mM EDTA) at 36V for 15 hours. Post-stain gel in TAE with ethidium bromide (0.5μg/mL, final concentration) for 20 min. Destain in TAE for 30 minutes. A concentration of reverse gyrase that produces a good activity profile is shown in **Fig A.4.**

Produce Positively-Supercoiled DNA

Reaction mixture in 500μL:

a. 50μg negatively-supercoiled plasmid DNA
b. 10μL reverse gyrase (at appropriate concentration as determined above)
c. 2mM ATP pH 7.0
d. 10mM NaCl
e. 10mM $MgCl_2$
f. 50mM Tris-HCl pH 7.9

If using the thermocycler, split into 50μL reactions. Incubate reactions at 95˚C for 8 minutes. Take 5μL aliquots at time 0, 15s, 30s, 1min, 2min, 4min, and 8min after incubating at 95˚C. Quench in 2μL stop buffer. After 8 minutes, quench reactions by adding stop buffer to a final concentration of 1% (w/v) SDS and 10mM EDTA pH 8.0. Run gel of fractions as described in step 5 of the **Test of Specific Activity** protocol. Proceed with Phenol Chloroform Extraction and Ethanol Precipitation as described below.

Phenol Chloroform Extraction

1. Add equal volume Phenol-Chloroform-Isoamyl alcohol mixture (25:24:1) to the quenched reverse gyrase reactions.
2. Spin tube at 14k for 2min. Gently remove upper aqueous layer and place in fresh 2mL eppendorf. Dispose of lower layer in appropriate bin.
3. Gently add an equal volume of chloroform to the aqueous fraction obtained in step 2.
4. Vortex for ~10s. Spin tube at 14k for 2min.
5. Gently remove upper aqueous layer and place in fresh 2mL eppendorf.

Ethanol Precipitation

1. Add ammonium acetate to the DNA (final concentration should be 2M). Use ammonium acetate instead of sodium acetate because it selectively precipitates DNA but not ribonucleotide.
2. Add 2 volumes of -20˚C 95% ethanol to the tube.
3. Incubate tube at -80˚C for at least 20 minutes.
4. Spin tube in cold room for 30 minutes at 14k.
5. Gently remove the ethanol. The pellet may be visible at this step. Do not decant the ethanol from the pellet because this may dislodge it.
6. Wash pellet in 2 volumes (original volume) of 70% ethanol to remove salt. Centrifuge for 20 minutes at 4˚C, 14k.
7. Gently remove ethanol. Pellet should be visible at this point.
8. Wick excess ethanol with a Kimwipe. Allow pellet to dry on the bench top (usually 10-20 minutes).

9. Resuspend in autoclaved ddH_2O to appropriate volume and measure concentration.
10. Aliquot, snap freeze in liquid nitrogen, and store at -80˚C. Never freeze thaw DNA samples. Thawed DNA can be stored at 4˚C for several months.

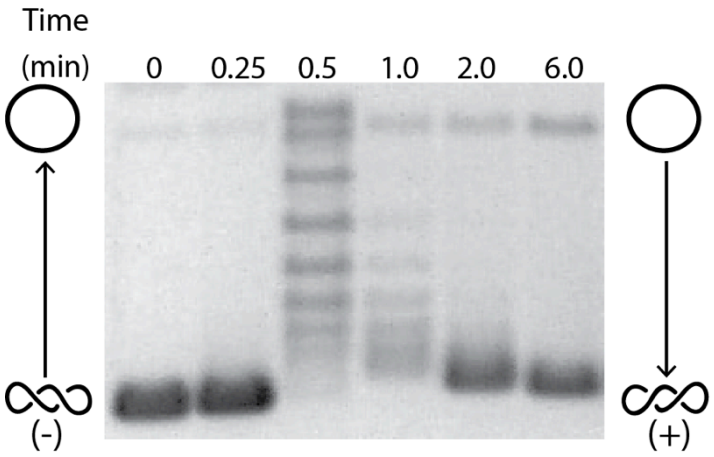

Fig A.4. Representative gel of reaction to produce positively-supercoiled DNA from a negatively-supercoiled plasmid substrate.
Plasmid substrate was incubated with reverse gyrase for various amounts of time. At 0.5 min, the negative supercoils have been removed and the plasmid runs primarily with relaxed topoisomers. With extended incubation periods, the plasmid becomes supercoiled again. Positive supercoiling is evident because the plasmid runs slightly slower than the negatively-supercoiled substrate and stains less intensely with ethidium bromide. Representative cartoons of relaxed and supercoiled DNA species are shown to the left and right of the gel to assist in identifying DNA species present over the course of the reaction.

Appendix 8: Gyrase supercoiling and topo IV relaxation assays

This is a general protocol for running topo IV or gyrase activity relaxation or supercoiling assays, respectively. This assay may require modification for different applications. For example, assays studying the effects of different protein•protein interactions, salt or DNA concentration, assay pH, or other additives will likely require further optimization. This protocol is a guide and is intended for determining the specific activity of gyrase/topo IV enzyme preparation.

Materials
Relaxed or supercoiled plasmid substrate resuspended in water (I typically use pSG483, 2927bps)
2M Potassium glutamate
1M Tris-HCl pH 7.9 (25˚C)
10mM Spermidine (topo IV assays only)
10mg/mL BSA
1M TCEP pH 7.0
1M DTT (topo IV only)
2M $MgCl_2$
200mM ATP pH 7.0
0.5M EDTA pH 8.0
SDS
6X Sucrose DNA loading buffer (see table A.4)
50% (v/v) Glycerol
Invitrogen UltraPure agarose
8-12 channel 20μL multi-channel pipette

Protocol

1. Form gyrase or topo IV tetramers on ice for at least 10 minutes and no longer than 15 minutes. Incubate equimolar concentrations of GyrA/ParC and GyrB/ParE to a final **tetramer** concentration of 20-40μM in a volume of 10-15μL. Bring the proteins up to the final 10-15μL volume by adding protein dilution buffer (**Table A.4**) **after** the subunits have incubated for 10-15 minutes.
2. Serially dilute reconstituted gyrase or topo IV. Perform in 2-fold (and 1 10-fold) dilutions to achieve to 500nM tetramer. The dilution scheme I use is drawn below (**Fig A.5**).
3. Once the gyrase and topo IV tetramers are diluted to 500nM, dilute in 2 or half log steps for 10 steps. This is to ensure a broad concentration series of enzyme to get an accurate idea of how active the enzyme is.

4. For general activity assays, remove 2μL of serially diluted gyrase/topo IV and place in a fresh set of wells in a 96-well plate. Use multi-channel pipette.
5. Add 2μL of protein dilution buffer to the gyrase/topo IV. NOTE: The protein dilution buffer can be modulated so that this buffer is not added at this step. I include this step because in subsequent experiments, I add a protein to gyrase/topo IV at this stage (**Table A.4**).
6. Incubate gyrase/topo IV with protein dilution buffer/protein on ice for 5 minutes.
7. Topo IV specific: Add DNA at this step. Incubate at RT for 5 min. (7.9nM final DNA concentration). I usually at 2μL of DNA.

a. Then add 10μL 2X buffer and water to bring the volume to 18μL. Incubate at RT for another 5 minutes (**Table A.4**).
b. To initiate the reaction, add 2μL 20mM ATP pH 7.0 (2mM final concentration, final reaction volume 20μL) and incubate at 37˚C.
c. Ten minutes after the addition of ATP, quench the reaction by adding 5μL stop buffer.

8. Gyrase specific instructions:
    a. Add 10μL 2x buffer, relaxed DNA substrate (7.9nM final), water to bring the assay to a final volume of 18μL, and 2μL 20mM ATP pH 7.0 (2mM final concentration, final reaction volume 20μL). Transfer reaction from ice to 37˚C.
    b. Incubate reaction at 37˚C for 30 minutes. Quench by adding 5μL stop buffer.

How to run a beautiful topo gel

Make fresh TAE buffer daily from solid sodium acetate. **DO NOT** make large stocks of TAE because the acetic acid will evaporate over time and will not be at the appropriate concentration.

Fresh TAE composition (1x)
50mM Tris-HCl pH 7.9
40mM Sodium acetate
1mM EDTA pH 8.0

Traditional TAE composition (1x)
40mM Tris base
20mM glacial acetic acid
1mM EDTA pH 8.0

1. Prepare medium gel box. Clean a 16-well comb and position so narrow side of comb is perpendicular to the bottom of the gel box.
2. To prepare gel, add 1.5g UltraPure Agarose (or another mass if running a cleavage assay or using a plasmid substrate other than pSG483) to 150mL gel buffer in 0.75-1L Erlenmeyer flask. Microwave for 1min at high power. Swirl gently. Microwave for another minute. When liquid begins to boil,

remove from microwave and swirl gently. Return to microwave and heat until liquid just begins to boil. **DO NOT** allow solution to reach a roaring boil.

3. Gently swirl solution, and avoid adding air bubbles. The agarose should be dissolved, if not microwave for another 15s and gently swirl. Place in 50˚C water bath. Cool until the glass can be placed against the wrist without burning the skin.
4. Gently pour cooled agarose solution into prepared gel box. Carefully remove air bubbles from the solution with a pipette tip.
5. Allow gel to fully set.
6. Prepare running buffer (1L). Mix 500mL TAE buffer used for the gel and 500mL traditional TAE buffer.
7. Add 6X sucrose loading dye to the samples.
8. Gently remove gel comb. Pour running buffer in gel box. Make sure gel is entirely submerged.
9. Load 20μL of sample into wells.
10. Run at 36V (2-2.5V/cm) for 15hrs or until dye front reaches the bottom of the gel.
11. Gently remove gel and place in staining container.
12. Mix running buffer with 0.5μg/mL ethidium bromide (final concentration). Stain gel for 20 minutes on orbital shaker. Shake gently.
13. Remove buffer from gel and dispose of in appropriate waste container. Rinse gel in ddH_2O two times. Pour water in appropriate waste bin.
14. Add 100mL running buffer to gel and destain for 30 minutes on orbital shaker.
15. Expose to UV transillumination and image. Usually a 3 second exposure is sufficient to resolve bands.

Table A.4. Buffers for gyrase and topo IV activity assays

Assay Buffers
Prepare these buffers in advance. Aliquot and store at -20˚C. This ensures consistency between reactions.

Protein Dilution buffer topo IV
6mM $MgCl_2$
150mM Potassium glutamate
50mM Tris-HCl pH 7. 9
10% (v/v) Glycerol
50mM Tris-HCl pH 7.9

Protein dilution buffer gyrase
150mM Potassium glutamate
25mM Tris-HCl pH 7.9
10% (v/v) glycerol
2.5mM $MgCl_2$

2X Buffer topo IV
20mM DTT
20μg/mL BSA
80mM Tris-HCl pH 7.9
9.6mM $MgCl_2$
2mM spermidine

2X Buffer gyrase
0.2mg/mL BSA
20% (v/v) glycerol
80mM Potassium glutamate*
1mM TCEP
10mM $MgCl_2$
50mM Tris-HCl pH 7.9*

Final assay conditions topo IV
6mM $MgCl_2$
30mM Potassium glutamate*
50mM Tris-HCl pH 7. 9*
2% (v/v) Glycerol
50mM Tris-HCl pH 7.9
10mM DTT*
10μg/mL BSA
1mM spermidine

Final assay conditions gyrase
70mM potassium glutamate*
5.5mM $MgCl_2$
0.1mg/mL BSA
0.5mM TCEP
30mM Tris-HCl pH 7.9
18% (v/v) glycerol

* Indicates buffer components that can be altered/omitted during optimization for specific reactions.

Stop buffer
10% (w/v) SDS
100mM EDTA pH 8.0.

6x Sucrose loading buffer
0.25% (w/v) Bromophenol blue
40% (w/v) Sucrose
pH solution with Tris-HCl pH 7.9 to pH 7.5-7.9. Filter sterilize and store at 25˚C.

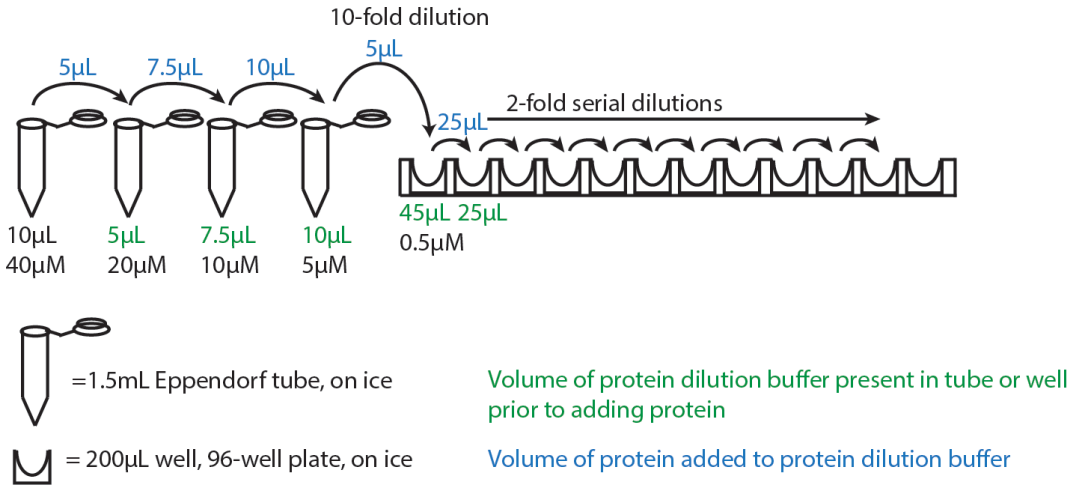

Figure A.5 Gyrase/topo IV protein dilution series.
Protein in 96-well plate will be added to reactions. Protein concentrations in each tube/well refer to reconstituted tetramer concentration.

Appendix 9: Explicit Solution for Simple Competitive Binding Equation

(As described by Wang *FEBS Letters* 1995 (Wang 1995))

This equation is useful for determining the affinity of a ligand in a fluorescence competition experiment. To perform a competition experiment using fluorescence anisotropy, the "receptor" concentration must be at an adequate concentration to observe at least half of the maximal binding signal. Under these conditions, ligand depletion must be taken into account. The following equation provides an explicit solution to the competitive binding equation. For complete derivation, see (Wang, 1995)

[P]= total "receptor" concentration
[A]= unlabeled ligand
[B]= labeled ligand
$[P]_f$=concentration of free receptor
KA= disassociation constant for "receptor" and unlabeled ligand
KB= disassociation constant for "receptor" and labeled ligand
F=fraction bound

$[P]=[P]_f+[PA]+[PB]$

$$[PB] = \frac{[P][B]}{KB + [P]}$$

$$[PA] = \frac{[P][A]}{KA + [P]}$$

Substitutions result in the following cubic equation:

$[P]_f^3+a[P]_f^2+b[P]_f+c=0$

$a=KA+KB+[A]+[B]-[P]_f$
$b=KB(A-[P]_f)+KA(B-[P]_f)+KA \bullet KB$
$c=-(KA \bullet KB \bullet [P]_f)$

$$[P]_f=\frac{-a}{3}+\frac{2}{3}\sqrt{(a^2-3b)}\ \cos\frac{\theta}{3}$$

$$\theta=\cos^{-1}\frac{-2a^3+9ab-27c}{2\sqrt{(a^2-3b)^3}}$$

$$\Delta F = \frac{[A](2\sqrt{(a^2-3b)^3}\cos\frac{\theta}{3}-a}{3KA+(2\sqrt{(a^2-3b)^3}\cos\frac{\theta}{3}-a)}$$

When using fluorescence anisotropy data, subtract the background. Then use the following modified binding equation to fit the data:

$$\Delta F = E + Bmax(-1\left(\frac{[A](2\sqrt{(a^2-3b)^3}\cos\frac{\theta}{3}-a}{3KA+\left(2\sqrt{(a^2-3b)^3}\cos\frac{\theta}{3}-a\right)}\right))$$

Bmax=maximal binding signal achieved for the specific ligand•receptor mixture.
E= constant for difference between the base of the curve and y=0 after background subtraction.

In this equation the concentration of the protein added to compete the labeled ligand from the receptor is the X value, or A.

Appendix 10: Rapid equilibrium kinetics to determine percent occupancy in a 2-protein complex

(As described by Jack Kirsch)

$[A]_T$=protein A total concentration
$[B]_T$=protein B total concentration
[AB]=concentration AB complex

1. $K_d = \frac{[A]_f[B]_f}{[AB]}$

Conservation of mass equations:
$[A]_f = [A]_T - [AB]$
$[B]_f = [B]_T - [AB]$

Substitute these equations into 1. :

$$K_d = \frac{([A]_T - [AB])([B]_T - [AB])}{[AB]}$$

$$K_d[AB] = ([A]_T - [AB])([B]_T - [AB])$$

$$0 = [A]_T[B]_T - [AB](K_d + [A]_T + [B]_T) + [AB]^2$$

Solve for AB:

$$[AB] = \frac{(K_d + [A]_T + [B]_T) - \sqrt{(K_d + [A]_T + [B]_T)^2 - 4([A]_T[B]_T)}}{2}$$

To solve for percentage bound:

$$[A]_f = [A]_T - [AB]$$

$$[A]_B = [A]_T - [A]_f$$

$$Fraction\ A\ bound = \frac{[A]_B}{[A]_{[T]}}$$